TESIS DE LA UNIVERSIDAD DE ZARAGOZA

2013

95

Irene Bolea Agüero

Heat transfer in oxy-fuel fluidized bed boilers

Departamento

Instituto Universitario de Investigación Mixto CIRCE

Director/es

Romeo Giménez, Luis Miguel

ISSN 2254-7606

Prensas de la Universidad Universidad Zaragoza

Universidad Zaragoza
1542

Tesis Doctoral

HEAT TRANSFER IN OXY-FUEL FLUIDIZED BED BOILERS

Autor

Irene Bolea Agüero

Director/es

Romeo Giménez, Luis Miguel

UNIVERSIDAD DE ZARAGOZA

Instituto Universitario de Investigación Mixto CIRCE

2013

Universidad Zaragoza
1542

Instituto Universitario de Investigación Mixto
circe
UniversidadZaragoza

HEAT TRANSFER IN OXY-FUEL FLUIDIZED BED BOILERS

PhD Thesis

Irene Bolea Agüero

Supervised by:

Dr. Luis Miguel Romeo Giménez

Instituto Universitario de Investigación Mixto
circe
UniversidadZaragoza

D. Luis Miguel Romeo Giménez, Catedrático del Área de Máquinas y Motores Térmicos del Departamento de Ingeniería Mecánica de la Universidad de Zaragoza y Miembro del Instituto Universitario de Investigación Mixto CIRCE-Universidad de Zaragoza:

Certifica que la memoria titulada *Heat transfer in oxy-fuel fluidized bed boilers,* presentada por la Ingeniera Industrial *Dña. Irene Bolea Agüero* para optar al grado de Doctor, ha sido realizada bajo mi dirección.

Así mismo, hago constar que la memoria aquí presentada se corresponde con el Proyecto de Tesis aprobado por el Instituto Universitario de Investigación Mixto CIRCE de la Universidad de Zaragoza en fecha 1 de febrero de 2011.

Por todo lo anterior, autorizo la presentación y defensa de la presente Tesis.

Zaragoza, 27 de mayo de 2013

Luis M Romeo Giménez

From the 19th century, the world has witnessed one of the most spectacular changes on the way of living along the History. The industrial revolution meant a drastic development for the economy, the quality of life, and the beginning of the society as we know it now, a globalized world. The steam generation was the breakthrough that let machines do double in half time than humans. And the coal has been the element accompanying men on such travel, followed later by the oil and the gas. But this story of success and progress had also hidden sides that we did not want to see until they were almost uncovered. Far from flattening, the curve of production and consumption has been never-ending exponential. From then on, manufacturing and transportation, the two pillars of the industrial era, are completely dependent on those non-infinite fuels. Globalization and progress meant not the same for every country and inequalities accentuate among them. And, in spite of this, the consequences of the progress of some will be paid by all. The climate change will be suffered by all the countries. But it is evident that those with infrastructure will cope better with the up-coming events. The dad *Development* must do his job and assumes *his* responsibilities. We, researchers are *his* tools, to carry out this hard task. Each of us must look for the piece of the jigsaw that is still not placed, to accelerate the change towards a fairer world and to lessen the irremediable repercussion of the acts of the teenager *Progress* that wanted to be *Development*.

ACKNOWLEDGEMENTS

First I would like to express my deep gratitude to my supervisor Prof. Luis Miguel Romeo. Since the very beginning of my career he has been an essential guide of my formation as professional researcher, not only in the technical issues, but also as a motivating leader and as a contagious optimistic.

I feel very grateful to Dr. David Pallarès for offering me the possibility of spending a fruitful and pleasant time in Chalmers University of Technology. Without his invaluable guidance and his opportune advices, this thesis would not have been what it is. I would like to acknowledge Prof. Bo Leckner for his helpful comments and ideas, some of which have been the seeds of parts of this work.

I would like to give special thanks to my team, the *Oxicocos*, Isabel Guedea and Carlos Lupiáñez, with whom I learnt much about oxy-fuel combustion in fluidized beds … but I learnt much more about patience, support, understanding, team-working and friendship.

Along these years I had the luck to meet exceptional people in CIRCE, always available to help and assist in whatever I needed. Some of them have become very good friends, willing to patiently listening to any worry about my projects, or to share some laughs in front of a beer.

Thanks to my family, for their backing, their confidence, their sensitivity and their love. Especially to my brother David that is in the beginning of his research career, I hope to be as encouraging as you have been for me.

Thank you Jose, you are part of this work as much as the words that are written in it.

RESUMEN

A pesar de la estabilización de la demanda de carbón en los países desarrollados, su papel en el *mix* energético de las próximas décadas es fundamental todavía. El uso de carbón como combustible incrementará particularmente en las economías desarrolladas, como India, o China, donde este combustible es abundante y permite moderar la dependencia energética de potencias extranjeras. Paralelamente, la comunidad internacional coincide en la importancia de dirigir esfuerzos hacia políticas que se comprometan a reducir las emisiones de CO_2 a la atmósfera en el corto período hasta 2015. Se han realizado ya avances considerables con respecto a la eficiencia energética de las plantas de potencia, lo que conlleva la reducción de las toneladas de CO_2 producidas por KWh. Sin embargo, la disminución de emisiones globales ha de ser más drástica para amortiguar sus consecuencias. A este respecto, la captura y almacenamiento de CO_2 (CCS, Carbon Capture and Storage) presentan un potencial de reducción de emisiones de CO_2 de fuentes estacionarias de un 25%, en cuanto se encuentren en un desarrollo comercial.

Las tecnologías CCS se agrupan generalmente en tres grandes grupos: las de post-combustión (final de tubería), pre-combustión (tratamiento del combustible previo a la combustión) y oxicombustión (combustión con oxígeno sin presencia de nitrógeno del aire). La oxicombustión de combustibles sólidos, como la combustión convencional, puede ser implementada en calderas de combustible pulverizado o en calderas de lecho fluido (CFB, *Circulating Fluidized Beds*). Esta última tecnología exhibe unas características de operación especialmente adecuadas para la aplicación de la oxicombustión. En primer lugar, la versatilidad de combustibles que pueden ser utilizados, desde biomasa a diferentes rangos de carbones, o incluso, residuos, tiene un enorme potencial para ser aplicado en el mix energético de una manera muy flexible. La temperatura moderada y uniforme en el lecho, evita por un lado la formación de NO_x térmico. Por otro, con la adición de sorbentes cálcicos, esta temperatura optimiza las reacciones de sulfatación y se minimizan las emisiones de SO_2. Si además se implementa la tecnología de captura de CO_2 en oxicombustión, el resultado se aproximaría por fin al concepto de *combustión limpia de carbón*.

El interés de la oxicombustión en lecho fluido ha crecido mucho en la última década. Existen algunas plantas piloto en el mundo dedicadas a profundizar en aspectos fundamentales del proceso. La planta más grande de oxicombustión en lecho fluido se encuentra precisamente en Ponferrada, León, y funciona exitosamente desde 2011. Es una planta demostrativa de 30 MW térmicos, exclusivamente dedicada a investigación.

Las implicaciones de la oxicombustión en lechos fluidos a gran escala, particularmente con altos porcentajes de O_2 en la corriente oxidante, solo se pueden pronosticar por el momento, a través de modelos matemáticos. En el Capítulo 2 de esta tesis, se ha realizado un modelo unidimensional de un lecho fluido circulante en oxicombustión de gran tamaño. La primera parte de dicho capítulo se dedica a revisar los modelos existentes y validados para la combustión con aire. Las mismas estrategias se han aplicado al modelado de la oxicombustión, dividiendo el modelo en tres módulos interdependientes entre sí: la fluidodinámica, la combustión y sulfatación, y la transferencia de calor. La validación real de los modelos de oxicombustión a gran escala no es posible, ya que no existen plantas reales operando en estas condiciones. En la literatura existen dos grandes compañías que han publicado los resultados de sus modelos de oxicombustión en grandes lechos fluidos. Aunque no es posible encontrar los detalles de dichas simulaciones, sus resultados se han comparado con los del modelo desarrollado aquí, para comprobar si el grado en que los resultados del modelo son coherentes y fiables.

Los resultados del modelo de oxicombustión en un lecho fluido de gran tamaño se han analizado desde tres perspectivas diferentes. Por un lado, los futuros lechos fluidos en oxicombustión permitirán reducir el tamaño de caldera y, con él, los costes de capital. A medida que se incrementa la concentración de oxígeno en la corriente oxidante, el área transversal de la caldera habrá de disminuir, para obtener velocidades adecuadas de fluidización. Los resultados indican que, incrementando la concentración de oxígeno hasta un 60%, el tamaño de la caldera pude reducirse un 66%. En consecuencia, el área disponible para intercambiar calor en las paredes de la caldera, disminuirá también considerablemente. Para refrigerar la caldera de manera adecuada, los sólidos recirculados habrán de incrementarse desde 7.8 kg/m^{2}s, hasta 32.7 kg/m^{2}s. La posibilidad de manipular el caudal de sólidos arrastrados y recirculados, permite una gran flexibilidad para trabajar a diferentes potencias de combustible. Por ejemplo, para regular

adecuadamente la temperatura de una caldera con una geometría determinada, que aumente su potencia de 600 MW a 800 MW, los sólidos recirculados habrán de incrementar 14.3 kg/m^{2}s. De manera análoga, el incremento de concentración de oxígeno en la corriente oxidante, permite mayor alimentación del combustible, dado por la estequiometria. De esta manera, con 40% de oxígeno a la entrada, la temperatura en la caldera puede regularse con dos estrategias complementarias: o bien incrementando el caudal de sólidos recirculados, hasta 20.7 kg/m^{2}s y enfriarlos hasta 720ºC antes de introducirlos de nuevo al lecho; o bien, no modificar dicho caudal, pero disminuir la temperatura a la que los sólidos son recirculados, hasta 620ºC.

Todo este análisis apunta a un protagonismo particularmente relevante de un equipo de extracción de calor externo a la caldera, el denominado *External Heat Exchanger*, EHE. Estos intercambiadores de calor se usan en ocasiones en las grandes calderas de lecho fluido circulante de combustión convencional, pero en la oxicombustión, su uso será esencial e inevitable, para poder controlar las temperaturas en niveles adecuados.

Los EHEs son, en general, intercambiadores de calor de lecho fluido en régimen burbujeante. Constan de haces de tubos que los atraviesan transversal o longitudinalmente. Su uso en calderas de lecho fluido en oxicombustión va a entrañar dos particularidades que aún no han sido abordadas por ninguna investigación: la diferente composición del gas de fluidización con respecto a su funcionamiento con aire y la mayor cantidad de sólidos que habrán de ser enfriados para conseguir las temperaturas de lecho adecuadas.

Por un lado, la composición del gas con el que será fluidizado el EHE, será diferente. Convencionalmente se ha tratado de aire. En muchos casos, parte del oxígeno del aire, permite la combustión de partículas inquemadas que llegan al EHE desde el ciclón. En el caso de la oxicombustión, el aire no puede ser introducido en el sistema, ya que el objetivo último es obtener una corriente concentrada de CO_2, y la presencia de N_2 contaminaría los gases de salida. El gas con el que se fluidice el EHE será una extracción de los propios gases de escape, que estarán compuestos de altas concentraciones de CO_2. La transferencia de calor en lechos fluidos burbujeantes se ha estudiado extensamente a lo largo de las décadas. El mecanismo fundamental de transferencia de calor en este régimen es el debido a la conducción transitoria de las partículas cuando contactan con la pared

de intercambio (convección de partículas). Además, el mecanismo de radiación de las partículas, y la convección del gas, tanto de la fase burbuja como de la intersticial entre las partículas, empiezan a dominar para mayores velocidades de fluidización y menores densidades del lecho. Sin embargo, la influencia en la transferencia de calor global del cambo de atmósfera que ocurre durante la oxicombustión, no se ha cuantificado todavía. El Capítulo 3 aborda este asunto experimentalmente. En el lecho fluido burbujeante de CIRCE se han llevado a cabo campañas de pruebas en combustión con aire, en oxicombustión con mezclas de O_2/CO_2 y en oxicombustión con recirculación de gases de escape. Gracias a las camisas que se usan para la refrigeración y, a partir de los correspondientes balances de energía, se han medido los coeficientes de transferencia de calor en un amplio rango de concentraciones de O_2 y de temperaturas. El análisis de los resultados se llevó a cabo desde dos enfoques diferentes. El enfoque puramente empírico trata la transferencia de calor de manera análoga a la convección forzada gaseosa, por medio de correlaciones experimentales. El enfoque mecanístico semi-empírico, que plantea la conducción transitoria de los paquetes de partículas, y utiliza relaciones empíricas para los términos que no pueden ser medidos experimentalmente: el tiempo de residencia de las partículas en la superficie, y la conductividad térmica efectiva del empaquetamiento que contacta la superficie de intercambio. Entre las correlaciones empíricas, la que mejor aproxima los valores obtenidos en oxicombustión, es la propuesta por Molerus y colaboradores (1995). El enfoque mecanístico, sin embargo, es el que mejor ajusta los datos obtenidos en este estudio. Se recomiendan la correlación de Xavier y Davidson (1985) para modelar mejor la conductividad térmica efectiva de los empaquetamientos en atmósferas de oxicombustión y la expresión desarrollada por Zarghami et al. (2007) para calcular el tiempo de residencia de los empaquetamientos. La expresión resultante, incluye además el término asociado a la resistencia térmica adicional de la pared gaseosa, durante los instantes en que los empaquetamientos intercambian el calor por condicción transitoria. Este término diferencia la transferencia de calor en oxicombustión y en combustión con aire. El ajuste del parámetro empírico involucrado en esta expresión, permite establecer dos valores óptimos diferentes para los dos modos de operación. La expresión resultante para la transferencia de calor durante la oxicombustión en lecho fluido burbujeante, permite una estimación de los valores experimentales con una desviación media de 8.6%.

La otra particularidad a la que se enfrentará la operación de los EHE en calderas de oxicombustión, residirá en la elevada cantidad de sólidos que habrán de recorrer este equipo y enfriarse hasta temperaturas adecuadas, para cumplir los requerimientos del balance de energía en la caldera. Existe escasa información en la literatura sobre las consecuencias de la distribución no uniforme de los coeficientes de transferencia de calor entre los tubos de un EHE. Aún así, todos coinciden en que el caudal de sólidos afecta dicha distribución, apareciendo zonas de transferencia de calor más intensa, y otras con fluidización más pobre, que no permiten tanto intercambio de calor con los tubos. En el Capítulo 4 se aborda esta cuestión desde la experimentación en un modelo frío de EHE y el modelado detallado de un EHE, para integrarlo en el modelo global de CFB desarrollado al comienzo.

El modelo frío de EHE estaba originariamente conectado a un CFB bidimensional. Para poder alimentar manualmente caudales de sólidos en un rango amplio, el EHE se ha desacoplado del CFB para ser operado independientemente. De esta manera, se han podido manipular las dos variables: la velocidad de fluidización y la cantidad de sólidos que atravesaban el EHE. Los resultados de los experimentos mostraron que los coeficientes de calor locales se incrementaron en general, con respecto a aquellos obtenidos cuando no había sólidos alimentados. Sin embargo, mayores caudales de sólidos promueven también más desigualdades de los coeficientes locales entre unas zonas y otras.

Para poder extrapolar los resultados de los coeficientes locales, el coeficiente medio de transferencia de calor se ha evaluado con respecto al tiempo que las partículas alimentadas necesitan para atravesar el equipo hasta la tubería de recirculación. De esta manera, se ha obtenido un factor de corrección que, aplicado al coeficiente de transferencia de calor sin aporte de sólidos, cuantifica el aumento de éste debido la circulación de sólidos.

A partir de estos resultados, y los obtenidos en el Capítulo 3, se pueden obtener unos coeficientes de transferencia de calor que tengan en cuenta los parámetros particulares de las calderas de oxicombustión. Así, se ha desarrollado un modelo de EHE, en base a los detalles geométricos publicados por Man et al. (2012) de un EHE real. Integrando este módulo con el modelo anterior, se han obtenido las áreas de intercambio de calor que serían necesarias para las diferentes concentraciones de O_2 planteadas al comienzo de la tesis. A pesar de que el incremento de superficie

de intercambio era evidente, dada la cantidad de calor que habría de evacuar el EHE, este aumento queda moderado por el incremento de coeficiente de transferencia de calor dado por el mayor caudal de sólidos calientes que atraviesan el equipo.

Con esta tesis se ha demostrado que las superficies de transferencia de calor en los lechos fluidos de oxicombustión habrán de adaptarse a las nuevas características de operación. La relevancia del EHE será particular de los grandes CFB. La predicción de los coeficientes de transferencia de calor en este equipo diferirá de los modelos utilizados en la combustión convencional. En consecuencia, para optimizar el rendimiento de las futuras calderas de oxicombustión en CFB, el diseño de la configuración del EHE tendrá que tener en cuenta los aspectos tratados en esta tesis.

CONCLUSIONES

Las grandes calderas de lecho fluido en oxicombustión van a requerir mayor caudal de sólidos recirculados, para poder moderar la temperatura de manera adecuada. Esto conllevará un diseño particularizado de los intercambiadores de calor externo (EHE). Las contribuciones de esta tesis se dirigen a demostrar teórica y experimentalmente los puntos más diferenciadores en los EHE de un lecho fluido en oxicombustión de uno en combustión convencional:

- El modelo unidimensional estacionario de lecho fluido circulante (CFB) a gran escala desarrollado en esta tesis permite cuantificar la evacuación de calor necesaria en los EHE para las diferentes condiciones de concentración de O_2 en la corriente oxidante y diferentes tamaños de caldera. La relevancia de este equipo apunta a dos diferencias fundamentales con los EHE asociados a la combustión convencional: la composición del gas de fluidización, y el aumento de sólidos recirculados
- El estudio teórico original de los modelos de transferencia de calor en lechos fluidos burbujeantes, tanto desde el punto de vista empírico como mecanístico, ayudan a predecir las posibles influencias de los cambios de

composición en las atmósferas de oxicombustión respecto a las de combustión con aire.

- Los coeficientes de transferencia de calor en el lecho fluido burbujeante de 90 kW se miden y presentan por primera vez en esta tesis durante la oxicombustión con mezclas de O_2/CO_2 y con O_2 diluido en gases de escape, para comparar los resultados con los medidos en combustión con aire.
- El tratamiento de los datos experimentales desde los números adimensionales y desde el enfoque mecanístico, permite proponer una expresión completa que predice los valores de coeficientes de calor obtenidos experimentalmente durante la oxicombustión en lecho fluido burbujeante
- La influencia de los sólidos recirculados en la transferencia de calor de un EHE se analiza experimentalmente en un modelo frío a escala, desacoplado del CFB original. Los resultados muestran un incremento de la transferencia de calor con el caudal de sólidos recirculados, a la vez que las los valores de los coeficientes de calor de unos tubos a otros también aumentan.
- Por primera vez se propone una expresión que modifique el coeficiente de transferencia de calor sin recirculación de sólidos, y que tenga en cuenta el tiempo que tardan las partículas en abandonar el EHE
- La simulación de une EHE, integrado en el modelo de CFB previamente desarrollado, incluirá el cálculo de los coeficientes de transferencia de calor tal y como se propone en esta tesis. Este modelo incluirá además el efecto de la re-carbonatación y sus posibles consecuencias en la de-fluidización del EHE.
- Finalmente se ha calculado el área de transferencia de calor requerida en el EHE para diferentes condiciones de concentración de oxígeno a la entrada del CFB. Gracias a las expresiones desarrolladas aquí, que tienen en cuenta de manera más realista las condiciones propias de la oxicombustión, las superficies de transferencia de calor resultantes aumentan a medida que se incrementa la evacuación de calor necesaria en el EHE, pero de manera más moderada de lo esperado.

NOMENCLATURE

A	area	m^2
A_0	gas-distributor area per nozzle	m^2
BFB	Bubbling Fluidized Bed	
C	molar concentration of a gas compound	kmol/ m^3
CFB	Circulating Fluidized Bed	
CCS	Carbon Capture and Storage	
c_p	specific heat capacity	J/kgK
d	diameter	m
D	bed diameter	m
D_g	diffusivity of oxygen in nitrogen	m^2/s
D_{sh}	horizontal dispression coefficient	m^2/s
D_{sv}	horizontal dispression coefficient	m^2/s
E	enthalpy	J/kgK
EHE	External Heat Exchanger	
f	fraction of time of a phase conctacitng a suface	
g	gravity constant	m/s^2
Gs	elutriated solids mass flux	kg/m^2s
H	bed height	m
h	heat transfer coefficient	W/m^2K
HT	Heat Transfer	
k	conductivity	W/mK

k_{bm}	backmixing parameter	
K_c	apparent kinetic constant for surface reaction	m/s
k_D	calcination kinetic constant	m/s
l	characteristic length scale	m
L	length	m
LHV	Low Heating Value	kJ/kg
LS	loop seal	
m	mass flow rate	kg/s
M	dimensionless parameter for the film thermal resistance estimation	
n	number of	
p	proportion of particle types	-
P	pressure	bar
Pp	partial pressure	bar
Q	heat	kW
r	radius	m/s
R	thermal resistance	m^2K/W
R_c	calcination rate	
RFG	Recycled Flue Gas	
s	path length	m
S^2	typical deviation	
T	temperature	ºC
$\overline{T}$	average temperature	ºC
t	time	s
t_{ce}	contact time of clusters in the emulsion	

t_δ	wall thickness	m
t_e	emulsion contact time	s
t_{pc}	contact time of particles attached to bubble	
t_R	time for recycled particles to cross the EHE	
u	fluidizing velocity	m/s
$\bar{u}$	average velocity	
U	uncertainty	
UA	Overall heat transfer coefficient times heat transfer area	W/m^2
V	measured water volumetric flow	m^3/h
V_{Cu}	volume of copper	m^3
V_W	volume of water	m^3
x_{cc}	carbon fraction in the core	
z	height above distributor	m

Greek Symbols

α	thermal diffusivity	m^2/s
δ	volume fraction	
ΔP	pressure drop	bar
ΔTl_n	mean temperature logarithmic	ºC
ε	void fraction	
ε_r	radiative emissivity	-
ε_f	fouling coefficient	m^2/W
φ_s	particle sphericity	
η	efficiency	
H	dimensionless heat transfer coefficient	

κ	absorption coefficient	1/m
v	coefficient of kinematic viscosity for flue gas	m^2/s
ξ	a ratio of solids that effectively exchanged heat in the EHE	
ρ	density	kg/m^3
σ	Bolzman constant	m^2kg/s^2K
τ	residence time	s
Θ	dimensionless time	
Ψ	dimensionless visible bubble flow	

Subscripts

ave	average
b	bubble
B	bed
bb	bottom bed
br	bubble rising
c	cluster
conv	convection
d	dense phase
disp,h	height of disperse phase
e	emulsion
eq	equivalent
eff	effective
f	fluidizing/fluidized
g	gas

gc	gaseous convection
HT	heat transfer
i	cell or tube numbering
in	instantantaneous
lat	lateral flow
m	number of measurements
mf	minimum fluidization
Pa	packet
p	particle
pc	particle convection
r	radiation
ref	riser height interval from 0.135 to 1.635 m above gas distributor
RS	recycled solids
s	solids
sat	saturation value
tf	throughflow
t	terminal
vis	visible flow
VOL	volatile matter
w	wall/wakes

Non-dimensional groups

Ar	Archimedes	$\frac{g d_p^3 \rho_g \left(\rho_p - \rho_g\right)}{\mu^2}$
Fo	Fourier Modulus	$\frac{Dt}{l^2}$

Nu	Nusselt	$\frac{hd_p}{k_g}$
Pr	Prandtl	$\frac{c_{p,p}\mu}{k_g}$
Re	Reynolds	$\frac{\rho_g u d_p}{\mu}$
Sh	Sherwood	$\frac{kl}{D}$

LIST OF FIGURES

LIST OF TABLES

CHAPTER 1

CONTEXT, JUSTIFICATION AND OBJECTIVES

1.1 THE GLOBAL SCENE

In 1992, the United Nations Framework Convention on Climate Change (UNFCCC) set an intergovernmental framework aimed to be a starting point to cope with the global climate change. The ultimate objective of the Convention was *"to stabilize greenhouse gas concentrations at a level that will prevent dangerous human interference with the climate system"* (UNFCC, 1992). With 194 Parties, the UNFCCC has near universal membership. Under the Convention, membership governments committed to: i) gather and share information on greenhouse gas emissions, national policies and best practices; ii) launch national strategies for addressing greenhouse gas emissions and adapting to expected impacts, including the provision of financial and technological support to developing countries; and iii) cooperate in preparing for adaptation to the impacts of climate change. This Convention represented the universal acceptation that human activities are the major cause of the increasing greenhouse gas emissions in the atmosphere and the agreement of reinforcing the countries to cope with climate change in cooperation with the international community. The Parties agreed to take precautionary measures to anticipate, prevent or minimize the causes of climate change and mitigate its adverse effects.

The International Panel of Climate Change (IPCC) has been making an outstanding task of preparing a comprehensive review and recommendations with respect to the state of knowledge of the science of climate change; social and economic impact of climate change, possible response strategies and elements for inclusion in a possible future international convention on climate (IPCC, 2010). In spite of the international community commitment, facts of greenhouse gas (GHG)

emissions to the atmosphere in the last two decades are not as comforting as they should. According to the Fourth Assessment report by IPCC (2007): *"… the atmospheric concentrations of long-lived GHGs CO_2 and CH_4 in 2005 exceed by far the natural range over the last 650,000 years. Global increases in CO_2 concentrations are due primarily to fossil fuel use, with land-use change providing another significant but smaller contribution…."*. IPCC concluded that reductions of at least 50% in global CO_2 emissions compared to 2000 levels will need to be achieved by 2050 to limit the long-term global average temperature rise to 2-2.4ºC (IEA, 2010a).

Energy production is the human activity that represents the major source of CO_2 emissions in the developed countries, because CO_2 is an intrinsic waste from the combustion of fossil fuels for power generation.

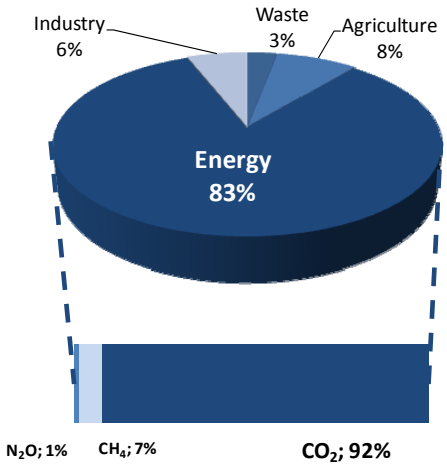

Figure 1.1. Shares of anthropogenic greenhouse-gas emissions in Annex I countries, 2009, adapted from IEA (2011a).

The economic growth, together with the increasing world population are narrowly related to the emissions of GHGs to the atmosphere, due to the dependence on the fossil fuel combustion as primary energy all over the world, in the so-called carbon-based economy. In spite of the smoother increment of the global GDP, the international indicators remain unaltered. The small variation of advanced economies does not alter the global tendency. The rate of growth of OCDE countries is estimated on 2% in the following 30 years, and the non-OCDE will grow more than 4.5% (ExxonMobil, 2012). Estimations of the world energy demand ranged from 30-40% in the following decades (BP, 2011a; ExxonMobil, 2012), while this growth will achieve 63% in a "usual as business" scenario (EIA, 2011).

Fossil fuels accounts for more than 60% of the electricity generation. Coal has been a key component of the electricity generation mix worldwide. It fuels more than 40% of the world's electricity, although this share is higher in some areas. In countries like South Africa, 93% of power comes from coal, in Poland, 92%, in China, 79%, in India, 69% and in the United States, 49% (IEA, 2010b). In Europe, the growth of coal demand is being progressively replaced by the gas, but still accounts for almost 40 % of the power generation share.

The reports coincide to recognize that energy efficiency continues to improve globally, and at an accelerating rate. The IEA World Energy Outlook (2011b) remarks the need to achieve an even higher pace of change, with efficiency improvements accounting for half of the additional reduction in emissions.

In 2009, 43% of CO_2 emissions from fuel combustion were produced from coal, 37% from oil and 20% from gas, Figure 1.2. Growth of these fuels in 2009 was quite different, reflecting varying trends that are expected to continue in the future. Global CO_2 emissions actually decreased by 0.5 Gt CO_2, between 2008 and 2009, representing a decline of 1.5%. However, trends varied greatly: the emissions of developed countries decreased, whereas the emissions of developing countries increased up to 54%.

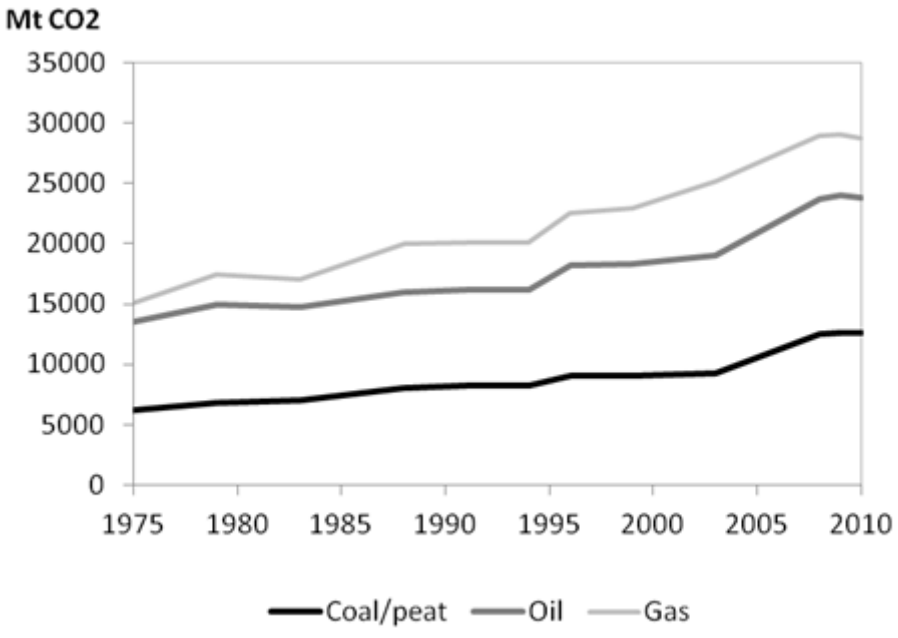

Figure 1.2. World CO_2 emissions by fuel. Adapted from IEA (2011a)

Urgent actions are needed for changing the directions of the CO_2 emissions trends, aiming for the long-term target of limiting the global average temperature increase to 2°C. Some scenarios are pessimistic about the effectiveness of policies to act quickly enough. And all of them coincide on pointing out the reduction of CO_2 emissions from fossil fuel sources as a priority for a real global reduction.

1.1.1 MAKING THE COAL SUSTAINABLE: THE CO_2 CAPTURE AND STORAGE CHAIN (CCS)

Electricity and heat generation accounts for more than 60% of the CO_2 emissions derived from coal combustion (Figure 1.3). This represents most of the stationary power plants. From a technological point of view, this should be a simplification when applying measures for emissions reduction from the source itself. This CO_2 reduction is based on increasing the power plants efficiency and on deploying CO_2 capture and storage technologies.

According to the IEA World Energy Outlook (2011b) widespread deployment of more efficient coal-fired power plants and carbon capture and storage (CCS) technology could promote the long-term prospects for coal. Therefore, it is necessary the development of clean fossil fuels power plants. The development of zero and near zero emissions power plant technologies is gaining importance worldwide and large demonstration projects are expected in the coming decade for new plants (IPCC, 2005). But if drastic reductions are requested in the medium term, it is also necessary to support and deploy technologies that could be able to capture part of CO_2 from existing power plants.

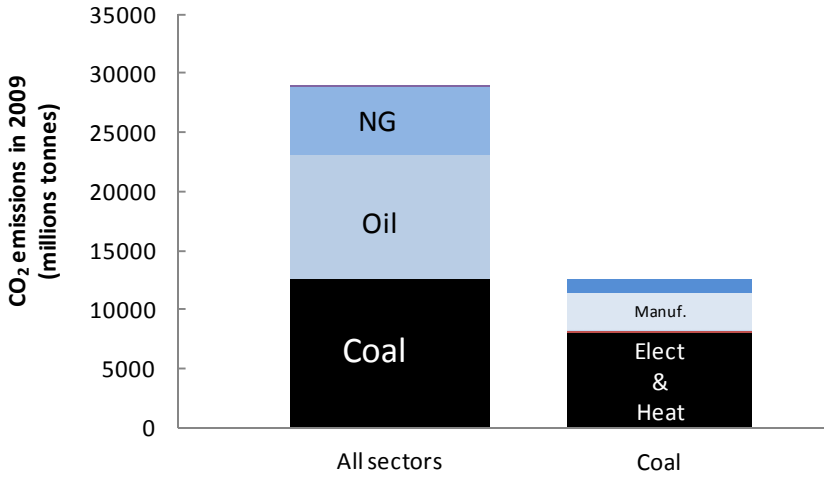

Figure 1.3. CO_2 emissions by fuel and sector. Data taken from IEA (2011a)

There are three main approaches to capture CO_2 from fossil-fired energy systems: pre-combustion, post-combustion, oxy-fuel. These technologies have application in large, stationary carbon emission point sources. However, capture is only one link in the CCS chain. A CCS system also requires CO_2 compression, a means to transport it and a storage site, as illustrated in Figure 1.4. This means a great complexity and effort required to successfully remove CO_2 from the atmosphere that goes beyond the carbon capture step.

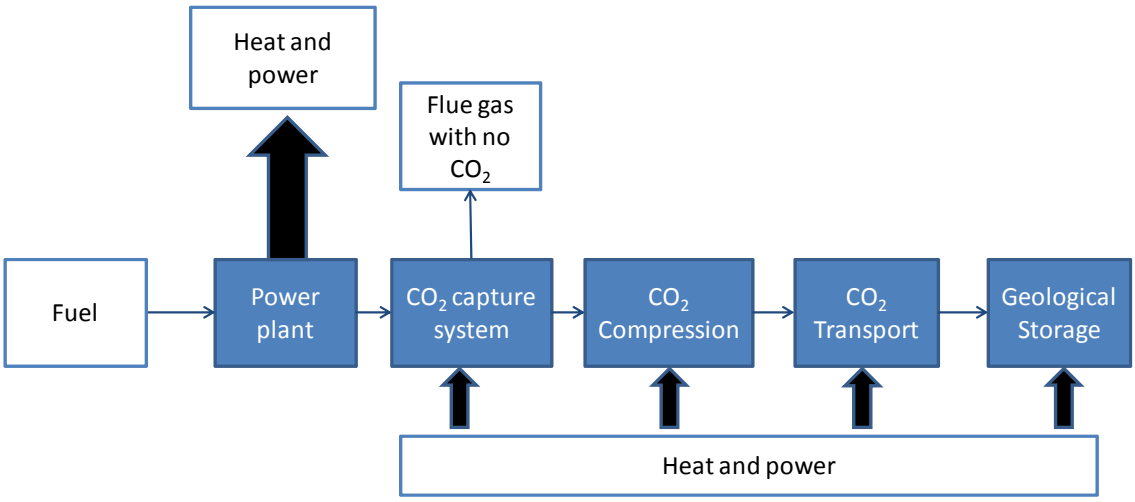

Figure 1.4. CCS chain scheme

Looking at Figure 1.4, it is clear that much of the barriers found by any CCS system to be economically feasible will relay on the way that energy requirements are minimized and integration of the overall power system with CCS chain components. Following, the technologies considered for capturing CO_2 from fossil fuel combustion in the near and medium term will be explained.

Pre-combustion capture

In pre-combustion capture, carbon dioxide is separated from a gaseous fuel mixture under reducing conditions prior to its combustion. The majority of commercially available pre-combustion CO_2 separation technologies rely on the use of liquid solvents for absorption of CO_2 from a gas stream (Kohl and Nielsen, 1997). CO_2 is usually separated by scrubbing with a physical solvent. A simplified diagram is depicted in Figure 1.5. It involves the conversion of a carbonaceous fuel, such as natural gas, coal, biomass or oil to a gaseous mixture that primarily consists of H_2 and CO, called *syngas*. The fuel conversion step during gasification or reforming is endothermic and requires supplementary heating, typically supplied by partial

oxidation of the fuel. In CO_2 capture applications, high-purity O_2 obtained from an Air Separation Unit (ASU) is often used as oxidant, yielding the high temperatures required to produce H_2 and CO-rich syngas.

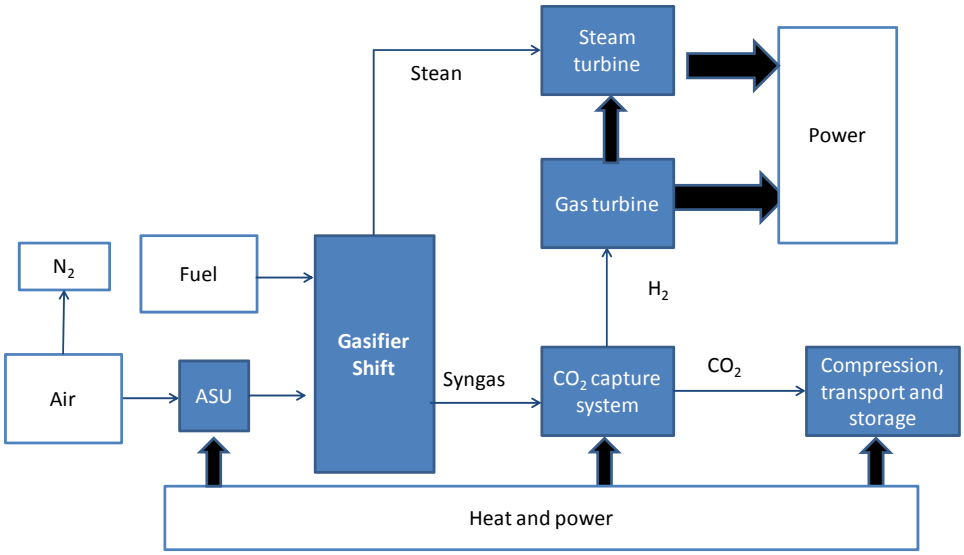

Figure 1.5. Pre-combustion capture scheme

The H_2 and CO in the syngas is converted to H_2O and CO_2 via the Water-Gas Shift (WGS) reaction. The WGS reaction is facilitated by commercially available catalysts, that are suitable for application under sweet and sour conditions, i.e. low and high sulphur (H_2S and COS) concentrations respectively. The CO_2 is then separated through physical absorption with a scrubbing solvent. The CO_2-rich solvent is later flashed by pressure reduction which releases the CO_2, while the regenerated CO_2-lean solvent is reused for CO_2 absorption. The recovered CO_2 is subsequently dried and compressed to facilitate its transport and storage, while the hydrogen-rich stream can be combusted in a combined cycle for generation of electricity or used for synthesis of chemicals.

This technology is very promising in terms of energy efficiency penalty, but it is the one in the earliest stage of development, and the capital cost is still elevated. A IGCC with capture would increase the construction costs 30% with respect to the case with no capture, whereas operation and maintenance costs would be 20% higher (Kyungtae et al., 2011). The first IGCC for CO_2 capture was run in the power plant in Puertollano, Spain. The pilot separates an annual equivalent of up to 36.5 ktonne CO_2 using the MDEA solvent, and 700 tonne H_2 employing a pressure swing adsorption unit (Romeo et al., 2010b).

Post-combustion capture

Post-combustion capture refers to the removal of CO_2 from flue gases downstream of fossil-fuelled emission sources. In broad terms, CO_2 can be captured using: a) liquid or solid absorption, b) solid adsorption, and c) membranes. The most mature post-combustion capture techniques involve liquid absorption using chemical solvents. Solid-based absorption and adsorption are in the early stages of development. Membrane technology is somewhat limited in application at the moment, but the research efforts in this area are significant.

Because post-combustion capture is often implemented in atmospheric air-fired combustion processes (i.e., low partial CO_2 pressure), CO_2 is captured by scrubbing the flue gases with a chemical solvent. Most solvent-based CO_2 absorption processes work in a similar fashion (Figure 1.6): the flue gas is cooled and channeled to an absorber where it flows counter-current of a chemical solvent. Most of the CO_2 leaves the absorber with the solvent, while the "clean" flue gas exits at the top. The CO_2-rich stream from the absorber is then sent to a stripper where CO_2 is recovered by the application of heat, regenerating the solvent. The regenerated solvent, also known as the CO_2-lean stream, is cooled and recycled to the absorber. The recovered CO_2 is then dehydrated and compressed for transport.

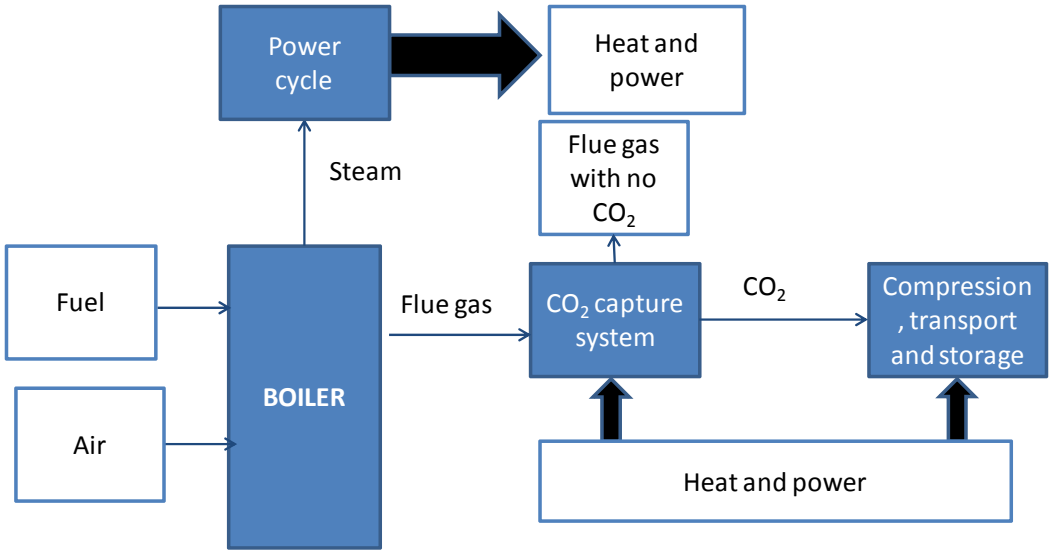

Figure 1.6. Post-combustion capture scheme

Key operational parameters that affect the techno-economics of solvent-based post-combustion CO_2 capture include: flue gas and solvent flow rates, desired CO_2 removal, and energy requirements. The flue gas flow rate determines the absorber

size and thus, largely sets the capital costs. The desired CO_2 removal affects costs and energy demands. Higher CO_2 recoveries require taller absorbers and incur higher ancillary energy demands, which are a function of the thermal energy for solvent regeneration and the electricity for pumps and compressors. The former is set by the activation energy and reaction kinetics of solvents while the latter is related to flue gas and solvent flow rates.

Although there are many solvents which can absorb CO_2, only a handful of them have been tested for CO_2 capture in post-combustion applications. Aqueous amines and blends of amines are currently the most suitable solvents, but novel solvents are under development. Efforts are lately focused on the energy integration of the capture system into the power plant, in order to reduce the energy penalty associated with the recovery of the solvent (Romeo et al., 2008).

Oxy-fuel combustion

The basic approach of oxy-fuel (OF) combustion is to carry out the combustion using pure oxygen as oxidant, instead of air. Thereby, the resulted flue gas stream consists mainly of carbon dioxide and water vapour. The steam is easy to remove by condensation and so, carbon dioxide is already concentrated for the required conditioning. Since high temperatures can be reached in the boiler, part of the flue gas is recycled back into the boiler with the so-called recycled flue gas stream (RFG). Therefore, it is possible to reach similar conditions of temperature and volumetric gas fluxes as in air combustion.

Since the oxidant stream contains higher O_2 concentration and the diluting CO_2 is denser that the air-N_2, the volume of produced flue gas decreases. This means a reduction in flue gas treatment equipments size and heat losses. This reduction would be a drawback, if the purpose were the use of sensible heat in the flue gases, like, in a convective heat exchanger. In Figure 1.7 the blocks diagram of an oxy-fuel combustion approach is represented.

One of the main advantages that make oxy-fuel combustion a suitable technology for CO_2 capture in power plants is the use of a conventional steam boiler technology. This is especially attractive when considering retrofit of existing power plants. However, there are also benefits in applying oxy-firing to new high efficient power plants, since their increased efficiency reduces the oxygen demand per unit of generated electricity.

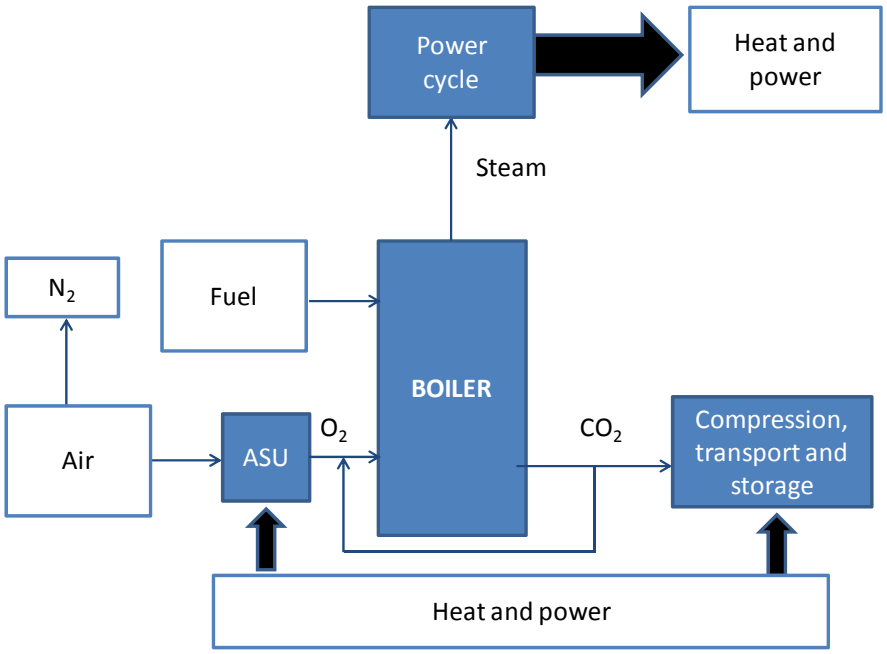

Figure 1.7. Oxy-fuel combustion capture scheme

When operating in oxy-fuel conditions, gaseous species are different. These will consist mainly of O_2, CO_2, and water vapour. Density and thermal capacity of gases and proportion of these compounds differ from conventional air combustion. This will mean substantial changes in the heat transfer, flame temperature and stability, combustion efficiency and pollutant emissions. These issues, together with the high energy requirements of ASU plant, are the main current research topics in oxy-fuel combustion.

1.1.2 STATE OF THE ART OF OXY-FUEL COMBUSTION

Status

Oxy-fuel (OF) combustion with the purpose of capturing CO_2 was first proposed in 1981 and earliest studies were carried out at Argonne National Laboratory (Kiga et al., 1997; Santos and Haines, 2007). The main reason was its potential for enhanced oil recovery. However, the oil crisis diminished the interest for CO_2 capture. In the late 1990s, attention grew again towards oxy-fuel technology, due to the imminent necessity of looking for solutions that decrease greenhouse gas emissions. Differences with the well-known air-combustion (AF) include the heat transfer mechanism variations, the combustion and ignition processes, the pollutant formation and the oxygen production technology.

Heat transfer

Radiation heat transfer is the dominant heat transfer mechanism in the furnace of a conventional pulverized coal boiler. Participative gases, as CO_2 and H_2O, are responsible for most of the radiation exchange, emitting, absorbing and scattering of the energy beams. In studies on retrofit applications, heat transfer show an increase in the furnace heat transfer but a decrease in the convective pass (Buhre et al., 2005; Sarofim, 2007; Smart et al., 2009). Convection heat transfer zones, located normally in cooler parts of the boiler are affected. An increase in the radiant heat exchange area requires lower temperature difference when passing through the convective pass. Furthermore, a lower volumetric flue gas flux implies a lower gas velocity, which also leads to lower convective transfer rates. Payne and co-workers (Buhre et al., 2005) studied the optimum recirculation rate in order to reach a heat transfer profile similar to the air-fired combustion system. They calculated that, with a factor of around 3, this requirement is matched and that, in the case of fluidized beds, this rate could be smaller, due to better control peak temperatures by the solids circulation.

In the case of oxy-fuel combustion in fluidized bed boilers attention must be paid when defining and locating heat transfer surfaces. Since there is less volumetric gas flows per unit of fuel, boiler size is reduced, but this reduction is limited by the required fluidization velocity inside the boiler. However, heat transfer surface must evacuate the same energy than in the air case. This leads to changes in the water walls design and optimization (Jäntti et al., 2007)

Combustion and ignition

The higher the O_2 concentration, the higher inflammability limit and the lower ignition temperature (Sarofim, 2007). Moreover, flame propagation velocity in O_2/CO_2 atmosphere is lower than O_2/N_2, for the same O_2 concentration. In general, CO_2 properties provoke flame instability in the case of using conventional burner designs. However, this effect could be compensated with oxidant enrichment.

For natural gas and coal combustion, optimum O_2 concentration was found to be between 30% and 35% dry basis, balancing with RFG CO_2. However, this optimum varies depending on the moisture in the fuel, in the RFG and in the ash. Additionally, O_2 partial pressure is higher in oxy-fuel combustion, which allows reducing O_2 excess in the flue gas, while still having a complete burnout.

Regarding oxy-fuel combustion in fluidized bed, the influence of particle size and lower temperature was recently explored by Guedea et al. (2013). They found different conversion patterns under O_2/N_2 and O_2/CO_2 atmospheres, finding lower reactivity of char in O_2/CO_2 mixture, due to lower diffusivity of O_2 in CO_2.

Emissions control

Pollutant emissions in the case of oxy-fuel combustion highly depend on the temperature, coal composition and O_2/RFG composition. Depending on which section of the flue gas treatment RFG is taken from, water vapour, SO_2, NO_x and other species could be present and these will be fed back to the boiler.

CO_2 concentration in the flue gas has reached up to 92% in some pilot scale experiments. Higher purities were difficult to reach due to air in-leakage into the boiler (Santos, 2009).

NO_x, so as SO_2 emissions tend to reduce during oxy-firing, although the mechanisms of this trend are not yet fully understood. In air-firing case, NO_x could be generated from the nitrogen found in the coal or in the air. Nitrogen from fuel is the main cause of NO_x formation, through a complex chain of reactions. In the case of NO_x from RFG reburning can take place and gets dissociated to form nitrogen.

CANMET research group (Croiset and Thambimuthu, 2001) observed a reduction of SO_2 formation from coal sulphur, compared with air-firing case. SO_2 removal has shown to be enhanced up to 30%, explained by higher kinetics of sulfation of ash, the inhibition of $CaSO_4$ decomposition in the high SO_2 concentrations and a more porous structure due to high CO_2 content in the gas.

SO_2 capture in oxy-fuel fluidized bed boilers is generally lower at bed temperature typical for air-firing, due to changes in the sulfation mechanisms and thus, the sorbent particle porous structure (de Diego et al., 2011). NO_x emissions is, in general, lower in oxy-fuel fluidized bed boilers, although numerous factors affect its formation-destruction mechanism, and this issue needs further research (Lupiáñez et al., 2012).

Oxygen production

Up-scaling oxy-fuel combustion development towards industrial plant sizes depends mainly on the feasibility of obtaining large quantities of oxygen economically. Nowadays, there are several technologies for oxygen separation from

nitrogen, but only cryogenic is considered feasible for large scale applications. The largest industrial ASU reported produces 4000t/d, and design studies have been performed for 7000 t/d, for a single train (Anheden et al., 2005).

Pilot and demo plants

The deployment of oxy-fuel technology involves the whole R&D chain, from basic research to the technology development. Therefore, the role of the pilot plants and experimental facilities is rather essential for the acceleration of the implementation of the CO_2 capture technologies.

Five independent main pilot plant studies, carried out by EERC-ANL, IFRF, IHI, CANMET and B&W-Air Liquid, with furnace sizes ranging from 0.3 to 3 MW, during late 1980s to 2000s, demonstrated the feasibility of oxy-fuel combustion and concluded that no technical limitations exist (Santos and Haines, 2005). However, they recommended further studies for heat transfer issues, especially because of the differences in temperature distribution along the furnace and the radiation characteristics.

Two main technologies for coal combustion are applied for large scale power generation: Pulverized Coal (PC) and Fluidized Bed (FB) boilers. Currently several industrial scale steam generation plants are projected and some of them are already in the commissioning phase. In Table 1.1, main pilot and projected demonstration plants for oxy-firing combustors are gathered.

Project/ Institution	Country	Size (MW_{th})	Status /Schedule	Boiler Type	Fuel	CO_2 capture dtails
Babcock & Wilcox	USA	30	Demonstration tests during 2007-2008	Pilot PC	Bit. SubBit, Lig	No Capture
Jupiter	USA	15	Start-up 2011	PC retrofit. No FGR	NG, , High sulphur coal	25% flue gases to be treated. No storage
Doosan Babcock	UK	40	Start-up 2009	Pilot PC		
Vattenfall	Germany	30	Start-up 2008	Pilot PC	Lig. Bit.	With CCS
Total, Lacq	France	30	Start-up 2009	Industrial. Steam for utilities	NG and Liq. Fuels	With CCS in gas depleted reservoir
Enel	Italy	48	Start-up planned 2012	Presurized PC		
Jupiter (Pearl Plant)	USA	66	Started-up 2009	22 MWe PC	Bit	Side stream
Callide	Australia	90	Air tests in March 2009 O_2/CO_2 plant contract: August 2009	30 MWe Retrofit PC	Bit	75 tpd to CCS. Road transport to a depleted gas field
Ciuden-PC	Spain	20	Start-up in 2010	Pilot PC	Antr. Pet cok	
Ciuden-CFB	Spain	30		Pilot CFB	Antr. Pet cok	
Babcock & Wilcox	USA	400		100 MWe PC CFB	SubBit	With CCS
Jamestown	USA	150	Announced for 2015	78 MWe gross /44 MWe with CCS	Bit, biomass	With CCS to Michigan Basin
Endesa	Spain	1500	Announced for 2015			With CCS
Vattenfall	Germany	1000	Announced for 2015	250 MWe PC	Lig. Bit.	With CCS
KEPCO (Young-dong)	Korea	400	Announced for 2016	100 MWe Repowering	SubBit, Bit	With CCS

Table 1.1. Pilot and demonstration plants of oxy-fuel combustion (Spero and Montagner, 2007; Total, 2007; McCauley et al., 2008; Barbucci, 2009; Burchhardt, 2009; Ochs et al., 2009a; Scheffknecht, 2009; Sturgeon, 2009; Wall et al., 2009; Alvarez et al., 2011; Spero et al., 2011; Schoenfield and Menendez, 2012)

Barriers and future prospects

Large Scale Oxygen production

One of the great drawbacks of oxy-fuel combustion comparing with other CO_2 capture technologies is the energy cost of oxygen production. Current technology, based on cryogenic air separation, for producing 95% purity O_2, requires around 200 kWh/tonO_2 (Sarofim, 2007). In a steam power plant this means energy losses of around 7%-10% of the LHV efficiency. Possibilities of achieving higher O_2 production efficiency with the current cryogenic ASU are limited. An added drawback of this technology is the residual N_2 that remains in the oxygen stream. It can reach up to 5% volume diminishing CO_2 stream purity. However, different concepts are also investigated: Ion Transport Membrane (ITM), developed by Air Products, is a promising technology. It operates at temperatures around 800-900ºC, at which the crystalline structure incorporates oxygen ion vacancies (White et al., 2009). Oxygen Transport Membrane (OTM), patented by Praxair, is also a new technology based on droped Zirconia, being able to consume 75% less power than cryogenic ASU (Wilsoon et al., 2009). Membranes show the advantage of avoiding presence of N_2 from air, and only bound N_2 would be present in the gas stream. Ceramics Autothermal Recovery (CAR) is under development by Linde and BOC (Santos, 2009).

CO_2 cleaning for disposal

Some research is needed to know the effect of recycling flue gas stream from the different points of the flue gas circuit: recirculation fans consumption, flue gas cleaning equipments sizing, or increase in accumulated pollutants in the boiler are some of the issues under study (Kather, 2007). Flue gas desulphurization tests were already carried out in Schwarze Pumpe, obtaining similar results as in air-firing cases (Yan et al., 2009)

On the other hand, uncertainties in the purity requirements for CO_2 geological disposal are still an issue, although some guidelines were determined from ENCAP project (Sarofim, 2007). In this respect, CO_2 stream from oxy-fuel combustion has more non-condensable species concentration than from other capture technologies (Seevam et al., 2008). Properties of gasses blends are not known around the critical point and changes in the phase diagram due to the presence of non-condensable gases in the CO_2 stream are difficult to determine. O_2 content in the flue gas

stream is around 3%. This represents a great drawback when the storage site is a depleted hydrocarbon site, because high probability of combustion reactions. In this case, O_2 should be removed before storage.

Moreover, undesired air ingress into the system is the major source of impurities in oxy-firing process. These leakages could be reduced by pressurizing gas feeding into the boiler. Especial care must be taken with NO_x, SO_2 and O_2 content, which represent around 0.25%, 2.5% and 3% vol. respectively. NO and SO_2, can react in the compressors in the presence of water and oxygen, forming H_2SO_4 and HNO_3.

New concepts are also proposed, for integrating captured CO_2 with compression phase (Romeo et al., 2009a). For diminishing compression costs, pressurized combustion systems would lead to a high pressure flue gas stream, for example, in the case of a pressurized fluidized bed. In the case of oxy-fuel, this would also help to avoid air leakages into the system, reaching a higher purity CO_2 stream.

Burners and boilers design

Adjustments in the burner designs need to accomplish several issues: higher oxygen feed concentration, different primary air for fuel conveying, different aerodynamics due to denser CO_2 gas around the burner and changes in flame staging because of NO_x feeding with RFG. With the help of computational fluid-dynamics modeling, new burner designs have been proposed by several researchers from academia and industry (Becher, 2008; Tchunko et al., 2008; Lee et al., 2009; Scheffknecht et al., 2009; Seltzer et al., 2009)

Regarding the boiler design, heat and energy balances are changing in the case of oxy-fuel combustion. As explained above, heat transfer is modified by the flue gases properties and flows. This leads to a re-sizing of the heat transfer exchange areas, reducing the radiant zone and increasing the area of the convective pass (Jordal et al., 2004; Jäntti et al., 2007; Ochs et al., 2009b). High ash fuels could also cause slugging and fouling problems in the radiant area (Scheffknecht, 2009).

Fluidized bed combustors are a highlighted option for implementing oxy-fuel combustion in the medium term time framework. In general, fluidized bed technology presents interesting characteristics when compared to pulverized fuel boilers, mainly related to the pollutant emissions control. This has allowed to improve the combustion performance of difficult, such as low-rank fuels, or fuels

that are difficult to pulverize. Additionally to these known advantages, fluidized bed present a remarkable feature that makes it suitable for burning under oxy-fuel conditions. Thanks to the high bulk density of inert particles and their movement, temperature is easier to control and uniform. For high O_2 concentration in fluidizing streams higher fuel is fed for the same boiler geometry. More compact boilers lead to less boiler wall surface to exchange heat. Along next section, fluidized bed combustion fluidized beds will be explored.

1.1.3 THE ROLE OF FLUIDIZED BED ON CCS

The particular characteristics of fluidized bed (FB) technology are caused by the fluid-like behavior of certain types of solids particles when a liquid or gas suspends them from below. Such a basic phenomenon provides an intense contact and interaction between the fluidization substance and particles and among the particles themselves. This allows FB to be susceptible to be applied to numerous industrial processes. Energy conversion in all its forms is one of the major applications for fluidized beds. Initially, fluidized beds were conceived by Fritz Winkler in 1912 for coke gasification. It was not until the 60's when Douglas Elliot recognized the possibility of burning coal in fluidized beds to generate steam (Basu, 2006).

The use of fluidized bed boilers has grown drastically in the last years. One of the main reasons is that environmental regulations have become stricter regarding pollutant emissions from combustion sources. Fluidized beds have the capability of capturing SO_2, thanks to the addition of calcium-based sorbents directly to the furnace. One of the main problems that fluidized bed combustion must cope with is the risk of inert matter agglomeration. This phenomenon is due to the melting of solids particles due to peaks of temperature. Melted particles become sticky and form agglomerates extremely quickly. This drives to a bed defluidization and consequent un-desirable operation turn off. For avoiding this problem, bed temperature must be always kept below ashes melting temperature. This is actually not a real handicap, having into account that optimum temperature for SO_2 capture under conventional air-firing is around 850ºC. Additionally, this temperature is sufficiently low for avoiding thermal mechanisms of NO_x formation, lowering the emissions of this compound as well.

For these reasons, fluidized bed is a very promising candidate to apply oxy-fuel combustion as a CCS technology. The support given by the European Commission to the deployment of oxy-fuel combustion to large circulating fluidized bed boilers, has been translated into two highly relevant projects within the Seventh Framework Program. First, the Flexi-Burn project, funded with 6.4 million Euros, started in 2009 and ended in 2012. Its aim was fully utilizing all the new CFB design and advancements for merging a CFB boiler with supercritical one through (OT) steam cycle and air separation unit, together with the CO_2 capture unit. The air/oxy flexible concept aim to have the capability of substituting 20% of the coal input with biomass fuels. The demonstration phase in this project took place, in parallel, in the CIUDEN 30 MW_{th} CFB plant, for the oxy-fuel tests, and in Lagisza plant, the 460 MW_e OT CFB boiler.

The second project, called O2GEN, within EU Seventh Framework Program was approved in the beginning of 2012, with a funding of 6 million euros. It will be coordinated by CIRCE. The focus is now to optimize and integrate the main components of the oxy-fuel CO_2 capture system, the ASU, the CFB boiler and the compression unit, aiming to reduce the overall energy penalty down to half of the current state of the art. The demonstration stage will be mainly developed in the 30 MW_{th} CFB unit in CIUDEN and the results will be deployed in the OXY-CFB-300 Compostilla Project (Table 1.1). The Compostilla Project was selected by the European Energy Program for Recovery (EPR) to receive funding of 180 milion Euros to develop the technology. It will be the first demonstration scale oxy-fuel power plant, based on supercritical CFB boiler, involving the whole CCS chain.

1.2 JUSTIFICATION

From a global point of view, the research community has an urgent task to develop instruments for avoiding CO_2 emissions to the atmosphere as soon as possible, as has been internationally recognized. The consequences of the climate change are imminent, and the necessity of mitigate CO_2 emissions from anthropogenic origin is an issue of absolute priority. One of the most relevant sources of CO_2 is the large fossil fuel combustor used in the energetic and the steel and concrete sectors.

It is clear that avoiding emissions from large stationary sources, such as said boilers and combustors, the essential contribution CO_2 capture and storage

technologies, has been recognized by the international authorities, as revealed by the Working group III report for the UNFCC on CO_2 mitigation (Sims et al., 2007). Still, it must be beard in mind, that CCS must be a transition technology towards the decarbonization of energy sources (IEA, 2011c).

The CCS chain technology acquires especial relevance for the appliance to de-localize, low-cost and carbon intensive fuels, such as coal. Indeed, coal is the fuel with the largest R/P ratio (reserves-to-production) and the world proved reserves in 2010 were sufficient to meet 118 years of global production. Moreover, in 2010 the world coal production grew around 6% over the historical average, and Asia Pacific region accounted for 89% of global growth. Solely China is planning to build 110 GWe of supercritical power plants by 2015 (BP, 2011b). Additionally given the successful commissioning of the first supercritical CFBC at Lagisza (Poland), both China and Russia are initiating programs for constructing supercritical CFBC units (Burnard and Bhattacharya, 2011).

It is then clear that fluidized bed technology is gaining importance because its unique features for burning broad range of local solid fuels. Particularly relevant is its capacity of avoiding SO_2 emissions by the addition of limestone based sorbents inside the boiler, contributing this way to the use of low-rank local lignite, indigenous of many regions around the world. The possibility of keeping temperatures, also below the point of NO_x thermal generation, drives fluidized bed combustion process to the concept of *clean coal technology* approach. It appears then as an outstanding opportunity for applying oxy-fuel combustion into this type of technology. This will be the first step towards developing a realistic concept of zero-emissions coal power plants.

From this perspective, oxy-fuel stands as one of the three feasible technologies to be implemented in the near term and, in fact, already at the demonstrations stage. Although the ratio of CFB combustors over the PC combustors for conventional air-firing was only around one fourth in North America and Europe was in 2007 (Koornneef et al., 2007), the oxy-fuel pilot and demonstration roadmap shows that both technologies are considered equally suitable. In fact, the two options are already working at a demonstration scale, 30 MW. Oxy-fuel PC was commissioned in 2008 in Schwarze Pumpe (Germany) and oxy-fuel CFB began operation in CIUDEN (Spain) in 2011 (Alvarez et al., 2011).

With this global picture in mind, research must be focused on overcoming the barriers to make oxy-fuel (OF) technology a reliable option for the new power plants generation. Expected differences with the well known air-firing (AF) technology have been early recognized. The main research groups that have carried out experiments on oxy-fuel pilots plants are summarized in Table 1.2.

As seen in Table 1.2, one of the main concerns of scientific community is coping with the pollutant emissions inherent in solid fuels combustion, particularly coal. This is the reason why most of the studies focus on looking deeper inside the SO_2 capture and NO_x destruction during OF mode. Many of the groups, in fact, had experiences on the research on these topics and retrofitted existing plants to adapt them to OF, like in CANMET, Utah or VTT.

From the table it is noteworthy that little attention has been paid to the behavior of the fluidizing bed itself. It has been widely recognized that the distinguishing particularities inherent to the fluidized bed technology are related to the movement of particles, strongly influencing heat transfer inside and thus, providing the outstanding characteristic of uniform and controlled temperature. Heat transfer during OF in FB has been only measured by ALSTOM (Nsakala et al., 2004), finding not remarkable differences between AF and OF heat transfer coefficients, although no numerical values were published. However, as stated by Eddings et al. (2009), the control of bed temperature when fixing exit O_2 will be critical when varying oxygen levels.

At great scale, some modeling results have been published, highlighting the role of a proper recycled solids rate and temperature for a proper control of bed heat balances (Nsakala et al., 2004; Saastamoinen et al., 2006; Seddighi et al., 2010). This temperature control will be an issue narrowly related with the SO_2 capture process. On the one hand, as stated by García Labiano et al. (2011) optimum temperature for SO_2 capture will differ from AF conditions, increasing for OF mode. Also, as indicated by Varonen (2011) or Nsakala et al. (2004), there are high probability of recarbonation of fly-ash, giving place to problems in the heat exchanger tubes, or meaning a risk of de-fluidization in the large CFB external heat exchanger. Additionally, temperature in fluidized beds must be strictly controlled under the limits of agglomeration and sintering risk.

Group	Experimental facility	Modeling	Issues	Refs
CANMET	CFB ID 100 mm H= 5 m	No	•Sulfure Capture •NO_x emissions	(Jia et al., 2007)
VTT	CFB ID167 mm H=8 m	Yes, dynamic simulation	•Sulfure Capture •NO_x emissions	(Pikkarainen, 2007)
Czestochowa University of Technology	CFB ID 250 mm H=5 m	Yes, at large scale (not validated)	•Fuel conversión (S,N,C)	(Czakiert et al., 2010; Krzywanski et al., 2010a)
ALSTOM	CFB ID lower = 0.66 m ID upper = 1 m H = 18 m	Yes, at large scale (not validated)	•Sulfure Capture •NO_x emissions •Combustion efficiency •**Heat transfer**	(Nsakala et al., 2004)
CSIC-ICB	BFB ID 100 mm H = 0.6 m	No	•Sulfure Capture	(de Diego et al., 2011)
University of Utah	CFB ID 250 mm H = 6.4 m	No	•Sulfure Capture •NO_x emissions	(Eddings et al., 2009)
METSO	CFB 1 x 1 m2 H = 13 m	Yes	•Sulfure Capture •NO_x emissions	(Seddigh et al., 2011; Varonen, 2011)
Wien Technical University	CFB ID 150 mm H =5 m	No	•Sulfure Capture •NO_x emissions •CO emissions	(Tondl et al., 2011)
CNR	BFB ID 40 mm H = 1 m	Yes	•Sulfure Capture •Attrition	(Scala et al., 2011)
CIRCE	BFB ID 207 mm H = 2.7 m	Yes	•Sulfure Capture •NO_x emissions •CO emissions •Combustion efficiency •Fluid-dynamics •**Heat transfer**	(Romeo et al., 2010a; Guedea et al., 2011; Lupiáñez et al., 2011)

Table 1.2.. Research groups with experimental experiences on oxy-fuel fluidized bed pilot plant

For this reasons the current research is going to stress the attention on the heat transfer during the oxy-fuel fluidized bed operation. Results will have to be extrapolated towards the implications that these results will have on the future

large oxy-fuel boilers. Second generation designs of oxy-fuel boilers working with higher concentration of O_2 in the comburent, will need to handle greater heat removal with less available surface for this exchange.

1.3 OBJECTIVES AND SCOPE

In spite of the existence of several experimental pilot plants worldwide, running oxy-fuel experiments, none of them have measured heat transfer during oxy-fuel combustion in the bubbling zone of a fluidized bed. The relevance of this issue, resides not only in the quantification of heat transfer during the combustion in an oxy-fuel boiler. Large oxy-fuel boilers will have to handle greater solids rates and the overall heat balance of plant will change. The external heat exchangers attached to the CFB boilers in the solids recycled loop will gain an essential relevance. These devices work, in most of the cases, in a bubbling regime, to assure a proper conveying of solids back to the boiler. Heat from recycled hot particles will be removed partly on this device. It is assumed that the external heat exchanger will be fluidized with recycled flue gas, consisting mostly on CO_2. The conditions in an external heat exchanger of an oxy-fuel boiler, will be similar to those existing on our bubbling oxy-fuel fluidized bed. Hence, the study of the heat transfer in the bubbling fluidized bed under oxy-firing conditions will be essential to correctly make proper design assumptions in future external heat exchanger devices.

This thesis aims to demonstrate which will be the key aspects that will modify the heat transfer surfaces design in the future commercial scale oxy-fuel CFB boilers. With this purpose, this thesis will be addressed to:

- establish how the heat balance of a large CFB will change in oxy-fuel combustion
- quantify the heat transfer during oxy-fuel combustion in a bubbling fluidized bed, under several operating conditions
- assess which will be the practical consequences of these changes within the plant configuration
- evaluate the influence of larger solids recirculation on the performance of the external heat exchanger fluidized beds

By means of a mathematical model of a large-scale oxy-fuel boiler, results will highlight the relevance that extra heat transfer surfaces to acquire a proper heat

balance of the plant when applying oxy-fuel combustion to the boiler. The external heat exchanger (EHE) will be then an essential device in future oxy-fuel CFB boilers. A new sub-model of generic EHE will be developed and integrated in the CFB loop previously developed. The appropriate estimation of the heat transfer coefficients in the EHE during fluidization with recycled flue gases lead to great uncertainties to quantify the heat transfer surface needed in the EHE for certain cooling requirements. Since the conventional frame of operation of EHE are inside the bubbling regime, measurements of heat transfer in the oxy-fuel bubbling fluidized bed pilot plant in CIRCE will give useful information. Additionally the contribution of recycled solids through the EHE on the heat transfer coefficient will be also quantified, by means of experiments on a EHE cold model. Experimental derived expression will be then included in the EHE sub-model, to reach the heat transfer surface area required under several oxy-fuel conditions.

This work is divided into three different sections:

First, a comprehensive one-dimensional model of a large-scale circulating fluidized bed has been developed. Oxy-fuel conditions have been run in the model. Results of the energy balance and the main difference of the operation conditions are explained in Chapter 2. The reader will find a review of the main modeling approaches and the explanation of the model itself, dividing the overall program in three main sub-models: fluid-dynamics sub-model, combustion sub-model and heat transfer sub-model. Validation of the model in air-firing conditions is made against literature results of large-CFB boilers. The energy balance validation under oxy-fuel conditions is also compared with three published reports by different authors. The results are shown, analyzing the consequences of changing O_2 content at inlet, the temperature of recycled solids and the effect of the boiler geometry on the overall plant balance. An essential role of the external heat exchanger device is drawn from this study. This will lead to the next section, when heat transfer in an oxy-fuel bubbling fluidized bed will be studied.

Chapter 3 explores the main previous findings on heat transfer in fluidized beds, and the expected influence of oxy-fuel conditions, according to the known approaches. Heat transfer coefficient is then measured during the oxy-firing operation in the bubbling fluidized bed pilot plant in CIRCE. The bubbling fluidized bed pilot plant is described, and the way of cooling the bed during operation is explained. Influences of oxy-fuel conditions on the coefficients are

analyzed and the main parameters affecting heat transfer are determined. Further discussion is driven under the perspective of fully empirical models, and the mechanistic semi-empirical approaches. A complete expression for the evaluation of heat transfer coefficients under oxy-fuel combustion is proposed, fitting the experimental heat transfer coefficients measured.

In the next section of this work, the experiments carried out on the cold model of a EHE are explored and discussed. On the one hand, the non-uniformity of local heat transfer coefficient across the EHE is measured. On the other hand, the average heat transfer coefficient will allow quantifying the contribution of the solids recirculation to the heat transfer coefficient when no solids are recycled. The expression derived from the experiments can be then included in an EHE sub-model, to be integrated in the overall CFB loop. From a design point of view, the great differences of heat transfer surface needed for different operational conditions will be analyzed.

This thesis intends to be an important support for the second generation oxy-fuel boilers designs. It aims to cover the main implications of the heat transfer on the plant balance and so, being a breakthrough to reach the optimum boiler efficiency when working under oxy-fuel conditions.

CHAPTER 2

LARGE OXY-FUEL CIRCULATING FLUIDIZED BED BOILER MODELING

2.1 INTRODUCTION

Combustion in fluidized bed has outstanding characteristics that make it advantageous in some aspects compared to the conventional pulverized combustion boilers. However, due to the presence of a large amount of particles and the effect of interactions among them, numerous phenomena take place at the same time. Thus, in spite of being an acknowledged mature technology, its complexity makes research efforts be kept addressed towards a better understanding of the processes taking place inside the boiler for more accurate and less tedious prediction of the system behavior.

Processes modeling in general and fluidized bed modeling in particular, can level, at least, at one of the following objectives:

I. to interpret data obtained from experimental plants, like in Redermann et al. (2009) or
II. to scale-up processes that are already running at lab-scale (Breitholtz. and B., 2000);
III. to optimize existing systems, like the one developed by Heikkinen et al. (2009) and
IV. to predict changes in conventional process or operational conditions, as made by Krywanski et al. (2010a).

This last is the purpose of the present work. The main concern here will be assessing the effects of oxy-fuel combustion in fluidized beds at large scale. With this aim, a model is developed, based on the knowledge of conventional air-CFB combustors. A review of the main modeling strategies for large circulating fluidized

boilers will provide us the criteria to select the appropriate modeling approach to reach adequate results. A one-dimensional steady-state semi-empirical modeling has been applied then to the current programming. The model predictions will be first compared with air-firing public data from large plants. Since no oxy-fuel large scale plants are commercially available yet, results of the current model will be analogized with three models published. The analysis by means of the current model will be assesed from two different approaches: i) modification of boiler geometry, imposing certain operational requirements, from the design point of view; ii) variation of O_2 concentration and fuel input, for the operational perspective, keeping unchanged the boiler geometry.

The model will highlight the relevance of allocating extra heat transfer surface out of the conventional water walls, wing walls or convective pass, to properly control the bed temperature.

2.1.1 LARGE CFB MODELING

Mathematical modeling is an essential tool for predicting operational behavior of existing plants or analyzing effects on the process when conventional input parameters are changed. With this purpose, researchers and boiler companies have been trying to develop different ways of representing CFB performance. Different approaches can be found depending on the aim of the model itself, Figure 2.1. Modeling of the system response, when facing changes in the input parameters, is the focus of the dynamic approach. These models predict the system behavior with time when fuel load changes (Park and Basu, 1997; Chen and Xiaolong, 2006), or fresh particles are entering the system (Hartge et al., 2007). Changes on the comburent composition, like in the transition to oxy-fuel combustion, is being lately investigated by the group in VTT (Pikkarainen, 2007).

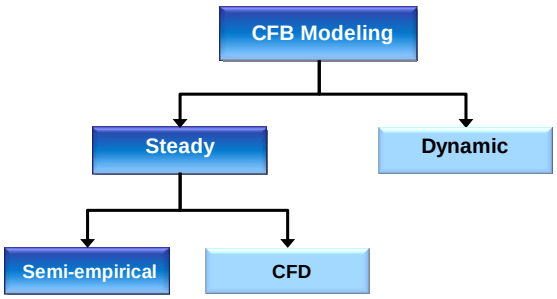

Figure 2.1. Types of CFB modeling, highlighted the one followed in the current work

Major number of models is focused on simulations assuming stable conditions with time. When considering steady-state simulations, two different types of models can be used: models based on a semi-empirical approach or models based on Computational Fluid-Dynamics (CFD). This last approach has been receiving increasing attention lately, but it must be considered under research, assuring a mesh, independent sub-grid model (Wang et al., 2010). One of the latest works on 3D CFD modeling of a large-scale CFB was performed by Zhang et al. (2010). They aimed to reach a virtual simulator of large-scale boilers. They reached a quite good fit of experimental data with modeling results, but still, complex phenomena such as mass and heat transfer processes were not included in the model. In Lappeenranta University the group of Timo Hyppänen is leading the CFD modeling of the Foster Wheeler 330 MWe Flexi-Burn boilers at large scale (Myöhänen et al., 2012).

Many researchers, however, bet for compromising accuracy at hydrodynamics prediction, by using empirical or semi-empirical expressions, with the aim of including fuel conversion and heat transfer phenomena into the model. Most of these models adopt a lumped model approach by dividing the boiler in dense and freeboard zones and, sometimes, sparse zone, dilute zone and exit zone are considered inside the freeboard as well. These parts are treated differently, depending on the processes taking place, but relations among them must always be included.

One of the extended one-dimensional CFB large scale models intended to become the basis for a common computer code was the one used by the IEA mathematical modeling group (Hannaes et al., 1995). The aim was to simulate the operation of a CFB defined by overall geometry, coal and limestone feed rates and composition, air feed and air staging ratios. One-dimensional hydrodynamics were on the vertical direction, and horizontal exchange was distinguished in the transition zone between core and annulus. A two-phase dense zone assumed bubble and emulsion phases. Additionally, different particles types were considered, differenced by size and density, taking into account primary fragmentation and attrition. Regarding combustion considerations volatiles were formed by CO, O_2, SO_2, H_2 NH_3 and char formed CO, CO_2 and NO. Volatiles were released instantaneously in the feed port. The heat transfer mechanisms, gas convection, radiation and particle convection, were estimated following the expressions:

$$Nu_g = 0.0175\, Pr^{1/3} Ar^{1/2} \left(\frac{u}{\bar{u}} \right)^{0.3} \qquad \text{Eq. 2.1}$$

$$h_r = 4\varepsilon\varepsilon\sigma^{3} \qquad \text{Eq. 2.2}$$

$$\frac{1}{Nu_p} = \frac{1}{Nu_{p,max}} + \frac{k_g / k_s}{4\left(1 - \frac{1}{\sqrt{\pi Fo}}\right)} \qquad \text{Eq. 2.3}$$

They compared their simulation results with tests run in a 120 MW power plant. The authors considered qualitative correct tendencies between experiments and model.

The same model was applied by Lee and Kim (1999) for simulating the 200 MWe Tonghae thermal power plant CFB boiler, designed to fire an indigenous Korean anthracite. They contrast their simulation results with the design values at different loads. These authors also analyzed the effect of different splitting ratios of primary air (PA) over total fed air (PA + SA). According to this model the temperature difference between the dense bed and the freeboard region decreases with increasing the split ratio (PA/PA+SA). The solid fraction in the dense phase increased from 0.163 to 0.74, but decreased in the lean phase.

Other authors such as Yang and co-workers (2005), included in the IEA-CFB the influence of particle residence time and segregation in the dense bed. They did not take into account combustion or heat transfer issues, but they could validate results of pressure drop profiles and solids distributions and sizing with data measured in the 135 MWe Zibo power plant.

Some models pay special attention to the evolution of particle diameter of the different groups of particles coexisting in the whole CFB loop, characterized by radius and density, for predicting optimum combustion performance as a function of particle sizing mass balances. An example applied to a large scale modeling is the model by Wang et al. (1999). They included a mass balance equation applied to every type of particle involved in the fluid-dynamics of the CFB. The model was applied to the simulation of the Chalmers 12 MW CFB boiler. Temperature profiles along the furnace and along the whole loop were fairly good fitted by simulations. Other comparisons regarding solids balances, such as the size particle distribution or average particle diameter profile, also showed good agreement, except for the

residual carbon content in particles that were underestimated by the model for coarse particles. However, this deviation was considered neglected because of the small portion of these type of particles in the dilute zone. Predictions of gaseous species were presented and well fitted by the simulation.

More recently a similar approach with a particle population model was developed by Redermann and co-workers (2009) and applied to the 105 MW Stadtwerke Neumünster combustion plant (Germany), which operates with refuse-derived fuel. The model aimed to calculate the solids mass flows as well as the corresponding particle size distributions at any point inside the combustion system. The hydrodynamics considered were quite simplified, but they included detailed attrition expressions, with fitted attrition constants from experiments in the same plant. They also added the cyclone sub-model and external heat exchanger (EHE) as a stirred tank reactor. They could compare measurements of pressure drop and solids volume concentration profiles with data measured in the power plant.

Measurements in large scale units are complicated and most of the times it is not possible to obtain data from the points that would be necessary for proper model validations. Because of this, Werther et al. (2009) proposed the so-called *simulation-assisted measurement*, consisting in introducing the measured values as inputs into the model for deducing information about the process at another location inside the combustion chamber. With this purpose they developed a 3D semi-empirical model. The horizontal velocity profile at every height was calculated as a potential flow field. In the dense zone, vertical and horizontal solids dispersion was considered but gas flowed in plug flow. In the upper part, splash, dilute and exit zones involved horizontal and vertical gas and solids dispersion. In the combustion sub-model, drying and devolatilization of fuel particles, primary fragmentation was assumed before volatile and char combustion. The aim was to determine secondary air penetration into the combustion chamber and its effect on the local combustion processes. The model was successfully developed for the 252 MWth CFB boiler of Stadtwerke Duisburg AG in Duisburg, Germany.

Most of the data published along the years from a semi-industrial scale CFB combustor were obtained in the 12 MW CFB boiler installed in the Chalmers University of Technology, in Sweden. In spite of being a commercial size boiler, available for its use during the winter, this facility was equipped with a comprehensive set of instrumentation taps for acquiring detailed and realistic

results on the plant performance during the operation. Long runs were possible, due to the commercial used availability, so realistic results were obtained continuously. Regarding fluid-dynamics, developments were gathered in the review paper by Pallarès and Johnsson (2006). Detailed heat transfer findings were also reported by Andersson (Andersson, 1988; Andersson, 1996).

2.1.2 OXY-FUEL CFB MODELING EXPERIENCES

The interest of applying oxy-fuel combustion into fluidized bed technology, has been growing in the last years. Some groups have developed their own models for their experimental pilot plants, as previously summarized in Table 1.2.

For the moment oxy-fuel CFB is not deployed at demonstration scale. Maximum thermal power size of pilot boilers currently running are less than 30 MW. Hence, modeling of oxy-fuel CFB is either a model of a small-rig and it is validated in the rig itself, or an existing and validated large-scale CFB model for air combustion adapted to oxy-fuel combustion conditions.

Large scale oxy-fuel modeling has been scarcely published in the literature. Four main group's works are available in the open sources. Three of them have experiences in oxy-fuel experimental fluidized bed facilities, but their modeling in large CFB cannot be validated.

Nsakala and co-workers (2004) published a comprehensive report about OF in FB. They showed some results from their experimental *Multi-Use-Fuel* facility and modelled a large-scale OF CFB. They did not find remarkable differences between AF and OF heat transfer coefficients inside the boiler or inside the external heat exchanger, arguing that heat transfer in both zones are dominated by particles. When comparing the heat balance between large-scale AF and OF CFB models, they encountered a significant importance of an external way of transferring heat from particles. This is due to a boiler size reduction for the OF case, resulting in less available area inside the boiler. However they stated an additional handicap of using an external fluidized bed as heat exchanger: the temperature of limestone to be calcined for high CO_2 partial pressures (around 900ºC) is higher than usual AF conditions (around 850ºC). Below this temperature, recarbonation of the formed calcium oxide from limestone would consume CO_2. In the case of an external heat exchanger fluidized with flue gas, they calculated that almost all CO_2 present in

the gas would be recarbonated at typical particles recirculation temperatures (around 650ºC). Thus, fluidization process would fail. For avoiding this, they proposed a moving fluidized bed, where no fluidizing gas was needed. Conventional AF temperature in oxy-fuel combustion were tested in the mini-CFB located in CANMET Energy facilities (Wu et al., 2011). They found $CaCO_3$ presence in ashes supporting the belief that calcination was avoided.

Saastamoinen and co-workers (2006) carried out experiments in a bench scale CFB-BFB facility, for different O_2/CO_2 ratios. They attained stable operation conditions and presented sulphur capture equally or more effective in oxy-fuel CFB than in air CFB combustion conditions. They also simulated a large scale CFB boiler, reporting some important re-design remarks for new oxy-fuel CFB boilers configuration. They calculated an available surface in a OF boiler being 38% smaller than the one for AF when feeding 60% O_2 at inlet. They estimate that higher heat flux surfaces would lead to significant reduction in the boiler size. They suggested that attention must be paid in arranging the heat transfer surfaces so that no blocking of gas or solids may occur and in locating surfaces not so close that suspension in between could cool down excessively (Jäntti et al., 2007). Related to oxy-fuel efficiency penalty, it has been proposed a *fire-more* concept for producing more steam with the same size boiler, based on higher heat transfer fluxes in oxy-fuel combustion (Hack and Shah, 2008).

Seddighi et al. (2010) modelled a large scale fluidized bed and predicted particle recirculation rates higher than 30 kg/m^2s for controlling bed temperature at O_2 concentration as high as 90% at inlet (Johnsson, 2010; Seddighi et al., 2010).

Krzywanski and co-workers (2010b) modelled an oxy-fuel boiler based on the 670 t/h lignite CFB boiler in Turow power station in Poland and simulated mixtures of O_2/CO_2 and O_2/N_2 atmospheres, confirming higher heat transfer to furnace walls when increasing O_2 concentration at inlet. They considered a limit of 60% of O_2 at inlet, stating that bed temperature over this concentration will exceed 1050ºC and so ash melting would take place.

We will now review the fundamentals of one-dimensional modeling air-firing CFB boilers. From them, the strategies selected to model the oxy-fuel CFB boiler will be selected, and further explained in section 2.3.

2.2 FUNDAMENTALS ON CFB MODELING

Process taking place inside a fluidized bed combustor can be grouped in three interdependent groups of phenomena: particles fluid-dynamics, combustion and heat transfer. In the Figure 2.2 interactions among said groups of phenomena are represented, as explained by Pallarès and Johnsson (2006):

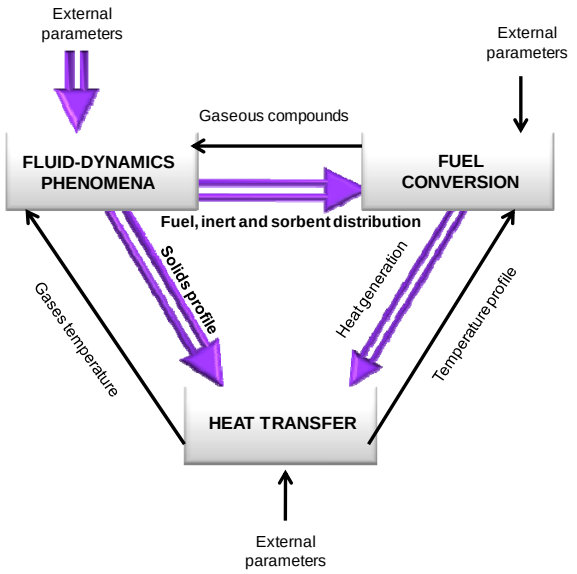

Figure 2.2. Interaction between the three great groups of phenomena occurring in a CFB combustor. Adapted from Pallarès and Johnsson (2006)

Double arrows highlight the sensitivity of heat transfer and fuel conversion with fluid-dynamics modeling. On the other hand, fluid-dynamics could be reasonably well modeled assuming certain typical values for combustion or heat transfer parameters. This is the feature that makes fluidized bed exhibit such unique characteristics, versus other combustion technologies. Movement of particles along the riser determines where and how well are the fuel particle burnt and also, how intense is the heat transferred to the boiler walls.

Ref	Type	Scope	Hydrodinamics			Fragm.	Combustion			SOx Capture	NO_x	HT		Validation /Scale	
			Level	**Zones**	**Phases**		**Devolatilization**	**Coal combustion**	**Shrinking**			**Gen**	**Rad**		
(Adánez and Diego, 1995)	CFB	A	II	A	B		A	C	Y	B	C	C	D	N	
(Aibéo and Pinho, 2003)	CFB	A	II	B	B				?			A	B	N	
(Arena et al., 1995)	BFB & CFB	A	I	A	B	Y	A	C	?			C	D	N	
(Krzywanski et al., 2010b)	OXY-CFB	B	II	B	C		A	D	N	B	B	B	B	N	
(Seddighi et al., 2010)	OXY-CFB	A	II	B	A		A	C	N	D	C	A	B	N	
(Chen and Saxena, 1977)	BFB?	A	I	A	A	N	F	A	N	B	C	D	C	Y	Literature
(Sotudeh-Gharebaagh et al., 1998)	CFB	A	I	A	A	N	A	D	N	B	B	D	D	Y	800 kW
(Gungor, 2009)	CFB	A	II	B	B		A	C	?			B	D	Y	50 kW
(Gayan et al., 2004)	CFB	A	II	B		Y	D	C	Y	D	C	C	D	Y	300 kW 100 kW
(Adanez et al., 2001)	Turbulent	A	II	A	B		A	C	Y	B	C	C	D	Y	300 kWth
(Alagöz, 2006)	BFB	A	I	A	B		A	C	?	B	C	A	C	Y	300 kWth 16 MW
(Chen and Xiaolong, 2006)	CFB DYN	B	II			Y	C	C	?	B	B	A	B	Y	410 t/h Pyroflow CFB (Steady state)
(de Souza-Santos, 2007)	BFB		I		B				?					Y	1.6 MW
(Werner, 2001)	CFB	A	II	A	B	N						A	E	Y	0.25m2
(Gungor and Eskin, 2008)	CFB	A	III	B	B	Y	A	D	Y	D	D	B	D?	Y	50 kW 160 MW (literature)
(Wang et al., 1999)	CFB	C	II	A	B	Y	A	D	N	B	B	A	A	Y	12 MW
(Huilin et al., 2000)	CFB	A	II	B	B	Y	A	D	Y	B	C	A	A	Y	30 MW
(Romeo and Cortés, 1998)	PFB	A	II	B	B	N	A	A	N	C	C	B	B	Y	80 MW
(Hannaes et al., 1995)	CFB	B	III	B	B	Y	E	C	Y	B	B	B	B	Y	120 MW
(Lee and Kim, 1999)	CFB	A	II	B	B	Y	A	D	Y	B	C	A	A	Y	200 MWe
(Werther et al., 2009)	CFB	B	III	A	B	Y	C	C	Y	D	C	D	D	Y	252 MWt
(Vepsalainen et al., 2009)	CFB	A	IV				E	D		B	B			Y	370 MWt

Table 2.1. Models of fluidized bed combustors

HYDRODYNAMICS:
- Scope:
  - A: Boiler
  - B: Boiler + Cyclone + Standpipe + Loop-seal (+EHE)
  - C: Steam cycle included
- Level:
  - I: 1D plug flow and stirred tank
  - II: 1.5D core-annulus structure
  - III: 2D numerically solved
  - IV: 3D
- Zones:
  - A: Two zones: dense and dilute
  - B: Three or more zones in the reactor
- Phases:
  - A: No distinctions between bubble and emulsion phases
  - B: Two phase model: bubble and emulsion phases
  - C: Three phase model: bubble, cloud-wake and emulsion phase
- Fragmentation included
  - Y: yes
  - N: no

COMBUSION:
- Devlolatilization:
  - A: Uniform in dense bed
  - B: Instantaneous at feed point
  - C: Rate related to solids mixing rate
  - D: Devolatilization kinetics
  - E: Particle movement model
  - F : Not considered
- Coal combustion
  - A: Difusionally controlled
  - B: Rate of CO oxidation comparable to other chemical reactions
  - C: Difusionally and kinetically controlled
  - D: Kinetically controlled
- Shrinking particle model:
  - Y: yes
  - N: no

SO_2 Capture:
- A: Desulfurization model
- B: Semi-empirical SO_2 kinetics
- C: Uniform in dense bed
- D: Not considered

NO_x
- A: Formation and reduction model
- B: Semi-empirical formation and reduction kinetics
- C: Not considered

HEAT TRANSFER
- A: Semi-empirical renewal model
- B: Empirical correlations
- C: Temperature is design variable
- D: Not included

Radiation:
- A: Zone Method
- B: Particle to gas heat exchange through Stefan-Boltzmann law
- C: Discrete Ordinates Method
- D: Not considered independently
- E: Two flux model (Schuster-Schwarzschild-approximation)

VALIDATION
- Y: yes
- N: no

Table 2.2. Nomenclature of Table 2.1

According to this scheme, numerous authors have developed their boiler models along last decades, with more or less level of complexity, depending of the aim on which the model was focused. In Table 2.1 some of these authors are shown,

attending at the strategies of modeling followed by each of the aforementioned fields.

2.2.1 FLUID-DYNAMICS

A very extensively used and experimentally confirmed way of modeling fluidized beds divides the combustor into several zones in which particles movement is different and so they are the processes taking place in each region. In the bottom part of a fluidized bed, a dense zone is clearly distinguished. Above this zone, concentration of solids decays dramatically. Some researchers include in their models an intermediate zone called *splash* zone. At the top of the riser, a fourth region can be considered, the *exit* zone, very much dependant of exit geometry. In Table 2.1 this division is shown in the corresponding column, distinguishing between those authors that consider dense and dilute zones (Adánez and Diego, 1995; Arena et al., 1995; Sotudeh-Gharebaagh et al., 1998; Wang et al., 1999; Adanez et al., 2001; Werner, 2001; Alagöz, 2006; Werther et al., 2009), and those that also include spares and exit zones (Hannaes et al., 1995; Romeo and Cortés, 1998; Lee and Kim, 1999; Huilin et al., 2000; Aibéo and Pinho, 2003; Gayan et al., 2004; Gungor and Eskin, 2008; Gungor, 2009; Krzywanski et al., 2010b; Seddighi et al., 2010).

The bottom zone

This region occupies a small volume in the overall CFB combustor, above the distributor, up to a height of around half a meter in large boilers. It is in this region, where particle density is hundred times higher than in the rest of the boiler and thus, most of combustion and chemical reactions occur here.

The way of modeling the bottom zone can be as simple as considering it a well mixed stirred tank or assuming the two-phase model or even including the cloud-wake phase and the mass transfer between the phases. The common point among these treatments is assuming that the bottom zone behavior is similar to that found in a bubbling bed regime. This was confirmed for example, with the experiments made by Svensson et al. (1996), that found that increasing fluidization velocities makes an increase in gas flow through the bubbles and the bubble dynamics, showing fluctuation frequencies similar to those in bubbling beds, around 1 Hz. In spite of these fluctuations generated by bubbles, dense bottom bed

has a quite uniform time-average void fraction. One of the main characteristics of the bubbling bed regime, observed in the dense part of a CFB, is the linear time-averaged vertical pressure drop profile above the distributor, as confirmed by the authors. If an homogeneous mixing is assumed, i.e. the effect of the particle side distribution (PSD) on jetsam/flotsam segregation can be neglected, void fraction along the dense bottom zone is also constant. It can be expressed as:

$$\varepsilon_b = \delta_b + (1+\delta_b)\varepsilon_{emulsion} \qquad \text{Eq. 2.4}$$

According to the two-phase model, bottom zone consists of a dense or emulsion phase, formed by bed particles and the interstitial flow between the particles; and a bubble phase, made of uprising gas bubbles, considered to be free of solids (Kunii and Levenspiel, 1991). First approaches assumed that all the gas in excess of u_{mf} flowed through the bed as bubbles, while the emulsion stayed at minimum fluidizing conditions. The expression for a single bubble rise velocity yields then:

$$u_{br} = 0.711(gd_b)^{1/2} \qquad \text{Eq. 2.5}$$

However, there have been experimental evidences that the flow of bubbles is overestimated by this assumption (Shen et al., 2004). This is because gas crosses a certain section of the bed, not only by translation of bubble voids, but also by the flow through the bubbles relative to them and the interstitial flow relative to the particles in the dense phase. So, the overall gas balance would fulfill the following expression:

$$u = u_{tf} + u_{mf} + u_{vis} \qquad \text{Eq. 2.6}$$

where the visible flow, u_{vis}, would yield:

$$u_{vis} = \delta_b u_b \qquad \text{Eq. 2.7}$$

Or it can be also expressed as the dimensionless visible bubble flow, Ψ:

$$\psi = \frac{u_{vis}}{u - u_{mf}} \qquad \text{Eq. 2.8}$$

Several empirical expressions have been proposed and used by researchers for estimating the bubbling velocity. Some of them are summarized in Table 2.3.

Reference	Correlation	
Farrokhalaee (1979) in (Davidson et al., 1985)	$u_b = u - 0.44u^{0.62}u_{mf}^{0.32}H^{0.23}exp\left(-0.24x/D\right)$	Eq. 2.9
Peters et al. (1982) in (Davidson et al., 1985)	$u_b = Y\left(u - u_{mf}\right)$ $Y = 0.785 - 0.13\left(u - u_{mf}\right) + 5\left(u - u_{mf}\right)^2$	Eq. 2.10
Werther (1983) in (Kunii and Levenspiel, 1991)	$u_b = 1.6\left[\left(u - u_{mf}\right) + 1.13d_b^{0.5}\right]d_t^{1.35} + u_{br}$	Eq. 2.11
Werther and Wein (1994) in (Pallarès and Johnsson, 2006)	$\psi = 1.45Ar^{-0.18}$	Eq. 2.12
	$\psi = f_{CFB}\left(h + 4\sqrt{A_0}\right)^4$	Eq. 2.13
Johnsson et al. (1991) in (Pallarès and Johnsson, 2006)	$f_{CFB} = 0.3121 + 0.129u^{-1} - 16.6d_b - 2.61\cdot 10^{-5}\Delta P_{ref}$ ΔP_{ref} being the pressure drop between riser height interval from 0.135 to 1.635 m above gas distributor	Eq. 2.14

Table 2.3. Correlations for estimating bubble velocity

The transport zone

When bubbles reach the limit of the dense bed they explode in the surface. Aggregates of particles are thrown into the splash zone. Due to the differences of particles physical properties, drag forces per unit weight also differs from one type of particle to another. A high drag force per unit weight makes the particles move upwards, whereas particles with low drag per unit weight will tend to sink to the bottom. During this instantaneous explosion of bubbles in the bottom bed surface, competition between both mechanisms, mixing and segregation, occur simultaneously. A strong back-mixing is caused in this region by the decay in the solids concentration. The transport region comprises the height between the dense bottom zone limit and the top of the riser. For covering both, the upper diluting and the lower dense regions, the following expression was proposed by Li and Kwauk in 1980 (Horio, 1997):

$$\frac{\varepsilon_p - \varepsilon_s}{\varepsilon_b - \varepsilon_s} = exp\left[-a\left(z - z_i\right)\right] \qquad \text{Eq. 2.15}$$

This way of modeling back-mixing and decay of solids concentration in the freeboard has been extensively used by most of models in Table 2.1

The decay constant for these models, a, is inversely proportional to the gas velocity. It represents fairly well the effect of the back-mixing of solids above the dense bed, dominated by clustered solids thrown up into the freeboard.

For this reason, Johansson and Leckner (1995) proposed a two-solid-phase model, consisting of a cluster and disperse phases. The first, describing a ballistic type of solids back-mixing, similarly to Eq. 2.15 and the second, dominating the contribution of the wall layer falling solids effect. The formed clusters in the dense bottom zone are immersed in the disperse phase but there are few that reach the top of the riser. So, particles are elutriated from the bottom rising upward along the central region of the riser. In this region, the flow is turbulent due to high slip velocities (the difference between the mean interstitial gas velocity and the mean upward particle velocity) and particles are thrown towards the wall. A falling film is then formed. This falling layer captures particles close to it and those particles are entrained back to the core less frequently. This makes the concentration of solids along the riser height adopting an exponential shape (Davidson, 2000). The expression derived by Johansson and Leckner (1995) including the mentioned back-mixing processes yields:

$$\rho = \left(\rho_{bb} - \rho_{disp,h}\right) exp\left(-a\left(z - H_x\right)\right) + \rho_{exit} exp\left(K\left(H_{exit} - z\right)\right) \qquad \text{Eq. 2.16}$$

Where a corresponds, as in Eq. 2.15, to the back-mixing from homogeneous clustering flow in the splash zone. K is the decay coefficient for the back-mixing in the wall-layer flow (Johansson et al., 2007). Zijerveld et al. (1997) calculated the decay constant using Eq. 2.15 and Eq. 2.16 in three boilers, the 12MWth CFB, a 1.2m x 0.8m and a 0.083 m ID CFB. They found that Eq. 2.15 fails to predict satisfactorily the concentration in the larger risers, so they suggest to avoid that expression for those commercial CFBs.

The exponential behavior of solids along the riser is then due to the lateral transport of solids from the core to the down-flow wall layer of solids. According to Horio (1997) there are two other ways of modeling the lateral solids transfer. One approach explains the core-annulus flow by the radial velocity distribution and radial density profile. The other explanation is based on time-average mass and momentum balances.

The wall thickness, t_δ, is the distance between the riser walls to the point where net flux of solids is zero in the vertical direction. This magnitude has been

extensively studied and several correlations have been proposed, like the one by Harris et al. (2002):

$$\frac{t_\delta}{D} = 0.5\left[1 - 0.4014\varepsilon_s^{-0.0247} Re^{0.0585}\left(\frac{H-z}{H}\right)^{-0.0663}\right] \qquad \text{Eq. 2.17}$$

In general, a clear dependence of wall thickness on riser height is observed. Some authors include the effect of solids circulation adding the average solids concentration term within their expressions, like the one proposed by Bi et al (1996). Johnsson et al. (1995) collected data from different unit sizes and conditions. For large-scale CFB boilers, this decrease in wall-layer thickness upwards is also observed. This reduction levels out for $(H-z)/D_{equiv} > 6$ from where a height-independent value for t_δ was proposed. Therefore, the expression for the wall-layer thickness was:

$$t_\delta = 0.0108(H-z) \text{ for } H_{sat} < z \le H_{duct} \qquad \text{Eq. 2.18}$$

and

$$t_\delta = 0.0648 D_{equiv} \text{ for } H_b < z \le H_{sat} \qquad \text{Eq. 2.19}$$

Gas composition seems to influence slightly on the explained theory of large one-dimensional fluid-dynamics modeling. The models including oxy-fuel conditions on their fluid-dynamic modeling do not include variations of the semi-empirical approaches developed for air-firing. However, few studies have been published lately, showing certain differences on the bubbling regime for high CO_2 concentration in the fluidizing gas, specially related to changes in viscosity and density (Guedea et al., 2011).

2.2.2 COMBUSTION AND POLLUTANT FORMATION

When a fuel particle enters the bed, the following processes take place:

- Heating and drying
- Devolatilization and volatile combustion
- Swelling and primary fragmentation
- Char combustion

The typical bulk temperature in fluidized bed boilers is over 800ºC. Then, at 100ºC heating and drying of the particles happens quickly and can be considered to occur almost completely in the dense part. Volatile content is considered a property of coal. There are methodologies to estimate the portion of carbon on volatiles but, in fact, to quantify coal volatile content, temperature, heating rate and particle diameter should be considered (Thunman et al., 2001). When a detailed model of the particle combustion is needed, fragmentation of the fuel particle must be regarded. Fragmentation takes place when steam or volatiles inside the particles are released, but the pore structure of the fuel particle does not let them escape. Thus, higher pressure is generated inside the particle and it can be then broken. One of the consequences of fuel particle fragmentation is the unburnt carbon entrainment (Daki et al., 1989).

In the range of 400-900ºC the temperature has a positive influence on the quantity of volatiles. If heating rates are below 600ºC/s, less volatile matter is released. In the case of lignites, it does not depend on pressure but for bituminous coals decreases with increase of pressure (Oka, 2003).

For understanding the devolatilization and volatile combustion of a single coal particle inside a fluidized bed, the study by Prins et al. (1989) gave a comprehensive data analysis. Huilin et al. (2000) suggested the expression developed by Peter and Poynton in 1992 for estimating the devolatilization time:

$$t_{VOL} = 10\left(\frac{1048}{T_g}\right)d_p \qquad \text{Eq. 2.20}$$

Devolatilization time, $t_{VOL,}$ is very short and depends mainly on temperature, T_g, and particle diameter, d_p. As seen in Table 2.1, most of models assumed that devolatilization occurred in the dense part of the fluidized bed, uniformly distributed along the bottom bed height. This is the assumption considered in this work.

Regarding char combustion modeling, it is often carried out including a kinetic model, like the one used by Huilin et al. (2000), Gungor and Eskin (2008) or Sotudeh-Gharebaagh et al. (1998). Some authors also included the diffusion mass transfer in their models. The shrinking unburned core model has been extensively used in these kind of detailed combustion model. Thus the shrinking rate of the particle radius could be expressed like suggested by Adánez and de Diego (1995):

$$-\frac{dr_i}{dt} = \frac{12C_{O_2}}{\rho_{char} x_{cc}\left(\frac{1}{K_c} + \frac{d_p}{ShD_g}\right)} \qquad \text{Eq. 2.21}$$

Where C_{O2} is the concentration of O_2 around the particle; K_c is the kinetic constant of burning char particles; Sherwood number is semi-empirically estimated, using two different expressions for the dense part and for the dilute zone; and D_g is the diffusivity of oxygen in nitrogen.

Fuel conversion in oxy-fuel fluidized beds was explored by the team from Czestochowa Technical University (Czakiert et al., 2006). They made experiments for different O_2/N_2 mixtures and compared it with O_2/CO_2 mixtures. Carbon conversion ratio increased with increasing oxygen concentration in the gas mixture, regardless the reactor's temperature level. This was explained because combustion rate increased by an increase in oxygen partial pressure. Increasing temperature had no effect on carbon conversion ratio. The carbon conversion in the O_2/N_2 mixtures was always higher than for O_2/ CO_2 mixtures, at the same oxygen concentration and combustor temperature. Tests reported by Nsakala et al. (2004) in the ALSTOM *Multi-fuel CFB* also observed, as expected, higher CO emissions, likely due to high CO_2 content of the flue gas, which hinders oxidation of CO.

Still, the influence of atmosphere on char combustion during oxy-fuel fluidized beds is not evident, as explained by Guedea et al. (2013). Char reactivity changes with varying the diluting gas in the atmosphere, but it is related with higher volatile matter content and porous residual char. Higher reactivity was found under O_2/N_2 atmosphere, due to higher diffusivity coefficients. On the other hand, in some cases, higher O_2 concentration implied higher velocity of reaction, concluding that different fuels are not affected in the same way by oxy-fuel conditions.

SO_2 formation

One of the main advantages of burning coal in fluidized bed is the capacity of in-furnace SO_2 capture, when adding a proper solid sorbent. This sorbent is usually limestone or dolomite mineral stones which do not influence the combustion process. Under certain conditions, they calcined, i.e. calcite crystals ($CaCO_3$) disintegrate into small lime crystals (CaO) due to CO_2 diffusion, according to the reaction:

$$CaCO_3 \Leftrightarrow CaO + CO_2 \qquad \text{R. 2.1}$$

The resulting porous structure depends on limestone and calcination conditions, i.e. temperature and CO_2 partial pressure, and dominates the subsequent sulfation phenomena:

$$CaO + SO_2 + \frac{1}{2}O_2 \Leftrightarrow CaSO_4 \qquad \text{R. 2.2}$$

Under conventional atmospheric air-firing conditions, where CO_2 partial pressure is around 0.12-0.15 bar, calcination takes place above 790ºC. Then, SO_2 and O_2 penetrate through the pores and react with CaO yielding $CaSO_4$. Formed $CaSO_4$ will not decompose until approximately 1580ºC, so it is thermodynamically stable at a range of conventional bed temperatures of 800-1000ºC. This is one of the reasons of keeping fluidized bed temperature within the mentioned range. Optimum desulfurization temperature is commonly accepted to be located near 850ºC. Nevertheless, this optimum temperature depends on sorbent properties and combustion conditions. For example, Mattison and Lyngfelt (1999) found that under alternating conditions, $CaSO_4$ reacts with CO or H_2, releasing SO_2 and breaking $CaSO_4$ layer. Therefore SO_2 capture efficiency is increased and optimum temperature is also lower than under oxidizing conditions.

By analyzing the equilibrium between CaO and $CaCO_3$, high CO_2 partial pressure does not let limestone to be calcined at conventional air-firing temperature and sulfation takes place in one step, also called direct sulfation:

$$CaCO_3 + SO_2 + \frac{1}{2}O_2 \Leftrightarrow CaSO_4 + CO_2 \qquad \text{R. 2.3}$$

Direct sulfation was previously addressed for pressurized fluidized beds (Snow et al., 1988), but it can also happen under atmospheric oxy-fuel combustion. The effect of CO_2 partial pressure on limestone conversion is commonly expressed with equilibrium pressure term, P_{eq}, at bed temperature, that coincides with the equilibrium constant of reaction, estimated from thermochemical data (García-Labiano et al., 2002):

$$P_{eq} = 4.137 \cdot 10^{12} exp\left(-\frac{20474}{T}\right) \qquad \text{Eq. 2.22}$$

Calcination rate becomes lower when P_{CO2} is increased. Figure 2.3 shows this tendency, represented by the expression (Stanmore and Gilot, 2005):

$$R_c = k_D\left(P_{eq} - P_{CO2}\right) \qquad \text{Eq. 2.23}$$

$$k_D = 1.22exp\left(-\frac{4026}{T}\right) \qquad \text{Eq. 2.24}$$

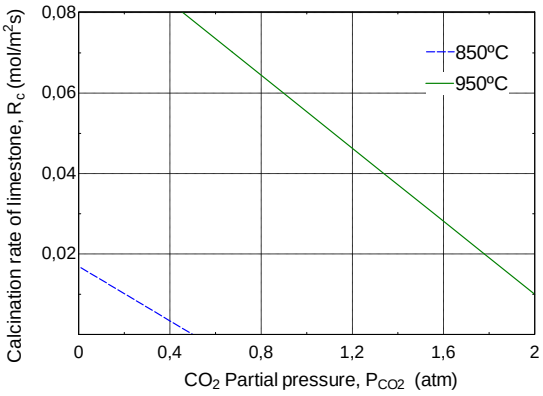

Figure 2.3. Dependence of calcination rate on partial pressure and temperature

When P_{CO2} is above P_{eq}, CO_2 cannot migrate out the sorbent particle, preventing calcination (García-Labiano et al., 2002). Nevertheless, although desulfurization rate is lower than in indirect process, $CaSO_4$ layer formed around the particle core has more and larger porous, allowing a higher Ca conversion (Hu et al., 2006). This improvement depends strongly on particle size and residence time (Liu et al., 2000). Unlike in indirect sulfation, there is no agreement on an optimum temperature for direct sulfation (Qiu and Lindqvist, 2010).

Since CO_2 partial pressure under oxy-firing atmospheres significantly differs from air-firing, desulfurization reaction mechanisms also change. For typical bed temperatures (800-900 ºC) and near to atmospheric pressure, direct sulfation takes place instead of the indirect sulfation, similarly as in PFB. De Diego and co-workers (de Diego et al., 2011; García-Labiano et al., 2011) analyzed the influence of temperature, particle size and CO_2 concentration during sulfation under oxy-firing conditions on desulfurization process in a thermogravimetric balance. They found lower particle conversion in direct sulfation which improved at higher temperature. The contrary happened for indirect sulfation. First results published about desulfurization under oxy-firing conditions in a CFB do not reveal a clear tendency of desulfurization efficiency using the same Ca:S ratio. Jia and co-workers (2010), reported lower efficiencies using two kinds of limestones and coals whereas Duan and co-workers (2011b) obtained higher values under oxy-firing for an anthracite and a bituminous coal with a similar CaO content in limestone (around 53%of CaO).

However, several studies confirm that indirect sulfation also occurs under oxy-fuel bed combustion if the temperature is high enough, and consequently desulfurization rate sharply increases, as shown in Figure 2.3. Higher bed temperature is required during oxy-fuel combustion for reaching similar SO_2 capture efficiency.

In the current model, SO_2 capture will be implemented because of its influence on CO_2 emissions and, mainly, in the energy balance. Calcination is an endothermic process, whereas sulfation is exothermic. Thus, SO_2 capture by the indirect way would consume heat of combustion if $CaCO_3$ excess is used.

NO_x formation

During coal combustion, NO_x is originated from the nitrogen present in air or from the N-fuel. Air-nitrogen generates NO_x at high temperature (thermal process), that are not usually reached in fluidized beds. It can be formed also by the prompt process, but this is not usual process in fluidized bed, since hydrocarbon free radicals and high temperature would be necessary. So 95% of NO_x in a fluidized bed is formed from the fuel nitrogen. During devolatilization, when coal particle is heating-up, nitrogen decomposes to yield gaseous HCN as the main nitrogen-containing specie. This hydrogen cyanide then forms the basis for most reactions leading to NO_x in the gas phase (Hayhurst and Lawrence, 1996).

Destruction of formed NO is usual as well. It can react with other species such as NH_2 yielding N_2. NO reduction is also possible with CH:

$$CH + NO + \Leftrightarrow HCN + O \qquad \text{R. 2.4}$$

This is the reaction that allows reburning, as a method for reducing NO_x emissions, feeding methane in the freeboard. Reburning can occur in fact during the incomplete combustion of volatiles. However, if O_2 is available, CH radicals oxidized quickly yielding CO and CO_2, before reacting with NO.

When fuel is present, NO can also be reduced by other species in atmosphere with NH_2:

$$NO + NH_2 \Leftrightarrow N_2 + H_2O \qquad \text{R. 2.5}$$

$$NO + NH \Leftrightarrow N_2 + OH^- \qquad \text{R. 2.6}$$

Char particles also help to heterogeneous reduction of NO to N:

$$NO + char \Leftrightarrow N_2 + CO \quad \text{R. 2.7}$$

$$NO + CO \overset{char}{\Leftrightarrow} \frac{1}{2} N_2 + CO_2 \quad \text{R. 2.8}$$

Nitrous oxides, N_2O, are formed similarly than NO_x. It is formed from N-fuel and it requires the same precursors: HCN and NH_3. So, reactions yielding these intermediate compounds are common for all nitrogen oxides:

$$NCO + NO \Leftrightarrow N_2O + CO \quad \text{R. 2.9}$$

$$NH + NO \Leftrightarrow N_2O + H \quad \text{R. 2.10}$$

Bed temperature is an important parameter. According to de Diego et al. (1996) bed temperature makes NO_x emissions decrease but N_2O increase. This influence is even greater for higher air excess. Also, when incrementing air excess, NO_x and N_2O increase. This is explained because higher O_2 concentration increases volatile and chars combustion and also, at the same time, concentration of char and CO is lower, so heterogeneous reduction of NO is decrease in the char surface.

N_2O is also increase by higher volatile (NH_3 and HCN) conversion via homogeneous reactions as:

$$HCN + O \Leftrightarrow NCO + H \quad \text{R. 2.11}$$

$$NCO + NO \Leftrightarrow N_2O + CO \quad \text{R. 2.12}$$

NO_x and N_2O is reduced by increasing secondary air injection. This is an extensively used method for control of pollutants. This is because combustion occurs in oxygen-limited conditions, favoring volatile conversion from N to N_2, instead to NO_x. Moreover, char is accumulated and higher CO concentration allows decomposition of NO via CO (R. 2.8) in the char surface. Finally, residence time of gas in the lower part increases. Thus, NO_x decreases because NO_x decomposition is faster than NO_x formation along the riser.

Mechanisms of formation and destruction for NO and N2O during fluidized bed combustion have been thoroughly studied in the literature. A clarifying way of understanding main conversion paths of fuel nitrogen during fluidized bed combustion was explained by Leckner (1997) and it is schematically present in Figure 2.4

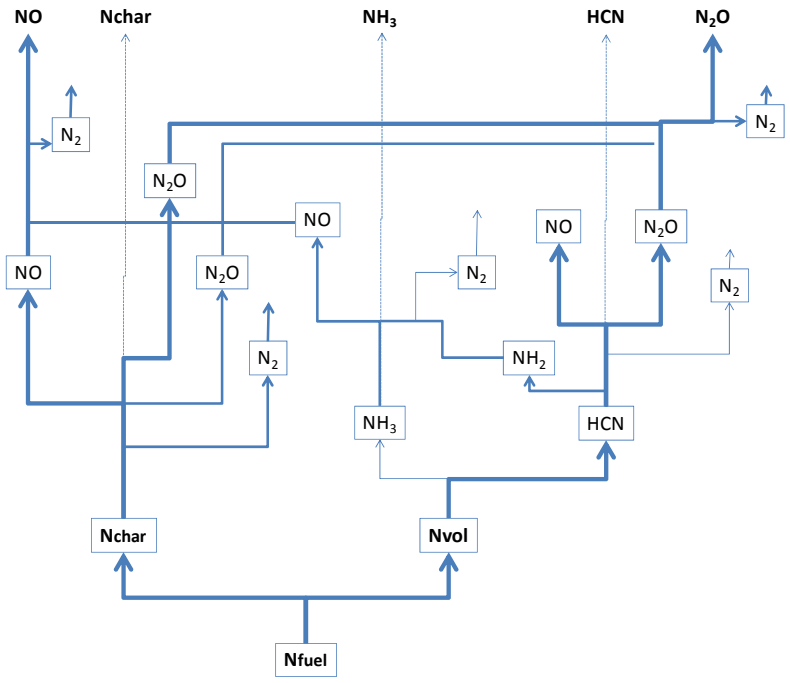

Figure 2.4. Main conversion paths of fuel nitrogen. Adapted from Leckner (1997)

In oxy-fuel combustion there have been numerous investigations of NO_x formation specially in pulverized coal combustion. Experiments from the Czestochowa CFB pilot plant (Czakiert et al., 2006) show a significant limitation of fuel-nitrogen conversion to NO_x during oxy-fuel combustion.

In the 50kW CFB in Southeast University in China the effect of operation parameters of oxy-fuel combustion on NO emissions were analyzed by Duan et al. (2011a). NO formation decreased in 21%/79% O_2/CO_2 atmosphere. They explained it as due to the less O and OH radicals formed under lower bed temperature. In addition, low temperature and high CO_2 concentration bring possibility of higher CO concentration in O_2/CO_2 atmosphere. As the O_2 concentration at inlet is increased gas velocity diminishes and this means longer residence time of fuel particles in the combustor, which would promote fuel-N conversion into NO_x precursors. Increasing bed temperature or oxygen stoichiometric ratio brings higher NO emission in O_2/CO_2 atmosphere, which is consistent with the results in air-fired CFB combustion. Stream staging is more efficient for controlling NO emission in oxy-CFB combustion than that in air combustion.

Another important issue in oxy-fuel is the positive effect of RFG on the decrease of NO emissions. Okazaki and Ando (1997) examined the effects of CO_2 concentration, together with the less recycled-NO in the flame, and the interaction of fuel-N and

recycled NO_x on the decrease of the final NO_x exhausted from the coal combustion system with the recycled CO_2. They concluded that the conversion ratio from the fuel-N to exhausted NO_x is reduced to less than one-fourth of that with air combustion, and the effect of a reduction of recycled-NO in the furnace was dominant and amount to 50%-80%.

In the current model, NO_x formation and destruction reactions are not included, since their energy interactions can be neglected, compared with combustion and sulfation reactions.

2.2.3 HEAT TRANSFER

For decades, there have been numerous investigations on heat transfer in fluidized bed, specially carried out in laboratory scale facilities. Although not completely independent, there is a generalized treatment of heat transfer from bed to surfaces as the contribution of three mechanisms: the transient conduction of particles when contacting the surface, also called particles convection; the gas convection, and the radiation heat transfer. In fast beds such as circulating fluidized bed, heat transfer is strongly dependent on particles fluid-dynamics. Parameters like rate of solids circulation, superficial velocity through the column, and particle size, will define the dominant heat transfer mechanism. Particles travel upwards along the core in the form of strands. When strands approach the wall layer, they change direction. Therefore, energy is transferred from particle strands or agglomerates at bed temperature that "enters" into the wall and exchange heat with the surface during certain residence time. This is called renewal packet theory and it is further explained in the next chapter.

Radiation heat transfer turns out the dominant heat transfer mechanism for the low density boiler zones. Normally, gas-particle suspension can be considered isothermal. Thus, the expression for the radiative heat transfer coefficient related to a plane grey heat transfer surface follows the expression:

$$h_r = \sigma \varepsilon_{bw} \left(T_b^2 + T_w^2 \right) \left(T_b + T_w \right) \qquad \text{Eq. 2.25}$$

Where

$$\varepsilon_{bw} = \frac{1}{\left(\frac{1}{\varepsilon_{ef}} + \frac{1}{\varepsilon_{w}} - 1\right)} \qquad \text{Eq. 2.26}$$

As stated by Baskakov and Leckner (1997) there is not a unique methodology for accurately estimate the value of emissivity of an isothermal suspension. All those methodologies coincide in indicating that particle emissivity is the main factor for the suspension emissivity, so as particle porosity. For estimating values of the radiative heat transfer, these authors separated the effect of gas phase convection heat transfer from the measures values, calculating the gas contribution by the expression:

$$Nu_{gc} = 0.003 Re^{0.8} Pr^{0.43} \qquad \text{Eq. 2.27}$$

The heat transfer coefficient in the membrane wall of the 12MWth CFB at Chalmers was 104 W/m²K. Convection and radiation heat transfer coefficients were estimated around 20 and 78 W/m²K respectively, confirming good fitting of aforementioned assumptions.

Basu and Nag (1996) collected heat transfer data from several commercial CFB units. Average heat transfer coefficients ranged from 80-220 W/m²K and shows great dependency on suspension density. He correlated data against suspension density and obtained the following expression:

$$h = a\rho_s^n \qquad \text{Eq. 2.28}$$

with $a = 40$ and $n = 0.5$, for $5 < \rho_s < 25\ kg/\mathrm{m}^3$ and $750 < T_{bed} < 850$ºC. Similar expressions were proposed by Divillo and Boyd (1994), where $a = 23.2$ and $n = 0.55$, although this was proven by Xie et al. (2003) to overestimate data for densities greater than 200 kg/m³.

Basu and Nag (1996) explained the dependence of heat transfer in large units with temperature. There is an obvious increase of heat transfer coefficient with increasing temperature, due to higher gas thermal conductivity and higher radiation. At a relatively high suspension density of 20 kg/m³ the increase in heat transfer coefficient with temperature was linear. This may not be the case at a more dilute bed where the radiation becomes dominant. Regarding fluidization velocity there were not much influence on heat transfer in large units. It was reported that change in secondary air rate did not affect the heat transfer

coefficient in the upper part of the furnace, but an increase in the primary air velocity did increase it (Andersson and Leckner, 1992). This happened because the increased primary air transported more solids to the upper section increasing the suspension density in that region of the bed. Particle size had a strong effect in laboratory units, but influenced much less heat transfer in large units. This is not the case for bubbling fluidized beds where the particle size is the most important factor influencing heat transfer irrespective of the plant size.

Breitholtz et al. (2001) reviewed heat transfer coefficients from laboratory and industrial scale fluidized bed boilers and proposed an exponential simplified expression for particle convection heat transfer that fit data of all the cases studied. Considering the different mechanisms to transfer heat as independent contributions, the overall bed-to-wall heat transfer could be expressed as:

$$h = h_{conv} + h_r = \alpha_0 \rho^b + \eta_r h_{r,max} \qquad \text{Eq. 2.29}$$

Where h_{conv} comprises particle and gas convection mechanisms and h_{rad} is radiation heat transfer coefficient. Parameters for the equation yields $a_0 = 25$ and $b = 0.58$. η_r refers to the radiation efficiency term, that gives an idea about the shadow effect of the boundary layer. In the extremes cases, this term would becomes 1 for a very thin optical wall layer, and 0.65 when optical layer is thick. η_r takes the form:

$$\eta_r = 0.86 - 0.14 \ arctan \left(\frac{\rho_s}{2.6} - 1.6 \right) \qquad \text{Eq. 2.30}$$

This expression shows an asymptotical shape on the value 0.65, i.e., for dense wall layer only 65% of the energy emitted by radiation will be seen by the wall.

Cheng and co-workers (2007) reviewed numerous measured heat transfer coefficients in large fluidized beds. They measured heat transfer in a 12 MWe, 50 MWe and 135 MWe CFB boilers and observed again the high dependence of these values with the solids concentration in the riser, and in different zones of the boiler, such as the cyclone, and the economizer. They confirmed that it is mainly influenced by solid suspension density and furnace temperature. They stated following a correlation in the form of:

$$h = K \rho_s^{\alpha} T_s^{\beta} \qquad \text{Eq. 2.31}$$

Being K, α and β regression coefficients, which are not specified in the paper. They proposed this expression because in the review of large CFB most of expressions for

prediction heat transfer coefficients were in the form of Eq. 2.28, and they stated that temperature had a remarkable influence and must be included in the correlation.

Recently, Krzywanski and co-workers (2010b; 2010a) applied the model developed for the 670 t/h CFB boiler operated in Turow Power Station in Poland. They calculated the heat transfer coefficients in the dilute zone, by the expression:

$$h = \frac{h_1}{1 + \varepsilon_f h_1} \qquad \text{Eq. 2.32}$$

$$h_1 = \xi\left(h_{conv} + h_r\right) \qquad \text{Eq. 2.33}$$

Where ε_f is a fouling coefficient ranging from 0.001-0.003 and ξ is around 0.85, representing the non-uniform flow near the heat transfer surface.

$$h_{conv} = 0.214 \frac{k}{D_{eq}}\left[\left(\frac{uD_{eq}}{v}\right)^{0.8} - 100\right] Pr^{0.4}\left[1 + \left(\frac{D_{eq}}{H_{mw}}\right)^{0.67}\right] \qquad \text{Eq. 2.34}$$

$$h_r = \sigma \frac{h_w + 1}{2} h_s T_g^3 \frac{1 - \left(\frac{T_w}{T_g}\right)^4}{1 - \frac{T_w}{T_g}} \qquad \text{Eq. 2.35}$$

α_s the emissivity of the gas-solid phase was calculated as the absorptivity of a path *s* through the gas-particle suspension expressed by Bouguer's law:

$$h_s = 1 - e^{-\kappa s} \qquad \text{Eq. 2.36}$$

Where

$$\kappa = \frac{1.5\rho_B}{\rho_p d_p} \qquad \text{Eq. 2.37}$$

$$s = \frac{3.6V_{furnace}}{A_w} \qquad \text{Eq. 2.38}$$

Comparison of both, the method by Breitholtz et al. and Krzywanski et al. is represented in Figure 2.5. In Figure 2.5a) it can be observed that estimated values of total heat transfer coefficient from the two approaches are closer for higher solids density in the riser. The model used by Krywanski gives very low values for small solids densities.

Looking at the estimated values for radiative heat transfer, Figure 2.5b), in the model of Krzywanski et al. they tend to zero for very low solids concentration, due to the form of Eq. 2.13. The influence of particle densities shows opposite behavior in the approach by Breitholtz et al. Denser riser leads to denser wall layer and the shadow effect to the heat transfer surfaces increases, and thus, heat transfer by radiation decreases. This is not the case of the expression used by Krzywanski et al. since the term for suspension absorptivity makes denser medium leading more intense radiation. The influence of the radiation path thickness is shown to influence remarkably on the estimation of the radiation. This term is not considered by Breitholtz et al. but the empirical term of radiation efficiency allows taking density of wall layer into account.

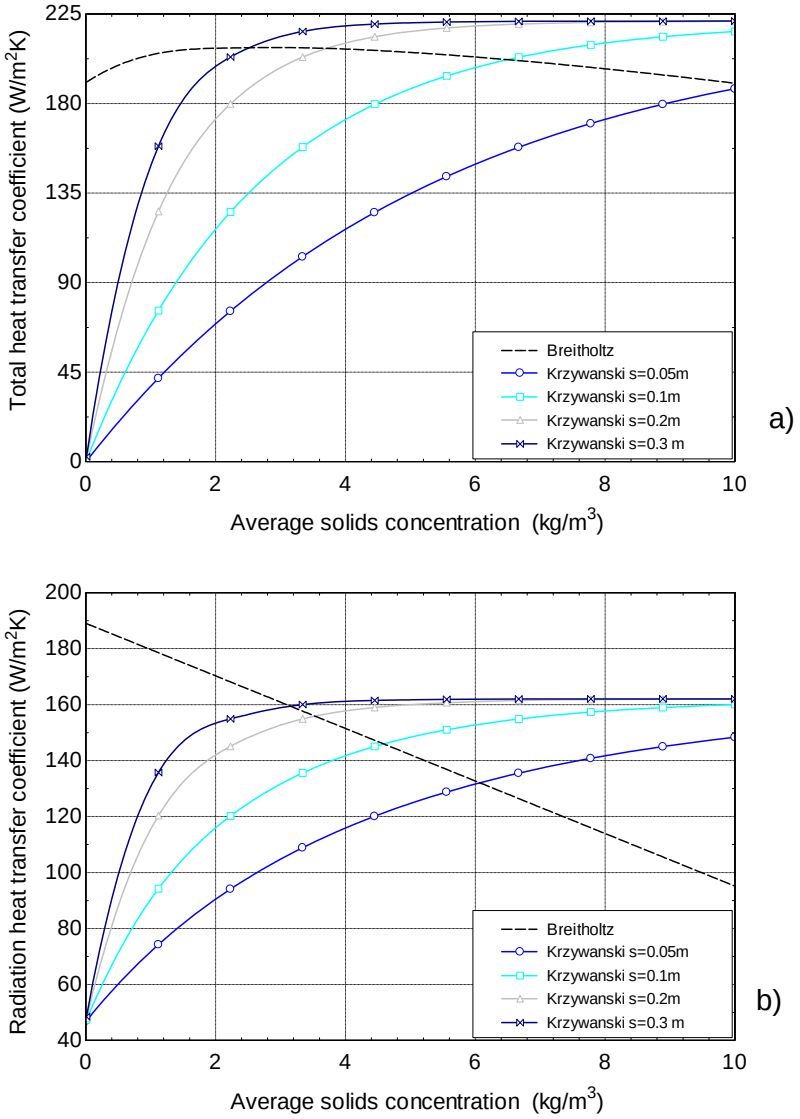

Figure 2.5. Dependence of the a) total and b) radiative heat transfer coefficient with the bed density according to Beritholtz and Leckner (1997) and Krzywansky et al. (2010b) for different radiating layer thickness, s

In none of the aforementioned models, radiative gas properties influence appreciably the radiative heat transfer coefficient. This is not the case for heat transfer in pulverized coal boilers, where radiation from the flame through the gas is the dominant heat transfer mechanism.

It is generally assumed that heat transfer under oxy-fuel combustion conditions behaves similarly to air-firing conditions, i.e. main parameters influencing heat transfer such as bed temperature, particles concentration, particles diameter or gas velocity affects heat transfer the same way as it does under oxy-fuel conditions. However, there are no experimental published data about this issue and models available in the literature takes the same models used for air-combustion.

2.3 THE OXY-FUEL CFB MODEL

The overall model for the OF in CFB has been sub-divided into three non-independent modules that interact with each other as shown in Figure 2.2: i) solids fluid-dynamics, ii) combustion and iii) energy balance. The sequence of sub-models arranged for CFB modelling is represented in Figure 2.6. Main initial considerations are following explained, for understanding the significant operational factors that would determine the overall CFB behaviour.

- *Fuel input and fuel characteristics*: Thermal power input is determined by fuel rate and by its composition and heating value. These parameters allow calculation of stoichiometric O_2 needed plus certain excess for assuring proper combustion. In the case of air combustion, an air-excess around 20% is generally accepted to reach around 3-6 % O_2 in flue gases. Similar oxygen contents in flue gas have been considered in the OF simulations. In any case, the fuel thermal input imposes the amount of oxidant flow.
- *Inert matter properties*: Main fluidization parameters such as fluidization velocity or terminal velocity are determined by the particle density of the bed material and particles size distribution, among other factors. A solids inventory consisting of particles with a diamter of 200 µm and a density of 2500 kg/m^3 (Geldart B type) has been assumed.
- *Boiler geometry*. The amount of gas entering the boiler and the boiler cross sectional area will settle the fluidization velocity and thus, how solids will

be distributed along the riser. Secondary gas inlet is located at 5 m height from the distributor.

- *Pressure drop along the combustor*: This parameter is easily measured with conventional pressure taps and bottom bed height can be estimated. Values around 9000-12000 Pa have been considered as average range on conventional air firing boilers. Thus, the pressure drop limits the height of the lower dense region (Yang et al., 2005; Redemann et al., 2009; Lu et al., 2010)

The first sub-module in the programme aims to estimate the solids concentration profile for certain fuel input, boiler geometry and pressure drop across the boiler. It calculates fluid-dynamics in the dense and in the transport zones, such as void fraction, gas velocity and wall layer thickness at every height. For estimating gas properties, temperature profile must be an input that will be calculated in the energy balance sub-model.

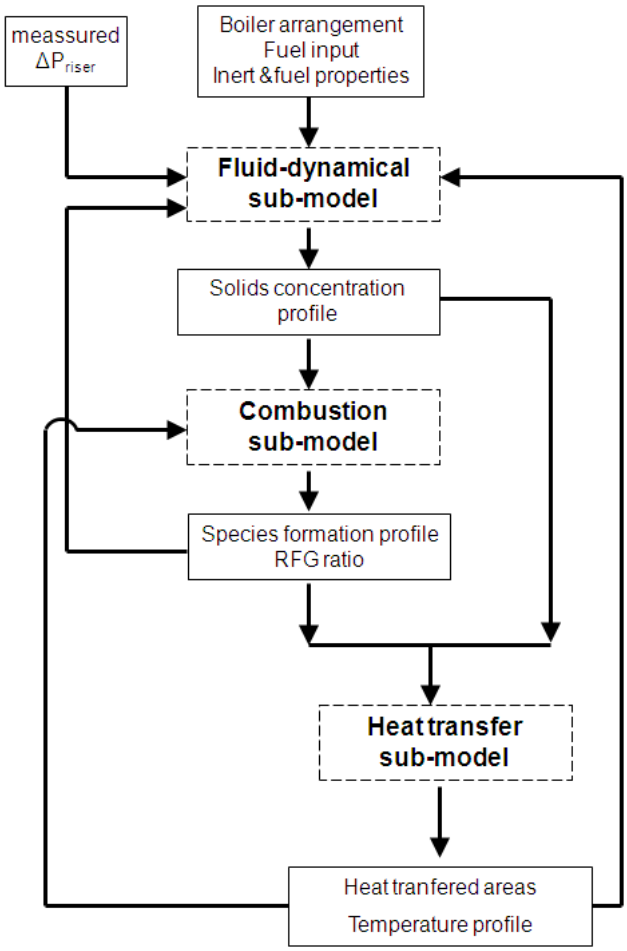

Figure 2.6. CFB model flow-chart

The combustion module calculates the main formed species based on disperse and cluster phases present at each cell. Temperature must be also an input for estimating if calcination of limestone takes place before sulfation, according to Eq. 2.22.

Finally, the energy balance sub-module will carry out the energy balance cell by cell, according to the combustion, heating of gases, heat carried by the solids and cooling at each height.

In Figure 2.7 it has been graphically represented the processes taking place in each part of the control volume considered in this model. Black arrows represent the flux of solids, modeled by the fluid-dynamic module, where primary and secondary gas are the inlets, so as the boiler geometry and pressure drop. Red circle arrows represent the heat of reactions. As can be seen, combustion in the loop-seal was not considered. During air firing combustion, unburnt fine particles are likely to be burnt by the O_2 present in the fluidizing gas. However, O_2 in the fluidizing gas of the EHE will be avoided, for economical reasons.

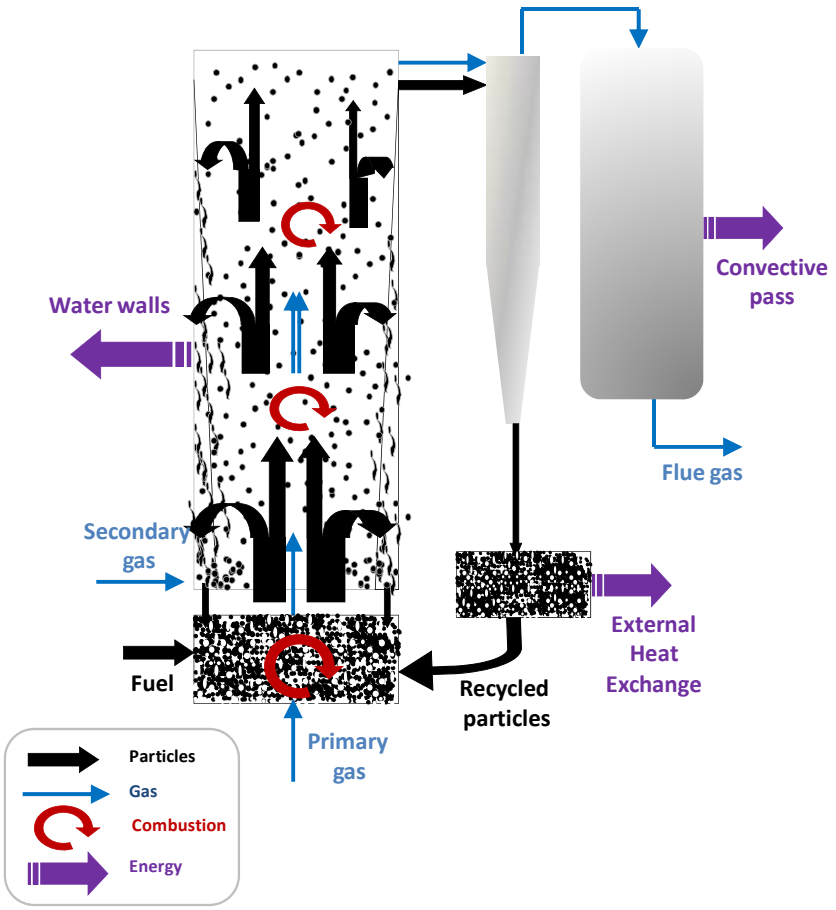

Figure 2.7. CFB boiler mass and energy balance scheme

2.3.1 FLUID-DYNAMICS SIMULATION

The fluid-dynamics simulation sequence is represented in Figure 2.8. Input parameters are:

1. Fuel input. During AF, this is given by the fuel input considered and so, by the stoichiometric O_2 required for combustion, plus a certain excess, for assuring adequate efficiency of combustion. For OF case, a higher O_2 concentration allows to introduce higher fuel inputs for a certain fluidizing velocity. Thus, the fuel feeding rate sets the volumetric flow of gases entering into the boiler.
2. The secondary gas ratio. Although it is evident that in real boilers there are several secondary air entrances, for the scope of this model, one secondary gas inlet is considered. By calculating the volumetric inlet gas required, together with the secondary gas ratio, the primary gas is calculated and then, the fluidizing velocity at the entrance of the distributor plate.
3. The pressure drop along the riser. In many simulations found in the literature, the entrained solids flow, Gs, and the dense bed height are estimated using semi-empirical expressions. However, in the current model, it has been considered that in a real boiler, certain pressure drop along the boiler can always be measured and reasonable values for these parameters are generally known. Thus, riser pressure drop will be an input parameter for the model
4. The model is developed using monosize inner matter particles and thus, no attrition is included.

Main assumptions used in the fluid-dynamical module are:

i. The bed is divided into two zones, the bottom dense bed and the transport zone
ii. Core-annulus structure is assumed in the transport zone
iii. Two-phase theory is used for calculating properties in the dense phase, according to Eq. 2.13.
iv. Dilute and cluster phases are considered for calculating the distribution of solids along the riser, Eq. 2.16
v. PSD has not been included, and particles are considered monosize, with a average particle diameter of 200 microns

vi. Density of inert matter is 2500 kg/m^3

vii. Wall thickness have been estimated using Eq. 2.19 and Eq. 2.20

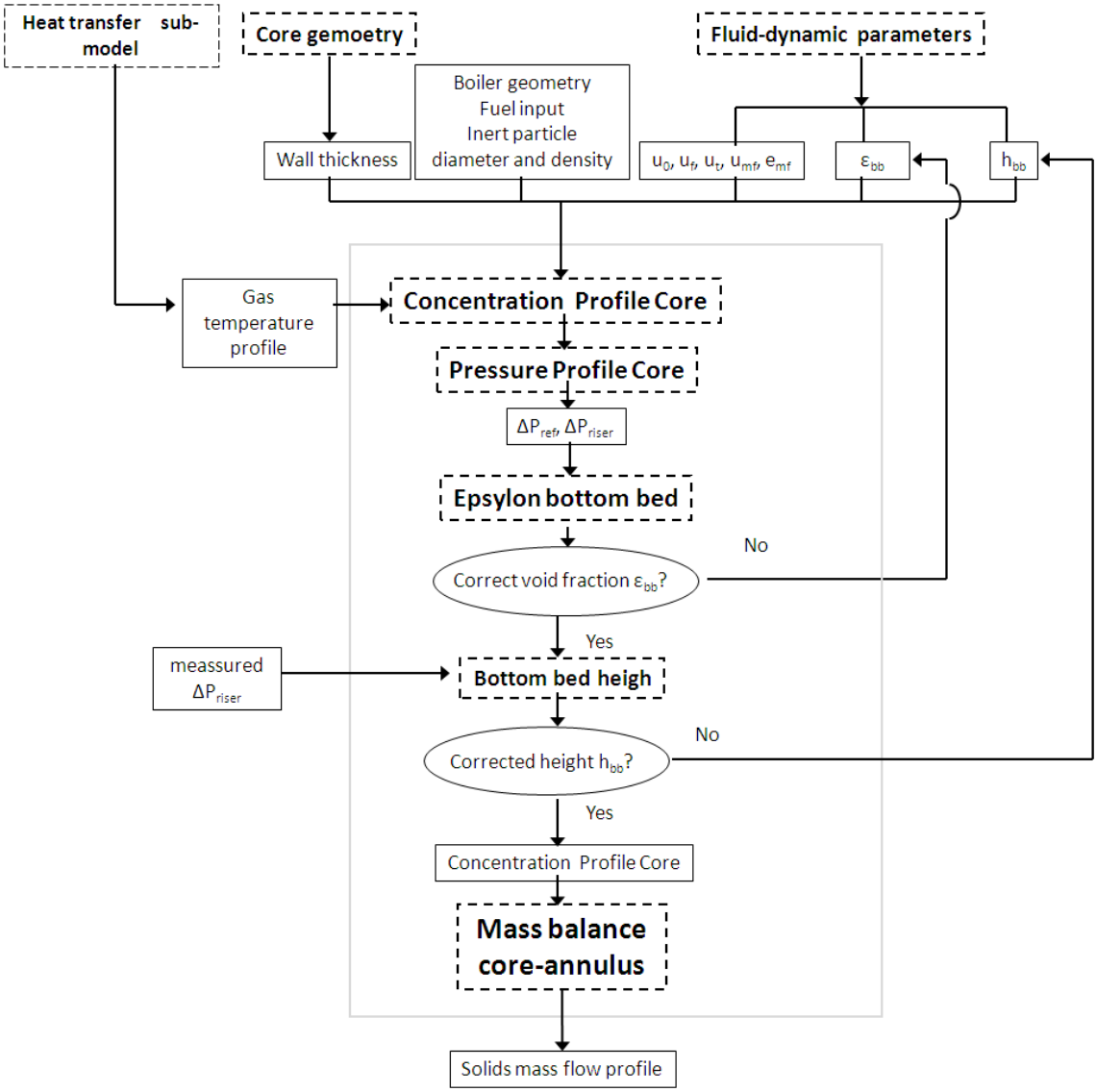

Figure 2.8. CFB fluid-dynamics modeling flow-chart

Minimum fluidization velocity, u_{mf}, minimum fluidization void fraction, ε_{mf}, and terminal velocity, u_t. were calculated using by Wen and Yu correlation (Wen and Yu, 1966):

$$Re_{mf} = \sqrt{C_1^2 + C_2 Ar} - C_1 \qquad \text{Eq. 2.39}$$

$$Re_{mf} = \frac{\rho_g \cdot u_{mf} \cdot d_p}{\mu_g} \quad \text{Eq. 2.40}$$

where C_1=27.2 and C_2=0.0408. And for minimum fluidization void fraction, Ergun correlation was solved (Ergun and Orning, 1949):

$$\frac{1.75}{\varepsilon_{mf}^3 \varphi_s} Re_{mf}^2 + \frac{150(1-\varepsilon_{mf})}{\varepsilon_{mf}^2 \varphi_s^2} Re_{mf} = Ar \quad \text{Eq. 2.41}$$

Bottom bed voidage, so as bubble properties were estimated with Eq. 2.4 –2.9 and Eq. 2.13 – 2.16. Wall layer thickness followed Eq. 2.18 –2.20.

The solids concentration along the riser considered the contribution of the cluster and dilute phase, Eq. 2.16, being the decay constants:

$$a(h) = 4\frac{u_t}{u(z)} \quad \text{Eq. 2.42}$$

$$K(h) = \frac{0.23}{u(z) - u_t} \quad \text{Eq. 2.43}$$

The decay constants depend on the gas velocity in riser. This velocity could vary if boiler geometry does, so as with secondary gas injection. And also, the temperature profile and the gas composition will vary gas velocity with the height of the riser.

Knowing the solids profile along the boiler, pressure drop profile is calculated:

$$\Delta P_{riser}(h) = \rho_{core}(h) g z \quad \text{Eq. 2.44}$$

From this calculation, ΔP_{ref} is re-calculated and used for the iterations of the bottom bed voidage. For estimating the height of the dense zone, pressure drop measurements must be compared with the calculated pressure drop and so, by interpolation, a new h_{bb} is calculated and introduced in the sequence again.

Once the core solids concentration profile is calculated, the solids up-flow in the core region, m_{core}, becomes:

$$m_{core}(z) = \rho_{core}(z) A_{transv\_core}(z) u_{slip}(z) \quad \text{Eq. 2.45}$$

Being the slip velocity:

$$u_{slip}(z) = u(z) - u_t(z) \quad \text{Eq. 2.46}$$

Up-raising solids decrease with boiler height, because some are transferred to the wall and falls down contributing to create the downward flow of solids in the so-called annulus. Thus:

$$m_{lat}(z) = m_{core}(z) - m_{core}(z+dz) \qquad \text{Eq. 2.47}$$

$$m_{wall}(z) = m_{wall}(z+dz) + m_{lat}(z) \qquad \text{Eq. 2.48}$$

The exponential decrease of solids with height, explained for solids concentration profile, was, in fact, experimentally verified for the solids mass flow. Application of Eq. 2.47 and Eq. 2.48 implied then these intrinsic assumptions:

- no dependency of velocity with height
- no dependency of core cross sectional area with height

With the aim of compensating mistakes dragged by these assumptions an additional term is included in the concentration profile expression:

$$\rho_{core}(z) = \left(\rho_{disp}(z) + \rho_{cluster}(z)\right)\frac{u_{slip_{BB}}}{u_{slip}}\frac{A_{core_{BB}}}{A_{core}} \qquad \text{Eq. 2.49}$$

This fluidynamics modeling calculates the solids density distribution along the whole boiler height and thus, also, the elutriated solids and the density and thickness of the wall layer of particles. This sequence must be up-dated with the values obtained from the combustion modeling, to account for the gas composition, and from the heat transfer modeling, to account for the temperature at every height.

2.3.2 COMBUSTION SIMULATION

Combustion modeling sequence is represented in Figure 2.9. Results from the fluid-dynamics module are the main inputs of this module. Coal proximate and ultimate analysis are needed, on the one hand for calculating the volatile composition and also, for setting-up the carbon combustion at each height. As seen in Figure 2.9 the temperature profile from the energy balance module is also an input. This input will be applied for determining the mechanism of SO_2 capture according to Eq. 2.22.

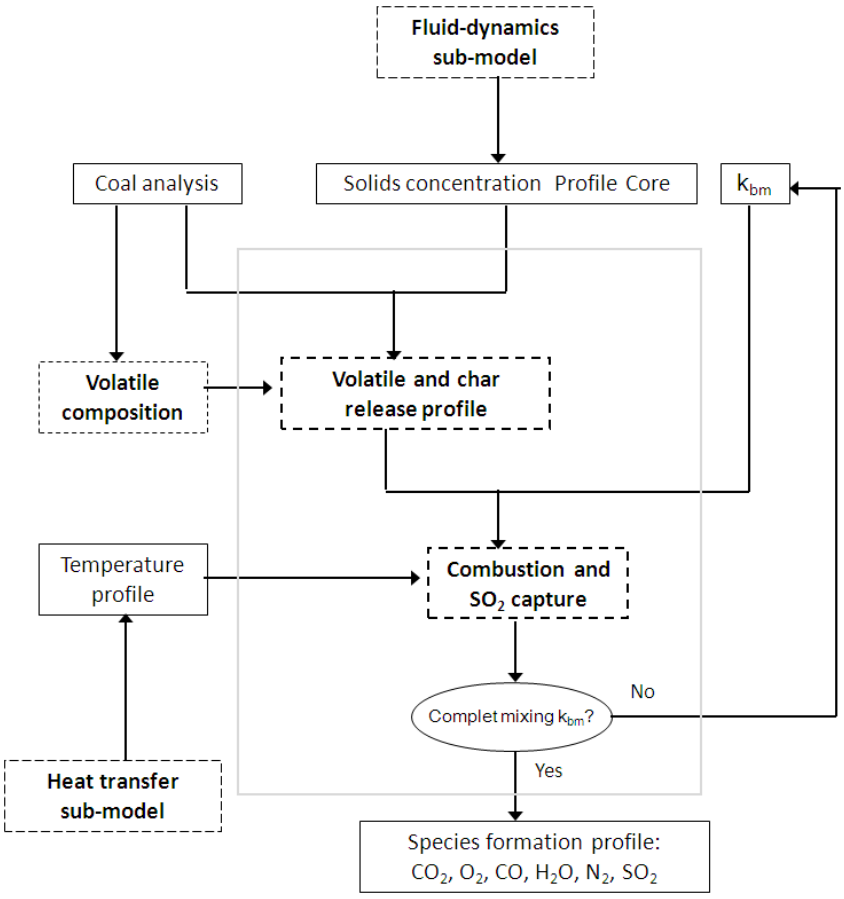

Figure 2.9. CFB combustion modeling flow-chart

	Spanish lignite	**Central Europe Antrhacite**
ANALYSIS DATE	22/02/2010	03/11/2010
HHV (Kcal/kg)	3420	7124
INMEDIATE		
Moisture	19,98%	2,04%
Volatile	23,81%	17,10%
Fixed C	28,15%	68,82%
Ash	28,05%	12,04%
ELEMENTAL		
C	37,52%	75,86%
S	6,16%	0,38%
H	3,77%	3,44%
N	0,26%	1,95%
O	24,24%	6,33%

Table 2.4. Coal composition used in the simulations

Volatile content in coal was considered as a coal property. Volatile composition was not known and needed to be estimated. Firstly, the methodology used by Thurman et al. (Thunman et al., 2001) was applied on two different coals considered for simulations: Spanish lignite and anthracite from Central Europe. Both coals compositions are shown in Table 2.4.

Calculations of volatile composition are based on the mass balance of O, H and volatile C, yielding CO_2, CO, H_2, H_2O and CH_4. This composition is also assumed by Hannes et al. (1995). Volatile heating value can be estimated from the balance:

$$LHV_{volatile} = LHV_{fuel} - (LHV_{drying} + LHV_{devolatilization} + LHV_{char}) \qquad \text{Eq. 2.50}$$

Mass and energy balance of volatile compounds gives a degree of freedom that could be solved by iteration. Energy for water vaporization and devolatilization is small compared with the rest of terms, so approximation values have been considered:

LHV_{drying} = 2253 kJ/kg

$LHV_{devolatilization}$ = 300 kJ/kg

Hence, equations system yields:

$$x\,C = \alpha CO_2 + \beta\,CO + \gamma CH_4$$

$$y\,H = \delta/2\,H_2O + \gamma/4\,CH_4 + \varepsilon/2\,H_2$$

$$z\,O = \alpha/2\;CO_2 + \beta CO + \delta H_2O$$

$$\beta\,\Delta H_{CO} + \gamma\,\Delta H_{CH4} + \varepsilon\,\Delta H_{H2} = LHV_{volatile}$$

This system has five unknown variables and four equations. The variables α, β, γ, δ and ε, are the molar rate of each component. The way of solving would be giving values to one of the unknowns. The system would look like:

$$\begin{bmatrix} 1 & 1 & 1 & 0 \\ 0 & 0 & 1/4 & 1/2 \\ 1 & 1/2 & 0 & 0 \\ \Delta H_{CO} & 0 & \Delta H_{CH4} & \Delta H_{H2} \end{bmatrix} \begin{bmatrix} \alpha \\ \beta \\ \gamma \\ \varepsilon \end{bmatrix} = \begin{bmatrix} x \\ y - \delta/2 \\ z - \delta \\ LHV_{volatile} \end{bmatrix} \qquad \text{Eq. 2.51}$$

Applying this methodology to the aforementioned coals found no convergence. Then, they were also included other components to the calculations, such as C_6H_6,

C_2H_6, C_2H_4 and C_2H_2. In none of the runs convergence on the volatile composition was reached. In the Figure 2.10, some of the simulations are shown: In Figure 2.10a), the basics components and in Figure 2.10b), C_6H_6 is added.

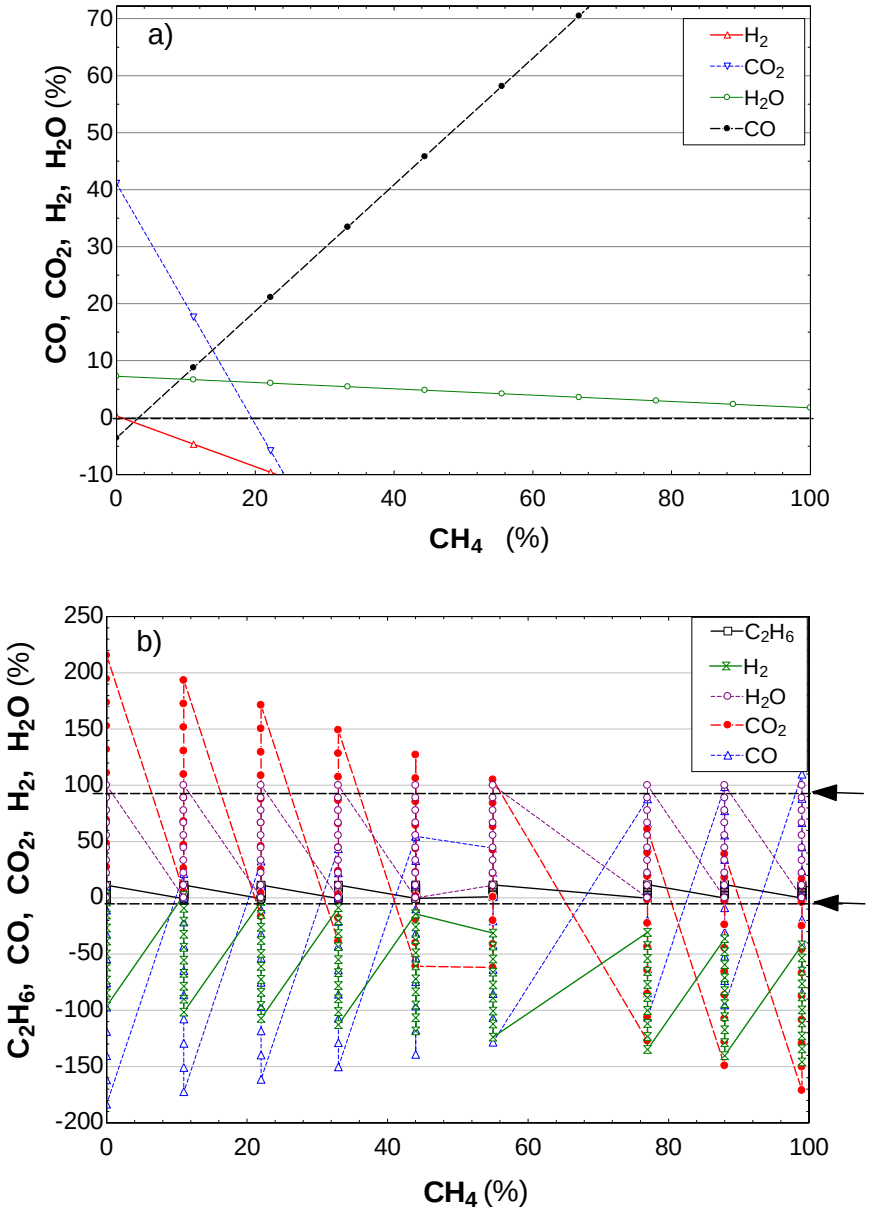

Figure 2.10. Simulations results of non-convergence of applying volatile composition methodology, considering. a) CO_2, CO, H_2, H_2O and CH_4; b) CO_2, CO, H_2, H_2O, CH_4 and C_6H_6

There is no point in which all parameters are above zero and below 100%, so no feasible solution is possible considering these compounds. The same occurred when adding other compounds to the iterations of Eq. 2.51. Possible causes of this lack of convergence could be that this methodology was developed for biomass fuel, with a higher volatile content than coal. An alternate possibility of estimating volatile

composition is by looking at the literature coal composition analysis. Hence, energy balance is compromised, by not fulfilling the heating value of the volatile part.

This leaded to adopt a simpler way of considering volatile composition that fulfilled the energy balance, by compromising accuracy in the mass balance, since the simulation was focused on looking at the overall system energy balance and minimum deviation in species formation could be neglected. Thus, all volatile carbon would yield CO_2. To complete the volatile heating value $LHV_{volatile}$, part of hydrogen would produce H_2 and the rest would be released in the form of H_2O and NH_3.

Once volatile composition is estimated, these compounds are released and burnt quickly, before fixed carbon. Volatile and moisture are released proportionally to the accumulated solids in the dense phase and to the cluster phase solids in the riser. This is in accordance with the assumption made by numerous authors of considering volatile combustion taking place completely in the dense zone of the boiler (Basu, 1999; Gungor, 2009) . In every cell volatile matter is oxidized before char, if oxygen is available. This means that volatile combustion is instantaneous and controlled by the devolatilization rate, as explained by Oka (2003).

Char is released proportionally to the accumulated solids in the dense phase and to the cluster phase plus the disperse phase solids in the riser. This agrees with the concept that elutriated fine char particles can burn along the riser. These fuel particles find an oxygen enriched zone after the secondary air injection. Un-burnt char particles that found reducing atmosphere in the dense phase during volatile combustion will have time to be in contact with oxidant before the exit zone.

Below secondary gas is injection, a reducing conditions zone can appear. This is because volatile combustion can consume the primary oxygen before the secondary gas is fed. In practice, the good back-mixing of gas and solids in the fluidized bed, allows oxygen from the secondary injection point encountering un-burnt carbon. For taking into account this good back-mixing of gas and solids, that ideally avoids un-burnt matter, a new parameter is considered. The back-mixing parameter, k_{bm} is applied to char and volatile matter in the oxidizing conditions areas, so that the result is a complete conversion of char. This is graphically represented in the Figure 2.11.

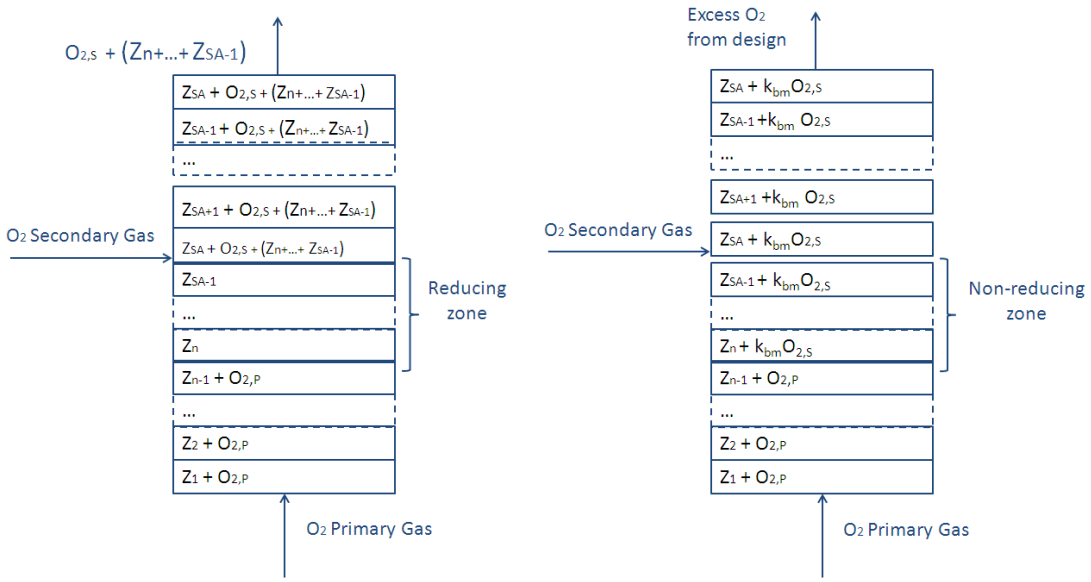

Figure 2.11. Scheme of applying back-mixing parameter, k_{bm}. Z being the char in each cell

In the left hand side of the Figure 2.11 O_2 from primary air is consumed before the secondary air is fed. Thus, it appears a region of reducing conditions. In the right hand side, the secondary air contact also with the unburned fuel below the feeding point, thanks to the application of the back-mixing parameter, k_{bm}.

Using the temperature profile input, from the energy-balance module, allows to estimate the equilibrium CO_2 partial pressure of the calcination-carbonation reaction, as expressed in Eq. 2.22. This value is compared with the CO_2 partial pressure at each height. Thus, it is possible to estimate if calcination is taking place or limestone is sulfated directly through the one-step reaction. Values of CO_2 partial pressure over this value, lead to calcination conditions. If P_{eq} values are higher than CO_2 partial pressure, direct sulfation would take place. Together with the efficiency values for each case, SO_2 emissions and CaO formation is calculated along the riser. S conversion to SO_2 occurs after volatile released and combustion. Efficiency values of 80% and 95% have been applied for direct and indirect desulfurization respectively. These values were experimentally obtained in Bolea et al. (Bolea et al., 2012a)

2.3.3 ENERGY BALANCE

The CFB system must fulfill the overall energy balance as shown in Figure 2.12. Fuel input and gas, together with the recycled solids from the loop-seal are the global entrances of the energy balance system. Heat transfer to walls, to the convective pass and to the external heat exchanger, must ideally complete the overall energy balance.

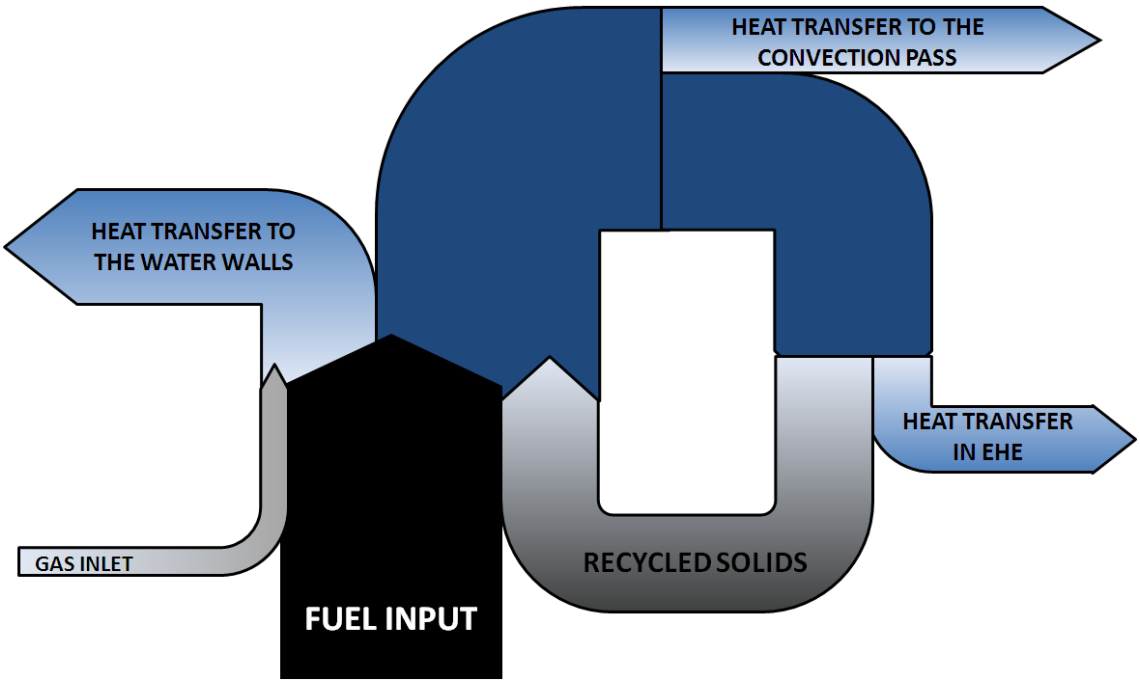

Figure 2.12. Sankey diagram of the CFB

Programming sequence begins then from bottom dense bed. Inputs are the temperature of this zone, primary gas and fuel entering the furnace. Also solids recirculation rate from the fluid-dynamical sub-model is needed. In this zone, combustion takes place as calculated in the combustion sub-model. An initial temperature for recycled solids is assumed. Another required initial value is a temperature value for solids falling down by the walls. Thus, temperature of elutriated particles is the input for energy balance of first cell in dilute zone. Energy balance of each cell in the core makes a first temperature profile for core cells. From the last core cell, energy balance to the annulus cell starts. When energy balance of wall cells takes place in the first wall cell, energy balance in the dense zone is actualized. Bed temperature profile is obtained by the energy balance applied to every cell. The programming sequence is represented in Figure 2.13:

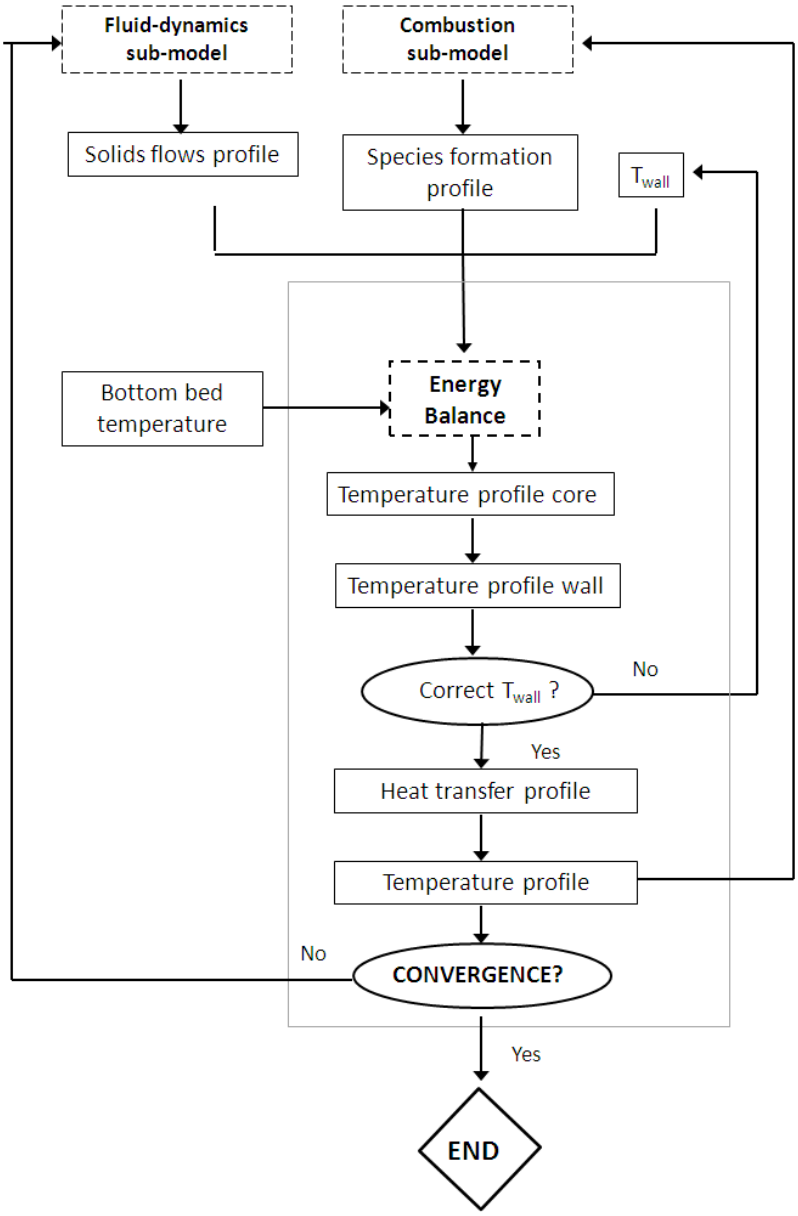

Figure 2.13. CFB energy balance modeling flow-chart

In Figure 2.13 represents how the temperature profile from this sub-model is introduced again in the combustion sub-model, and reaches the convergence by iterative process. This temperature is used for calculating equilibrium CO_2 partial pressure profile and so, estimating if direct or indirect sulfation conditions are taking place.

Dense zone and dilute zone are treated differently. The schemes of energy balance in both zones are represented in Figure 2.14 and Figure 2.15.

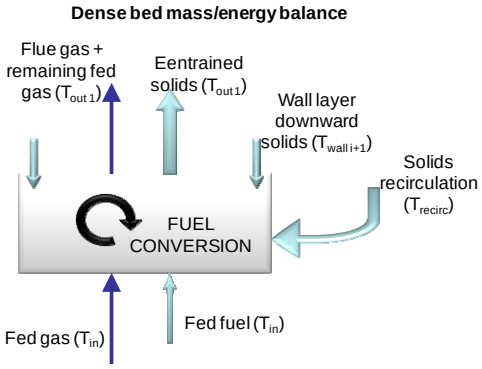

Figure 2.14. Energy balance scheme in the dense zone of the CFB

The dense zone is considered isothermal and no heat transfer surfaces are present in this zone, i.e. a constant temperature along bottom bed zone is assumed. This assumption is common in numerous models in the literature (Table 2.1). The intense fuel mixing of this area, together with high solids density and their high thermal capacity make this assumption fair enough.

Thus, the dense zone energy balance is treated as a whole, following the expression:

$$Cp_S\left(m_{RS}T_{RS}+m_{Wall,1}T_{Wall,1}-m_{Core,1}T_{bb}\right)+\left(m_{g,In}E\left(T_{g,in}\right)-m_{g,Out}\Big|_{bb}E\left(T_{bb}\right)\right)=\ldots$$
$$\ldots=Q_{comb,VOL}\Big|_{bb}+Q_{comb,CHAR}\Big|_{bb} \qquad \text{Eq. 2.52}$$

Right hand side of Eq. 2.52 is the combustion energy from the char and volatile reactions. This energy is invested in heating up the gaseous oxidant stream $m_{g,in}$, the solids from the recycled pipe, m_{RS} and the solids falling from the wall layer of particles, m_{Wall}. The output gaseous and solid flows are the elutriated solids to the transport zone, m_{Core}, and the resulting flue gas with the remaining oxidant, $m_{g,Out}$, respectively.

The energy balance in the dilute zone is divided into the core cells and the wall layer cells. The energy balance for each core cell is:

$$Cp_S\left(m_{Core,in,}\Big|_i T_{i-1}-m_{core,out,}\Big|_i T_i-m_{lat,}\Big|_i T_i\right)+\left(m_{gas,in,}\Big|_i E\left(T_{i-1}\right)-m_{gas,out,}\Big|_i E\left(T_i\right)\right)=$$
$$=Q_{comb,VOL}\Big|_i+Q_{comb,CHAR}\Big|_i-Q_{HT}\Big|_{core\rightarrow wall} \qquad \text{Eq. 2.53}$$

Volatile and char combustion heats up the solid and gaseous streams arriving at the cell, $m_{Core,in}$, $m_{gas,in}$, and leaving the cell, $m_{core,out}$, m_{lat} and $m_{gas,out}$ and heat is also transferred to the wall layer, $Q_{HT|core\rightarrow wall}$.

The energy balance of a wall layer cell is then:

$$Cp_S\left(m_{Wall,in,}\Big|_i T_{i+1} - m_{Wall,out,}\Big|_i T_i + m_{lat,}\Big|_i T_i\right) = Q_{HT}\Big|_{core\rightarrow wall} - Q_{HT}\Big|_{wall\rightarrow surface} \qquad \text{Eq. 2.54}$$

In the wall layer no combustion reaction is considered, and energy entering with the falling solids, $m_{Wall,in}$, and solids from the core, m_{lat}, together with the heat from the core cell, $Q_{HT|core\rightarrow wall}$, is transfer to the heat exchange surface $Q_{HT|wall\rightarrow surface}$ and to the falling solids, $m_{Wall,out}$.

The model by Breitholtz et al. (2001) shown in Eq. 2.29 was implemented to estimate heat transfer to the walls. Energy is transferred with the solids to the wall layer, according to the mass balance and the core temperature. The radiation from the core to the wall is calculated with Eq. 2.25. Heat transferred by radiation is not straight received by the walls. Instead, the core heats up the falling solids. The radiation efficiency of Eq. 2.30 is included, since high solids density is expected in oxy-fuel combustion, and thus, denser wall layer will increase the shadow effect to the radiation from the core. This could be clearer understood in Figure 2.15

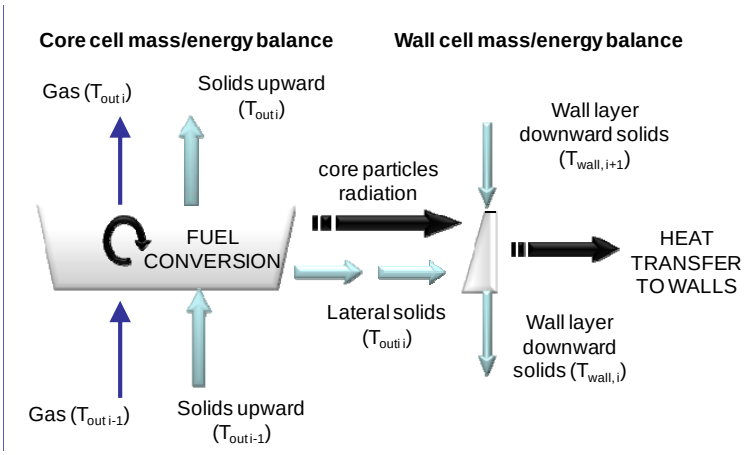

Figure 2.15. Energy balance scheme in a cell of the dilute zone of the CF

Once the integration of the three sub-models, fluidynamics, combustion and energy balance, converges, we obtain the temperature, pressure, gas composition and solids density at every height along the boiler. The results drawn from the model must be now compared to real values, in order to confirm the model validity and so, to enable to be used as a reliable tool to establish the implications of oxy-fuel combustion in large oxy-fuel CFB boilers.

2.4 MODEL VALIDATION

2.4.1 AIR FIRING

In spite of the scarce published data on commercial and large-scale fluidized bed boilers, some published measurements could be useful for confirming the model feasibility and reliability:

Published data	Author
Pressure drop profile	Yang et al. (2005)
Flue gas composition	Lee and Kim (1999)
Temperature profile	Hannaes et al. (1995)

The measurements published by Yang et al. (2005) has been taken as a reference for comparing pressure drop along the boiler. The 135We CFB boiler, located at Zibo power station was 38 m height, and the cross section was 6.6 x 13.1 m^2. They specified the coal used in the plant, that contained 45.39% of fixed carbon, 4.44% moisture and 16.73% of volatile matter. The heating value was 21060 kJ/kg. Some of the operation conditions at which measurements were taken were indicated. A temperature of 885ºC in one case and 896ºC in the other was average along the riser. Elutriated solids were 5.79 and 6.50 kg/m^2s respectively. With these inputs, comparison of measurements and model are shown in Figure 2.16.

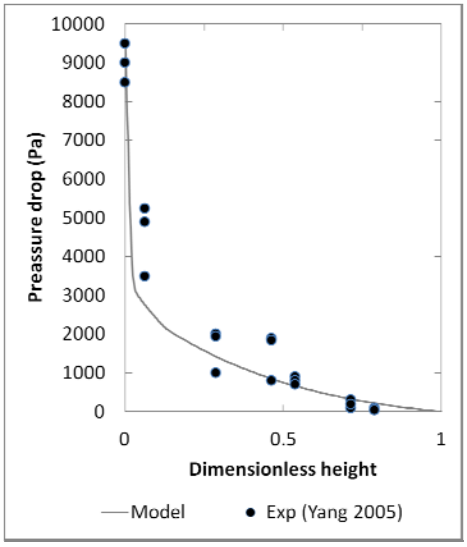

Figure 2.16. Comparison of model pressure profile prediction with the one reported in Yang et al. (2005)

From the Figure 2.16 it can be confirmed that realistic values of pressure drop profile are drawn from the model.

For main gas species concentration in the boiler, emissions of CO_2 and O_2, are reported by Lee and Kim (1999) and Hannaes et al. (1995), for a 200 and 120 MW boiler respectively. The former was a 32 m height CFB with a cross section of 19 m 7m. The coal used is a Korean Anthracite with 53.7% fixed carbon and only 4% of volatile matter and 3.3% moisture. Average temperature was 900ºC. Entering said parameters, comparison results are shown in Figure 2.17.

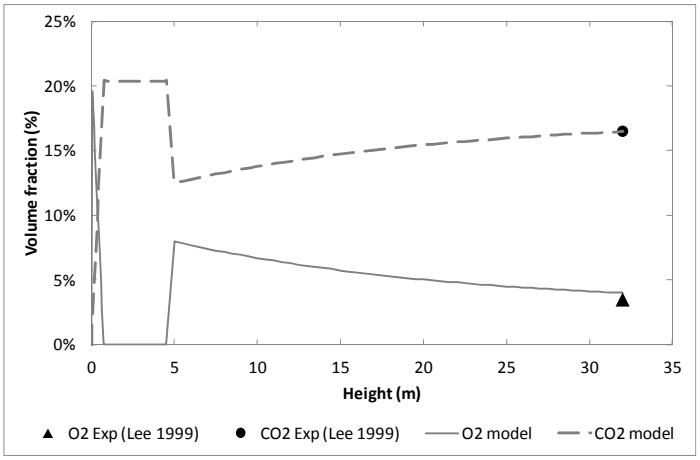

Figure 2.17. Comparison of flue gas composition prediction with the one reported in Lee and Kim (1999)

Figure 2.17 cannot be considered a proper validation, since measurements of the gas composition along the height of the riser were not available and the deviation of CO_2 and O_2 results is usually small, even for the simplest modelling approach. Even though, the common available data from real boilers are taken at the flue gas outlet. Figure 2.17 is also interesting for showing the estimated CO_2 and O_2 profile by the model. It shows the reducing zone commented in the section 2.3.2 and it can be also distinguished that most of the combustion reactions take place in the lower zone of the boiler.

Temperature profile measurements in a 120 MW boiler was reported by Hannaes et al. (1995), for validating the IEA-CFB model. The boiler is 30 m height and 38 m^2 in cross section. However, they do not specify the coal used in the tests, so a bituminous coal was assumed, with a fix coal fraction of 63%, 5.7% moisture and 24% volatile, and 24450 kJ/kg as heating value.

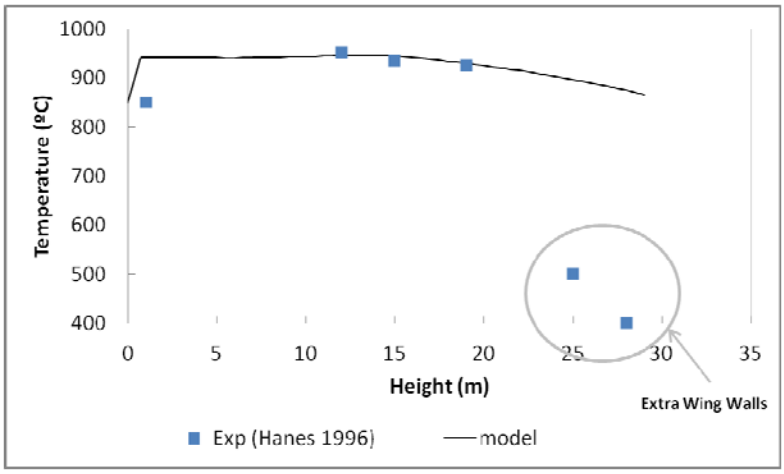

Figure 2.18. Comparison of the model temperature profile result with the one reported in Hannaes et al. (1995)

In Figure 2.18 the two highest thermocouples indicated a drastic decrease of temperature. The reason was the additional heat exchanger tubes located at this point. Solids at this location were then further cooled.

In general, the model developed in this work gives reliable results. It can be adapted to different input conditions, satisfactorily estimating the measurements from large scale boilers. More accurate predictions could be achieved, particularly with a more detailed combustion modelling. However, for the aim of this work, the model is more useful if it can be flexible for different configurations and inputs parameters.

2.4.2 OXY-FIRING

Since there is no available data from commercial CFB installations operating under oxy-firing conditions, the validation for these cases is based on a quantitative comparison of published simulations (Nsakala et al., 2004; Saastamoinen et al., 2006; Seddighi et al., 2010)

In order to validate the present model, heat transfer ratio per fuel input in the different heat transfer locations will be compared. Three main zones are distinguished in the the CFB system: furnace walls, including water walls and wing walls; external heat exchanger (EHE) in the loop-seals, for cooling down recycled particles before re-injected to the boiler; and the energy contained in the flue gas stream.

The models used for comparison are based on real boilers designs, so some of the operational parameters were not published. For example, no data about the fuel characteristics used for the simulations are given. The amount of elutriated solids is also unknown except for the simulation by Seddighi et al. (2010). These parameters that must be varied for adapting the present model results to the ones published, will give actually much valuable information about operation of the oxy-fuel commercial plant, as it will be later discussed.

The aim of the models is to reach a satisfactory temperature profile along the boiler. The optimum temperature for air-firing case was set between 850-900ºC in air-firing combustion for a proper combustion and optimum sulphur capture. Higher temperature than 900ºC is needed for having indirect sulphation (calcinations+sulphation) inside the boiler and so, higher SO_2 capture efficiencies.

Figure 2.19 illustrates a comparison between the heat transfer share results and the ones presented by Seddighi et al. (2010). Boiler size is 15 m wide, 6 m depth and 37 m height. As the boiler size remains unchanged, Figure 2.19 shows how thermal input varies from 257 to 900 MW with increasing oxygen concentration at inlet from air firing to 80% O_2.

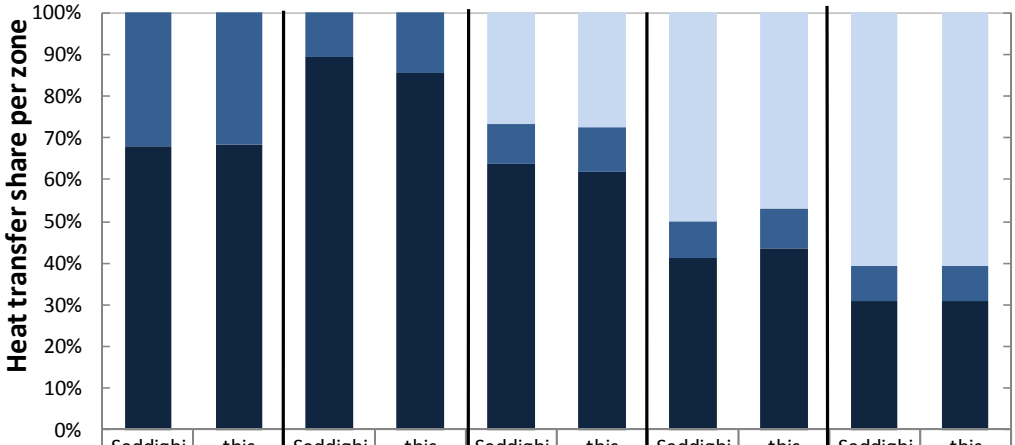

	Air		Oxy 24%		Oxy 40%		Oxy 60%		Oxy 80%	
	Seddighi et al.	this study	Seddighi et al.	this study	Seddighi et al.	this study	Seddighi et al.	this study	Seddighi et al.	this study
Rate Loop Seal	0.0%	0.0%	0.0%	0%	26.5%	27.5%	49.9%	47.0%	60.8%	60.8%
Rate Flue Gas	31.9%	31.5%	10.5%	14%	9.7%	10.5%	8.9%	9.6%	8.4%	8.3%
Rate Walls	67.8%	68.5%	89.5%	86%	63.9%	62.1%	41.3%	43.4%	30.8%	30.9%
Gs (kg/m2s)	1.9	2.4	1.9	7.8	5.2	7.0	14.8	14.2	24.2	22.4

Figure 2.19. Heat transfer share comparison of simulated results with those obtained by Seddighi et al. (2010)

According to Seddighi et al. (2010), solids recirculation flux, Gs, reaches values up to 25 kg/s·m^2 for the highest O_2 concentration case, as shown in Figure 2.19. For reaching the specified recycled solids, Gs, secondary air has been varied, between 12 to 40%. Although not specified, solids recirculation temperature has been estimated to be around 600ºC. This value fulfils the energy balance in the loop-seal, knowing recycled solids rate and considering their initial temperature around 850ºC, except for the highest O_2 concentration cases, 60% and 80% O_2, where bed temperature was around 900ºC.

These conditions of geometry and O_2 concentration are introduced in the model. A lignite coal has been considered as fuel, with a HHV of 14300 kJ/kg. As it can be observed, for air conditions and for oxy-fuel mode at 24% O_2, most of the heat is transferred along the bed riser (furnace walls and wing walls). No EHE is required, as in some boilers designs, because extra panels are located inside the furnace for increasing the heat exchange in this zone. While increasing O_2 concentration, less heat share is removed in the convective pass in OF mode due to reduction in flue gas rate. Increasing oxygen content, contribution of EHE heat transfer is strongly incremented, from 26.5% to 60.8% of the total fuel power input, due to higher solids to be cooled down before recirculation.

Although operational details of the simulations presented by Saastamoinen et al. (2006) and Nsakala et al (2004) are not published, the present model is able to fit their results adjusting the model input data, as shown in Figure 2.20. In simulation by Nsakala et al. combustor cross-sectional size for oxy-firing modelling is reduced down to 30% from the air case size, which means a reduction from 128 to 38 m^2 of cross sectional area. They considered 543 MW for AF mode and 529 MW for OF with 70% O_2 fed gases.

For air-firing, Saastamoinen et al. (2006) considered the boiler was 9.4 m x 20.3 m cross section and 40.8 m height for 649 MW thermal power output and 5.3 m x 12.5 m x 45 m and 617 MW for feeding gases with 60% O_2 concentration.

Developed simulation is able to reproduce the location of heat transfer in both cases with said input parameters.

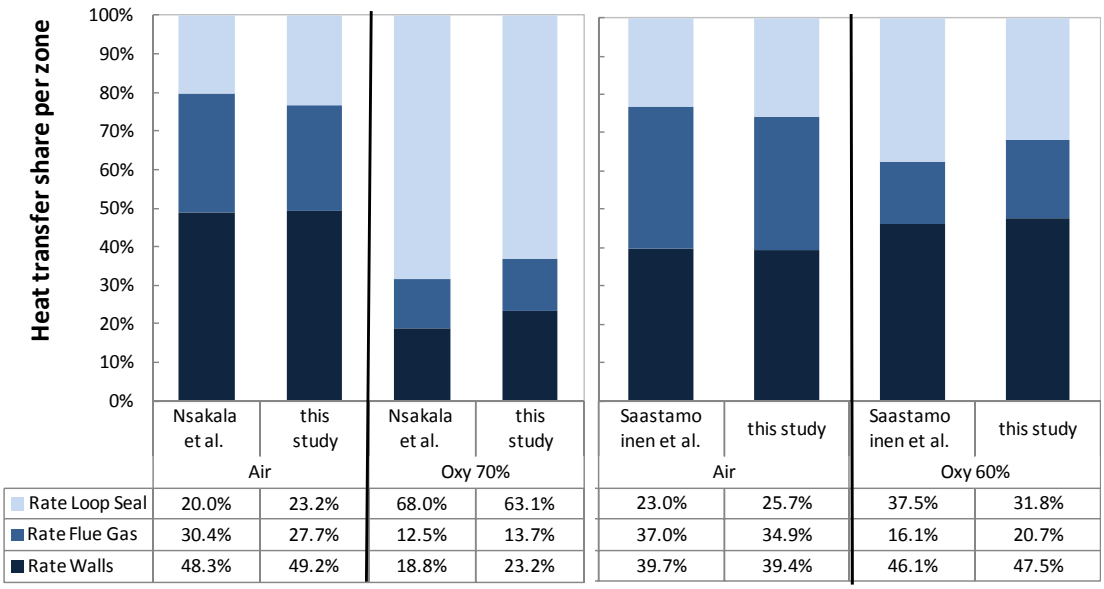

	Nsakala et al. (Air)	this study (Air)	Nsakala et al. (Oxy 70%)	this study (Oxy 70%)	Saastamoinen et al. (Air)	this study (Air)	Saastamoinen et al. (Oxy 60%)	this study (Oxy 60%)
Rate Loop Seal	20.0%	23.2%	68.0%	63.1%	23.0%	25.7%	37.5%	31.8%
Rate Flue Gas	30.4%	27.7%	12.5%	13.7%	37.0%	34.9%	16.1%	20.7%
Rate Walls	48.3%	49.2%	18.8%	23.2%	39.7%	39.4%	46.1%	47.5%

Figure 2.20. Heat duties share model results compared with heat duties estimated by Saastamoinen et al. (2006) and Nsakala et al (2004)

Good agreement with results by Nsakala et al. was obtained considering entrainment solids rate of 7.6 and 35 kg/m^{2}s, for AF and OF, cooling them down to 700 and 650ºC respectively. A bituminous coal fit the results with less volatile content and higher char and ashes ratios.

Regarding simulation by Saastamoinen et al., Gs was 8 kg/m^{2}s for AF and 19 kg/m^{2}s for OF, to fit the results, with same recycled solids temperature, around 700ºC and extra-panels inside the furnace for the case of OF. Fuel used was the same lignite type that was used in Seddighi et al. model.

Both simulations conclude an important augmentation of the heat transferred outside the furnace walls. This difference is larger in the work by Nsakala et al. changing from 20 to 68% and slighter in the one by Saastamoinen et al., from 23 to 37.5%. There are three main considerations that cause this difference. First, the higher O_2 concentration, 70% in Nsakala et al. and 60 % in Saastamoinen et al., that allows further boiler size reduction for similar fed fuel. Riser height is also 15 m less than in Nsakala et al. (2004). That means higher entrained and recycled solids, and so higher heat transferred in EHE. In spite of higher heat transfer coefficient, heat exchange area along the boiler is reduced and both effects could be compensated. Hence, cooling process inside EHE becomes essential. In Saastamoinen et al. riser walls heat exchange surface increases by considering higher boiler and so, solids are then further cooled.

In the model by Seddighi et al. (2010), boiler size was not modified and bed temperature was controlled by increasing the amount of recycled solids. Heat removed in the convective pass during oxy-fuel simulations represent 8-10% of the total thermal power fed and does not change significantly varying O_2 concentration at inlet. If gas flow rate per fuel input does not vary significantly and boiler temperatures keep similar, shared of heat that can be extracted by gas convection per unit fuel input is also similar within different oxy-fuel conditions.

2.5 THE ROLE OF THE EXTERNAL HEAT EXCHANGER

2.5.1 REDUCTION OF OXY-FUEL BOILER SIZE

New OF CFB boiler designs, using high O_2 concentrations in the oxidant stream, may lead to reduce boiler size and so, capital costs. This means also diminishing the mass flow of gas per unit of thermal fuel input. This will allow reducing the cross sectional area for reaching similar fluidizing velocities. However, decreasing the boiler cross sectional area involves a considerable reduction on the available area along the riser for heat exchange in the wall tubes.

The OF CFB model is used to estimate the consequences of the boiler size reduction. With this aim, four runs results are compared in , the AF case and three OF cases, at three O_2 concentrations. Fuel input is kept constant, at 650 MW, feeding low rank Spanish lignite. Temperature at which elutriated solids are recycled back into the boiler is 700ºC. The heat share called *Rate Loop Seal* is calculated by the elutriated solids and the energy difference between the bed temperature and the imposed recycled temperature. Average bed temperature is between 850ºC and 900ºC in all the cases. Fixing these parameters will allow isolating the effect of increasing O_2 at inlet, for a certain thermal power.

For fixed boiler geometry, AF case and 30% O_2 case require similar recycled solids rate, to lie within the appropriate bed temperature range, Figure 2.21. Energy contained in flue gases is lower in the case of OF than AF due to the change in gas flow rate. This is, O_2 concentration is higher in OF 30% than in AF (21%) so the mass flow of gas conveys less energy than in AF. This difference is distributed in an increment of 2 points on the EHE and 3 points in the walls. The increment in

the wall region is due to an increase in bed temperature around 40 ºC compared with the AF bed temperature.

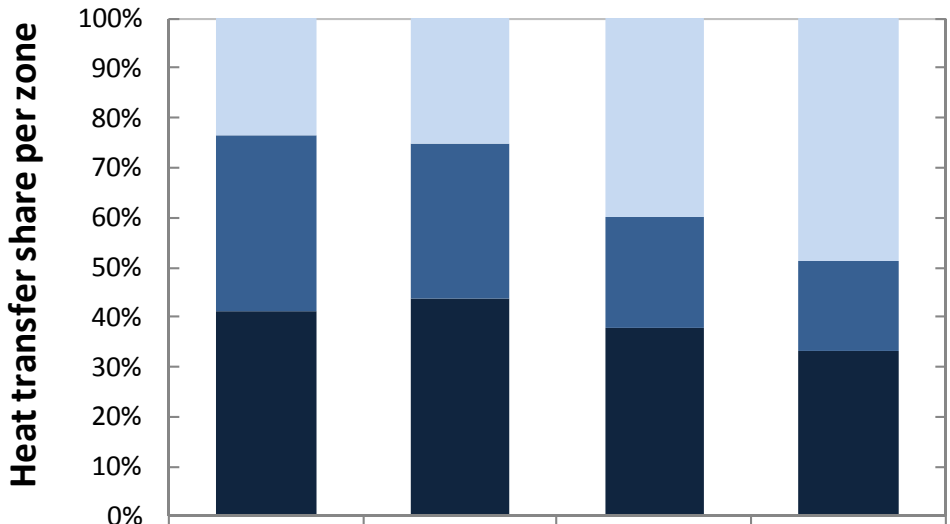

	Air	Oxy 30%	Oxy 45%	Oxy 60%
Rate Loop Seal	23.27%	25.34%	40.04%	48.76%
Rate Flue Gas	34.86%	30.82%	22.28%	17.91%
Rate Walls	40.68%	43.84%	37.69%	33.33%
Gs (kg/m2s)	7.8	7.8	18.5	32.7
A cross (m2)	190.8	190.8	103.4	64.0

Figure 2.21. Heat transfer share for different oxygen concentration, 650 MW power input

In the two other OF cases the O_2 concentration is incremented up to 45% and 60% respectively. This is to acquire an estimation of the increase of elutriated solids needed for controlling bed temperature and hence, the higher heat that the EHE must remove. The elutriated solids must augment up to 11 and 25 kg/m^{2}s respectively. Energy with gases almost halves the flue gases heat share in AF. As a consequence, the heat removed in the EHE is almost double. The cross sectional area for the 60% O_2 case is reduced to 34% from the original size. This also contributes to diminish the cooling capacity of the riser water walls 7%.

2.5.2 VARYING POWER INPUT

The flexibility that fluidized beds exhibit for working under different fuel loads resides on the possibility of reducing or increasing elutriated solids, Gs, for regulating the bed temperature. This can be a particular great advantage for OF combustion if an appropriately flexible EHE is available. Broad variety of thermal power output in the same boiler can be handled in a OF CFB. With the aim of

understanding this particular feature, a certain boiler size was fixed and the boiler geometry was selected, with a cross section of 12.5 m x 5.3 m and 40 m high. In the simulations results are shown in Figure 2.22. Oxygen concentration of 60% at inlet and solids are recycled at 700ºC were the input values in these runs.

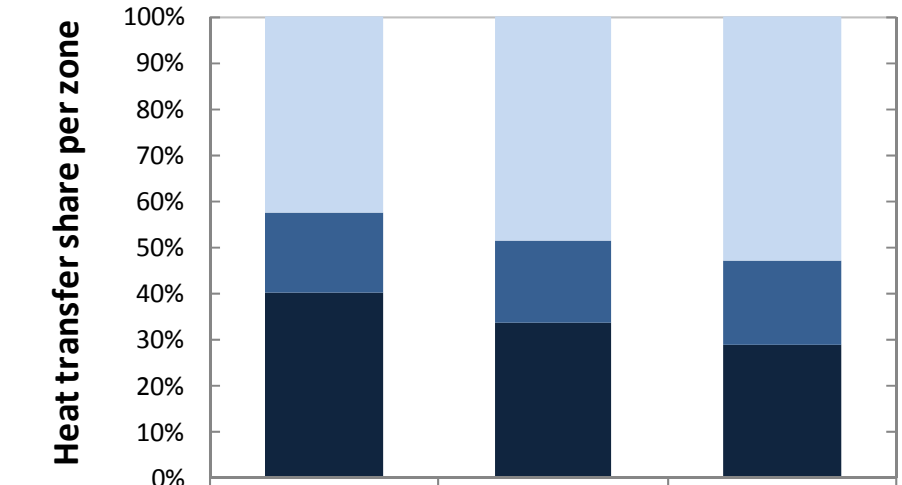

	600 MW	700 MW	800 MW
Rate Loop Seal	42.28%	48.28%	52.77%
Rate Flue Gas	17.22%	18.04%	18.16%
Rate Walls	40.00%	33.68%	29.07%
Gs (kg/m2s)	25.4	32.3	39.7
Sec Gas	20%	34%	43%

Figure 2.22. Heat transfer share for three fuel inputs and same boiler geometry

While increasing fuel input and so, the required stoichiometric O_2, the fluidizing gas is incremented. To achieve the adequate rate of Gs that made possible a proper regulation of bed temperature, between 850 and 900ºC, the secondary gas ratio, per total fed gas is manipulated. By increasing this ratio, the primary gas, and so, the fluidizing velocity, is controlled within the convenient limits to convey the proper amount of solids out o the boiler.

As observed in Figure 2.22, an increment of 200 MW in the fuel, means that more than double of the necessary combustion gas should be deviated, not being fed in the lower part of the boiler. If this deviation were not enough, the high fluidizing velocity would drag too many solids and thus, the bed would be cooled down below the acceptable limits.

In the runs results shown in Figure 2.22, fuel input from 600 to 800 MW, needs Gs ranging from 25 to 40 kg/m^{2}s, thanks to secondary air ratio, that was varied from

20-43%. In spite of keeping temperature difference between the bed and the recycled solids similar in all cases, the increase of Gs makes the contribution of the EHE increments from 42.3 to 52.8%.

2.5.3 VARYING O_2 AT INLET

The distinguishing characteristic of OF combustion versus AF combustion lies on the possibility of modifying the O_2 content in the fluidizing gas. While in AF, the only way of changing fluidizing velocity is by incrementing the air excess, in OF case, it also can be varied by manipulating the O_2 concentration at inlet.

In future concepts of OF CFB boilers it will be essential to know what flexibility is possible to achieve for a certain boiler arrangement similar to AF case. In the following runs an area of 16 x 9.4 m was considered, as the adequate size for air firing boilers.

Reaching AF temperature conditions is possible with an O_2 concentration around a 30% v. This statement has been extensively assumed for pulverized fuel boilers (Scheffknecht, 2009) but fluidized bed do not present such a great restriction in feeding wider range of O_2 concentration.

A proper temperature profile along the furnace is possible for higher O_2 concentrations, when fuel input is also increased. Therefore, higher volume of gases must be introduced into the boiler and so, higher velocity entrains more solids to the particles separator device (cyclone).

Figure 2.23 shows the distribution of heat transfer along the system, for keeping similar temperature profile in the boiler, but different conditions of the oxidant stream.

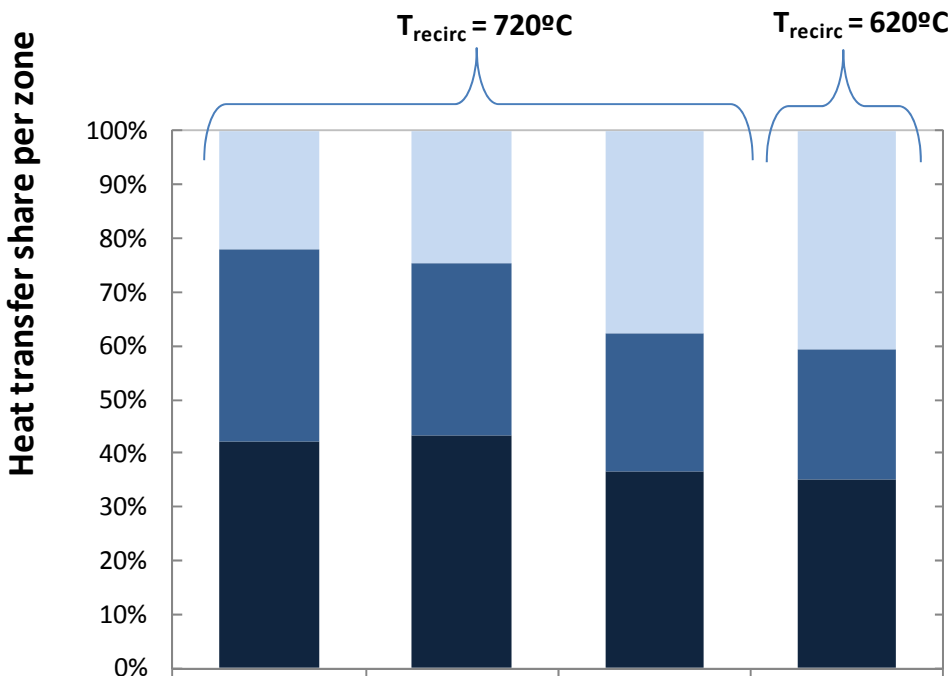

	Air	Oxy 30%	Oxy 40%	Oxy 40%
Rate Loop Seal	21.83%	24.61%	37.73%	40.80%
Rate Flue Gas	35.82%	31.94%	25.39%	23.98%
Rate Walls	42.36%	43.46%	36.68%	35.22%
Gs (kg/m2s)	11.0	11.2	20.7	10.6
Fuel input (MW)	570	580	850	730

Figure 2.23. Heat transfer share with air design boiler geometry and different O_2 concentrations at inlet

When O_2 at inlet is incremented up to 40%, it is possible to raise entrainment of solids, up to 20.7 kg/m^{2}s. More particles are managed by the EHE and so 36.7% of the total fuel input is removed in this part. But it is also possible to maintain the fluid-dynamical conditions by increasing the temperature difference of solids that comes out from the boiler. In the last column of Figure 2.23, Gs has been kept similar than in the 30% O_2 case, but solids have been cooled down to 620ºC. Hence, the contribution of EHE represents 35% of the overall fuel input, as high as the case of high Gs. In these runs, geometry has been kept constant, but Gs changes by varying fuel input, up to 730 MW. From the graph it is found that the possibilities of proper regulation of the fluidized bed operation fall on the external device for cooling down the particles that are coming back into the boiler. It is possible to recycle larger amount of solids, or to cool them down to lower recycled temperatures. In both cases, an important effort must be dedicated to a proper external heat exchanger design. Conventionally, EHE devices for CFB are bubbling fluidized beds or moving fluidized beds.

2.6 CONCLUSIONS

Two of the models of large-scale oxy-fuel CFB available in open literature have been developed by boiler companies, with long experience on air-firing large CFB. These models are presumably complex, and based on computational fluid-dynamics modeling, although modeling data are not public. In spite of this lack of details, the one-dimensional modeling developed up to here is able to predict the oxy-fuel boiler heat balance with similar results as those previously mentioned. The heat balance has been then compared using the heat ratios, dividing the overall energy balance into three shares: the energy removed by the walls, the flue gas sensible heat through the convective pass, and the heat removed in the external heat exchanger, the three of them, represented by unit of fuel input. The values obtained from the comparison made the model fairly reliable to be used for further analysis.

The effect of changing O_2 concentration on the design of certain boiler geometry was evaluated. Fixing the fuel input and the temperature at which solids are recycled, three different O_2 concentrations were run. The results indicated that a much compact boiler is required for the case of 60% O_2. For this case, the boiler cross sectional area was 33% less than the case of 30% O_2. This implied a reduction in the available surface for heat removal in the water walls. Consequently, the heat transferred in the EHE increased twice from the 30% O_2, to the 60% O_2 cases.

When boiler geometry was not variable, fuel input did increase for higher O_2 percentages, to reach the proper fluidizing velocity. Again, this led to higher heat removal requirements in the EHE up to 53% from the overall combustion heat.

Oxy-fuel applied in the CFB boiler presents outstanding operating flexibility, for a range of O_2 at inlet, analogous to the conventional case in which boiler load must change for adapting the energy market requirements.

On the other hand, the EHE is now an essential device for acquiring the mentioned flexibility and it will not be possible to disregard it in future oxy-fuel CFB boilers designs.

There will be then two essential differences in the operation between EHE attached to an oxy-fuel and an air-fired CFB. On the one hand, the fluidizing gas composition cannot be air, but it will consist of flue gases bleeding, in order to preserve the purity of the CO_2 concentrated flue gas, within acceptable limits for

transport and storage. On the other hand, higher recycled flow of solids will lead to non-uniformities along the tubes in the EHE. Consequently, the average heat transfer coefficient will be affected. Following, both issues will be experimentally assessed and discussed.

CHAPTER 3

HEAT TRANSFER IN CIRCE EXPERIMENTAL OXY-FUEL COMBUSTION BUBBLING FLUIDIZED BED

3.1 INTRODUCTION

The particular relevance of higher heat removal in the EHE of an oxy-fuel CFB leads the attention towards an adequate design of the heat transfer areas and the allocation of this equipment. EHEs work usually under bubbling regime conditions. This allows the proper displacement of solids from the bottom of the cyclone leg, to the recycling pipe. At the same time, low velocity fluidization regime prevents from excess of gas flow through the dip-leg solids column (Grace et al., 1997). The bubbling regime exhibits an intense heat transfer from the particles to the heat tubes, due to the dominant contribution of the particle convection mechanism. Unlike in conventional EHE, the oxy-fuel CFB's EHE will not be fluidized with air, but with RFG. Only one previous experience evaluated heat transfer coefficients under oxy-fuel fluidized bed conditions (Nsakala et al., 2004). They measured the heat transfer coefficients in the riser of a CFB, finding no significant differences with the ones measured under air-firing. In the CFB riser, the radiation contribution and gas convection prevails over the particle convection mechanism, unlike in dense beds. Thus, presumably, most researchers assume that the change on the gaseous atmosphere would not mean a significant difference on heat transfer. However, the change on gas composition would affect the conductivity and heat capacity of the gas layer adjacent to the wall. This gas layer is, in fact, the limiting actor to the heat flow. The fluid-dynamics is also assumed to behave similarly in OF than in AF mode by most of researchers, although the bubbles were

found to be slightly smaller and with more vigorous bubbling than in air-firing case (Guedea et al., 2011). This affects the fraction of time during which particles are in contact with the surface.

Heat transfer in an oxy-fuel bubbling fluidized bed (BFB) is measured in this work. This will allow evaluating the differences with the known air-combustion operation. The two main approaches used for the prediction of heat transfer coefficients in fluidized beds, the empirical and the mechanistic approaches, are examined to forecast the differences between air and oxy-fuel operation. The heat transfer coefficients measured during the pilot plant operation will allow proposing a complete expression for the heat transfer coefficient during oxy-fuel combustion in fluidized beds.

3.2 HEAT TRANSFER IN FLUIDIZED BEDS

3.2.1 PREVIOUS FINDINGS

Heat transfer between a surface and a gas flowing through a bed of particles is many times higher than expected for the same flow in an empty column. Thus, the heat transferred through particles in movement is rather more intense than the gas convection alone. Heat from hot particles to the cold inlet fluidization gas is transferred intensively. Thus, bed and gas temperatures are generally considered equal to the average bed temperature, even in the vicinity of the distributor. Researchers confirmed this phenomenon and it was mostly represented by means of empirical expressions. Compendium of correlations of heat transfer between gas and solid particles in fluidized beds can be found in general literature of fluidized beds like (Botterill, 1989; Howard, 1989; Kunii and Levenspiel, 1991; Oka, 2003; Basu, 2006). Although these quantification is particularly relevant for the modeling of fuel particle conversion, in this work the heat transfer from the particles to the gas will be considered high enough to be neglected.

The mechanisms involved in the heat transfer between the bed and the surface include:

- The solid conduction that takes place while solid particles contact the surface. The emulsion phase contains the majority of solid particles, but

there is also a small proportion in the bubble phase. Although it is based on solids conduction, this mechanism is known as particle convection, because the movement of solids greatly enhances the energy transfer, h_{pc}.

- The gas convection from both, the bubble phase and the gas found in the emulsion, $h_{gc.}$
- The radiation heat transfer from the layer adjacent to the wall, $h_{rad.}$

As an engineering approximation the contribution of these mechanisms are regarded as independent, from each other, and the heat transfer coefficient is then written as:

$$h = h_{gc} + h_{pc} + h_r \qquad \text{Eq. 3.1}$$

The particle convection heat transfer mechanism prevails in fluidized bed region for bubbling fluidized beds and in the freeboard, radiation mechanism dominates. Thus, heat transfer coefficients to immersed surfaces in the fluidized region can range from 250 to 700 W/m^{2}K and in the freeboard these coefficients are less than 100 W/m^{2}K (Breitholtz et al., 2001; Oka, 2003). The transition in the heat transfer values in the splash zone was measured by Pidwerbecki and Wely (1995). Moreover, radiation heat transfer is often neglected when the bed temperature is lower than 600ºC. Numerous authors analyzed the parameters influencing heat transfer at low temperature, isolating the radiation contribution. In most of cases, the cooling rate of a heated surface (van Heerden et al., 1953; Ziegler et al., 1964; Schmidt and Renz, 2005; Patil et al., 2006) or sample probe (Grewal and Saxena, 1981; Mathur et al., 1986; Sunderesan and Clark, 1995) is used to measure the energy transfer. Since the earliest studies it was stated that the greatest influence on heat transfer intensity is that of the fluidization velocity and particle size:

On the one hand, fluidizing velocity influence is usually described in three stages:

- At fixed bed regime, heat is transferred by conduction of particles in contact with the surface and by convective gas flow between bed particles. With onset of fluidization, particle convection heat transfer starts. At minimum fluidization velocity, heat transfer increases sharply.
- With further increase in fluidization velocity, heat transfer coefficient continues to increase, and it reaches a maximum at an optimal fluidization velocity. Below this limit, the major contributor to heat transfer is the particle convection, increasing with particle mixing.

- With velocities higher than the optimal velocity, the key mechanism of heat transfer is gas convection. Since bed density is lower, the influence of particle convection decreases.

Particle size, on the other side, determines the relative influence of each mechanism. With increasing particle diameter, optimal fluidization velocity increases and the maximum heat transfer coefficient is significantly smaller. In fluidized beds of small particles less than 0.1 mm, particle convection makes for more than 90% of heat transfer, while in beds with particles greater than 1 mm, it makes only 20% of particle heat transfer. A detailed review of the influence of particle diameter on heat transfer can be found in Decker and Glicksman (1983). The role of gas convection becomes significant when the gas flow occurs at particle diameters greater than about 800 µm. For particles of this size and larger, the convective component of heat transfer by gas becomes significant and total heat transfer coefficient does not depend much on the particle size.

Additionally, the solids density is closely related to both, the fluidizing velocity and the particle size. Breitholtz et al. (2001) gathered experimental data from pilot and large plants, and established a simple correlation that directly related the global heat transfer coefficient with the solids suspension density. Their study focused on circulating fluidized bed boilers, but they highlighted the adequacy of bed density for satisfactorily predict the heat transfer coefficients in a generalized way.

Empirical approaches

One of the most widely recommended expressions for estimating heat transfer in fluidized beds is the one proposed by Zabrodsky (1966). Due to simplicity and also, the reasonable predictions given, it has been extensively used along decades (Botterill, 1989; Howard, 1989; Basu, 2006).

$$h_{max} = 37.6\left(\frac{\rho_s}{\rho_g}\right)^{0.2} k_g^{0.6} d_p^{-0.36} \qquad \text{Eq. 3.2}$$

Note that the energy units for this expression were not S.I. but $kcal/h$. Botterill et al. (1984) recommended that a value of about 70% of that predicted by Eq. 3.1 represents a conservative estimate for h_{max}.

Earlier common approaches for modeling heat transfer to surfaces in fluidized beds assumed similarity to gaseous convection and assigned thermal resistance to a

boundary layer at the heat transfer surface. The enhancement found at gas velocities greater than u_{mf} is attributed to the decrease of effectiveness of the film thickness (Wagialla et al., 1990). Models following this approach attempted to correlate a Nusselt number with the Prandtl number, a modified Reynolds number and the Archimedes number, using either the particle diameter or the tube diameter and other non-dimensional parameters. Hence, the influence of factors related to operation conditions, bed geometry or solids and gas properties were correlated.

Table 3.1 gathers some of these empirical expressions for the heat transfer from bed to vertical surfaces.

Heat transfer to the walls	
$Nu = 0.55\,\mathrm{Re}^{0.8}\left(\frac{\rho_p C_p}{\rho_g C_g}\right)^{0.25}\left(\frac{d_t}{d_p}\right)^{0.03}\left(\frac{H_f}{d_t}\right)^{-0.65}\left(\frac{1-\varepsilon_f}{\varepsilon_f}\right)^{0.25}$	Dow and Jakob (1951)
$Nu = 0.58Pr^{0.5}\left(B\,\mathrm{Re}\right)^{0.45}\left(\frac{C_p}{C_g}\right)^{0.36}\left[\frac{\left(1-\varepsilon_{mf}\right)\rho_s}{\rho_g}\right]^{0.18}$	van Heerden et al. (1953)
$Nu = 0.6PrRe^{0.3}$	Levenspiel and Walton (1954)
$Nu = 0.16Pr^{0.4}Re^{0.76}\left(\frac{\rho_p C_p}{\rho_g C_g}\right)^{0.4}\left(\frac{u_f{}^2}{g d_p}\right)^{-0.2}\left(\eta\frac{H_{mf}}{H_f}\right)^{0.36}$	Wen and Leva (1956)

Table 3.1. Empirical expressions for the prediction of heat transfer coefficient from fluidized bed to vertical walls

The Dow and Jacob correlation (1951) was deduced under the assumption that there were not only a boundary layer of gas participating in the heat transfer, but also a boundary layer of particles moving along the wall and hindering the heat transfer. Van Heerden et al. (1953) compared the wall with the film of laminar flow along a vessel wall containing well-stirred liquid. Levenspiel and Walton (1954) supposed an artificial structure for the fluidized bed and assumed that particles were arranged in horizontal layers. So, the boundary layer was disturbed in its plane, forming intervals between layers. Wen and Leva (1956) proposed to include

particle velocity in the heat transfer relationships, since they observed that particles had scoring action in the boundary layer.

Although authors agreed in the importance of fluid-dynamics on heat transfer, the expressions failed to predict the tendency with Reynolds number as shown in Figure 3.1

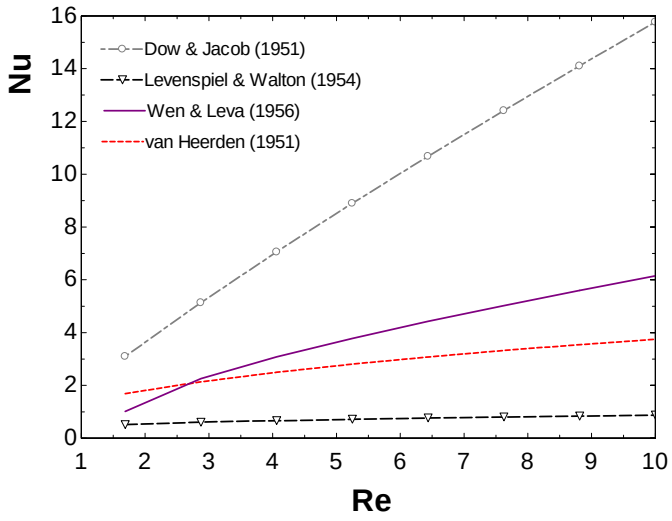

Figure 3.1. Effect of Reynolds on Nusselt number prediction by different authors

The increase of Nusselt number with Reynolds is not so for the whole range of Reynolds numbers. In fact, the behavior of heat transfer with Re, follows analogous curve as the heat transfer coefficient with fluidizing gas velocity. An example of experimental results obtained by Mathur et al. (1986) is shown in Figure 3.2. The well known optimum heat transfer point marked the difference between a fully dominant heat transfer by particle convection, and an increasing relevance of gas convection, due to increasing on excess gas velocity. In the secondary axle, the solids volumetric fraction is also represented.

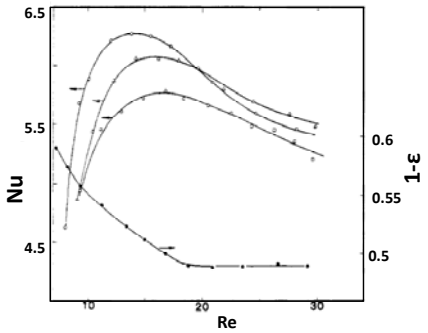

Figure 3.2. Dependence of Nusselt number with Reynolds number for vertical tubes immersed in 500 µm silica sand fluidized bed (Mathur et al., 1986)

Molerus et al. (1994) proposed a new fully empirical correlation, deduced from the two limiting conditions for heat transfer in fluidized bed: fully dominant gas convection ($10^5 < Ar < 10^8$) or fully dominant particle convection ($Ar < 10^2$).

$$\frac{hl_l}{k_g} = \frac{0.125\left(1-\varepsilon_{mf}\right)\left[1+33.3\left(\sqrt[3]{\frac{u-u_{mf}}{u_{mf}}}\sqrt[3]{\frac{\rho_p c_p}{k_g g}}\left(u-u_{mf}\right)\right)^{-1}\right]^{-1}}{1+\frac{k_g}{2c_p\mu}\left(1+0.28\left(1-\varepsilon_{mf}\right)^2\left[\frac{\rho_g}{\rho_p-\rho_g}\right]^{0.5}\left[\sqrt[3]{\frac{\rho_p c_p}{k_g g}}\left(u-u_{mf}\right)\right]^2\frac{u_{mf}}{u-u_{mf}}\right)} + \ldots$$
$$\ldots + 0.165 Pr^{1/3}\left(\frac{\rho_g}{\rho_p-\rho_g}\right)^{1/3}\left[1+0.05\left(\frac{u-u_{mf}}{u_{mf}}\right)^{-1}\right]^{-1} \qquad \text{Eq. 3.3}$$

Eq. 3.3 was deduced from cold tests, but still, it appears as a quite reliable expression for predicting the behavior of changes in gas composition, as in oxy-fuel combustion. The existing expressions were modified to represent the dependence of heat transfer on the slip velocity parameter. This expression was compared with numerous experimental data from other authors and agrees in the prediction of the real tendency of heat transfer with Reynolds number.

Mechanistic approaches

Although there is no universal theory for the mechanisms of heat transfer in fluidized beds, it is generally accepted that heat transfer in BFB is best explained by the packet renewal model, developed by Mickley and Fairbanks (1955), explained and recommended in numerous general studies (Xavier and Davidson, 1985; Chen, 2003; Basu, 2006). They analyzed the simple case of aggregates of particles, named packets, receiving heat while contacting an isothermal flat surface. Thus, packets of particles at bulk bed temperature are swept to the heat transfer surface due to the action of bubbles. They stay in contact with the exchange surface for a period of time τ and then they are swept back to the bed. During this time, unsteady state heat transfer takes place between the packet and the surface. Eq. 3.4 yields the instantaneous heat transfer coefficient:

$$h_{in} = \sqrt{\frac{k_{Pa}\rho_{Pa}c_{p,Pa}}{\pi\cdot\tau}} \qquad \text{Eq. 3.4}$$

Where the subscript *Pa* indicates the packet properties. This concept was experimentally confirmed by researchers who were able to measure transient

variations of particle concentration at heat transfer surfaces, for example, with surface capacitance sensors with flush mounted electrodes, as Chen et al. (2005). Techniques such an optical probes (Kurosaki et al., 1995) or pressure fluctuation measurements (van Ommen and Mudde, 2007) are also used for obtaining quantitative voidage values. All of them allow to obtain real-time measurements of fluctuating particle concentration at surfaces in fluidized bed (Werther, 1999). These experiments confirmed that particle concentration is highly dynamic and varies dramatically over time. An additional heat transfer resistance to the particle packet transient conduction was first proposed by Baskakov (1964), considering that the contact zone is time-independent with changing properties and it could not be considered as a continuous medium. Particle concentration alternates between pure gas (bubble phase) and high concentration similar to that for packed beds (emulsion packet phase). These evidences support the renewal model where the time average heat transfer coefficient involves proportional contributions from the bubble phase coefficient and packet phase coefficient (Xavier and Davidson, 1985), Eq. 3.5:

$$h = (1 - \delta_b) h_{pc} + \delta_b h_{gc} \qquad \text{Eq. 3.5}$$

There are two difficulties added to the evaluation of the transient conduction term. On the one hand, time-domain parameters are not easy to measure or evaluate. These parameters include f_d, the fraction of time when surface is in contact with dense phase and τ, the root mean residence time of packets at the heat transfer surface. According to the two-phase approach for fluid-dynamics in a fluidized bed, where bubbles as composed by pure gas, the frequency at which solids packets are contacting the wall is related to the residence time through the bubble fraction δ_b as shown in Eq. 3.6:

$$(1 - f_d) = \frac{1 - \delta_b}{\tau} \qquad \text{Eq. 3.6}$$

On the other hand, Eq. 3.4 is reasonably accurate for long packet residence times or very small particle diameters, because it ignores variations in bed voidage with distance normal to the surface. Thus, physical and thermal properties of packet near the surface must be estimated as *effective properties* (Xavier and Davidson, 1985; Kunii and Levenspiel, 1991), taken at one-half of the penetration depth of the temperature wave for the given operation conditions (Chen, 2003). In 1964 Baskakov modified this model by adding a time-independent contact resistance

between the packed and the surface to account for the zone with variable properties (Xavier and Davidson, 1985).

Effective thermal conductivity

From the earliest studies on heat transfer (Zabrodsky, 1966), it was observed that temperature gradient in the proximity of the wall dramatically dropped. This indicated that the resistance due to the conductivity in the wall layer was more elevate than the bulk of particles conductivity. The fluidized bed effective thermal conductivity is higher than the gas or solid particles thermal conductivity. This is due to the interaction among the particles in bed and the number of contacts between them and the wall. Furthermore, experiments showed that effective thermal conductivity in axial directions is one order of magnitude lower than in the radial direction. This effective conductivity was studied first based on bulk void fraction and later, on the near-wall void fraction. The importance of accurate prediction of thermal conductivity has gained importance in the last decade, thanks to the development of computational fluid-dynamics modeling, which includes particle-particle interactions in their approaches (Patil et al., 2006; Yusuf et al., 2012).

Kunii and Levenspiel (1991) proposed Eq. 3.7 to account for the added contribution to the effective conductivity from the particle through the gas layer and through the contact point between particles. They corrected the model in which heat would flow through parallel paths, to account for the geometry of the particles. Based on analogous approach, Xavier and Davidson (1985) recommended the estimation of both components of the effective conductivity, as shown in Eq. 3.9. In the equation it was approximated the solution in packing of spheres and cylinders. The first is independent of the fluid flow, and second represents the effect of the diffusion in the fluid phase. Chen et al. (2005) simplified these expressions correlating the results by other authors in Eq. 3.10.

Kunii and Levenspiel (1991)	$k_{eff}\big\|_0 = \varepsilon_{mf} k_g + (1-\varepsilon_{mf}) k_s \dfrac{1}{\varphi_b \dfrac{k_s}{k_g} + 2/3}$	Eq. 3.7
	$k_{eff}\big\|_w = \varepsilon_{mf} k_g + (1-\varepsilon_{mf}) k_s \dfrac{1}{\varphi_w \dfrac{k_s}{k_g} + 1/3}$	Eq. 3.8
Xavier and Davidson (1985)	$k_{eff} = k_g \left(\dfrac{k_s}{k_g}\right)^{0.28-0.757\log\varepsilon-0.057\log\left(\frac{k_s}{k_g}\right)} + 0.1\rho_g c_{p_g} d_p u_{mf}$	Eq. 3.9
Chen et al. (2005)	$k_{eff} = (3.5-2.5\varepsilon)\left(\dfrac{k_s}{k_g}\right)^{(0.46-0.46\varepsilon)}$	Eq. 3.10

Table 3.2. Effective thermal conductivity of particulate phase by different authors

Figure 3.3 shows the effect of temperature on the effective thermal conductivity, estimated with Eq. 3.10. The discontinuous line represents the air-firing case and the oxy-fuel lines are estimated for two O_2 concentrations, 40% and 60%. The effective conductivity during oxy-fuel is higher than in air-firing, and the temperature influence exhibits similar dominance on this value than the proportion of O_2 in the mixture.

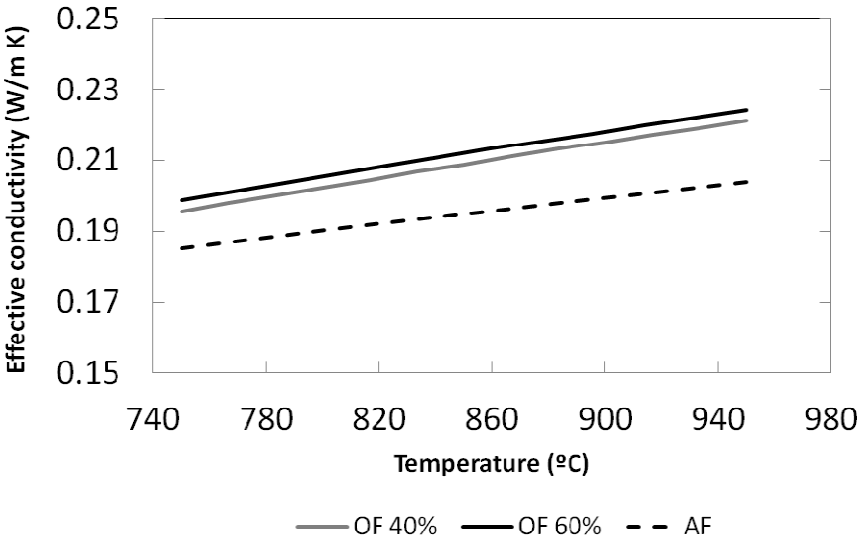

Figure 3.3. Temperature effect on effective thermal conductivity

Estimation of time-related parameters

In exchange surfaces of the order of some centimeters, the renewal of particulate phase near de surface is not complete, due to the numerous contacts of particles with the surface, at different positions. The values for the surface renewal frequency are around 0.7- 2 Hz and the bubble motion is the phenomena that lead the particles mixing. The surface temperature mainly changes while the rising bubble contacts, whereas during the passage of the emulsion phase, the oscillation is limited. This allows approaching the renewal frequency with the bubble frequency term (Di Natale et al., 2008). Di Natale et al. (2008) developed a single-particle model and proposed the following expression for estimating the renewal frequency, deduced from the correlation of data from different authors, Eq. 3.11:

$$1 - f_b = \frac{k Re_p^{0.287}}{d_p} \qquad \text{Eq. 3.11}$$

With the coefficient of proportionality k equal to $2.045 \cdot 10^{-4}$ m/s.

Based on experimental results, Chen (2003) confirmed that larger particle diameter lowered the frequency and also, higher fluidizing velocity enhances the replacement of solids and so the frequency. They proposed the following expression:

$$\xi \cong 2.32\sqrt{\alpha_p \tau} \qquad \text{Eq. 3.12}$$

Where ξ was the distance into the packet emulsion where 90% of the temperature change is obtained in residence time τ and α_p as the thermal diffusivity of the particles. The expression proposed for local void fraction at positions less than one particle diameter from the surface yielded:

$$\varepsilon = 1 - 2.04\left(1 - \varepsilon_b\right)\left(\frac{x}{d_p}\right)\left(1 - 0.51\left(\frac{x}{d_p}\right)\right) \qquad \text{Eq. 3.13}$$

However, this author also recognized that further experimental is needed for reaching a more universal expression representing any of the temporal parameters. In fact, Zarghami et al. (2007) found that the particle-wall contact time in a bed of sand particles decreases with gas velocity in the bubbling regime of fluidization, reaches its minimum at the onset of turbulent fluidization and increases beyond that. They considered the contact time of solids at the wall consisting of two factors, t_{pc} the contact time of particles attached to bubble and t_{ce}, the contact time of clusters in the emulsion phase:

$$\tau = t_{pc} + t_{ce} \qquad \text{Eq. 3.14}$$

The fraction of time in which the surface is bathed by particles attached to bubbles is proportional to the volume fraction of emulsion in the vicinity of the surface:

$$t_{pc} = \frac{\delta_e}{n_b} = a\delta_e \frac{d_b}{\delta_b u_b} \qquad \text{Eq. 3.15}$$

Being a an empirical correction factor to take into account the ratio of the existence probability of bubbles near the surface to their probability within the bed.

For t_{ce} it is considered that the clusters are pushed towards the wall by the bubbles and so, the contact time of the clusters in the emulsion phase is proportional to the bubble fraction. It is also added a correction factor b for the probability of cluster being near the surface:

$$t_{ce} = \frac{\delta_b}{n_c} = b\delta_b \frac{d_c}{\delta_c u_c} \qquad \text{Eq. 3.16}$$

So, the proposed formula for particle-wall contact time is expressed as:

$$\tau = a\delta_e \frac{d_b}{\delta_b u_b} + b\delta_b \frac{d_c}{\delta_c u_c} \qquad \text{Eq. 3.17}$$

Factors a and b are correction factors for taking the wall effect into account and so, evaluating radial distribution of bubbles and cluster. According to their experiments Zarghami et al. observed less frequently clusters in the wall than in the center, less frequently bubbles in the center than in the wall. They compared the experimental results of Hamidipour et al. (2005) with the model developed and with the expression proposed by Lu et al. (1993):

$$\tau = \frac{2(1-\delta_b)}{3\delta_b \frac{u_b}{d_b}} \qquad \text{Eq. 3.18}$$

Looking at the influence of slip velocity in residence time, Figure 3.4 illustrates the prediction by the above-mentioned authors.

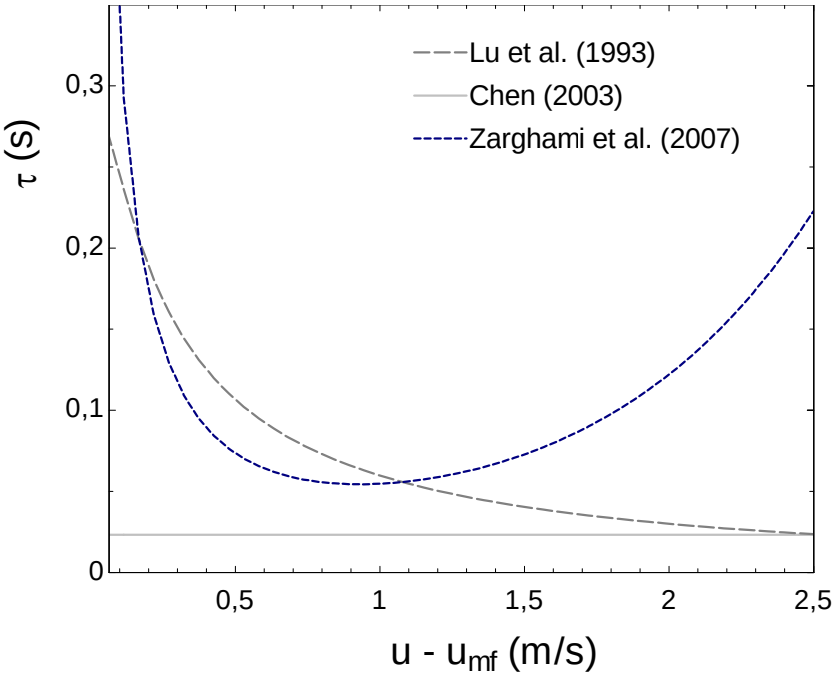

Figure 3.4. Predicted residence time dependence on fluidizing velocity, by different authors

The bath shape of Zarghami et al. approach appears a realistic prediction of the effect of velocity in the residence time of particles. This would agree with the velocity influence on heat transfer, commented above, in which there would be an optimal velocity at which residence time were lowest and the packet presence at the wall had the major importance.

Radiation heat transfer

Radiation heat transfer mechanism begins to contribute appreciably to the overall heat transfer in bubbling fluidized beds at temperature greater than 500ºC. Measurements of radiant heat transfer in dense beds are scarce. Yamada et al. (2001) affirmed that the reason was that conclusion from models are contradictory among authors. In their experiments they showed that the real contribution to this radiant heat transfer lies on the particles adjacent to the surface, and hinders the radiation heat transfer between the surface and the higher temperature particles in the depth of the bed. They measured the influence of particle diameter and fluidizing velocity on the radiant energy transfer to the surface. In the transport zone of circulating fluidized beds radiation models are proposed, and extensive research is available (Luan et al., 2000; Eriksson and Golriz, 2005; Glicksman, 2007). Basu and Konuche (1988) reported that the radiative component is 70%-90% of the total heat flux transferred from the suspension to the wall at 600ºC-885ºC.

The high percentage of radiation to total heat transfer in CFBs compared with bubbling fluidized beds is attributed to relatively low convective heat transfer due to low particle concentrations (Luan et al., 1999).

A simple approach to estimate radiation, used by many authors (Botterill, 1989; Wirth, 1994; Molerus et al., 1995b; Molerus et al., 1995a; Baskakov and Leckner, 1997; Basu, 2006), is to treat the radiation transfer as the exchange between opaque gray bodies separated by a nonparticipating medium. Then, the expression for radiation exchange yields as previously stated in Eq. 2.25. Where, for two parallel planes much larger than the distance between them, Eq. 2.26 showed the calculation of the bed-to-wall emissivity. In that expression, the term of bed emissivity ε_b is difficult to accurately estimate. It appears that it exceeds the value of particle emissivity, ε_p, because of reflections from particles near the bed surface. This was attributed to the same reason that an irregular surface has a higher emissivity than a smooth surface of the same material. Effective emissivity of fluidized bed has been correlated against different bed and wall temperatures and shown in Botterill (1989). A more simple expression was, however proposed by Baskakov and Leckner (1997) yielding:

$$\varepsilon_b = \varepsilon_p^{0.64} \qquad \text{Eq. 3.19}$$

The heat transfer of the layer of particles near the wall is controlled by a thermal resistance, R_w. This resistance is determined by the thickness of the gas layer between the heat transfer surface and the layer of particles. If the value of R_w is small, particles close to the surface at surface temperature influence is low.

The increase of heat transfer when increasing bed temperature is not only attributable to radiation heat transfer (Glicksman and Decker, 1982). Gas conductivity also augments, causing the corresponding increase on conduction mechanisms. They actually proposed to use an additional *radiative conductivity* for including the radiation heat transfer for particles adjacent to the surface. They added this conductivity term to the effective thermal conductivity and yielded:

$$k_r = \frac{8}{9} d_p \sigma T^3 \qquad \text{Eq. 3.20}$$

3.2.2 THEORETICAL INFLUENCES OF OXY-FUEL CONDITIONS

The immediate difference between the air-firing and oxy-firing modes resides on the atmosphere composition in which combustion and fluidization takes place. High concentration of CO_2, instead of N_2 is present in the gases. For acquiring an impression of how the gas properties would vary in both cases Figure 3.5 shows the theoretical properties of a mixture of O_2/N_2 (Air) and a mixture of O_2/CO_2 at different O_2 proportions, at 850ºC. Density and heat capacity were evaluated as proportional with gas composition, while conductivity and viscosity follow the recommendation by Lindsay and Bromley (1950) and Wilke (1950), respectively:

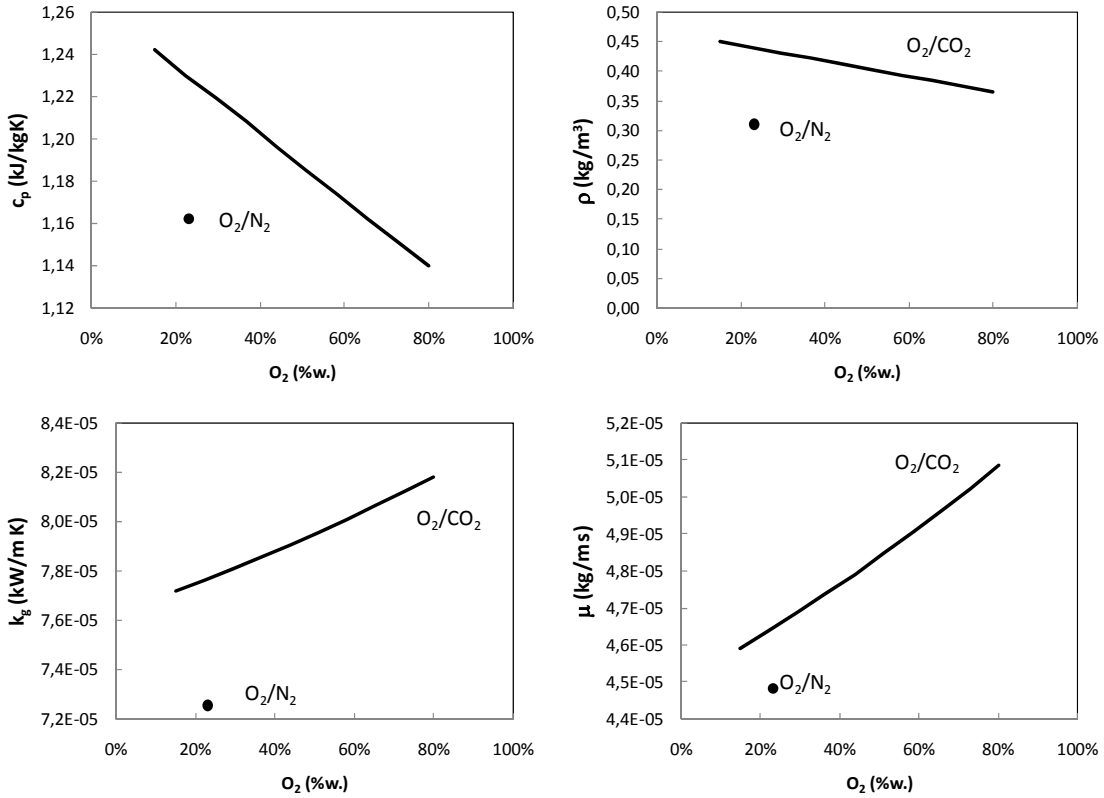

Figure 3.5. Gas properties variation for different O_2 concentration at inlet: a) density; b) viscosity; c) conductivity; d) specific heat capacity

In the four properties observed here, for the same O_2 proportion, O_2/CO_2 mixture shows higher values. The greatest difference turns out in the gas density, which is 45% higher in the mixture with low O_2 compared with O_2/N_2 mixture. While increasing O_2 in the mixture, the gas density decreases 18%. Heat capacity diminishes 9 percentage points from the lowest O_2 content case, to the highest,

approaching the values in O_2/N_2 case. The gas conductivity value for low O_2 percentages is only 2% higher than the air case, but it increases up to 13% with respect to the O_2/N_2 mixture. The similar ascendant tendency is found in the gas viscosity, increasing 11% from the lowest O_2 ratio case to the highest.

The higher density of O_2/CO_2 means an increase on fluidizing gas mass flow rate, for certain fluidizing velocity. The fluidizing velocity is settled by the desired fluidization regime, the boiler geometry and, particularly, by the stoichiometric conditions. This means that for a certain fuel input in a fluidized bed, fluidizing gas velocity decreases. Apart from the increase in gas density, this occurs predominantly because the higher the O_2 concentration at inlet, the less flow rate of gas feeds the combustion. This variation of fluidizing velocity is represented in Figure 3.6.

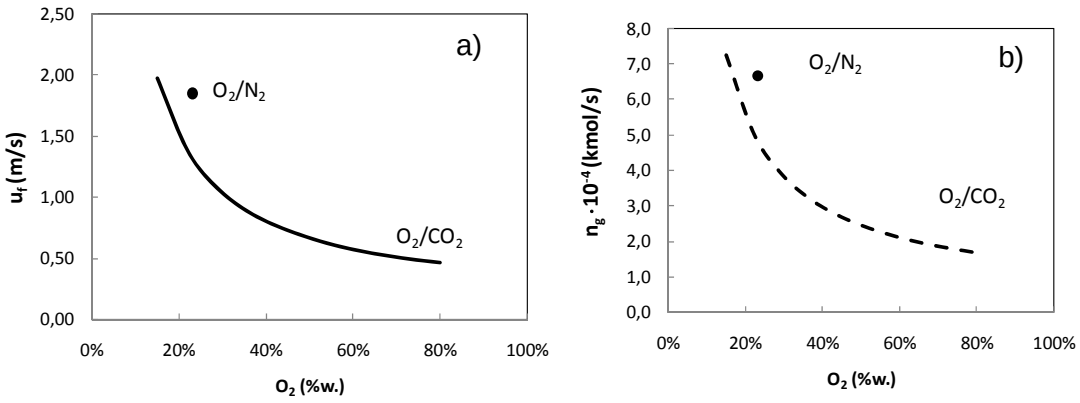

Figure 3.6. a) Variation of fluidizing velocity, u_f, with O_2 content in the gas mixture (constant molar rate of O_2) and b) the variation of the total gas molar rate

The potential shape in Figure 3.6a) illustrates the inverse relationship between the O_2 percentage and the fluidizing velocity, due to the stoichiometry, as shown in Figure 3.6b).

The influence of gas viscosity is closely related to fluidization, since it represents the resistance to the movement of particles in the fluid. These terms are included in the Reynolds number ($u_f d_p \rho_g / \mu$), the ratio between inertial and viscous forces. This non-dimensional variable is the key parameter when correlating the heat transfer by fluid convection, since it was for conceiving the laminar, turbulent or transitional regime, at which the stream is flowing. Slightly modified Reynolds

number, is used, referred to the particle diameter instead to any longitudinal parameter.

Archimedes number ($d_p^3\rho_g(\rho_p-\rho_g)/\mu^2$) also comprises the effect of particle diameter and solids and gas densities on the fluidization regime (Rabinovich and Kalman, 2011; Shaul et al., 2012). The term of Archimedes number has been usually related to the contribution of gas convection heat transfer component, like the expressions used by Kunii and Levenspiel (1991), Xavier and Davidson (1985) or by Botterill et al. (1989). In circulating fluidized beds the influence of Archimedes number is more evident. Wirth (1995) established a direct relation between the Archimedes number and the influence of the gas conductivity in the component of heat transfer by gas. He stated that, for high Archimedes numbers, the conductivity of gas did not influence the heat transfer coefficients, unlike for low Archimedes numbers that based the gas heat transfer on the gas conduction. Archimedes number is also related to the void fraction of the bed. Void fraction at minimum fluidization velocity, together with the Archimedes number, are the most influencing parameters for determining the bed porosity, according to Di Natale et al. (2008).

Thermal properties of gas, such as conductivity and specific heat capacity, are higher for O_2/CO_2 mixtures, diminishing with the O_2 content in the case of c_p. Prandtl number ($c_p\mu/k_g$) includes both variables and reflects the predominant influence of either convection or conduction heat transfer. This is also a common parameter participating in forced internal convection correlations. Prandtl varies slightly for certain gas composition and its value is usually around 0.7 for gaseous phase.

The influence of gas composition at inlet is now reviewed, by means of non-dimensional parameters included in Table 3.1. With this aim, Figure 3.7 shows the influence of gas composition and temperature on the densities ratio, $(1-\varepsilon_{mf})\rho_s/\rho_g$, the Archimedes and Prandtl numbers, respectively, at three different temperatures 750ºC, 850ºC and 950ºC. These three temperature values approach the lower, average and upper limit of temperature in a fluidized bed boiler.

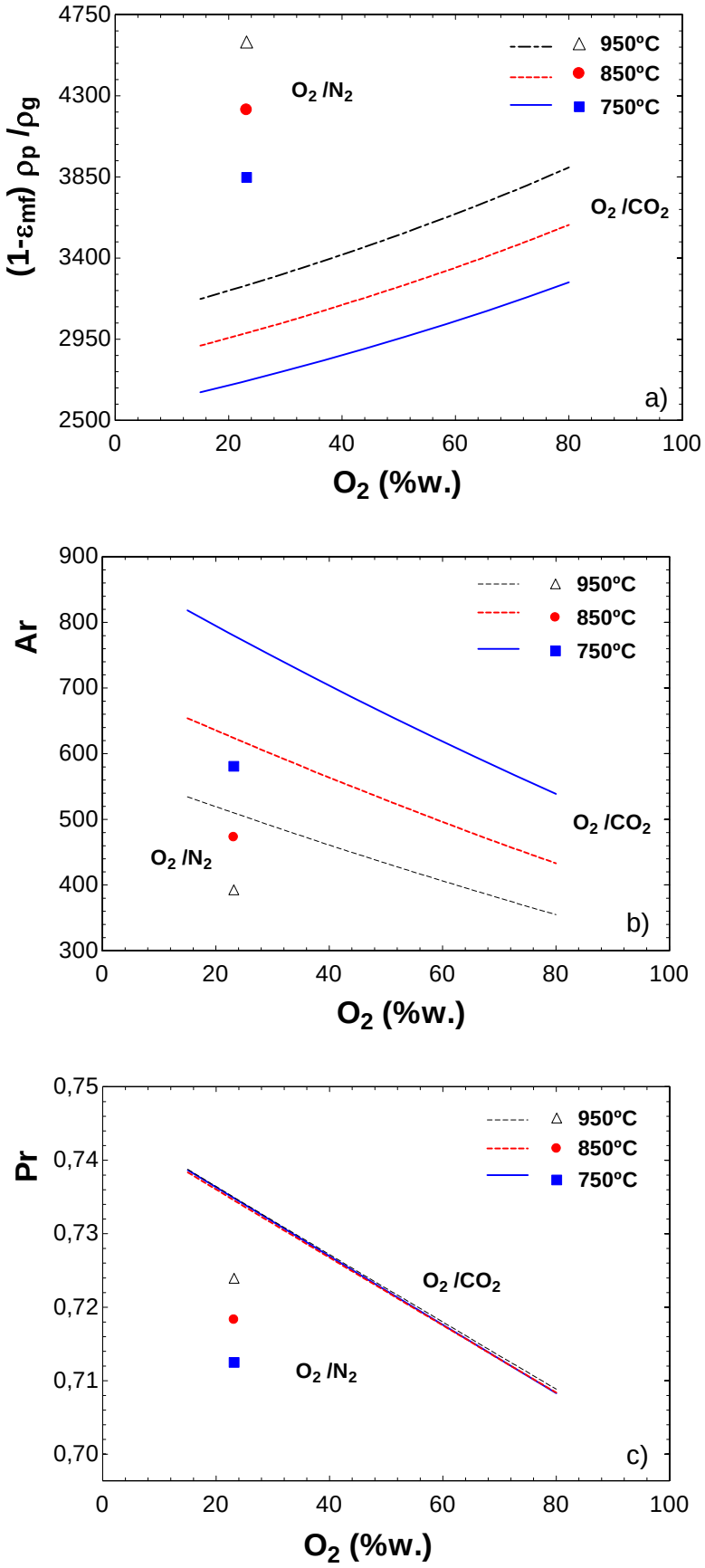

Figure 3.7. Variation of non-dimensional parameters with O_2 content in the gas mixture a) densities ratio, b) Archimedes number, c) Prandtl number

Regarding Figure 3.7a) the term of minimum fluidization voidage, ε_{mf}, was calculated using Ergun and Orning (1949) and Wen and Yu (1966) correlations. The densities ratio is 35% lower in O_2/CO_2 mixture for O_2 content similar to air. While increasing O_2, this ratio reaches values still 13% lower than the O_2/N_2 mixture ones. This parameter diminishes with temperature. This tendency is particular of this parameter, unlike the other non-dimensional parameters, that increases with O_2 content.

Archimedes number is 33% higher in O_2/CO_2 mixture than O_2/N_2 mixture, for the same O_2 percentage (Figure 3.7b)). It diminishes with the O_2 content, down to values close to those of air. This decrease on Archimedes number, given a non-changing particle diameter, is dominated by descendant viscosity of the mixture. Values of Archimedes number are higher for lower temperatures, which is again the added effect of higher gas density and lower viscosity when temperature decreases.

The temperature influence on Prandtl number for O_2/CO_2 mixture is negligible, compared to O_2/N_2 mixture, Figure 3.7c). The decrement of this parameter with O_2 proportion coincides both, with an increment of gas conductivity and a decrement of gas specific thermal capacity (Figure 3.5). Still, this decrement represents only 2% of the value in O_2/N_2 mixture.

Knowing the differences on gas velocity when fluidizing with O_2/CO_2 or air (Figure 3.6), Reynolds number is following represented in two ways. In Figure 3.8 a) gas velocity varies with O_2 content, but fuel input is constant, which means that molar rate of O_2 in the stream must be constant. Figure 3.8b) represents constant fluidizing velocity, regardless of the fuel that should be fed for each O_2 percentage.

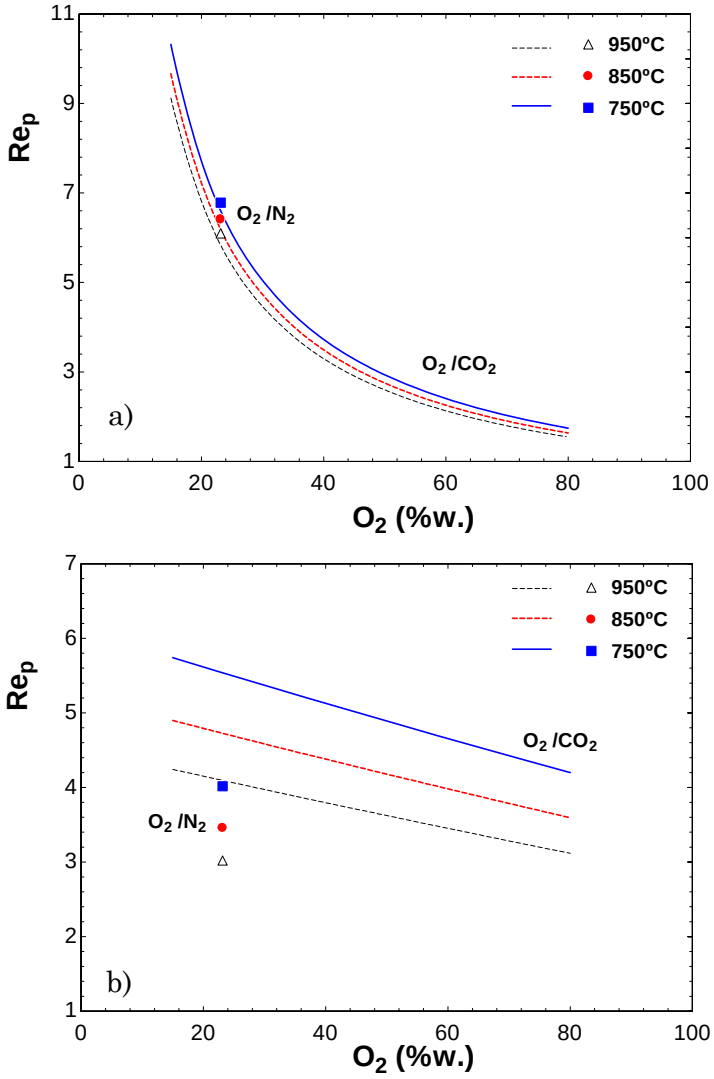

Figure 3.8. Variation of Reynolds number with O_2 content in the gas mixture: a) for a molar O_2 rate b) for constant u_f = 1 m/s

Looking at the constant velocity graph, Figure 3.8b) the decrease of Reynolds with O_2 is then due to the gas density and viscosity variation. Still, it remains higher than O_2/N_2 mixture, but approaches the air values at higher O_2 contents. The Figure 3.8a) however, remarks the importance of gas composition on the fluid-dynamics parameters, dominating over gas properties variation, neither by gas composition nor gas temperature.

The differences in gas composition influence, predicted by the expressions in Table 3.1 are depicted in Figure 3.9. In spite of the differences on the tendencies of non dimensional parameters, the air-firing coefficients are to some degree over the ones in oxy-firing, following a descendant tendency with increasing O_2.

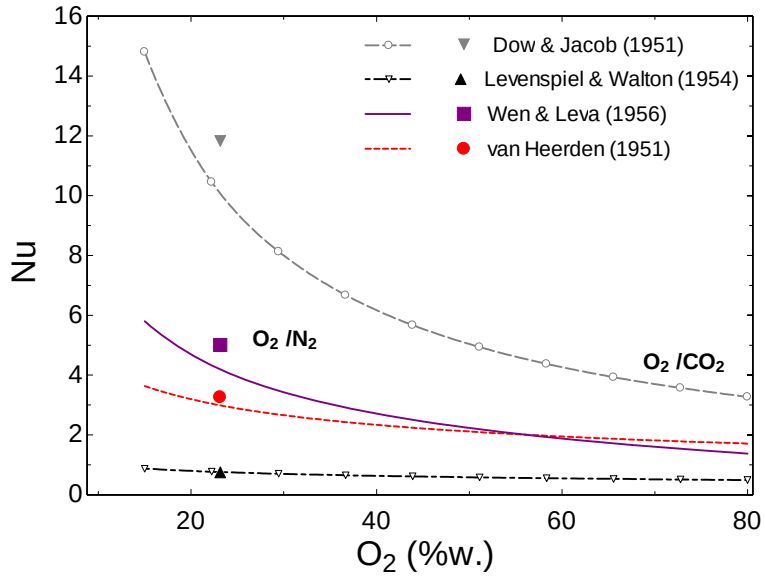

Figure 3.9. Effect of O_2 content in the gas mixture on Nusselt number predicted by different authors

The Figure 3.10 shows the prediction by Zabrodsky (1966), Eq. 3.2, for two gas mixtures, O_2/CO_2 and O_2/N_2, at three temperatures. Since the gas density and gas conductivity varied with opposite tendencies, the influence of O_2 content at inlet is almost offset. According to this, the heat transfer would be higher under oxy-firing conditions, but the influence of O_2 concentration would not be relevant. The heat transfer coefficient decreases only 5% while increasing O_2 in the mixture. According to this expression, the effect of temperature would decrease the heat transfer coefficient down to 8%, due to the changes on gas properties (since radiation is not included in this expression).

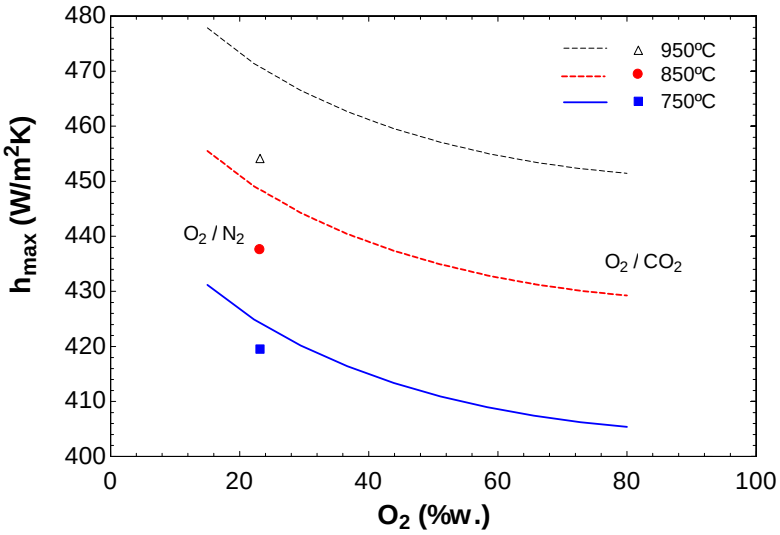

Figure 3.10. Prediction of heat transfer coefficient by the Zabrodsky expression (Eq. 3.2)

Radiation contribution from the gas phase is, in many cases, neglected in dense bed. However, it must be carefully considered for the dilute zone of oxy-fuel fluidized beds, since participative gas CO_2 partial pressure is now higher. The expression in Eq. 3.21 (Baukal, 2000) can be used to calculate the emissivity of a mixture of gases:

$$\varepsilon_g = \varepsilon_{CO2} + \varepsilon_{H2O} - \Delta\varepsilon \qquad \text{Eq. 3.21}$$

Being ε_f the emissivity of the mixture, and ε_{CO2} and ε_{H2O}, the emissivity of the two compounds at the operating temperature. $\Delta\varepsilon$ considers the overlapping of the emission bands of H_2O and CO_2. Figure 3.11 shows the influence of the CO_2 content in the gas for three different cases of H_2O content, considering a freeboard temperature of 700ºC. The presence of H_2O inhibits the mixture emissivity. The value of the gas emissivity differs up to 15% for high CO_2 content in the gas. At lower gas temperature ε_{H2O} dominates over ε_{CO2} for both air and oxy-fuel modes, at 27% O_2 at inlet (Andersson and Johnsson, 2006).

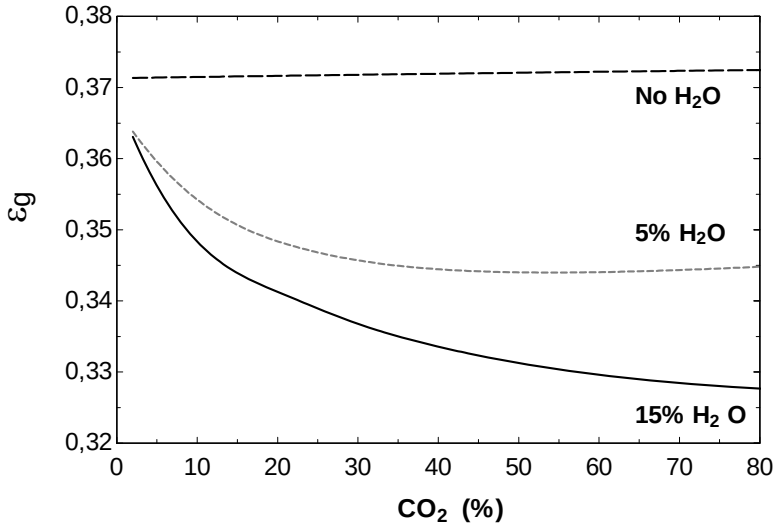

Figure 3.11. Emissivity of a gas mixture of CO_2 and H_2O

From the variation of emissivity values in Figure 3.11 the contribution of radiation mechanism will be treated as in air-firing case, including only the wall and particles emissivities, and not the gas phase radiative properties.

3.2.3 SUMMARY

Heat transfer in fluidized beds has been widely investigated along the last decades. The movement of particles is the main responsible for the exchange of heat with the immersed or wetted surfaces. Together with this mechanism, the gas convection and the radiation are also involved in the overall heat transfer. In the earlier decades, researchers looked for empirical expressions that fairly represented the phenomena occurring during the contact of particles with the exchange surface, through the gas layer in the proximity of the wall. In spite of their simplicity, some predict the influences of operational parameters similarly to the more mechanistic models. Empirical correlations, however, have been developed usually for small rigs and their extrapolation to a different geometry and conditions must be carefully treated. The theoretical analysis of heat transfer during oxy-fuel in fluidized beds is assessed for the first time. The predictions from some of the expressions forecast different values for oxy-fuel case. In most of them, however, the value of heat transfer in oxy-fuel is slightly higher than in air-firing. This will be quantified and analyzed in the following sections. The mechanistic approach turns out as a suitable option for including the differences in the fluidizing atmosphere. Particular attention should be paid to the effective properties of the particle phase and to the residence time of particles when gas properties change. Although the heat transfer coefficients in oxy-fuel combustion are not expected to be far from those during air-firing, there is no study yet pointing at this line.

From this lack of experimentation on heat transfer in oxy-fuel fluidized bed, we now characterize the heat transfer experimentally in a pilot plant working both, under oxy and air-firing conditions.

3.3 EXPERIMENTAL SET-UP

3.3.1 PREVIOUS EXPERIENCES ON OXY-FUEL FLUIDIZED BEDS PILOT PLANTS.

In the last decade, some fluidized bed pilot plants operating under oxy-firing conditions were erected. Details can be found in Table 1.2. In general, they estimate the heat transfer coefficients analogously to the air-firing mode of operation. In spite of the remarkably importance of the proper heat transfer surfaces allocation in oxy-fuel fluidized beds, there is only one study that included the measurement of heat transfer coefficients under oxy-fuel conditions. It was carried out by Alstom in their 3MW *Multi-Use Combustion Test Facility* (Nsakala et al., 2004). For measuring heat transfer at two different sections of the furnace, they installed two single tube test sections in the furnace. The pipes were 2 and $1^{1/4}$ inch, for assuring a high water velocity and so, low heat transfer resistance. They concluded that there was no clear difference in the heat transfer to the test sections between air and oxy-fuel operation. Still, they did not show any numerical results of these measurements. Furthermore, the particular relevance that the external heat exchanger will gain in the future oxy-fuel designs, points out the need of measuring the heat transfer coefficient also in the dense part of the fluidized beds.

A pilot plant that were initially conceived for operating under conventional air-firing conditions and that was retrofitted for oxy-firing should have included additional heat removal systems or should have considered this cooling flexibility from the initial design. It is difficult to find, in the published description of existing oxy-fuel pilot plants, the techniques used for controlling the bed temperature. Some of the facilities, used water cooled pipe, introduced vertically into the fluidized bed (de Diego et al., 2012). During operation they can move the pipe upward and downwards, controlling so the heat transfer surface and easily regulating the temperature. In other cases, the cooling methods are less sophisticated, and they consist of removing layers of isolating wool, for external walls natural convection enhancement (Czakiert, 2011).

Despite there are no other studies in which attention were particularly paid to heat transfer during oxy-fuel combustion in fluidized bed, there are important issues

closely related to the heat removal of oxy-fuel fluidized beds and the control of bed temperature:

- One of them and the most influencing for the proper future oxy-fuel large boilers have already explained in the previous chapter, regarding the heat transfer balance in the overall plant between AF and OF cases. The external heat transfer in fluidized bed heat exchanger will not be fluidized with air anymore but, most probably, with recycled flue gases. The composition will be predominantly CO_2. Probably with certain O_2, H_2O or N_2 from air-leakages. This change in gas composition is closer to the oxy-fuel atmosphere in a bubbling fluidized bed, as will be further explained here.
- Other fundamental issue regards the mechanisms of in-bed SO_2 capture. These change from usual air fluidized bed conditions. Garcia-Labiano et al. (2011) found that higher bed temperature would be needed for obtaining similar SO_2 capture efficiencies than with air. Calcination previous sulfation of limestone, the two-step reaction that usually occurs in conventional firing at around 850ºC, will not take place under oxy-firing conditions. Higher CO_2 partial pressure existing on oxy-fuel boilers avoid calcination of limestone at that temperature, and thus, lower SO_2 capture efficiencies. The authors proof this in a small fluidized bed rig (de Diego et al., 2011) and recommended higher bed temperature for optimum SO_2 capture under OF. This was confirmed at greater scale by Lupiañez et al. (2012) If higher temperature level is needed, heat removal along the boiler requires a more accurate design. The risk of ashes agglomeration in hot spots is then more probable. Moreover the proper allocation of the heat transfer surfaces along the boiler need to be carefully design for optimizing the combustor efficiency, since higher heat recovery will be needed in the convective pass of the boiler.
- Another important concern is also related to the calcination of limestone for SO_2 capture. If calcination takes place the excess of CaO arrives at the external heat exchanger. It will meet there the fluidizing gas consisting mostly on CO2. Below certain temperature, this CO_2 would react with the arriving CaO and the external heat exchanger could be instantaneously defluidized. Control of temperature in this device will then be of an essential importance, for avoiding such problem. In the literature, the 4 MW

pilot plant unit, owned by Metso Power, reported this kind of difficulties (Varonen et al., 2012).

CIRCE oxy-fuel bubbling fluidized bed was initially designed based on flexibility criteria. Different fuel ranks, from lignite to bituminous coal, and also biomass and coal blends have been characterized under oxy-fuel combustion (Romeo et al., 2011). A wide range of O_2 percentages at inlet have also been tested. This plant has been used by other components of the research group, for assessing the influencing of oxy-fuel combustion on the pollutant emissions, such as NO_x and SO_2 (Romeo et al., 2009b; Lupiáñez et al., 2011). Fluid-dynamics differences between AF and OF have also been addressed (Guedea et al., 2011). Combustion performance was analyzed and reported. The focus is addressed now towards the heat transfer measurements and the influence of oxy-fuel conditions on it.

3.3.2 CIRCE OXY-FUEL BUBBLING FLUIDIZED BED PILOT PLANT

In 2008 erection of the oxy-fuel bubbling fluidized bed combustor was finished and first characterization tests were run. The pilot plant was designed to burn up to 90 thermal kW under oxy-fuel conditions. Figure 3.12 represents the whole arrangement of plant equipments. Figure 3.13 shows a picture of the facility.

The combustion takes place in a bubbling fluidized bed, 203 mm internal diameter. Freeboard height was fixed at 1.8 m with an estimated maximum dense-bed height of 0.7 m. A propane burner pre-heats the bed material, up to the ignition temperature, which depends on the fuel. The induced draft fan is needed for the preheating stage, since it facilitates combustion flue gases to be conducted along the bed and the auxiliary equipments and so, heating up the overall facility.

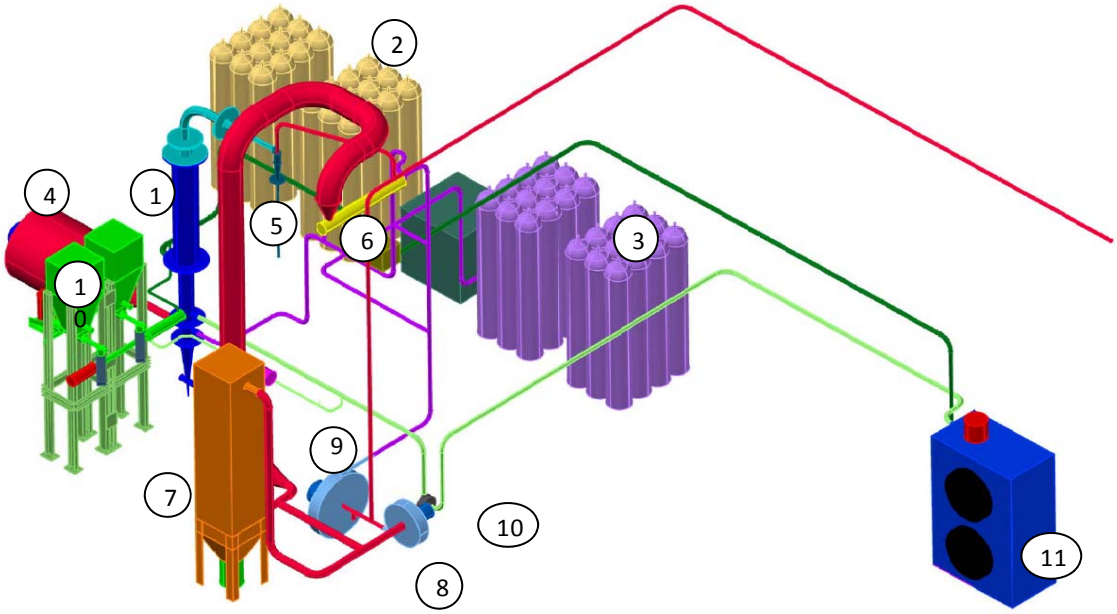

Figure 3.12. Pilot plant scheme: 1- Bubbling fluidized bed. 2-O_2 supply bottles. 3-CO_2 supply bottles. 4-Propane burner pre-heater. 5- Cyclone. 6-Flue gas heat recovery exchanger. 7-Bag filter. 8-Induce draft fan. 9-Forced or recirculation draft fan. 10-Cooling water pump. 11-Air-Water cooler

Figure 3.13. Photo of the fluidized bed pilot plant

Regarding the fuel and fresh sorbent supply, two 0.2 m^3 hoppers are located besides the reactor. When using coal and coal mixtures, one hopper contains the

fuel and the other limestone. When solids with different properties are used, such as coal and biomass, it is necessary to feed them separately, because segregation could take place easily inside the hopper. Each hopper discharges into endless screws controlled by variable-frequency drives and so, independent flow rates can be fed from every hopper. Each endless screw discharges in a faster one that feeds the combustor in the lower part, at 0.1 m over the distributor plate. While operating the plant under air-firing conditions, a forced-draft fan (or recirculation fan) introduces air into the boiler. When feeding oxygen with carbon dioxide mixtures from the gas canisters, this fan is no needed but is used again when substituting commercial CO_2 by RFG. In any case, an induced-draft fan evacuates the flue gas from the reactor. Fans nominal flow rates are 45 Nm^3/h and 130 Nm^3/h, respectively. O_2/CO_2 mixture is initially taken from 2 blocks of 12 canisters each. The proportion of each compound in the oxidant is controlled in a gas-mixer and the mixture is stored in small tank before it is fed. Once the operation is stabilized, a bleed from flue gases is recycled by the recirculation-draft fan, replacing the consumption of CO_2 cylinders.

Particles present in flue gases from the fluidized bed combustor are first removed by a fall chamber and later by a high efficiency Stairmand cyclone, designed for a cut size of 2 μm. Sensible heat from flue gases can be used in a 9kW shell-and-tube heat exchanger, where oxidant gas can be preheated, or by-passed depending of the required temperature level. At the end, a fabric-filter bag is located for additional particle retention.

For monitoring and controlling purposes, measurement instruments, valves, motor starters and variable-frequency drivers, are connected to a PLC (Programmable Logic Controller). Signals from thermocouples, pressure gauges, flow-meters and control valves are connected by distributed I/O. Some automatic sequences are programmed, to execute well-defined operating actuations. The supervision is carried out by Supervisory Control and Data Acquisition Application (SCADA).

Initially, the bed was designed for being cooled down thanks to a cooling jacket that covered the dense part, but the design was modified for accomplishing four independent jackets.

The constructive division of the combustor consists of two separated zones, the lower part, 0.8 m height, and the upper part, 1.6 m height and refractory lined. The lower part is where most of the combustion and reactions occurs. For controlling

bed temperature, four cooling jackets are surrounding the bed (Figure 3.14). The lower jacket is 50 mm height and the other three, 100 mm. Water can flow through either of the jackets independently, or through none of them.

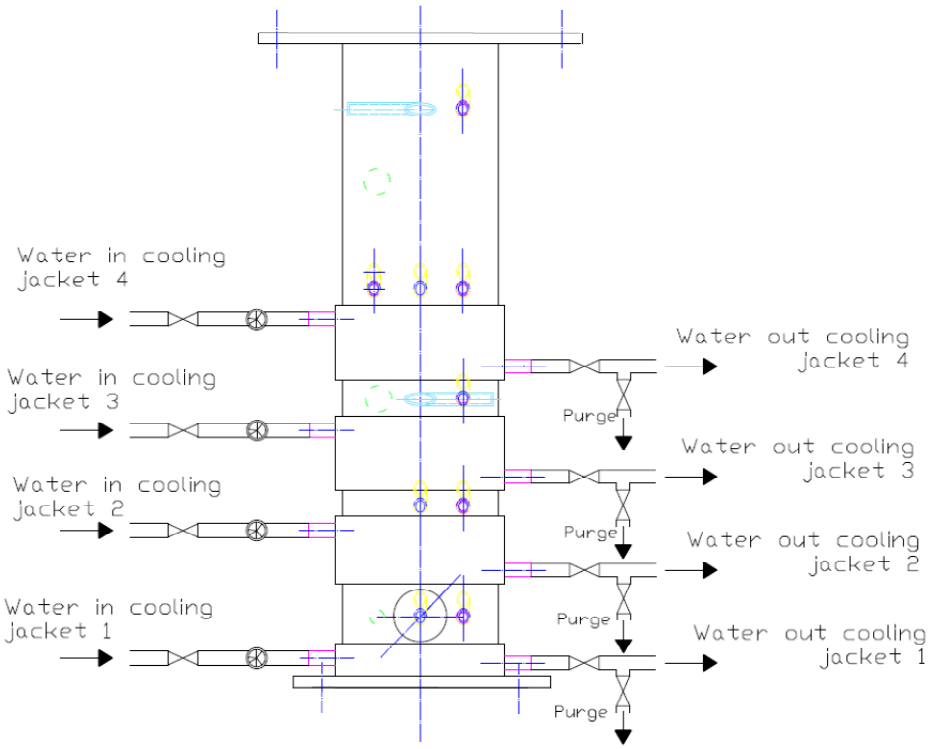

Figure 3.14. Lower section of the bubbling fluidized bed. Constructive scheme.

Total water flow is measured more accurately by an electromagnetic flow-meter. Additionally, every jacket includes a turbine flow-meter and a butterfly valve, allowing or not the water circulation. The purge valve opens only in the first instants of cooling, to evacuate the steam bubbles formed before stable cooling is reached.

3.3.3 EXPERIMENTS PLANNING

It was previously stated that the most important parameters influencing heat transfer in fluidized beds are the fluidizing velocity, the bed temperature and particles size. This last parameter was not varied in the plant operation, and thus, it was no included in the experimental planning. The value of fluidizing velocity and bed temperature are no directly manipulated, but by means of other operational parameters, such as oxidant stream flow rate, temperature and composition; fuel input and type; and cooling. Table 3.5 intends to summarize these

variables limits and monitoring devices, aiming at operating inside a proper range of values for fluidizing velocity and bed temperature.

The first column in Table 3.5 shows the parameters of the plant and inert matter that keep constant during the tests. These are the boiler geometry, the distributor plate arrangement, sand characteristics and its particle size distribution. The central section of Table 3.5 indicates the variables that can be manipulated during the plant operation. u_f and T are then indirectly varied:

- The fluidizing velocity is determined by the stoichiometric oxygen related to the fuel fed, the proportion of diluents: CO_2, recycled flue gas or air-N_2 and the bed temperature. The temperature influences the density of gases and thus, the velocity inside the reactor. For fitting into the desired bubbling regime, velocities were kept between 0.8 and 1.6 m/s
- The bed temperature is uniform in the dense part of the bed. Oxygen concentration affects the temperature profile. Particularly in this installation, temperature in the freeboard will be remarkably higher under oxy-fuel that under air-firing. Keeping temperature below 1000ºC will be essential for avoiding agglomeration problems.

Although fuels tested in the plant ranged from anthracite to lignite and blends with biomass, the experiments considered for the heat transfer coefficient assessment were the ones using anthracite type of coal. The other fuels exhibited lower heating values and so, lower thermal output during operation. As a consequence, the heat of combustion was not enough to keep stable cooling and heat transfer coefficients were not considered. The two types of Spanish anthracite used in the tests are shown in Table 3.3.

The ranges of experiments planned and finally achieved are summarized in Table 3.4. The range of oxidant composition was varied in oxy-fuel mode up to 65% O_2 concentration. Gas velocities were lower under oxy-fuel combustion, compared with air-mode.

Fuel:	Anthracite 1	Anthracite 2
HHV(Kcal/kg)	5095	5350
INMEDIATE ANALYSIS (%w.)		
moisture	2,05	1,00
volatile matter	10,84	7,55
fixed carbon	61,11	59,90
ashes	26,00	31,55
PROXIMATE ANALYSIS (%w.)		
C	64,46	60,66
S	1,04	1,33
H	2,32	2,16
N	1,20	0,87
O	4,98	3,43

Table 3.3. Composition of fuels used in the tests

MODE	O_2 inlet (% v.)		T_{bed} (C)		u_f (m/s)	
	Planned	**Achieved**	**Planned**	**Achieved**	**Planned**	**Achieved**
AF	N/A	N/A	800-850	785-850	0,8-1	0.95
OF	25%-35%	31%-32%	800-850	-	0,8-1	-
	35%-45%	36%-44%	800-850	827-855	0,8-1	0.74-0.94
	45%-55%	50%-54%	800-850	-	0,8-1	-
	55%-65%	57%-60%	800-850	833	0,8-1	0.86-0.98
OF-RFG	30%-35%	36-37%	800-850	796-830	0,8-1	0.84-0.85
AF	N/A	N/A	850-900	859-958	0,8-1	0.95
OF	25%-35%	31%-32%	850-900	877-895	0,8-1	0.84-0.98
	35%-45%	36%-44%	850-900	858-964	0,8-1	0.78-0.94
	45%-55%	50%-54%	850-900	889-943	0,8-1	0.82-0.98
	55%-65%	57%-60%	850-900	885-918	0,8-1	0.86
OF-RFG	30%-35%	36-37%	850-900	859-887	0,8-1	0.85
AF	N/A	N/A	800-850	785-850	1-1,2	1.3-1.6
OF	25%-35%	31%-32%	800-850	-	1-1,2	-
	35%-45%	36%-44%	800-850	827-855	1-1,2	-
	45%-55%	50%-54%	800-850	-	1-1,2	-
	55%-65%	57%-60%	800-850	833	1-1,2	-
OF-RFG	30%-35%	36-37%	800-850	796-830	1-1,2	1.05
AF	N/A	N/A	850-900	859-958	1-1,2	1.3-1.6
OF	25%-35%	31%-32%	850-900	-	1-1,2	1.02-1.23
	35%-45%	36%-44%	850-900	858-964	1-1,2	1.04
	45%-55%	50%-54%	850-900	889-943	1-1,2	-
	55%-65%	57%-60%	850-900	885-918	1-1,2	1.05
OF-RFG	30%-35%	36-37%	850-900	859-887	1-1,2	-

Table 3.4. Experiments planning matrix, planned and achieved ranges

Fixed Parameters		Parameters that can be modified during operation				Parameters that defined the plant operation		
Parameter	**Range**	**Parameter**	**Control device**	**Monitoring**	**Range**	**Parameter**	**Monitoring**	**Range**
Bed geometry	-207 mm diameter -Lower 1 m no refractory lined -Upper 2 m additional refractory lined	**Gas inlet flow rate**	-Forced-draft fan with variable-frequency drives (AF) -Valves (OF)	Flow-meters	30-150 m^3/h	**Fluidization velocity**	Flow-meters	0.7-1.2 m/s
Inert matter	Sand	**Comburent composition**	-Gas bottles mixer (OF)	Gas analyzer	Air, 25%-65%O2, FGR			
Particle size distribution	500-800 microns	**Thermal power**	Fuel endless screw with variable-frequency drives.		30-100 kW	**Bed temperature**	Thermo-couples	750-980ºC
		Fuel Type	Proximate and ultimate analysis		Coals, biomass, coke…			
Distributor plate	Flat plate with 210 orifices	**Cooling**	-Valves opening to the cooling jackets -Aero-cooler	Water thermocouples Water flow-meter	5- 60 kW			
		Gas inlet temperature	Proportional valve bypassing the heat exchanger		35-180ºC			

Table 3.5. Experimental operational ranges and devices

3.4 HEAT TRANSFER COEFFICIENTS MEASUREMENT

3.4.1 MEASURING PROCESS

Heat transfer coefficients are measured by an indirect way. When cooling is required for keeping a proper bed temperature, one of the cooling jackets valve is opened, at inlet, allowing water to pass through it. In the first instant of water crossing the jacket, the purge valve is opened. Water is around 40ºC when it enters the jacket, and the bed wall is near bed temperature, at more than 850ºC. Thus, during cooling start a great overpressure takes place, because of steam bubbles generation. Opening the purge valve releases this initial steam, protecting also the welding of the jackets. When water is not vaporized anymore, the purge valve is closed and the valve at outlet is opened, to close the water circuit. Heat transfer coefficient is measured at this instant.

Water mass-flow measurements and water temperature are averaged for every cooling period to calculate the energy removed by the water is approximated with Eq. 3.22:

$$Q_{cooling} \approx m \cdot c \cdot \left(T_{water;OUT} - T_{water;IN}\right) \qquad \text{Eq. 3.22}$$

Being m the water mass flow, c the average water thermal capacity and $T_{water;OUT}$ and $T_{water;IN}$ temperatures at outlet and inlet of the cooling jacket respectively. This expression assumes the approximation of considering the water calorific value, c, constant at the water average temperature.

The energy transferred to the cooling jackets is analogous to the Newton Cooling Law, calculated by means of the global heat transfer coefficient UA, yielding:

$$Q_{cooling} = UA \cdot \Delta T \qquad \text{Eq. 3.23}$$

ΔT is the logarithmic temperature difference evaluated as:

$$\Delta Tln = \frac{T_{water;OUT} - T_{water;IN}}{ln\dfrac{T_{bed} - T_{water;IN}}{T_{bed} - T_{water;OUT}}} \qquad \text{Eq. 3.24}$$

Bed temperature is measured at different heights in the bed. Particularly the temperature measured at the lowest position is located at 99 mm from the distributor. Then, bed temperature of the first jacket is approximated to the average between the oxidant stream temperature and the value from the first thermocouple.

Neglecting the conduction through the bed wall, UA involves two main contributions, the water convection coefficient, h_{water}, and the fluidized bed coefficient, h_{bed}:

$$\frac{1}{UA} \approx \frac{1}{h_{water} A_{water}} + \frac{1}{h_{bed} A_{bed}} \qquad \text{Eq. 3.25}$$

Water circulates through the jacket at high velocity, since the jacket is only 6 mm width. Water convection heat transfer coefficient is estimated using the formula by Gnielinsky, recommended by Mills (1995), for calculating heat transfer coefficient in the water side. The water heat transfer coefficient reaches values around 2500 W/m^{2}K. This is around an order of magnitude higher than the heat transfer coefficient in fluidized beds and, it can be neglected from Eq. 3.25.

Following criteria have been established for selecting an appropriate time-framework of measurements:

- At least 1 minute of stable operation on water parameters: mass flow rate and temperature at outlet and inlet (avoiding bubbling phase)
- During this time, fed fuel must be also constant
- During this time, fan drivers frequency is not varied.
- Registered emissions delays at least 3 minutes after any change inside the combustor. With this premise, 1 minute of stability in emissions measurements is also considered after the moment of stability in the water parameters.
- Values for calculations are averaging over the stability range selected
- The number of values increases when the time framework is longer, and this will allow reducing uncertainty, as it will be later explained.

A usual cooling curve is shown in the Figure 3.15. Here they are represented the water inlet and outlet temperature, the water flow rate and, in the secondary axle, the bed temperature. The frame remarks the time of operation at which values of

measurements are considered for calculations. First seconds of cooling are instable, due to bubbles formation inside the jacket

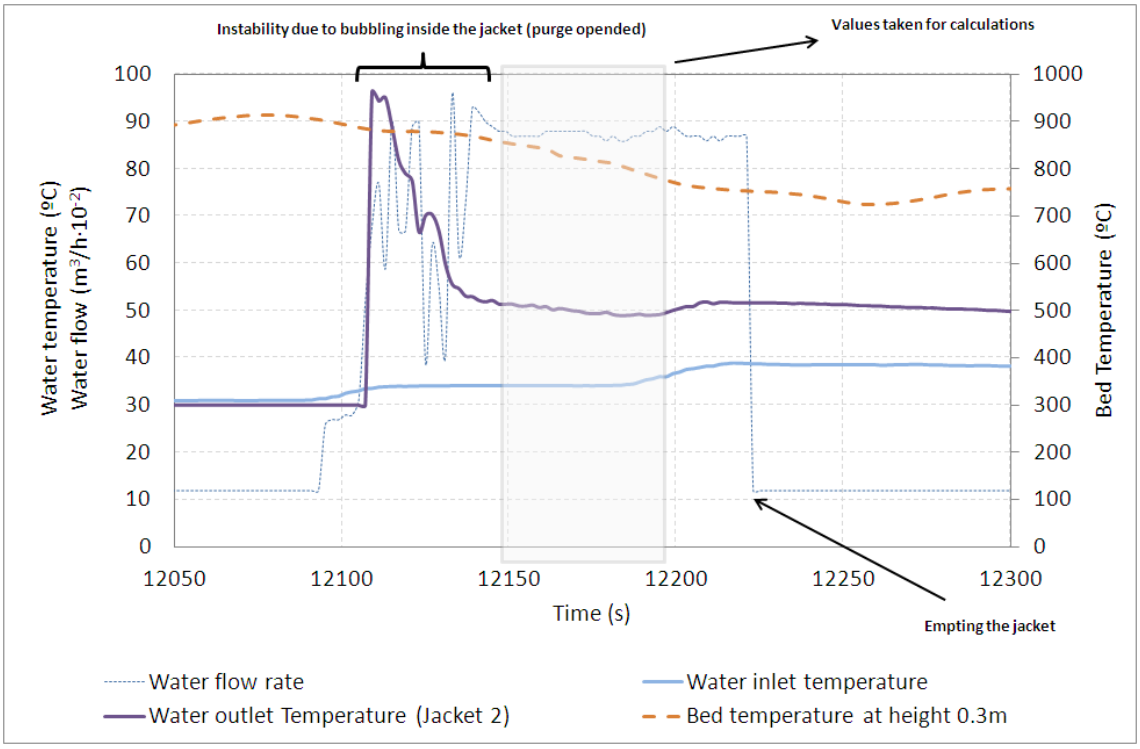

Figure 3.15. Example of the beginning of the bed cooling (17/02/2011)

In Table 3.6 stable measuring AF stages are gathered. Fuel input up to 60 kW was fed. Higher thermal power was not possible under AF conditions, due to limitation of inlet velocity. A wide range of bed temperatures were reached with the high calorific value fuels (Table 3.3). Every test carried out in the pilot plant begins with an AF phase.

In Table 3.7 the stable points for heat transfer calculation during oxy-fuel combustion tests are collected. A wider range of fuel inputs was possible, up to 100 kW. Last column of Table 3.7 shows the proportion of O_2 at inlet, from the commercial canisters. The high proportion of O_2 at inlet has been scarcely experimented before. One of the reasons could be precisely, the low cooling capacity of retrofitting fluidized beds. In these experiments we reach O_2 concentrations at inlet as high as 59.6%, with a fuel thermal input up to 100kW. Cooling was possible by opening the two central cooling jackets.

Oxy-fuel tests with recycled flue gas (RFG) mode were also carried out, as shown in Table 3.8. The column indication the CO_2 concentration from the mixture from the bottles is lower than in OF tests. The PLC had a control routine implemented to

regulate this concentration. Data from the gas analyzers indicated O_2 and CO_2 concentration present in flue gas that was recycled. The flow concentration of both compounds from the bottles was programmed for keeping a constant O_2 concentration at combustor inlet, around 36%.

Fuel	MODE	Q_{fuel} (kW)	T_{bed} (C)	V_{in} (m^3/h)	Exhaust gas composition (d.b.)		
					CO_2 (%v.)	CO (ppm)	O_2 (%v.)
Anthracite1	AF	60.5	785	59.2	14.2	1748	4.8
Anthracite1	AF	60.5	790	59.9	14	1245	5.2
Anthracite2	AF	43.4	817	54.0	13.5	431	3.5
Anthracite1	AF	35.6	819	57.3	16.3	2056	5.2
Anthracite2	AF	43.4	824	56.5	12.8	378	5.1
Anthracite1	AF	34.9	831	57.1	18.3	1747	4.8
Anthracite1	AF	54.8	832	61.5	14.4	696	5.1
Anthracite1	AF	54.8	832	61.5	14.4	695	5.1
Anthracite2	AF	32.2	834	53.8	14.6	1650	3.6
Anthracite2	AF	50.9	840	54.9	19.1	3564	5.4
Anthracite1	AF	30.5	840	56.9	18.5	1378	4.8
Anthracite2	AF	32.2	843	37.0	11.6	255	5.6
Anthracite2	AF	32.2	845	59.8	11.1	183	6.5
Anthracite2	AF	46.2	846	64.5	13	608	4.9
Anthracite2	AF	32.2	859	42.9	13.4	581	4.2
Anthracite2	AF	32.2	868	56.5	11.6	246	6.7
Anthracite2	AF	32.2	870	58.7	13.5	399	4.4
Anthracite2	AF	32.2	871	56.6	15.1	4029	2.6
Anthracite2	AF	49.0	907	66.9	11.7	225	6.3
Anthracite1	AF	54.8	954	54.7	14.6	490	5.0
Anthracite1	AF	54.8	958	58.9	16.1	2223	3.5
RANGE	MIN	30.5	785	37.0	11.1	183	2.6
	MAX	60.5	958	66.9	19.1	4029	6.7

Table 3.6. Summary of AF tests stable zones for heat transfer measurements

Fuel	MODE	Q_{fuel} (kW)	T_{bed} (C)	V_{in} (m^3/h)	Exhaust gas composition (d.b.)			O_2 inlet (%v.)
					CO_2 (%v.)	CO (ppm)	O_2 (%v.)	
Anthracite1	OF	30.5	888	50.2	72.8	246	17.4	30.9
Anthracite1	OF	30.5	889	50.1	84.6	348	7.7	31.1
Anthracite1	OF	30.7	894	52.1	87.7	2635	4.7	31.2
Anthracite2	OF	71.4	877	43.7	79.7	166	8.9	31.2
Anthracite1	OF	50.3	896	62.3	90.8	1830	4.6	31.3
Anthracite1	OF	66.1	884	57.6	90.2	3527	3.3	31.4
Anthracite2	OF	54.6	882	45.2	80.2	241	9.1	32.0
Anthracite2	OF	32.5	847	39.0	79.9	2016	3.5	36.3
Anthracite2	OF	50.3	861	48.5	78.6	288	5.5	37.0
Anthracite2	OF	51.8	831	48.5	76.7	223	6.9	37.2
Anthracite2	OF	49.0	858	48.5	76.8	224	6.8	37.3
Anthracite2	OF	64.4	827	47.7	76.5	224	7.2	37.3
Anthracite2	OF	32.2	964	42.6	79.2	5120	1.9	40.8
Anthracite1	OF	50.9	891	51.4	81.0	1310	7.2	41.2
Anthracite1	OF	50.9	893	44.2	85.0	2756	6.2	41.3
Anthracite2	OF	32.2	944	37.1	79.2	5120	2.5	41.8
Anthracite2	OF	32.6	898	39.8	78.0	306	8.2	43.0
Anthracite2	OF	54.6	884	41.6	76.8	250	9.3	43.9
Anthracite2	OF	68.3	902	44.2	80.2	380	9.2	49.9
Anthracite2	OF	72.3	943	44.8	79.6	200	7.0	50.4
Anthracite2	OF	74.4	895	45.3	79.7	375	8.5	50.5
Anthracite2	OF	77.0	889	43.4	69.9	300	13.4	50.7
Anthracite2	OF	77.0	918	38.4	67.1	319	15.8	50.9
Anthracite2	OF	78.0	894	43.6	72.4	283	13.1	53.5
Anthracite2	OF	77.0	918	48.3	77.9	227	6.2	57.5
Anthracite2	OF	99.4	833	48.4	65.5	434	18.0	57.8
Anthracite2	OF	99.4	885	40.4	75.6	5045	6.9	59.6
RANGE	MIN	30.5	827	37.1	65.5	166	1.9	30.9
	MAX	99.4	964	62.3	90.8	5120	18.6	59.6

Table 3.7. Summary of OF tests stable zones for heat transfer measurements

Fuel	MODE	Q_{fuel} (kW)	T_{bed} (C)	V_{in} (m^3/h)	Exhaust gas composition (d.b.)			CO_2 bottles (%v.)
					CO_2 (%v.)	CO (ppm)	O_2 (%v.)	
Anthracite2	OF+RFG	65.8	887	49.2	55.6	1332	5.7	34.7
Anthracite2	OF+RFG	65.8	864	49.3	49.2	284	7.1	30.3
Anthracite2	OF+RFG	77.0	796	46.8	48.9	218	9.0	30.4
Anthracite2	OF+RFG	77.0	830	45.6	47.9	267	9.8	30.5
RANGE	MIN	50.7	796.5	26.9	41.1	218.2	5.7	30.3
	MAX	77.0	886.6	49.3	55.6	2977.3	23.8	44.4

Table 3.8. Summary of OF+RFG tests stable zones for heat transfer measurements

3.4.2 HEAT TRANSFER RESULTS

The results of the heat transfer coefficient estimations for the bed to the wall in every mode are then calculated and represented in Figure 3.16.

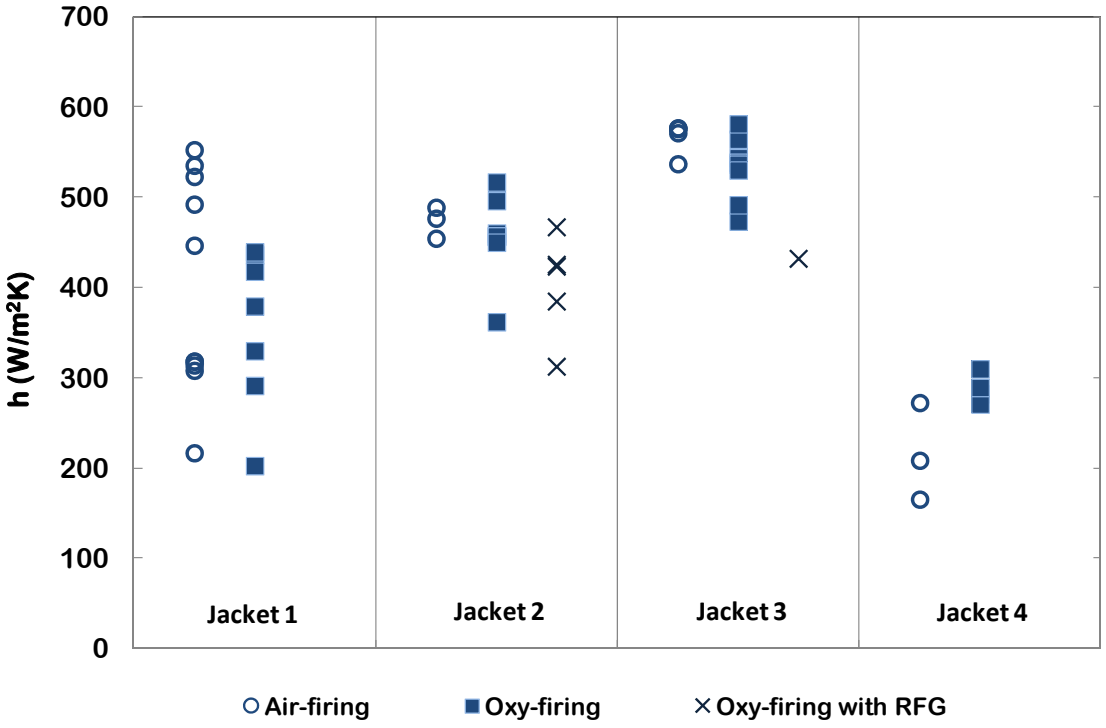

Figure 3.16. Fluidized bed heat transfer coefficients measured in each jacket

The most important conclusion drawn from Figure 3.16 is that values estimated for AF, OF and OF+RFG modes of operation are enclosed within similar ranges, within 200 to 600 W/m²K. These results demonstrate and agree with the fundamental mechanism of heat transfer in the bubbling beds, based on the movement of particles and their contacts with the wall, rather than on the gas composition.

In the fourth jacket, the values are the lowest. This is because it is located at the limit height of the dense bed, coinciding with the exploding bubbles zone. Bed density here is lower and so it is the influence of particle convection heat transfer. The first jacket exhibits the widest dispersion of coefficients. The geometry of this jacket is slightly different from the others. It is half height and it is welded to the lower flange. At first sight this disposition can be act as an extended surface for heat transfer and could influence the heat transfer evaluation. After a transient heat transfer evaluation in this zone the influence of the flange was not relevant for the heat transfer coefficients results. The reason of the lower values in first jacket resides then on the temperature of this zone, where cool oxidant enters the combustor, rapidly reacts with the fuel present and increases the temperature, creating a temperature peak in the zone near the distributor. So, the temperature of the bed at the first jacket location, below the first thermocouple, is lower than in the rest of the bed in many cases.

In all tests, the bed height is higher than the third jacket, so the second and third jacket heat transfer coefficients dwell within a narrower range of values. The three modes of operation show closer values. The discussion will lie in the factors influencing heat transfer and the role of oxy-fuel atmosphere on the influences of the heat transfer coefficients, in section 3.3.4.

The following section explores the uncertainties of these measurements, as criteria to accept or reject any of the measurements.

3.4.3 UNCERTANITY ANALYSIS

In order to complete the previous results, we must evaluate the uncertainties, due to deviations in the sensors measurements and averaging process, from which they are calculated.

h must be expressed as a function of water volumetric flow and inlet and outlet temperature, bed temperature and the properties of water, ρ and c, at the average temperature:

$$h = \frac{\rho_{water} \, V/3600 \cdot c \cdot \left(T_{water;OUT} - T_{water;IN}\right)}{A_{cooling} \cdot \Delta Tln} \qquad \text{Eq. 3.26}$$

Uncertainties associated with heat transfer coefficients are calculated by propagation of uncertainties principle Eq. 3.27 (Coleman and Steele, 1999):

$$\frac{U_h^2}{h^2} = \left(\frac{T_{water;IN}}{h}\frac{\partial h}{\partial T_{water;IN}}\right)^2\left(\frac{U_{T_{water;IN}}}{T_{water;IN}}\right)^2 + \left(\frac{T_{water;OUT}}{h}\frac{\partial h}{\partial T_{water;OUT}}\right)^2\left(\frac{U_{T_{water;OUT}}}{T_{water;OUT}}\right)^2 + \cdots$$

$$.. + \left(\frac{T_{bed}}{h}\frac{\partial h}{\partial T_{bed}}\right)^2\left(\frac{U_{T_{ned}}}{T_{bed}}\right)^2 + \left(\frac{V}{h}\frac{\partial h}{\partial V}\right)^2\left(\frac{U_V}{V}\right)^2 + \left(\frac{A}{h}\frac{\partial h}{\partial A}\right)^2\left(\frac{U_A}{A}\right)^2 \qquad \text{Eq. 3.27}$$

Where U_h, $U_{TwaterIN}$, $U_{Twater,OUT}$, U_{Tbed} and U_{TA} are the uncertainties related to the corresponding variables, respectively: heat transfer coefficient h, inlet and outlet $T_{waterIN}$ and $T_{waterOUT}$, bed temperature T_{bed} and cross sectional area for the water flow, A. This area is considered a constant value during each experiment.

The PLC registers the measurements every two seconds. Each instant, h is calculated and averaged within the stability period. Every instantaneous measure of h has an uncertainty associated with the measurements device and calculated by Eq. 3.27.

The systematic uncertainty of the thermocouples type K was calculated from the standard limit of errors, 0.75%, using Eq. 3.28.

$$U_T = \sqrt{\left(\frac{limit^2}{3}\right)} \qquad \text{Eq. 3.28}$$

The water flow measurement given by the turbine flow-meters was calibrated with the electromagnetic flow-meter, since this is a much more accurate device. The

systematic error includes then a term for the absolute uncertainty of both, electromagnetic and turbine devices and the influence of temperature. The absolute uncertainty of volume flow yields:

$$U_V = K\sqrt{\left(U_{sample}^2 + U_{calibration}^2 + \frac{\Delta V_{temperature}^2}{3}\right)} \qquad \text{Eq. 3.29}$$

Since the instantaneous value of h is averaged during the measuring period, the variance and the number of samples must be included and the absolute uncertainty of h yields:

$$U_h = K\sqrt{\left(U_{instantaneous}^2 + \frac{S_m^2}{n_m}\right)} \qquad \text{Eq. 3.30}$$

Where, S_m^2 is the variance of the measurements of h along the period of time considered. The constant K is usually equal to 2, assuming an enough number of data for the calculation. Instantaneous and absolute uncertainties are summarized in Table 3.9, averaging the uncertainties obtained for each value of h measured:

	Instantaneous uncertainty				**Sample period uncertainty**			
Jacket	**1**	**2**	**3**	**4**	**1**	**2**	**3**	**4**
max U_h	5.8%	2.6%	2.9%	3.8%	10.8%	1.6%	1.5%	8.8%
min U_h	28.4%	8.1%	11.6%	7.2%	34.3%	25.8%	30.3%	10.1%
average U_h	11.6%	5.2%	5.0%	5.1%	18.8%	9.3%	10.8%	9.5%

Table 3.9. Instantaneous and averaging relative uncertainty for heat transfer determination

The results of the instantaneous uncertainties assigned the most important source of errors to the water thermocouples, since the possible range of measurement of this device is much wider than the values of water temperature. The jackets 2, 3 and 4, presented uncertainties around 5% in the measurement of h, whereas the jacket 1 showed higher values, up to 12% averaged.

In the following analysis we discard the values obtained in the first jacket, since they involve double uncertainty ranges than the other three. We must also remove the fourth jacket measurements, because, as previously explained, the bed limit is below the jacket and thus the conditions are not comparable with the other jackets. Finally, the measurements of heat transfer during the OF+RFG mode will not be considered, since they are too few to be representative.

3.5 DISCUSSION ON THE RESULTS OF THE HEAT TRANSFER IN OXY-FUEL BFB

Along the current section, the results obtained of heat transfer during air and oxy – combustion tests are analyzed under the two perspectives revised in section 3.2. First, non-dimensionalized heat transfer values are compared with the conventional non-dimensional numbers involved in the majority of empirical approached for particle convection. Additionally, the expression by Molerus (Eq. 3.3) will also be explored and it will better estimate the influence of Reynolds number. The measurements will be then contrasted with the semi-empirical mechanistic approaches for heat transfer calculation. Here it is proposed the expression that better fits the experimental values in oxy-fuel combustion. This approach aims at being extrapolated to different facilities of similar characteristics, such as external heat exchangers attached to circulating fluidized beds.

3.5.1 EMPIRICAL APPROACH ANALYSIS

The theoretical distribution of non-dimensional numbers in oxy-fuel fluidized bed combustion was reviewed at the beginning of this chapter. Now, the experimental results are shown in terms of these set of parameters, in order to forecast the experimental heat transfer obtained during the operation.

Figure 3.17 shows the non-dimensional numbers calculated from the experimental conditions, and represented as a function of the O_2 content at inlet of the reactor. The Archimedes number is slightly higher in OF than AF. These values get closer for higher O_2 concentrations. The bed temperature in AF is in general lower than in OF, and this makes the values of Archimedes in OF approach those in AF. Analogously, Reynolds in OF is close or even lower than in AF. Apart from the bed temperature influence, as in Archimedes case, fluidizing velocities in AF were higher than in OF in the majority of cases, approaching so the values of both modes. Finally, Prandtl number follows the theoretical curve represented in Figure 3.7, where the temperature influence affects the AF values, but not OF.

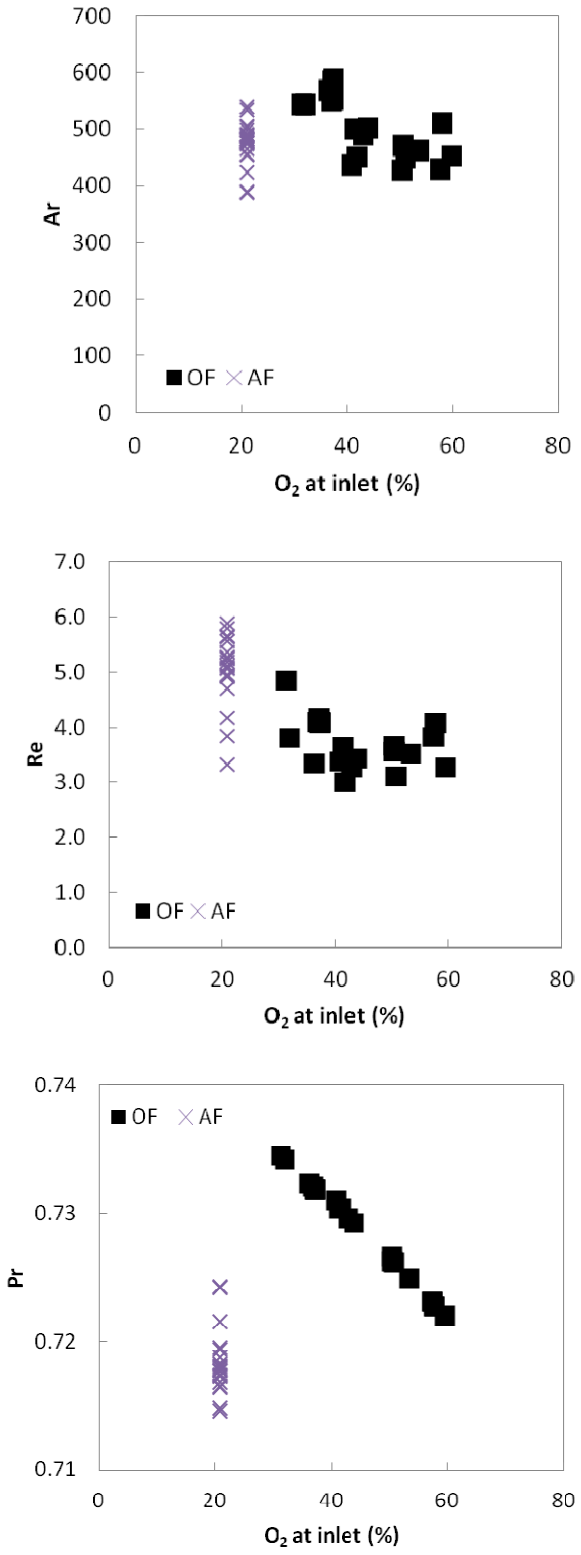

Figure 3.17. Influence of O_2 content on non-dimensional parameters

Although fully empirical expressions cannot assure and accurate estimation of heat transfer coefficient values for conditions different from those used for their development, they can help to anticipate influences of different non-dimensional

numbers on Nusselt numbers, representing the dissimilar conditions of air and oxy-firing modes. Similarly to the theoretical analysis carried out at the beginning of this chapter, the influence of non-dimensional numbers is here evaluated with the experimental results.

In Figure 3.18 the experimental Nusselt number is compared with the Prandtl, Reynolds, Archimedes, heat thermal capacity ratio, thermal conductivity ratio and bulk-gas density ratio.

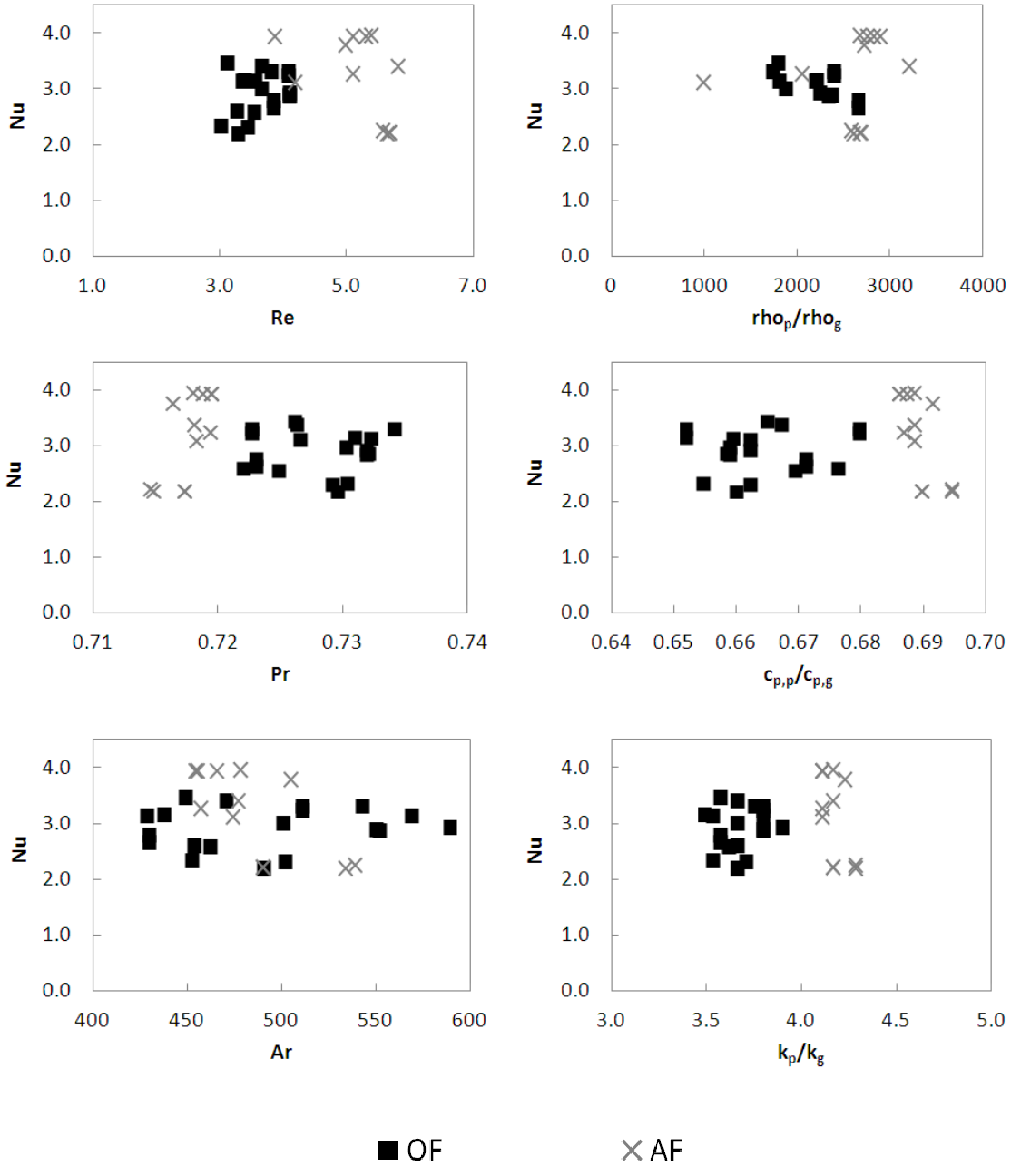

Figure 3.18.Influence of non-dimensional parameters on Nusselt number

Prandtl number is slightly higher in OF than AF, around 2%, so the influence on Nusselt number is not evident. Values of Archimedes numbers are overlapped between AF and OF and no tendencies are distinguished on the Nusselt number. Conductivity ratios seem not to affect the heat transfer at first sight, in spite of being a predominant factor on heat transfer. Density ratios influence is not obvious here, mainly due to the narrow range of voids fraction for keeping the bubbling regime of fluidization. Reynolds number and the ratio of thermal heat capacities turn out as the two factors affecting heat transfer perceptively. Both show higher values in air-firing and increasing tendency with O_2 at inlet. This agrees with the known influences explored in the literature widely.

During air-firing tests, gas velocities were mostly higher than in oxy-firing. Gas velocities, together with particle diameter and bulk density, are the three factors dominating particle convection mechanism. The particle diameter is not changing during the tests, and the bulk density is strongly influenced by the fluidizing velocity, but also by the gas conditions of gas and viscosity. Aiming at isolating the effect of fluidizing velocity on the influence of non-dimensional parameters on heat transfer, we now look now at two tests of air and oxy-firing with similar fluidizing velocity. In Figure 3.19 we represent Nusselt numbers from the tests of close fluidizing velocity in air and oxy-firing, corresponding to 1.2 m/s and 0.95-1 m/s, respectively. They coincide with the maximum velocity range during oxy-firing and the minimum in air-firing. O_2 concentration at inlet ranged from 50% to 57%, the maximum values tested. Temperature varied between 832ºC and 918ºC. In the air-firing case, temperature was 887ºC, also among the highest values reached.

By isolating the gas velocity effect, the variation of Reynolds number with gas properties is considerably lower. The ratio of thermal capacities involves both, variation of temperature and also, changes on gas composition. The value of Nusselt number in the air-firing case is now more similar to the ones during oxy-firing. None of the non-dimensional numbers in Figure 3.19 evidence any clear tendency of Nusselt number.

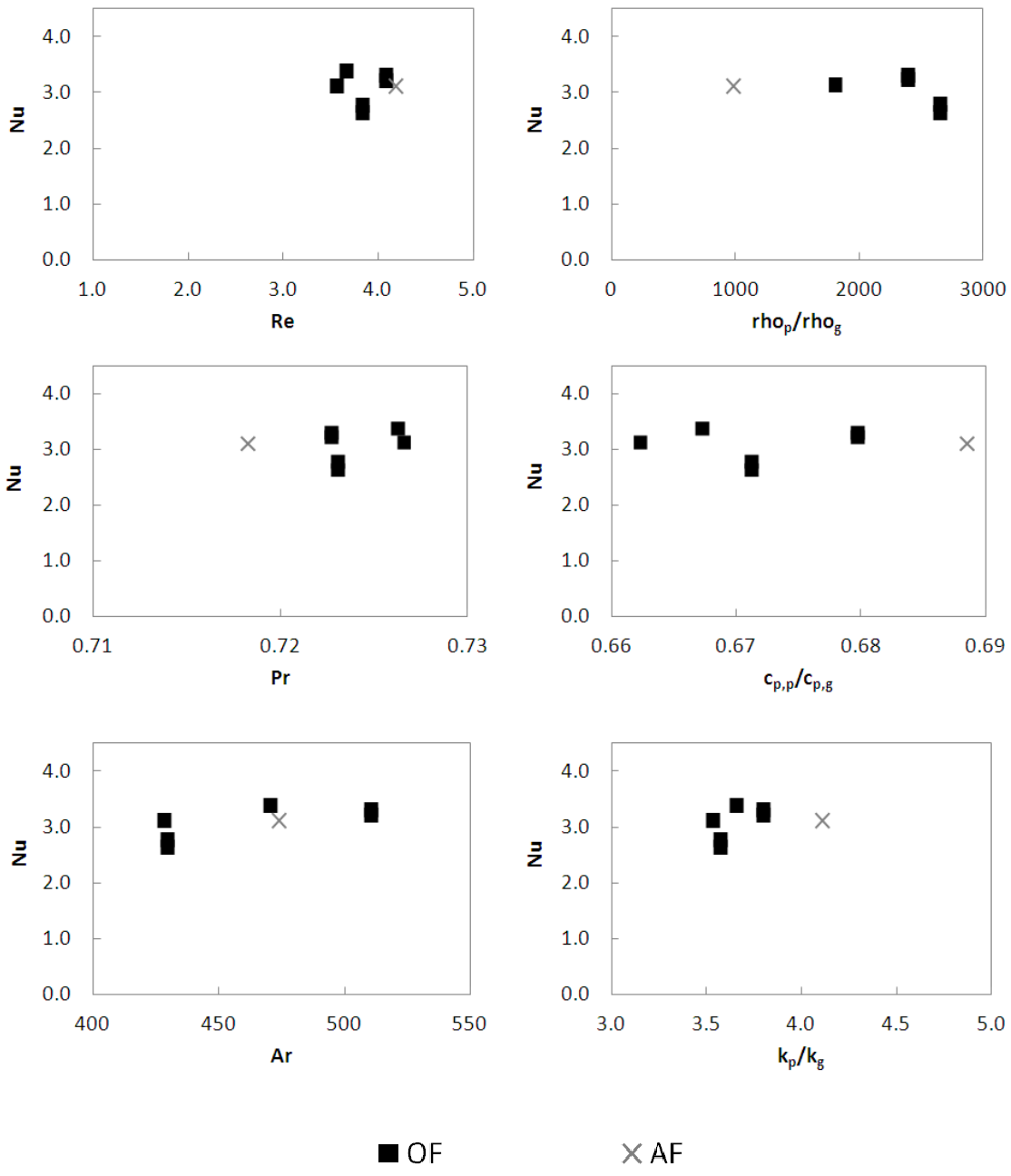

Figure 3.19. Influence of non-dimensional parameters on Nusselt number for similar fluidizing velocities

In Figure 3.20 the values of similar temperature, ranging from 823ºC to 884ºC are represented. In these graphs, the influence of the parameters on Nusselt number can be better distinguished. Lower Reynolds numbers in OF diminishes Nusselt with respect to AF cases. Gas conductivity for similar temperatures also displays an effect on heat transfer, keeping lower in OF tests. In general, Nusselt numbers in the OF tests are below the ones obtained during AF.

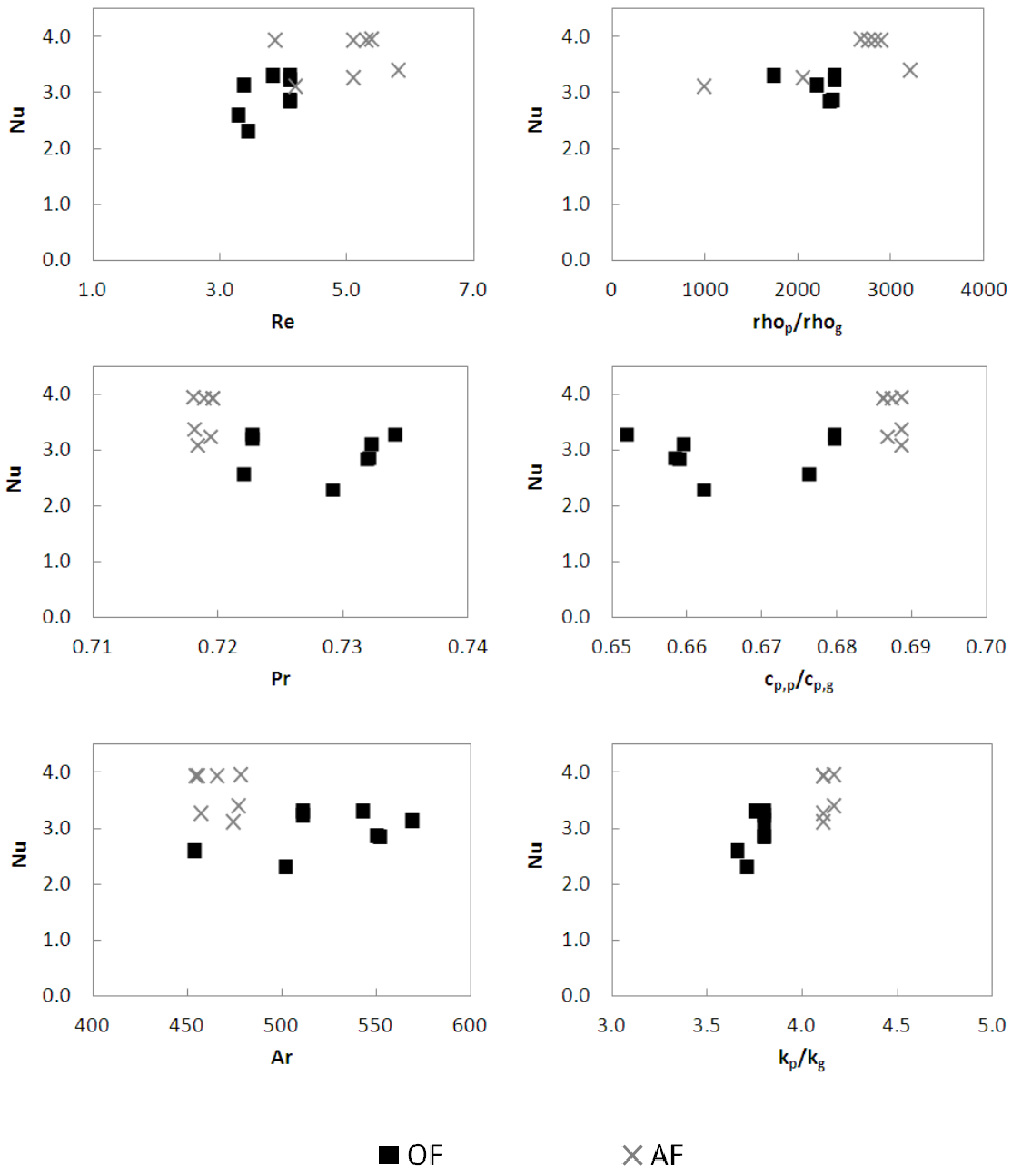

Figure 3.20. Influence of non-dimensional parameters on Nusselt number for similar bed temperature

Reynolds influence appears then as the distinguishing factor between air and oxy-firing due to differences on gas velocity. For this reason, the Molerus model (Molerus et al., 1995b), turns out more appropriate for evaluating the experimental results and it is going to be following explored.

MOLERUS MODEL

For similar conditions of bed density and temperature, and certain constant value of O_2 at inlet, non-dimensional heat transfer coefficients do not exhibit evident influence by differences on gas composition. The effect of Reynolds number on the Nusselt number, however, describes a general known tendency, according to the mechanism of heat transfer predominantly acting: up to a maximum Reynolds number, heat transfer increases, because particle convection is predominant. By increasing Reynolds number, heat transfer diminishes describing a smooth slope, because bed density also decreases and heat transfer by gas convection begins to participate more frequently in the heat transfer. To take all the parameters influencing the heat transfer into account, the expression proposed by Molerus et al. (1995b), Eq. 3.3, is applied. Heat transfer coefficients predicted by this correlation are compared with the experimental results in Figure 3.21. They are represented the values predicted by Molerus correlation (empty circles) with the experimental conditions in each case. Bold circles are the experimental results of heat transfer. The discontinuous line represents the theoretical tendency with constant values of density and temperature in air firing, to display the tendency of Nusselt number within the whole range of Reynolds values.

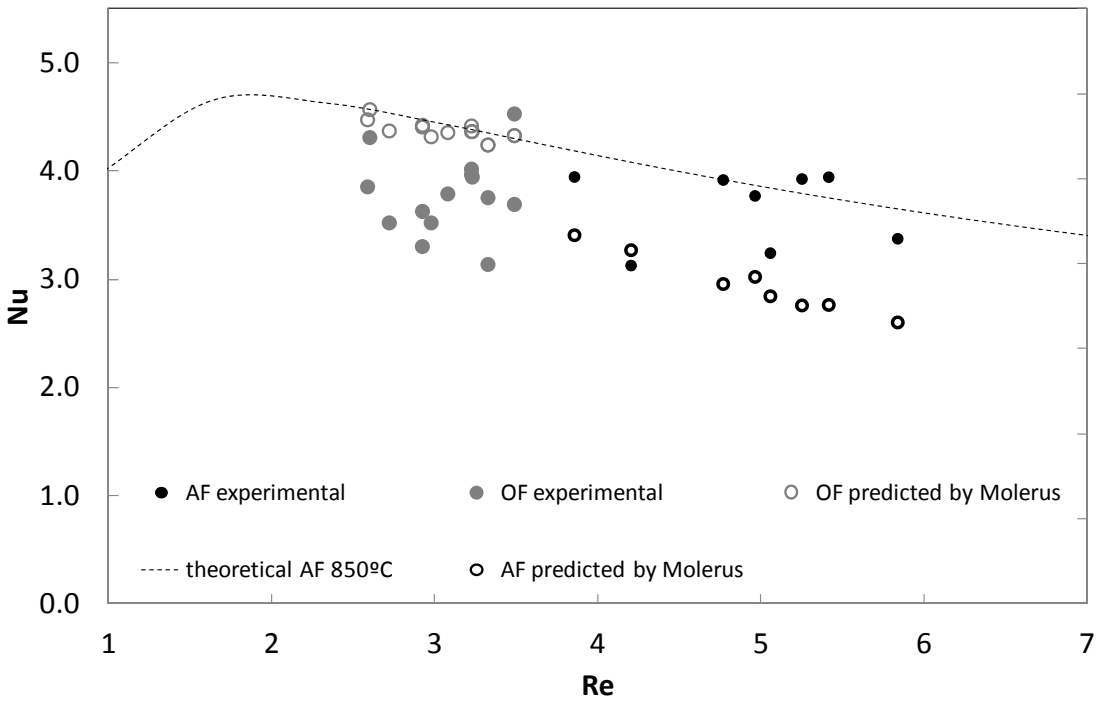

Figure 3.21. Comparison of tests results with prediction by Molerus correlation

The higher gas velocities in air-firing operation, locates the operational window further from the optimal heat transfer coefficient. Still, since this maximum is different in both modes, within this range of operation, the values of heat transfer remains close in air and oxy-firing.

Molerus et al. correlation fairly fits the tendency of heat transfer during oxy-fuel combustion, although this expression slightly over-predicts the experimental results, particularly far from the optimum heat transfer value. The correlation derived from cold tests at a wide range of velocities and particle diameters, although they also validated their results with data from the literature. The fitting curve with high temperature measurements, did not fit as good as the cold tests. This influence of gas temperature on gas properties would lead to the over-prediction observed in Figure 3.21.

Empirical correlations exhibit an obvious simplicity for the estimation of heat transfer, but semi-empirical models based on mechanistic approach have more predictive power and their use is extended in the last decades. Both modeling strategies must account for the contribution of heat transfer by radiation.

3.5.2 CONTRIBUTION OF RADIATION HEAT TRANSFER

For dense fluidized beds, like the case of the bubbling regime, the contribution of radiation to the overall heat transfer is rather smaller than in more diluted zones. This is because it is the first layer of particles the one that contributes to radiation. This layer hinders the radiation stemming from the particles in the core of the bed. The contribution of radiation to the overall heat transfer is calculated with Eq. 2.25, including the concept of "radiation efficiency" used in the previous chapter and proposed by Breitzholz and Leckner (1997). The results are shown in Figure 3.22.

According to Botterill (1989), apparent emissivities are around 0.43, when wall temperature was 300ºC, and up to 0.78 when wall temperature was 850ºC. They include these terms to account for the lower temperature of the particles adjacent to the wall and so, the reduced contribution to radiation. Values obtained using this methodology is slightly over the ones predicted by Figure 3.22. The percentages obtained in Figure 3.22 agree with those collected by Glicksman and Decker (1982).

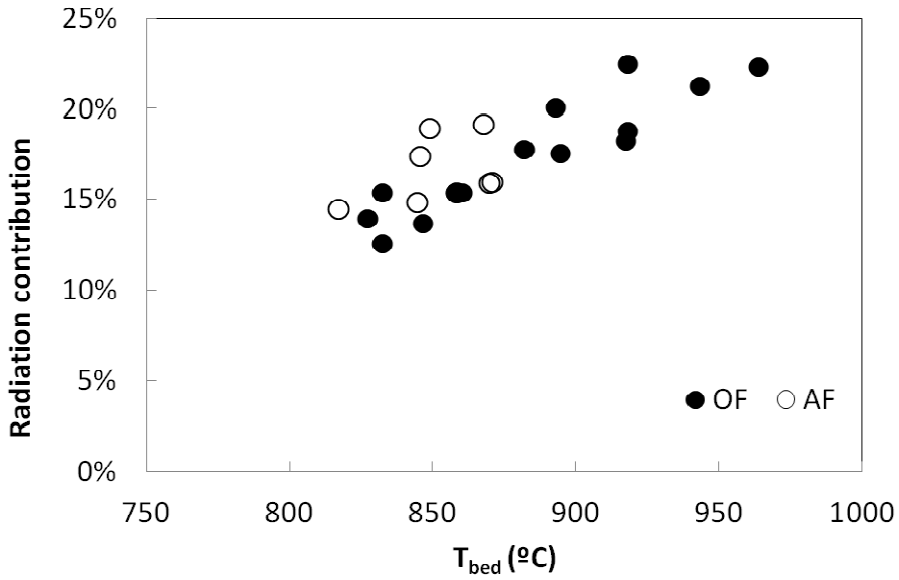

Figure 3.22. Estimation of the variation of radiant heat transfer coefficient with bed temperature

The heat transfer contribution by radiation during oxy-fuel tests reached similar values to those estimated for air-firing tests. This would not be the case in a more diluted zone of the combustor. The higher CO_2 partial pressure in flue gases increases the emissivity of the flue gas mixture and the contribution of radiation from gaseous phase will be higher. This was not evaluated here, since no heat transfer surfaces were located in the higher part of the combustor and gas radiation contribution could be neglected.

3.5.3 MECHANISTIC APPROACH AND PROPOSAL OF MODIFICATION FOR OXY-FUEL CONDITIONS

The trend in the modeling of heat transfer goes towards using more realistic approaches, as explained in section 3.1. Still, empirical expressions must be included for those terms difficult to measure, like the effective conductivity and the residence time of particles at the wall, with the aim of effectively simplify the prediction of heat transfer coefficients. Heat transfer will be then the addition of the radiation mechanism contribution, h_r, and the heat transfer by particle convection, during the contact time of the packets with the surface, accounting for the film resistance of the gaseous layer at the heat transfer surface:

$$h = h_r + (1-\delta_b)\frac{1}{\frac{1}{h_{packet}}+\frac{1}{h_{film}}} \qquad \text{Eq. 3.31}$$

Where h_{packet} is the transient conduction of heat from the particles packet to the surface, by integrating Eq. 3.4. If considering all packets contacting the surface for the same length of time, τ, this term becomes (Kunii and Levenspiel, 1991):

$$h_{packet} = 1.13\left(\frac{k_{eff}\rho_s(1-\varepsilon_{mf})c_{p,s}}{\tau}\right)^{1/2} \qquad \text{Eq. 3.32}$$

The gas resistance, h_{film}, proposed by Baskakov (1964) accounts, time-independently, for the variation of the gas layer properties. The packet renewal term predicted excessively high heat transfer coefficients for short particle residence times (Botterill, 1989) and this induced to include an additional series thermal resistance. This term was much influenced by gas thermal conductivity and particle diameter and it can be defined as:

$$h_{film} = M\frac{k_g}{d_p} \qquad \text{Eq. 3.33}$$

The term of film resistance offers the possibility of straightforward taking into consideration the change on gas composition in oxy-fuel combustion and its influence on the heat transfer coefficient.

The reviewed expression by Zhargami et al. (2007) for residence time prediction, together with the model for the effective thermal conductivity explained by Xavier and Davidson (1985), Eq. 3.9, is applied to deduced the best value of the empirical variable *M*, in order to properly correlate the experimental values obtained on heat transfer.

The maximum and average deviations of Eq. 3.31 with the experimental results are represented in Figure 3.23, for different values of *M*. The minimization of these functions indicates that, the best value of *M* for oxy-firing case, to optimize the maximum deviation, is 5.47, whereas for air-firing, this parameter reaches 10.64. To optimize the average deviation between predicted and experimental values, the parameter *M* increases. The fitting process suggests 6.51, as appropriate value to reach average deviations of 8.6% in oxy-fuel tests. For air-firing case, this value becomes 11.33, achieving average deviations of 10.2%.

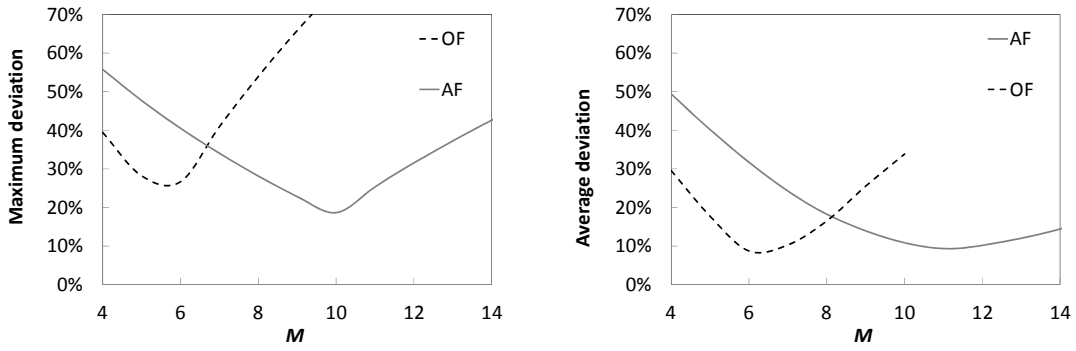

Figure 3.23. Maximum and average deviation of predicted values for different values of M

The expression for estimating the heat transfer coefficient by using the mechanistic approach yields:

$$h_{packet} = \ldots \left[\left(k_g \left(\frac{k_s}{k_g} \right)^{0.28 - 0.757\log\varepsilon - 0.057\log\left(\frac{k_s}{k_g}\right)} + 0.1\rho_g c_{p_g} d_p u_{mf} \right) \rho_p (1-\varepsilon) c_{p,p} \left(0.7\delta_e \frac{d_b}{\delta_b u_b} + 6.52\delta_b \frac{d_c}{\delta_c u_c} \right)^{-1} \right]^{1/2}$$

k_{eff} τ

Eq. 3.34

$$h_{film} = M \frac{k_g}{d_p}$$ with M=6.51 for oxy-firing and *M=11.33* for air-firing Eq. 3.33

Figure 3.24 represents the comparison of the calculated heat transfer coefficients and the experimental values obtained during air-firing and oxy-firing tests. In Figure 3.24 a) the heat transfer coefficients obtained and predicted for the particle convection contribution is represented. Values in both mode of operation are satisfactorily predicted.

Figure 3.24b) illustrates the Nusselt number calculated for the global heat transfer coefficient, i.e., taking the radiation term into consideration. The higher values obtained in air-firing are due to the higher value of gas conductivity in the oxy-fuel cases.

There are not public results on heat transfer coefficients in oxy-fuel dense fluidized beds. Thus, validation is not possible for a different plant arrangement, as it would be desirable.

Since the basis of the Eq. 3.31 to Eq. 3.36 lies on the mechanistic model, already used in a wide range of facilities, the proposed expression for heat transfer under oxy-firing conditions would be capable to estimate the heat transfer coefficients from bubbling fluidized bed to surface, for an atmosphere different from air, as in the case of external heat exchangers of large circulating fluidized beds

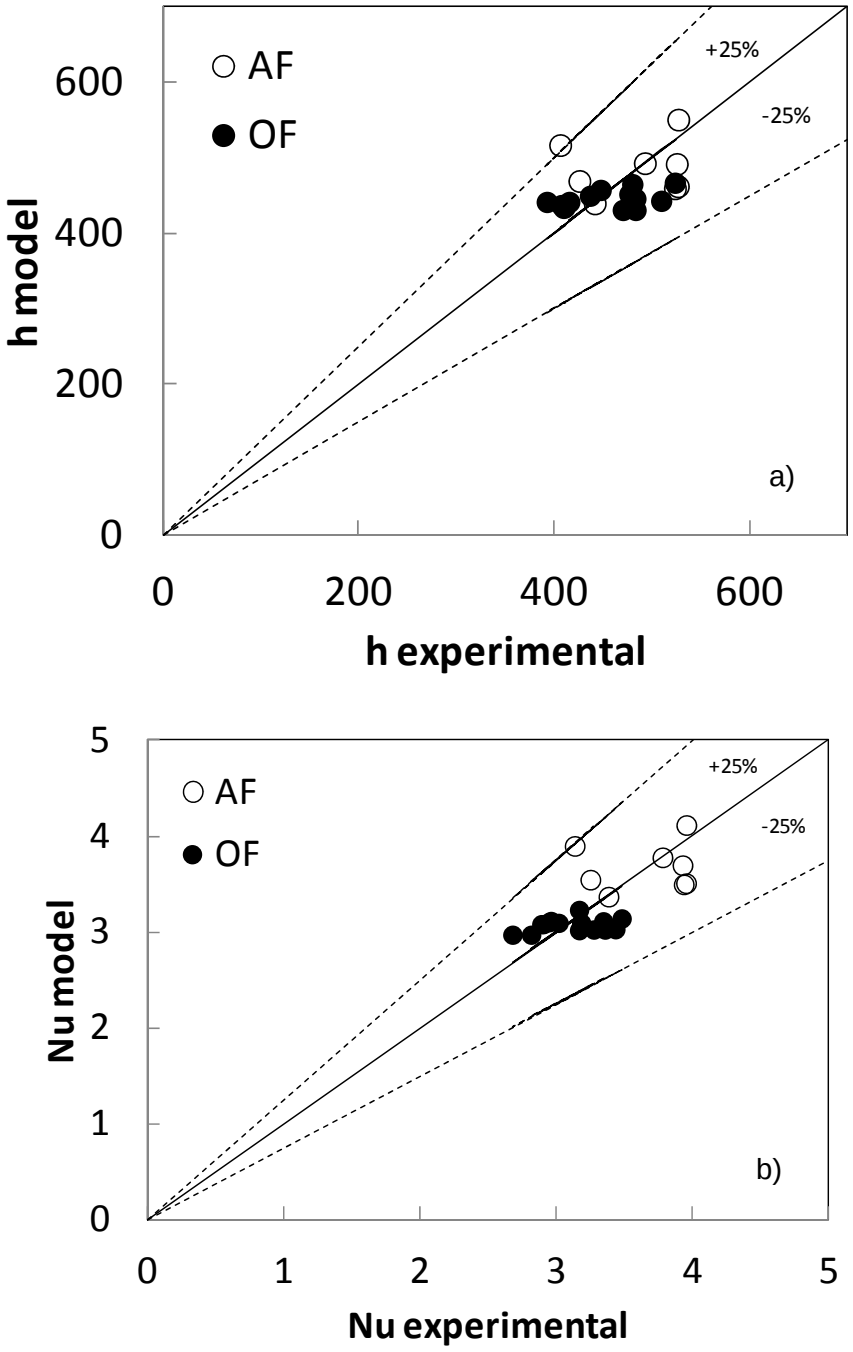

Figure 3.24. Validation of calculated heat transfer coefficients

.

3.6 CONCLUSIONS

For the first time the heat transfer coefficients during oxy-fuel combustion in a bubbling fluidized bed have been quantified and presented. Measurements were carried out during the combustion experiments in the CIRCE BFB, operated under conventional air-firing conditions, oxy-fuel with O_2/CO_2 from commercial canisters and O_2 with RFG. Due to the plant flexibility, operation conditions varied along a wide range of O_2 concentrations at inlet and bed temperatures. Heat transfer data were collected during the cooling stages in the plant operation.

The extended literature on heat transfer in fluidized bed traditionally approaches the prediction of the coefficients by two ways, fully empirically by experimental correlations, or by semi-empirical mechanistic models. The available studies on heat transfer in bubbling fluidized beds are found in the earliest studies on this issue, particularly to vertical walls instead of tubes bundles. In the last decades, further effort was devoted to heat transfer in the transport zone of circulating fluidized beds, since the majority of steam generation heat transfer tubes are located in this zone. However, the relevance of heat transfer in bubbling beds, with atmospheres different from the conventional air-firing ones, turns now up again as a key issue, due to the importance of external heat exchanger on future large CFB oxy-fuel boilers.

The values of heat transfer during air-firing and oxy-firing operation allowed here the assessment of the particular key factors that differentiate both operational modes.

The non-dimensional analysis, indicated that, the change in Reynolds, Prandtl and Archimedes number, caused by the variation of gas composition, is offset by the differences on fluidized gas velocity. Additionally, bed temperature in oxy-fuel cases were over that in air combustion, bringing closer the Reynolds and Archimedes numbers in both, AF and OF. In most of the tests, fluidizing velocity was lower in oxy-firing tests than in air-firing. According to Molerus correlation, this translates into higher heat transfer coefficients, because the operational points locate closer to the optimum Reynolds number for heat transfer. However, this correlation over-predicted the values obtained during oxy-fuel combustion.

The mechanistic approach is recommended to more adequately predict heat transfer coefficients. It was propose the appropriate expression to estimate the residence time and effective thermal conductivity, among those available in the literature. The empirical variable included in the film resistance expression shows different values for air and oxy-firing. The results of heat transfer coefficients in oxy-firing mode were then satisfactorily predicted.

CHAPTER 4

THE INFLUENCE OF SOLIDS RECIRCULATION ON HEAT TRANSFER IN AN EXTERNAL HEAT EXCHANGER

4.1 INTRODUCTION

In oxy-fuel CFB, the external heat exchanger (EHE) presents two particularities, with respect to the conventional air-firing CFB. The one related to the change on gas composition has been previously addressed. With the experiments in the oxy-fuel bubbling fluidized beds, we could propose the adequate semi-empirical expressions to predict the heat transfer coefficients. This allows including the influence of gas composition on both, the effective thermal conductivity and the residence time of particles, so as in the film resistance term.

The other particularity of oxy-fuel CFB EHEs is related to the higher amount of recycled solids that the EHE will manage and drive to the recycling pipe. Scarce literature has addressed this issue, and they all coincide in pointing out the influence of solids trajectory on the heat transfer coefficients distribution. The heat transfer will differ from the different locations in the EHE tubes bundle.

With the aim of examining the influence of recycled solids on the EHE heat transfer, experiments have been carried out in a cold model of a scaled-down EHE. The EHE was uncoupled from the original CFB loop and thus, the Gs and aeration velocity was independently varied along a wide range of values.

The heat transfer measured in every tube will be averaged, with the objective of deducing an expression that can take into account the influence of the time of recycled particles in the EHE. This will give rise an empirical correlation that

modifies the previously proposed heat transfer coefficient with no recycled solids, and so, involving the gain of this coefficient due to the flow of particles.

Together with the previous analysis on the influence of the combustion atmosphere on heat transfer coefficients, we will achieve a new heat transfer coefficient expression adapted to the EHE conditions of an oxy-fuel CFB boiler.

4.2 HEAT TRANSFER IN EXTERNAL HEAT EXCHANGER FLUIDIZED BEDS

4.2.1 HEAT TRANSFER TO TUBES BUNDLES

In the first designs of fluidized bed combustors, bubbling regime was extensively used, especially for burning difficult type of fuels, such as residues or slugs (Peña, 2011). Heat transfer surfaces were usually located in the dense part of the boiler. Different types of heat transfer surfaces were used, such as vertical or horizontal tubes bundles. For horizontal tubes immersed in fluidized bed, nearly no bubbles does contact with the top of the tubes. During the time that a bubble contacts the surface, heat transfer coefficient is significantly lower, since gas convection is a non-dominant heat transfer mechanisms in dense beds. Therefore, the effect of no bubble presence in the top of the tube does not mean that heat transfer is increased, rather than the solids transferring heat at this point are not enough frequently replaced and thus, heat transfer in this location is smaller than in the rest of the tube surface. Heat transfer coefficient is also lower in the bottom part of the tubes than in the sides, due to voids frequently formed below the tube. Experimental observations in this regard are summarized by many authors (Grewal, 1981; Kunii and Levenspiel, 1991; 2003; Oka, 2003; Masoumifard et al., 2008).

The heat transfer surfaces located in the bed region of a bubbling fluidized bed were usually steam superheater tubes. Vigorous fluidization caused high erosion loses and also, the presence of burning fuel caused metal carbonization and local high temperatures that hence, resulted in high material loss rates (Stringer, 1995). Because of these reasons, this approach was almost abandoned and heat transfer surfaces are usually located in more diluted zones in the boilers, like water walls along the CFB riser or coil surfaces in the convective pass (Oka, 2003).

Last decades, attention has been paid to the external fluidized bed heat exchangers employed to enhance heat transfer capacity in circulating fluidized beds, removing heat from recycled particles, patented by Abdulally and Randolph (1989). There are scarce published works about how heat is transferred in these types of devices. However, detailed information drowned from these studies referring to fluid-dynamics around the horizontal tubes. One of these works was carried out by Umekawa and co-workers (1999), visualizing particles movement around the tubes by neutron radiography. The tests were performance with bed material being sand, with 2555 kg/m^3 and a particle diameter of 218 μm. An example of their visualization results is shown in Figure 4.1:

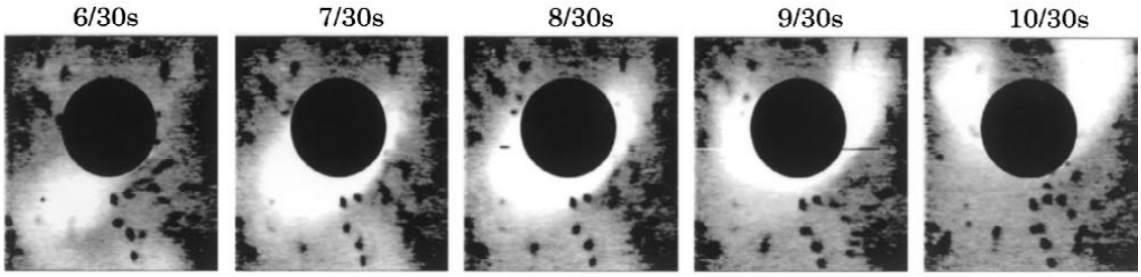

Figure 4.1. Void fraction around an horizontal tube (Umekawa et al., 1999)

Their experiments were carried out at low temperature and radiation was neglected. They also were able to measured the heat transfer coefficient around a tube, and detected maximum in the obtained values, at 90^o and 270^o (Ozawa et al., 1998). For fluidizing velocities close to minimum fluidization velocity, heat transfer was lower and both maximum were symmetric at both sides of the tube. Values obtained ranged from 100–300 W/m^{2}K for in-line arrangement and up to 400 W/m^{2}K for staggered arrangement. Higher velocities increased heat transfer, reaching values around 600 and 700 W/m^{2}K for in-line and staggered arrangements respectively. Also higher velocities induced more uniform heat transfer around the tube. This uniformity was clearer for arrangement where distance between tubes was decreased. They related this behavior to the flow pattern around the tube contour. The jet passed through the side passage of a first row of tubes and collided on the stagnant region of the 2nd row tube.

A detailed study on predicting heat transfer coefficient in fluidized bed heat exchanger was carried out by Kim et al. (2003). For taking into account differences between heat transfer coefficients around the tube surface, they measured heat

transfer in five locations along one tube at 0, 45º, 90º, -45º, -90º, by means of an optical probe. Then, they obtained an average heat transfer coefficient by averaging the obtained local heat transfer in the eight points around the tubes, the five points measured and the other three by symmetry. They calculated differently the heat transfer coefficients in the five bottom locations than in the three top locations. For the upper part they used the following gas convection correlation:

$$Nu_{top} = 47.56Re^{0.43}Pr^{0.33}\left(\frac{D}{d_p}\right)^{-0.74}\left(\frac{c_{p,s}}{c_{p,g}}\right)^{-1.69} \qquad \text{Eq. 4.1}$$

For $0.97 \leq \text{Re} \leq 12.56$, $93.46 \leq \frac{D}{d_p} \leq 157.73$, $0.67 \leq \frac{c_{p,s}}{c_{p,g}} \leq 0.79$ and Pr = 0.71.

And for the bottom part they considered the packet renewal theory (Chapter 3). In this model, during the emulsion phase contact heat is transferred by transient conduction. Then, the predicted time-average heat transfer coefficient is expressed as rearranging Eq. 4.2:

$$h_{bottom} = (1-\delta_b)2\left[\frac{k_e\rho_s c_{p,e}(1-\varepsilon_e)}{\pi t_e}\right]^{1/2} + \delta_b h_g \qquad \text{Eq. 4.2}$$

The authors measured and correlated values of the bubble fraction at the tube bottom, using the expression:

$$\delta_b = 0.19\left[\frac{d_p g}{u_{mf}^2\left(\frac{u}{u_{mf}} - A\right)^2}\right]^{-0.23} \qquad \text{Eq. 4.3}$$

Where A= 1-(projected tube area/bed area).

The emulsion contact time t_e is also correlated against Froude number ($u^2/g\ d_p$) as:

$$t_e = 1.2\left[\frac{d_p g}{u_{mf}^2\left(\frac{u}{u_{mf}} - A\right)^2}\right]^{0.3}\left(\frac{d_p}{D}\right)^{0.225} \qquad \text{Eq. 4.4}$$

So, they finally proposed an expression averaging both terms, the heat transfer coefficient in the denser bottom part of the tube, h_{bottom}, and the heat transfer coefficient in the top, h_{top}:

$$h_{ave} = \frac{5}{8} h_{bottom} + \frac{3}{8} h_{top} \qquad \text{Eq. 4.5}$$

Their findings coincide with the ones by Ozawa (1998), obtaining maximum heat transfer at the side of the tube and minimum at the top, down to 200 W/m²K for fluidizing velocities around minimum fluidizing velocity. Maximum heat transfer was observed for velocities around twice the minimum fluidizing velocity, reaching values of 450 W/m²K.

4.2.2 INFLUENCE OF SOLIDS RECIRCULATION

The movement of solids in the horizontal direction of a fluidized bed could be neglected compared with the vertical movement of solids. This difference could be expressed in terms of the vertical and horizontal dispersion coefficients. With the aim of acquiring an idea of the magnitude of these terms, following, Figure 4.2 represents both dispersion coefficients versus the ratio of velocities.

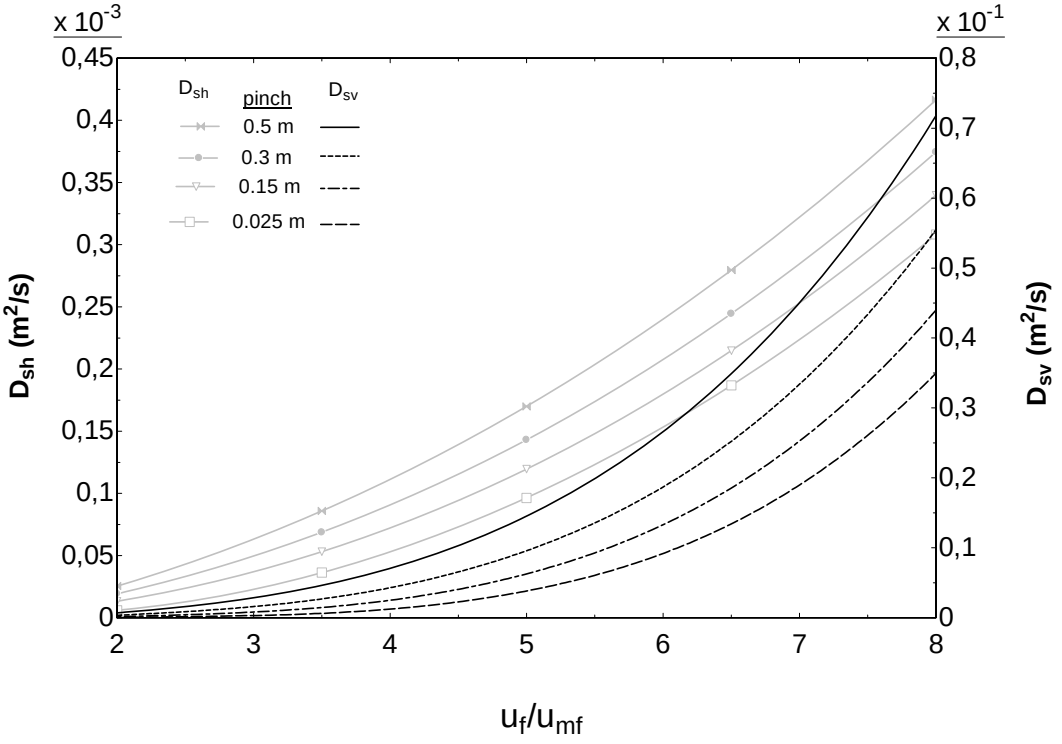

Figure 4.2. Dispersion coefficients calculated for different fluidization velocities and different tubes arrangements, according to Eq. 4.6 and Eq. 4.7.

The dispersion coefficients shown in Figure 4.2 have been calculated according to Kunii and Levenspiel (1991) proposal. The horizontal dispersion coefficient, D_{sh}, yields:

$$D_{sh} = \frac{3}{16}\left(\frac{\delta_b}{1-\delta_b}\right)\left(\frac{\alpha^2 u_{mf} d_b}{\varepsilon_{mf}}\right) \qquad \text{Eq. 4.6}$$

α is the ratio between the wake size and the bubble size. It is recommended α=1 for small Geldart A and AB particles and α=0.77 for larger solids.

The vertical dispersion coefficient, D_{sv}, is expressed as:

$$D_{sv} = f_w^2 \varepsilon_{mf} \delta d_b \frac{u_b^2}{3u_{mf}} \qquad \text{Eq. 4.7}$$

In this expression f_w represents the fraction of wakes according to the counterblow solid circulation model (Kunii and Levenspiel, 1991). Values for this term would be between 0.3 and 2.

As seen in the Figure 4.2 tendencies of both terms are similar for different distances between tubes, but vertical dispersion coefficient is two orders of magnitude greater than the horizontal term, what makes it possible to neglect it in most of cases.

As mentioned before, heat transfer surfaces immersed in dense fluidized bed are particularly important in external heat exchangers of circulating fluidized beds. In these devices particles not only move in one direction but they must be conveyed along the heat exchanger to reach the solids recycling pipe. Consequences of this additional dimension have been scarcely studied and it will play an essential role for the next generation of oxy-fuel fluidized bed combustors.

With the aim of observing such effects of recycled solids on the heat transfer in an external heat exchanger, Wang and co-workers (2003) designed a cold model of loop-seal with external heat exchanger. The solids rate was controlled by diverting part of the particles from the standpipe by changing fluidizing velocity of both, loop-seal and external heat exchanger. Heat transfer probes were located in different positions in the external heat exchanger. The results are shown in Figure 4.3:

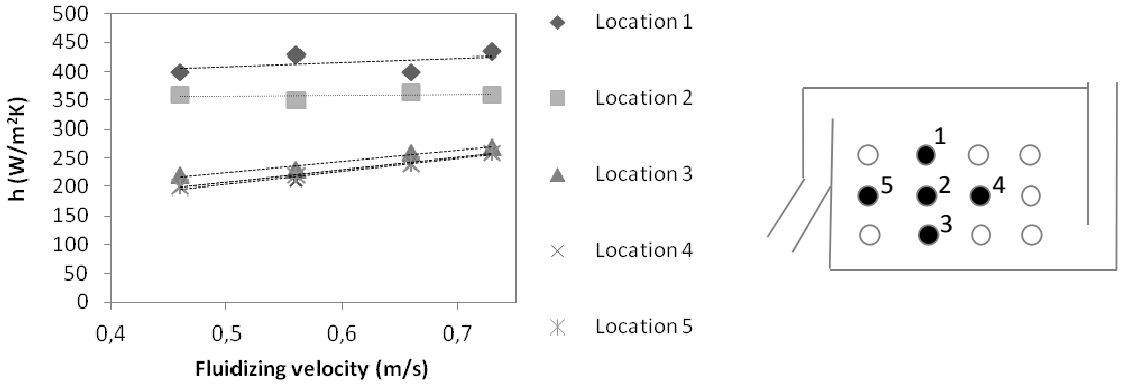

Figure 4.3. Results from the heat transfer measurement in a cold model of an External Heat Exchanger. Adapted from Wang et al. (2003)

Heat transfer is not uniform in each location of Figure 4.3. This confirms the influence of fluid-dynamics and tubes location on heat transfer. The maximum heat transfer coefficients are obtained in locations 2 and 1, the central tube and the point near the splash zone respectively. Lower and similar coefficients are obtained in positions 3, 4 and 5, near the walls and the distributor plate. Increasing the solids rate crossing the heat exchanger they observed higher heat transfer coefficients, particularly in position 1 and 2. Difference between the maximum and minimum heat transfer surfaces were almost of 45%. This indicated insufficient fluidization areas with poor gas-solids mixing near the wall and near the distributor plate.

Johansson et al. (2006) they studied a 1/3 scale cold model of an existing loop-seal with immersed tubes bundle. The aim of the work was twofold: analyzing the performance of the sealing, by measuring the solids in the down-comer and the pressure drop across the seal and measuring heat transfer coefficient in different locations along the loop-seal. They were able to compare their findings with the EHE of a commercial scale CFB. Results of their experiments are plotted in Figure 4.4:

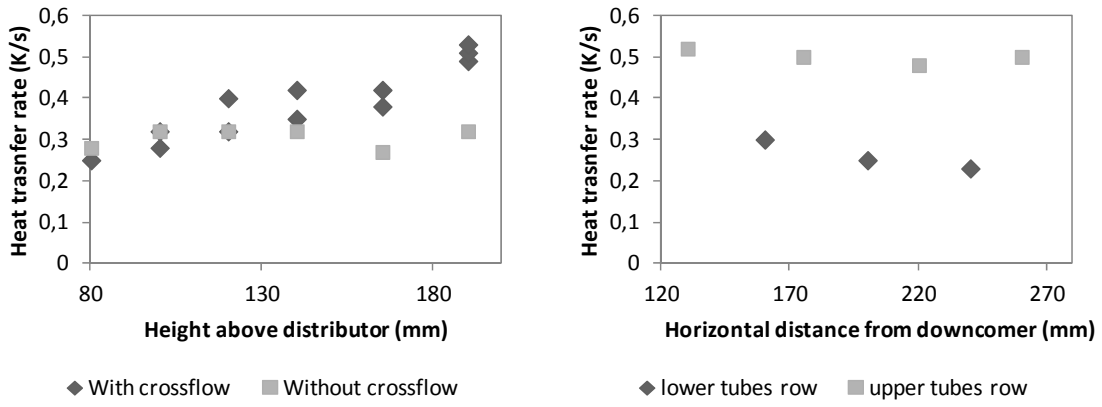

Figure 4.4. Heat transfer rates at different locations of a loop-seal heat exchanger. Adapted from Johansson et al. (2006)

These results agreed with the findings commented above by Wang et al. (2003). Heat rates were higher in the upper part of the heat exchanger. Higher exchange of solids took place in the upper part of the device. Moreover, heat transfer diminished with the distance from the downcomer. This finding showed that the main flow direction through the tube bundle was horizontal and that the time averaged particle velocity was higher laterally than vertically. Interestingly, for comparing the results obtained in the cold model with the behavior of the 30 MW loop-seal, measurements of CO gave a fairly good idea of the solids flow pattern. This was possible because CO flows with the inert matter and enters the loop-seal through the cyclone.

A shallow fluidized bed heat exchanger was investigated by Rodriguez et al. (2002). It was connected to a fluidized bed combustor, so that hot particles arrived to the heat exchanger where 5 longitudinal tubes were located. The aim of the study was to optimize the heat exchanger effectiveness by means of baffles addition. In their measurements, heat transfer coefficient profile along the heat exchanger decreased asymptotically. When they compared their measurements with correlations found in the literature, there was not proper agreement with results. At the first stage of the heat exchanger, correlation predicted fairly well the measured coefficients but as the distance to the particles feeding increases, predictions did not agree with measured coefficients.

All these works coincided to indicate that the trajectory of solids along the fluidized bed heat transfer device influence the local heat transfer coefficients, and thus, the average EHE heat transfer.

4.2.3 REAL EXTERNAL HEAT EXCHANGERS

There are few public data about heat transfer in real external fluidized bed heat exchangers. In some cases, this could be due probably to confidentiality issues, but in general, the access to the devices is usually obstructed by other components of the plant and, particularly in heat exchangers, inserting probes involves high risk of damaging tubes bundles.

One of the most complete studies focused on the fluid-dynamics and heat transfer in a real loop-seal heat exchanger was the one carried out by Werdermann and Werther (1993) in an existing BFB EHE of 10 m long and 3 m wide and 5 m height. A heat transfer probe was used to measure heat transfer at eleven different ports in the first chamber. Unfortunately, this was the chamber with no heat exchanger tubes because introducing the probe in the other chambers was considered too risky. Still, important findings were drawn from the study. Non-uniformities in the temperature profiles were detected in the first chamber. This was attributed to the reaction of the unburned carbon in the ash, when contacting with oxygen from fluidizing air.

They measured heat transfer coefficients at two different distances from the front wall and at three different heights from the distributor. Maximum heat transfer was measured in the position further from the front wall at 0.322 m, reaching values around 1600 W/m^{2}K at the row near the distributor, but far from both side walls. In the same position but at 0.114 m from the wall, the heat transfer coefficients were only around 250 W/m^{2}K.

When the heat transfer probe was introduced from the top of the chamber, at the height near the limit of the bed, at 3.468 m, heat transfer was between 500 W/m^{2}K and 1000 W/m^{2}K, whereas at higher position than this, heat transfer coefficient decreases down to 100 - 550 W/m^{2}K.

Results obtained in this study are represented in Figure 4.5:

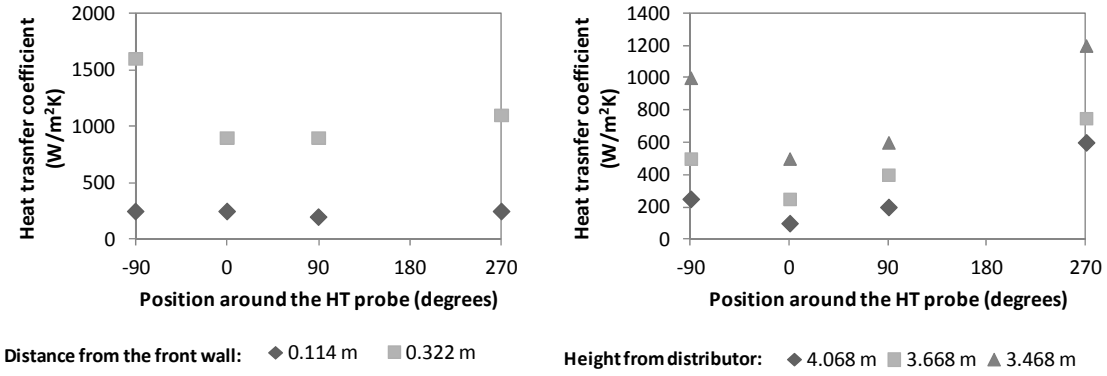

Figure 4.5. Heat transfer coefficients measured in different positions in a real HHE. Data taken from Wedermann and Werther (1993)

In the Figure 4.5 is easy to detect an intense heat transfer at height near the bed limit, where bubbles are exploding and particle-gas mixing is more intense. This would be expected also in a stationary fluidized bed with no horizontal particles movement. There was the great difference of measured heat transfer values at different distances from the walls. These results agreed with results seen before on cold models. Still, the average measured heat transfer values shown in Figure 4.5 are particularly higher than the ones predicted by the cold models described. Higher temperatures leads to additional radiation heat transfer, but in the dense beds, this contribution means around 100 W/m²K. In the paper, the authors also paid attention to this issue. The average heat transfer coefficient, measured by energy balance in the rest of the chambers, with tube bundles inside, showed values around 450 W/m²K. The explanation for this was given by the non-uniform fluidynamics along the fluidized bed heat exchanger. Thus, only part of the ashes did take part of the heat exchange, but the rest flow straight to the next chamber. The stirred tank model is then not valid anymore. They suggested an additional term ξ representing the fraction of solids that, in fact, exchanged heat with the tubes.

Recently, measurements on a fluidized bed heat exchanger in a 300 MW CFB boiler were published by Man et al. (2012). They give detailed information about the geometry and arrangement of the heat exchanger. Their measurements of heat transfer coefficients were based on the energy balance with the water and ashes mass flows and temperatures at outlet and inlet. Their study was focused on the change of the values of the heat transfer coefficients for different boiler loads. During operation at higher boiler loads, higher solids flux where circulating in the

solids loop. This is analogous to the increase of fuel input when increasing O_2 concentration at inlet, as resulted in Chapter 2 simulations. Results of these measurements are shown in Figure 4.6.

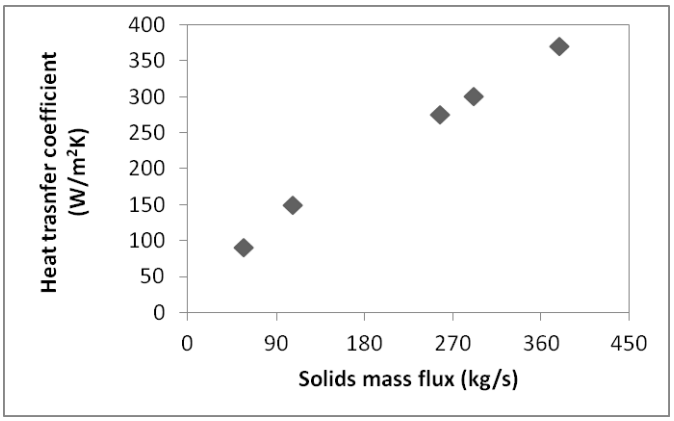

Figure 4.6. Heat transfer coefficients measured in one of the chambers of the external heat exchanger. Data taken from Man et al. (2012).

They found a direct relation between the solids rate arriving at the external heat exchanger and the heat transfer coefficient. They proposed a simple correlation taken into account both, the solids flux and the bed temperature, for estimating the changes of heat transfer coefficients at different boiler loads.

$$h_{EHE} = 0.8m_{solids} + 0.12T_{solids,in} - 38.1 \qquad \text{Eq. 4.8}$$

These results can be explained also by the model suggested by Werdermann and Werther (1993). They considered a ratio of solids that effectively exchanged heat with the water tubes, based on the solids and water temperature, on the tubes geometry and conductivity, and, particularly, on the heat transfer coefficients measured in the chamber with tubes and in the first chamber with no tubes. The expression yielded:

$$\zeta = \frac{T_{solids,in} - T_{solids,out}}{T_{solids,in}\frac{h}{h^*}\left(T_{solids,in} - T_{water}\right) - T_{water}} \qquad \text{Eq. 4.9}$$

with

$$h = \left[\frac{d_o}{d_i h_{max}} + \frac{d_o}{2k} ln\frac{d_o}{d_i} + \frac{1}{h_o}\right]^{-1} \qquad \text{Eq. 4.10}$$

$$h^* = \left[\frac{d_o}{d_i h_{max}} + \frac{d_o}{2k} ln \frac{d_o}{d_i} + \frac{1}{h_1} \right]^{-1} \quad \text{Eq. 4.11}$$

They considered maximum heat transfer coefficient, h_{max}, of 1000 W/m²K in the first chamber, with no tubes, and an average heat transfer coefficient of 750 W/m²K in the same chamber, h_0. The term h_1 was the average heat transfer coefficient in the chamber with tubes bundles, measured indirectly by energy balance, having a value of 400 W/m²K.

From the Eq. 4.9 to Eq. 4.11 it seems no relation between the mass flow and the heat transfer coefficients, being ξ no dependent directly on this parameter. However, if the term ξ remains constant, when incrementing solids flux, the flow of solids effectively exchanging heat with tubes also increases, which actually can be a plausible explanation for the effects of mass flow seen in Figure 4.6. Thus, the simple expression in Eq. 4.8 proposed by Man et al. (2012) can actually represent also this effect.

The relevance of the EHE on the energy balance of future CFB will reside predominantly on the increasing flow of recycled solids compared with the air-firing case. The available literature reviewed on the cold models revealed an un-even distribution of heat transfer along the EHE tubes bundle. In real EHE, the average heat transfer coefficient was also dependant on the mass flow of solids crossing the EHE. The following experimental campaign aims at looking for the relation between both effects, particularly for a wide range of solids mass flow rate.

4.3 EXPERIMENTAL SET-UP

The loop-seal heat exchanger cold model used by Johansson et al. (2006) in their work was un-coupled from the original two dimensional CFB set up. This allowed operating the loop-seal independently from the CFB operational parameters. The scheme is represented in Figure 4.7 and Figure 4.8 shows the photo of the arrangement.

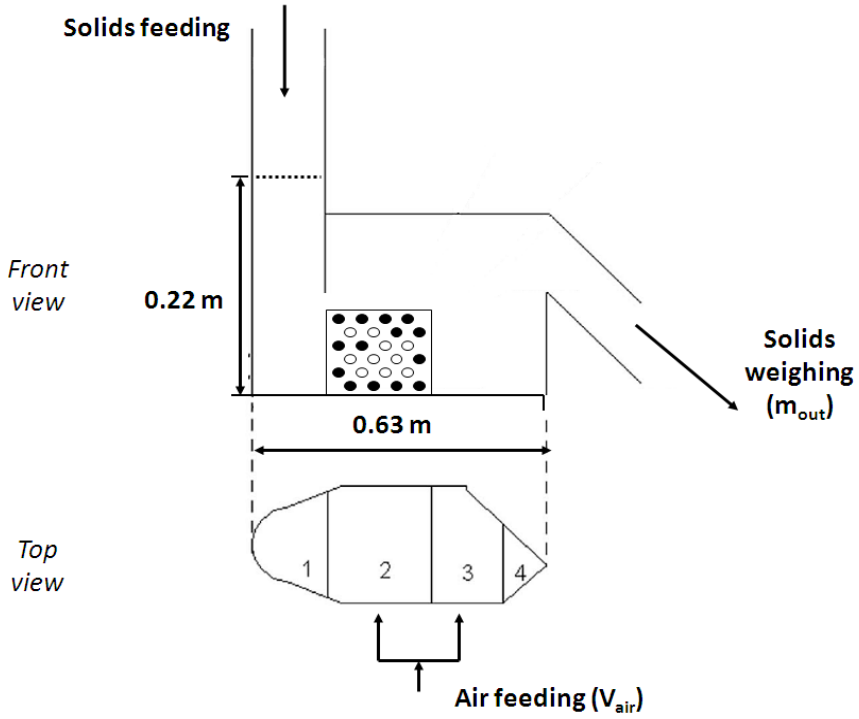

Figure 4.7. Experimental set-up. Filled circles indicate the thermocouples location

Figure 4.8. Photo of the loop seal, the instrumented tubes bundle, and the air supply

The EHE is located in the Chalmers University of Technology. It consists of a Plexiglas loop-seal, with 24 copper tubes crossing horizontally. Solids were fed from the top of the down-comer. After traveling along the loop-seal, they arrived to the recycling pipe, originally attached to the bottom zone of the CFB. Solids from the recycling pipe were weighted for estimating an average flow rate of solids in every test. Air entered directly to the chambers 2 and 3 through perforated plates. A rotameter flow-meter with a manual globe valve allowed varying de fluidizing gas velocity. Tap warm water circulated inside the tubes, reaching a maximum temperature around 40ºC. 15 of the 24 tubes (filled circles in Figure 4.7) had attached thermocouples in the surface. The water temperature was approximately that of the tubes, because of the high conductivity of copper.

Once the water circulation stoped, we estimated the cooling rates in each tube with the following expression:

$$\frac{\Delta T}{\Delta t} = \frac{T_2 - T_1}{t_2 - t_1} \qquad \text{Eq. 4.12}$$

Capital letters represent temperature in the moment t_2 and t_1 respectively. Figure 4.9 displays a typical cooling curve and the initial 10 seconds that were used for the cooling rate estimation.

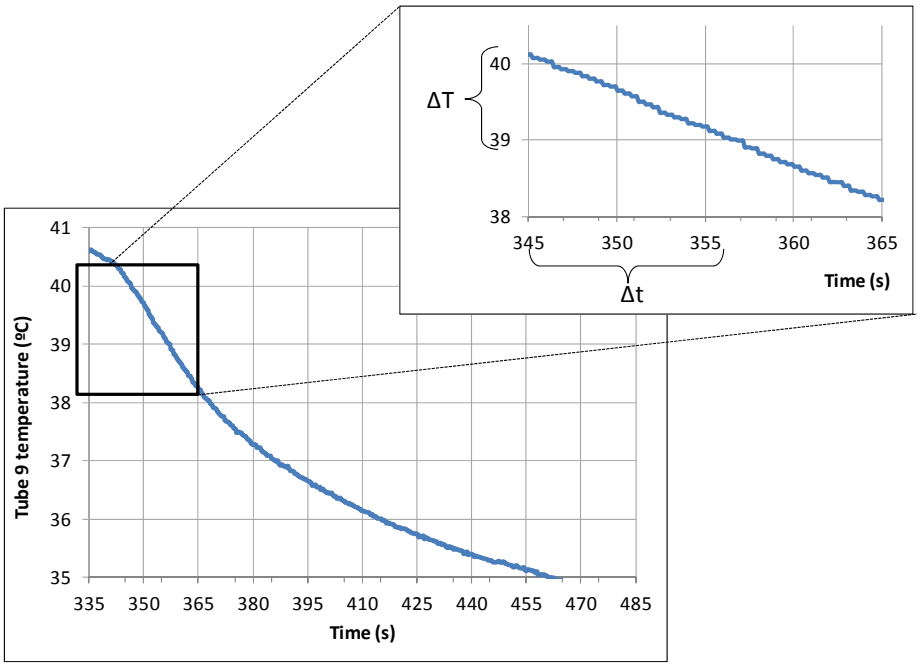

Figure 4.9. Example of cooling curve for a testing tube. Zoom to the first seconds of cooling to calculate the cooling rate.

In order to compare the influence of solids recirculation on the heat transfer performance in the loop-seal, the mass flow fed by the dip-leg was widely varied. Thanks to the un-coupling with the overall CFB arrangement, the solids rate could vary within a wide range of values. On the other hand, this uncoupling, did not permit a good regulation of solids feed, particularly at high rates. These ranges are presented in Table 4.1. The fluidizing velocity was kept below 5 u_{mf}, in order to avoid the return of gas trough the dip-leg.

m_{out} (kg/s)		u/u_{mf}	
planned	achieved	planned	achieved
0	0	0	0
		1	1.2-1.5
0-5	0.8-4.7	1-3	2-3
		3-5	3.6
5-15	5.3-13.5	1-3	2.4-2.8
		3-5	3.6-4.8
15-30	15-23.4	1-3	1-2.8
		3-5	3.2
>30	30-71.8	1-3	1.6-3
		3-5	3.6

Table 4.1. Experiments planning matrix for the operation of the cold EHE

The cooling rate in every tube was measured. The tubes with attached thermocouples are widespread among the tube bundle. They provided information at different locations in the loop-seal: along height and from the dip-leg to the recycling pipe area.

4.4 RESULTS OF HEAT TRANSFER IN THE COLD EHE

4.4.1 COOLING RATES

The cooling rates are negative values, because of the sign of the calculated slope. This is, the further the cooling, the more negative the cooling rate value, and the higher the heat transfer in that position. We can so identify the conditions at which cooling are uneven distributed along the tubes. In order to easier visualize the cooling rates results, in the following graphs, these are represented against the tubes position in the horizontal distance from the down-comer. Figure 4.10 illustrates three cases for the first row of tubes, one with no solids feeding crossing the EHE, and two different solids flow, 7 kg/s and 8.7 kg/s, respectively.

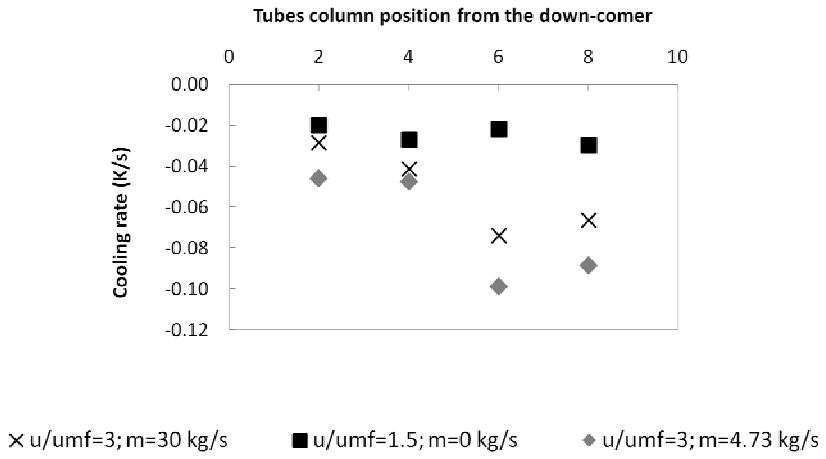

Figure 4.10. Cooling rates at the first row, near the distributor, low velocities

The case of no solids feeding presents uniform cooling rates along the loop-seal, and the lowest values out from the three cases. When solids are fed and fluidizing velocity increases, more intense cooling takes place far from the downcomer. The values showed that uniformity of cooling observed in the reference case, is disturbed when solids cross the EHE. These observations agree with the previous findings, in which the trajectory shaped by solids influenced heat transfer coefficients at the different locations.

In Figure 4.11 and Figure 4.12, cooling rates are represented in the lowest (1st) and highest (6th) tubes positions. Figure 4.11 shows the reference case with no solids feeding (the same as in Figure 4.10), and two cases with different mass and air flows: 4.7 kg/s with $3u_{mf}$ m/s, and 15 kg/s with $4u_{mf}$ m/s. Here, the increase of cooling rates is also higher in the cases with solids feeding, compared with the reference case. Interestingly, a markedly inequality is shown by the case of medium air velocity and solids flow, doubling the value of cooling rate near the down-comer. With highest solids flow, cooling rates are more uniform, particularly in the 6th row.

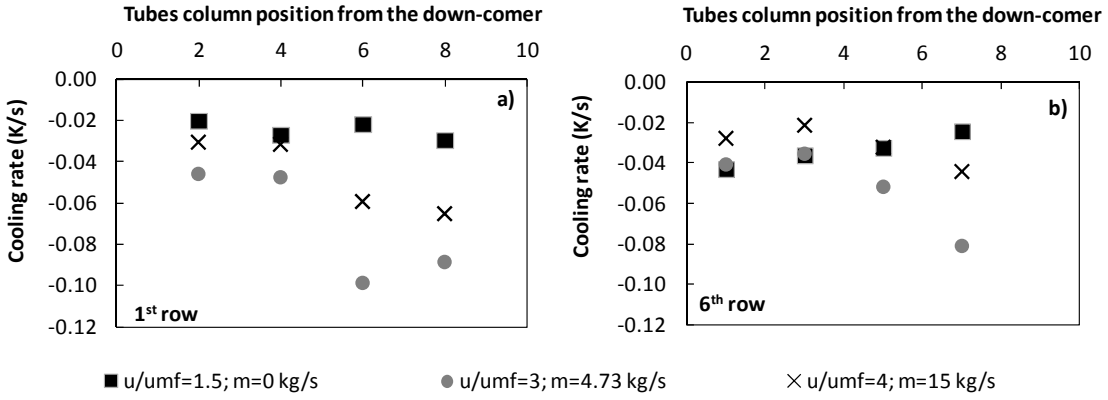

Figure 4.11. Comparison between low and higher tubes with two solid rates

Figure 4.12 shows two cases, with low solids rate and different fluidizing velocities, together with the reference case with no solids feeding. On this occasion the cooling is slightly higher in the case with higher aeration velocity and this is also the conditions at which inequalities at different positions are increased.

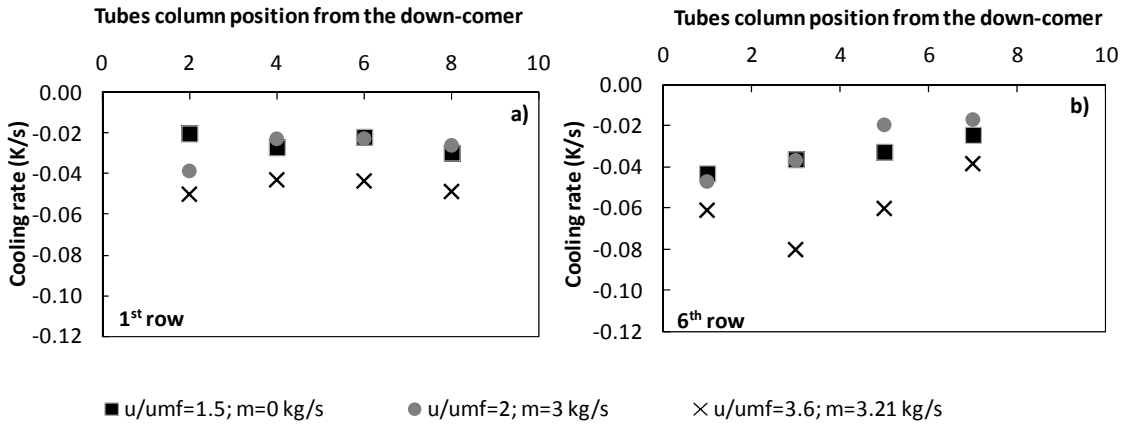

Figure 4.12. Comparison between low and higher tubes with two aeration velocities

Unlike in Figure 4.11, in Figure 4.12 the distribution of cooling along the tubes in the 1st row for the highest velocity case is more even. The major cooling occurs in the last row, in the tubes near the down-comer, and it diminishes with the distance.

Up to here, the influence of fluidizing velocity on the cooling rate turns predominant over the mass flow of solids traveling across the EHE. However, heat transfer is increased when solids travel through the EHE. The uneven cooling among the tubes must be due to the different distribution of warm solids at the different locations in the EHE. This is related to the combination of the fluidizing

velocity that allows a proper solids mixing, and the solids flow rate that permits the warm particles to contact all the tubes before abandoning the EHE.

In order to compare influence of solids rate and velocity, the distribution of the cooling rates along the vertical direction, is presented in Figure 4.13 for four different conditions. Figure 4.13 shows the reference case, where no solids are fed in the EHE. More intense cooling is perceived in the 5th and 6th row of tubes than in the lower tubes, but the distribution is near uniform. Figure 4.13b) presents the case with low solids rate and high aeration velocity. Average heat transfer is increased, and heat transfer is very even in all tubes, except in the 5th row, near the recycling pipe, where cooling is markedly more intense. In Figure 4.13c) and d) aeration velocity is similar, but solids rate is higher in c). Average cooling rates increase compared to the reference case. Non-uniformities are differently located in both cases. Higher solids rate exchange more heat near the recycling pipe, whereas the cooling in the case of low solids rate is higher in the tubes near the down-comer.

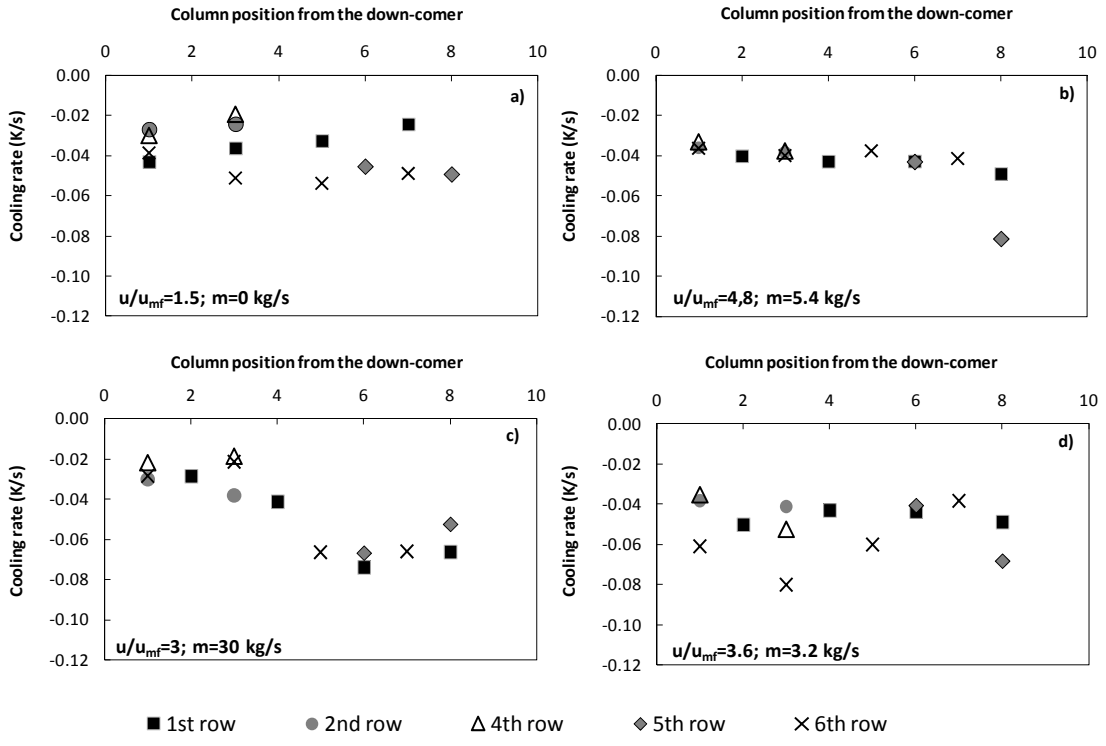

Figure 4.13. Comparison of four tests at different row heights

Tests carried out in the cold fluidized bed heat exchanger model reveal that heat transfer in the loop-seal is highly influenced by solids travelling across, and un-

uniformities of heat transfer coefficients along the loop-seal are caused by the trajectory of these solids in their way to the recycled pipe. Heat transfer near the bed limit is more intense. Higher velocities could allow better solids mixing and hence, would reduce differences on heat transfer from one area to another in the loop-seal.

Up to this points we can conclude that high flows of solids arriving at the loop-seal EHE enhances heat transfer. However, the un-even distribution of tubes cooling is caused by this flow of solids. The non-uniformities are also related to adequate aeration velocities that allow proper mixing of solids. This translates into that maximum cooling rates were not found for the case of highest velocity and highest solids rate.

The local cooling rates measured in the previous experiments will be used to following calculate the local heat transfer coefficients in each tube.

4.4.2 UNEVEN DISTRIBUTION OF HEAT TRANSFER COEFFICIENTS

Cooling rates previously presented are a transient heat transfer process (Mills, 1995). The heat exchange between tubes and bed, Q, can be written as:

$$Q = hA_{HT}\left(\overline{T} - T_B\right) = \left(\rho_{Cu}V_{Cu}C_{Cu} + \rho_w V_w C_w\right)\frac{dT}{dt} \qquad \text{Eq. 4.13}$$

The $\rho_{Cu}V_{Cu}Cp_{Cu}$ and $\rho_w V_w Cp_w$ terms are the lumped thermal capacitance of copper and water respectively. A_{HT} is the surface of tubes available for heat exchange. T_B indicates the value of the bulk of particles. Rearranging Eq. 4.13, the heat transfer coefficient in each tube yields:

$$h_i = \frac{\left(\rho_{Cu}V_{Cu}Cp_{Cu} + \rho_w V_w Cp_w\right)\Delta T_i / \Delta t}{A_{HT}\left(\overline{T} - T_b\right)} \qquad \text{Eq. 4.14}$$

Where index i represents the coefficient and temperature at each tube. Tubes diameter were 1/4" and cupper density and specific thermal capacity were 8932 kg/m^3 and 0.3854 kJ/kgK, respectively.

Following the heat transfer coefficient will be displayed against the horizontal position from the downcomer of the respective tube. In Figure 4.14a) and b), different solids rates are represented, for low and high aeration velocity,

respectively. In Figure 4.14a) two cases are represented, in which the ratio u/u_{mf} is 4.8 and the solids rate is 2.4 and 5.4 kg/s. The case with lower solids rate present also lower heat transfer values. Moreover, uneven distribution of heat transfer is more evident in the lower solids rate case, with a variation around 80%.

In Figure 4.14b) solids rate varies from 22.7 and 8.7 kg/s, with lower velocity ratio, 2.8. In this cases, the inequalities in the heat transfer values is up to four times the minimum values in the position near the down-comer, and even higher close to the recycling pipe.

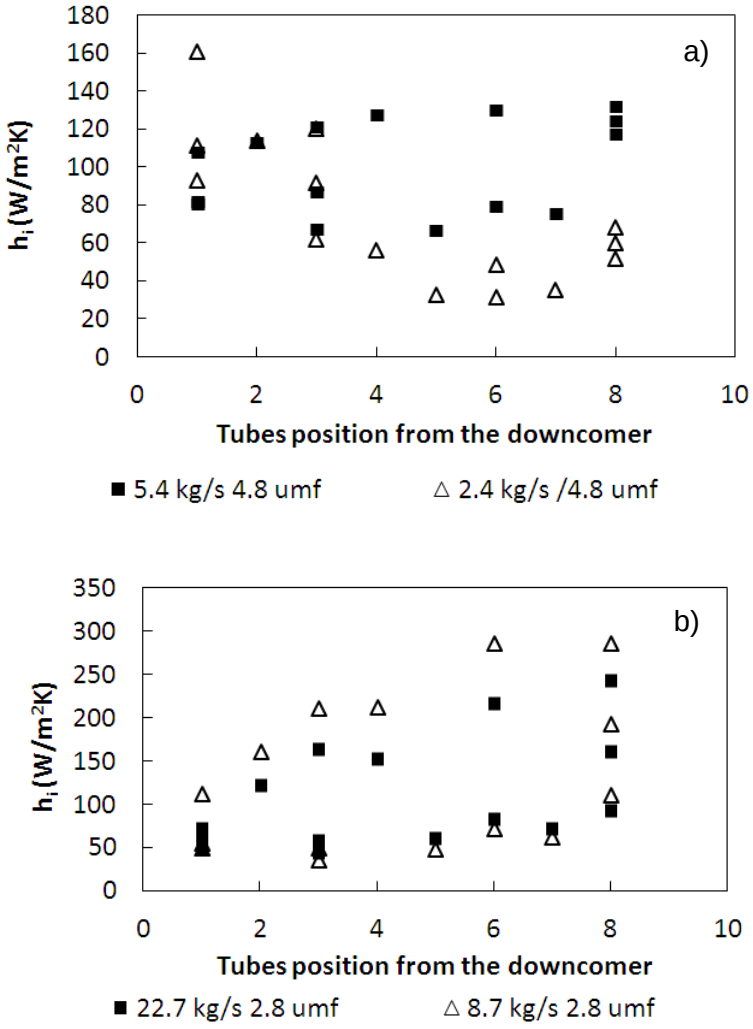

Figure 4.14. Heat transfer coefficients, a) high velocity and increasing solids rate; b) low velocity and different solids rate

Figure 4.14 reveals that aeration velocity and solids rate must be adequately related in order to obtain not only high heat transfer coefficients, but optimum distribution among the heat exchanger tubes. Another example of this affirmation is shown in Figure 4.15. They are represented the cases with lowest fluidizing

velocity and a considerable amount of solids traveling through the EHE, and a higher velocity ratio with less solids rate. The average heat transfer coefficient is, in both cases, around 100 W/m²K, although the higher solids rate induces further inequalities in the heat transfer among the tubes.

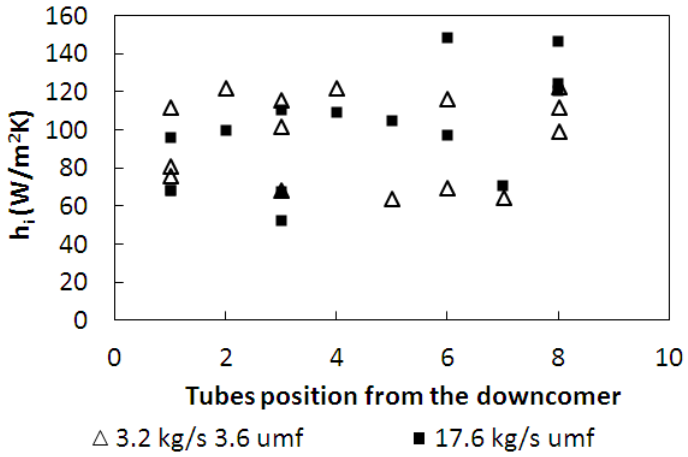

Figure 4.15. Heat transfer coefficients with two velocities and solids rate conditions

Increasing aeration velocity would lead to higher gas flow in the chamber 3. Pressure drop in this chamber is lower than in chamber 2, because no tubes are present. Then, certain reflux of aeration gas could have intensified cooling rates of last tubes columns. However, in the experiments where aeration velocity was as high as 4.8 times the minimum fluidizing velocity, heat transfer coefficients distribution kept uniform. The dominant cause of dissimilarities of heat transfer lied on the increment of Gs.

In the conventional operation of an EHE, the different heat transfer coefficients at different tubes locations are not usually considered for the design, but the average heat transfer coefficient. The average heat transfer coefficient among the local values previously obtained, will allow establishing a relationship between Gs and heat transfer coefficient, to account for the enhancement of heat transfer due to solids recycling, in spite of dissimilarities of heat transfer among the tubes.

However, since elutriated solids rate of an oxy-fuel CFB are expected to considerably increase, a specific design of tubes bundle will be desirable for optimum design of future EHE. This should be carefully considered and it will be propose as future work at the end of this document.

4.4.3 AVERAGE HEAT TRANSFER COEFFICIENT

Averaging the tubes heat transfer coefficients helps to ascertain the influence of operating parameters particular of an EHE. The average heat transfer coefficient is represented versus solids rate and fluidizing velocity ratio in Figure 4.16. These two parameters have opposite effect on heat transfer. On the one hand, increasing solids rate crossing the EHE improves heat transfer. The relation shown in Figure 4.16 a) is not lineal, but follows a potential shape, i.e. up to certain Gs, the heat transfer coefficient does not improve visibly. On the other hand, gas velocity has an opposite effect on heat transfer. This means that gas convection mechanisms begins to dominate the overall heat transfer, over the particle convection mechanism, probably due to higher bed void fraction.

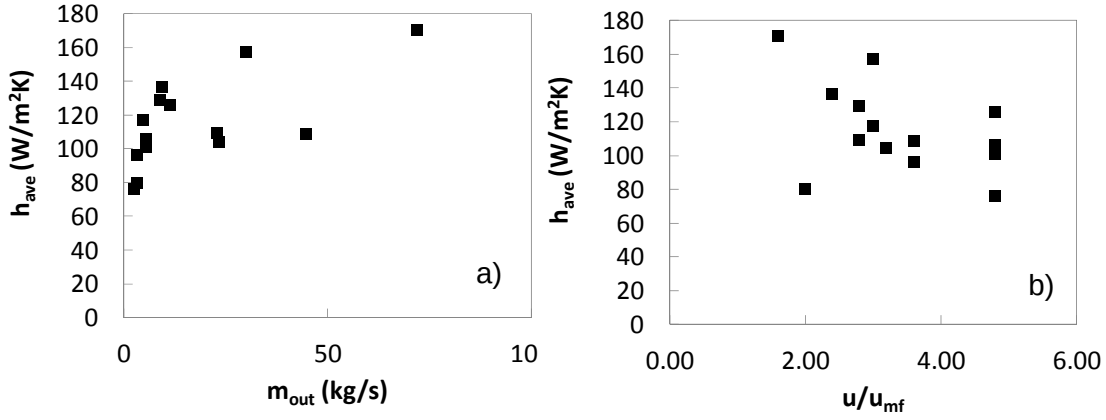

Figure 4.16. Influence of a) solids flow, and b) velocities ratio, on the average heat transfer coefficient

In the conventional operation of a loop-seal there is evidently a relationship between the aeration velocity and the recycled solids. Simultaneously it must fulfill the adequate pressure seal for the proper solids circulation in the fluidized bed loop. This was experimentally analyzed and quantified by Kim (2001). They observed a lineal relationship between aeration velocity and solids recirculation up to certain velocity, from which solids recirculation did not depend on fluidizing velocity anymore. The operation of an EHE can comprise different arrangements. If it works as the CFB loop-seal, this relationship between Gs and u_f would be essential. Another approach is to redirect part of the solids from the loop-seal to the EHE. Thus, the sealing would not be the main role of the EHE, and Gs and

aeration could vary in wider ranges, within the desired heat exchange requirements.

The residence time of particles inside the EHE, t_R, is calculated in Eq. 4.15. This term condenses both: the flow rate of particles from crossing the EHE and the fluidizing velocity by means of the void fraction.

$$\frac{1}{t_R} = \frac{\dot{m}}{(1-\varepsilon)\rho_s A_{cross} L} \qquad \text{Eq. 4.15}$$

The void fraction, ε, is function of the fraction of bubbles in bed, and thus, of the bubbling velocity. We estimated these parameters following the procedure proposed by Kunii and Levenspiel (1991).

Figure 4.17 shows a potential shape curve of heat transfer coefficient while increasing residence time of particles in the loop-seal. The two opposite effects of mass flow and gas velocity explains this behavior, being predominant the effect of solids rate. Higher solids rate leads to quicker replacement of solids in each zone of the EHE. This also means that solids temperature decreases slower.

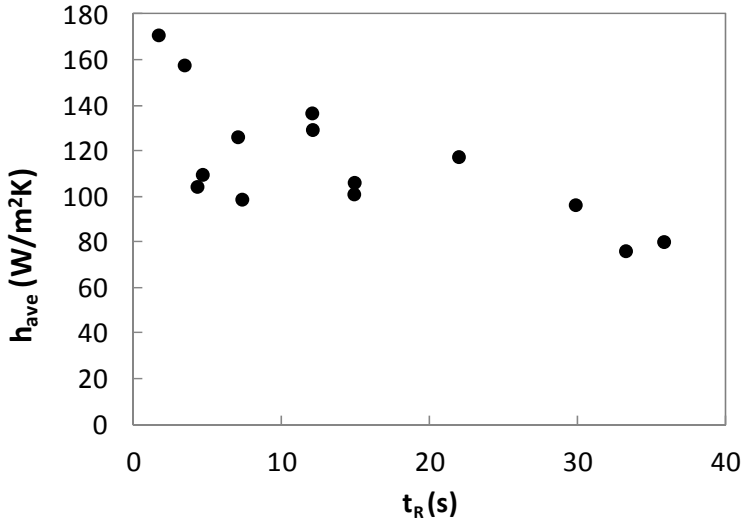

Figure 4.17. Residence time influence on the average heat transfer coefficients

The decreasing tendency observed in Figure 4.17 agrees with the transient conduction concept, exhibiting that during the time t_R, particles are transferring energy and so, diminishing temperature. Thus, when they contact the next surface, the heat transfer diminishes. The descendant curve described in Figure 4.17 shows

that, in the extreme case in which t_R is infinite, the heat transfer set in a constant value. This is the case in which no solids were recycled.

The average heat transfer coefficients and residence times of recycled solids obtained for the cold model are now represented in the dimensionless form, H and Θ, respectively. This allows including the values measured in a real EHE, reported by Man et al. (2012), and previously explored. Figure 4.18 displays results from both, the cold model and the real EHE, in dimensionless form. The values follow a decreasing potential shape that stabilized in the minimum heat transfer coefficient. This minimum heat transfer coefficient will approach the value in which solids are not crossing the EHE, i.e. there is not lateral flow of warm solids.

The curve that fits the values in Figure 4.18 is correlated by the expression (R^2=0.65):

$$H = 2.7324\ \Theta^{-0.322} \qquad \text{Eq. 4.16}$$

Eq. 4.16 allows modifying the heat transfer coefficient estimated for non recycled solids conditions, and estimating how much this coefficient is enhanced by the solids flow traveling through the EHE.

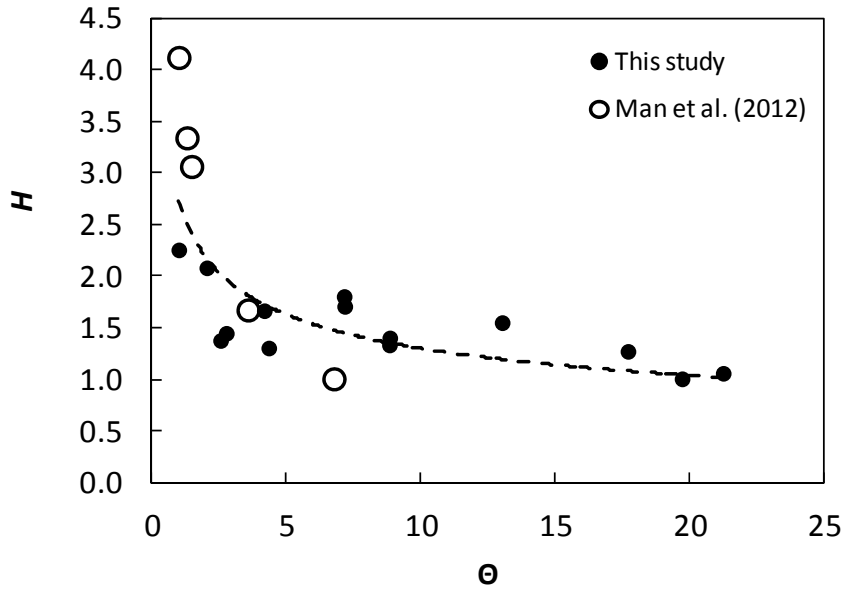

Figure 4.18. Influence of residence time of recycled particles on heat transfer coefficients in the cold model and in the real EHE

With the expression proposed in Eq. 4.16 accounting for the influence of Gs on heat transfer, and the heat transfer semi-empirical approach deduced in last chapter, Eq. 3.34, we are ready to extrapolate these expressions to the sub-model of an EHE to include it in the modeling of the large CFB boiler.

4.5 INTEGRATION OF THE EHE MODEL IN THE OXY-FUEL CFB MODEL

4.5.1 FLY-ASH RE-CARBONATION

Before developing the sub-model of the external heat exchanger fluidized bed, a relevant issue, particular of oxy-fuel operation, must be addressed. This is the possibility that re-carbonation of fly ashes, coming from the cyclone, takes place in the EHE. Under oxy-firing conditions, conventional bed temperature is not high enough to allow limestone calcination and direct sulfation takes place. This was further addressed in section 2.2.2. This leads to a decrease of SO_2 capture efficiency compared to indirect sulfation using the same calcium to sulfur ratio.

Higher bed temperature can be a solution for reaching similar SO_2 capture efficiency during oxy-fuel combustion. In this case, limestone is calcined yielding large amount of CaO. Sulfation process occurs in the particles surface, until external pores are blocked by $CaSO_4$ layer. Diffusion to the CaO core is then difficult for SO_2. Thus, an excess of Ca:S over stoichiometric is necessary for assuring proper SO_2 capture. Still, considerably CaO surface is available after travelling along the riser.

Conventional temperature in the external heat exchanger ranges between 750ºC-650ºC (Nsakala et al., 2004) and these are the temperature values obtained for proper bed temperature in the previous analysis. At this temperature and high CO_2 partial pressure, CaO tends to quickly re-carbonate. Then, if calcination had been taken place, large amount of CaO would arrive to the loop-seal. In oxy-firing conditions, loop-seal is fluidized with CO_2 or RFG that can easily react with the available CaO. In Figure 4.19 CaO-$CaCO_3$ equilibrium is represented and conditions in boiler and loop-seal are indicated. It can be distinguished that conditions at which a loop-seal works are clearly in the carbonation area. The

optimum air-firing temperature is also marked and calcination is not likely to occur under high CO_2 partial pressure proper of oxy-fuel combustion.

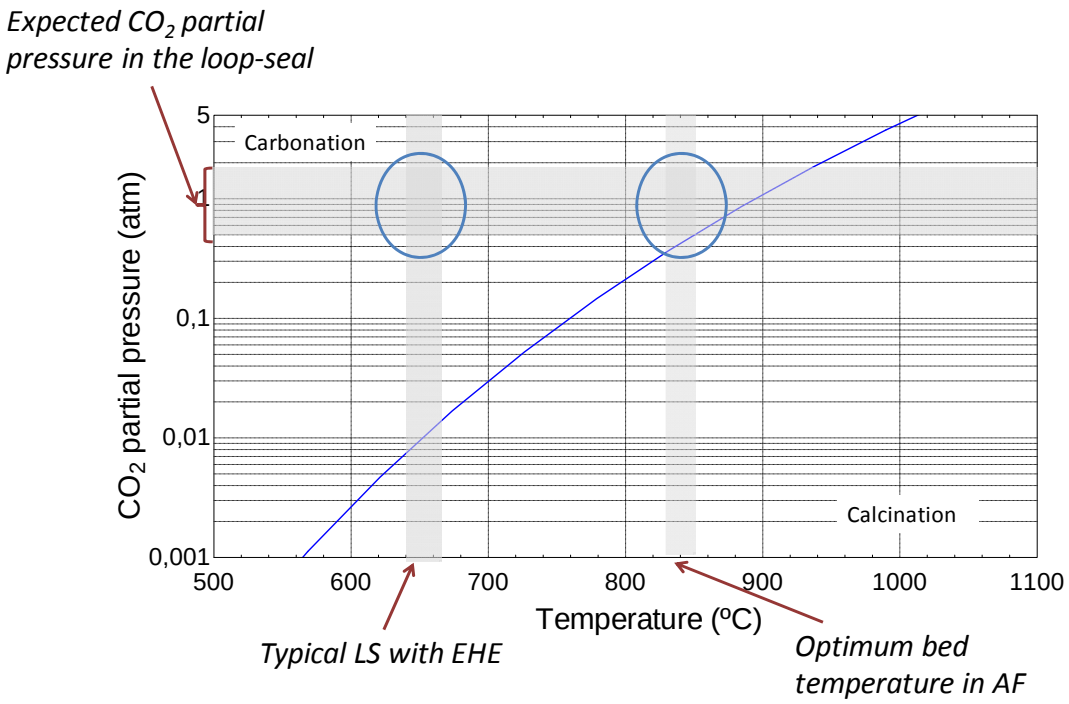

Figure 4.19. Carbonation-calcination equilibrium

With the aim of exploring the influence of direct and indirect sulfation on the CaO rate reaching the EHE, the CFB model developed in Chapter 2 is now run, for two temperature levels, and two oxygen concentrations. Figure 4.20 illustrates the results at 850ºC and 900ºC, with the 40% O_2 concentrations in the oxidant stream. Figure 4.21 graphs simulations results when feeding 60% O_2 at the same two average bed temperatures. In both graphs, zoom is made on the bottom part of the boiler, where most of reactions take place. The equilibrium pressure is represented in bold line for both cases, according to Eq. 2.23. The higher temperature level, around 900ºC is depicted in dotted line and the lower in discontinuous line. When the values of CO_2 partial pressure are higher than those of the equilibrium curve, indirect sulfation occurs. The contrary happens if the partial pressure of CO_2 is lower, i.e., sulfation occurs in one step. Figure 4.21 shows that, with O_2 concentration as high as 60%, direct sulfation occurs in the lower part of the boiler, even at high temperature, which reduces the sulfation efficiency, although CaO available in the solids loop is also lower.

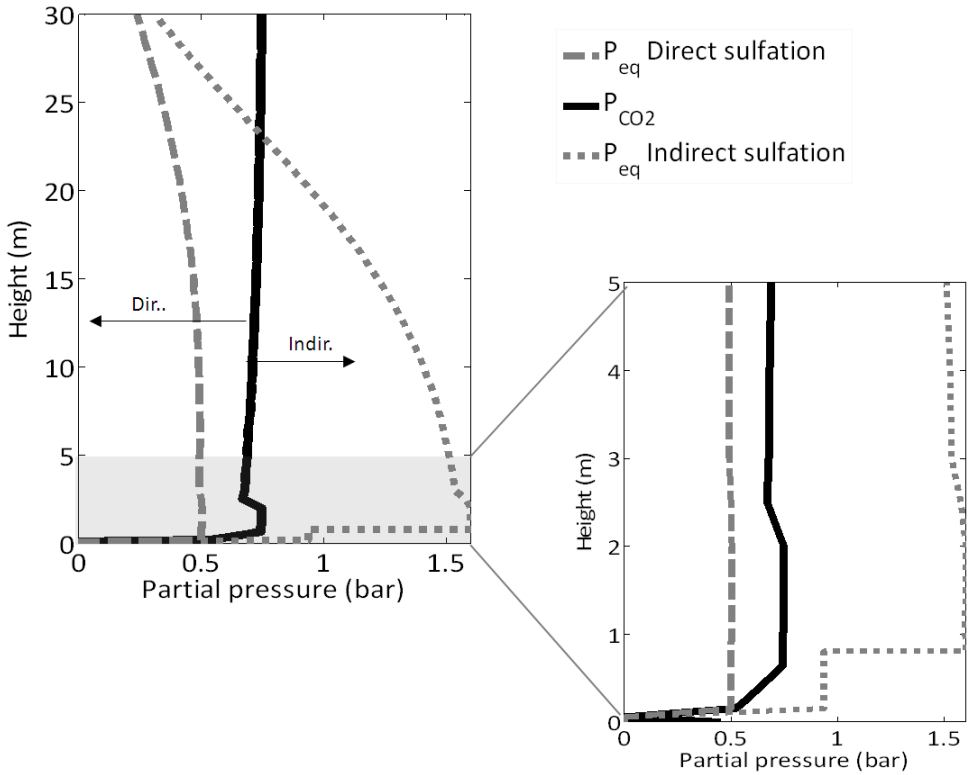

Figure 4.20. Partial pressure and equilibrium pressure of CO_2 along the riser, 40% O_2 at inlet

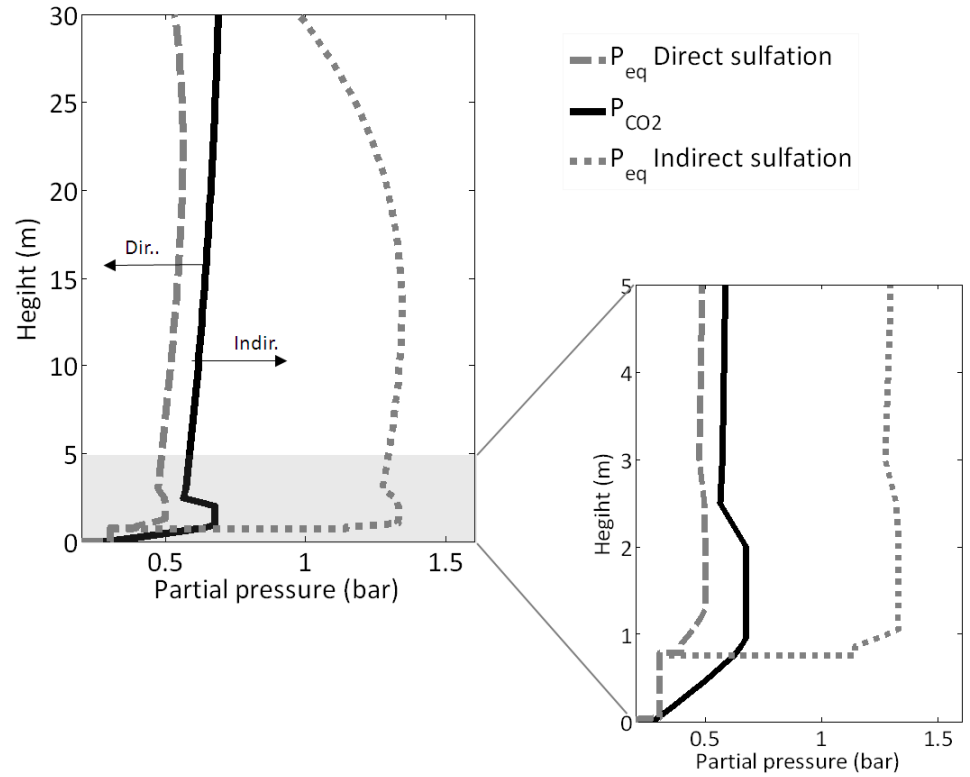

Figure 4.21. Partial pressure and equilibrium pressure of CO_2 along the riser, 60% O_2 at inlet

The sulfur capture efficiencies for the direct and indirect sulfation cases are 80% and 95% respectively. These values are set from the experiments run in the CIRCE pilot plant. These experiments in the OF BFB are described in Bolea et al. (2012a). The results were obtained from the oxy-fuel combustion of a blend of two different coals, 46% of lignite, 30% of bituminous coal. The rest 24% was limestone with a Calcium-Sulfur ratio of 2.5. The sulfur capture efficiency was measured in two air-firing tests and two oxy-firing tests at 25% O_2. Bed temperature was always kept below 900ºC. The experimental efficiencies values have been coupled to the large-scale OF CFB model.

In the model, to reach indirect conditions, average bed temperature was over 890ºC, with 40% O_2; the boiler size was enlarged up to 3.9 m depth: lower velocity for the same gases volume promotes less elutriation and thus, average boiler temperature is higher. This is due to a higher heat transfer when increasing riser density. In the simulation of 60% O_2, boiler size was kept constant and fed fuel was varied between 190 to 170 MW. Thus, as before, increasing fuel input makes necessary to feed higher gas volume for reaching stoichiometric conditions. Then, velocity increases, higher solids concentration enhances heat transfer rates in the freeboard and the global temperature decreases. Table 4.2 shows these inputs.

Results of the simulations are shown in Table 4.3. The molar rate of CO_2 for fluidizing the EHE is the same order of magnitude than the CaO elutriated in the case of indirect sulfation. Not all the CaO surface is available for reactions, since part will be covered by $CaSO_4$ layer formed during sulfation in the combustor and it will be difficult for CO_2 to diffuse to the CaO core. Works like the one published by Sun et al. (2007) found that carbonation of CaO is reduced down to 30% with SO_2 present, for 10 cycles of carbonation-calcination loops.

Case	O_2/CO_2	Sulfation	Power (MW)	Sizes (m^2)	Gs (kg/m^2s)
1	40/60	Direct	90	3.5x4.5	10.9
2		Indirect	90	3.9x4.5	7.2
3	60/40	Direct	190	3.5x4.5	34.7
4		Indirect	170	3.5x4.5	24.5

Table 4.2. Recarbonation inputs for the simulations

Case	Emitted SO_2[a] (ppm)	Elutriated $CaCO_3$ (kmol/s)	Elutriated CaO (kmol/s)	CaO available for carbonation (kmol/s)	Loop-seal fluidizing CO_2 (kmol/s)
1	1361	0.011	-	-	0.0164
2	319	-	0.011	0.0033	0.0182
3	2174	0.0247	-	-	0.0164
4	963	-	0.0216	0.0065	0.0164

[a]Normalized SO_2 emissions: $C_{SO_2\,6\%O_2} = C_{SO_2\,O_2,meas}\,\frac{C_{O_2\,in} - 6}{C_{O_2\,in} - C_{O_2\,out}}$

Table 4.3. Recarbonation results from the simulations

For higher O_2 ratios at inlet, molar flow of CaO arriving at the loop-seal is twice the molar flow of CO_2 needed for fluidization. The values obtained by Sun et al. (2007) for estimating the available CaO surface available were considered here. According to this paper, the factor of 0.3 is applied to the total flow of CaO arriving to the loop-seal and indicated in the column called *CaO available for carbonation*. Still, in the case of 60% O_2 at inlet, de-fluidization is highly probable.

When indirect sulfation is the predominant SO_2 capture phenomena, the risk of defluidization of the loop-seal is a problem that must be tackled in this CO_2 capture technology. Particularly, when wet flue gas recirculation took place, the presence of steam on RFG would catalyze the carbonation reaction, probably due to formation of transient hydroxide species (Wang et al., 2008). The presence of steam would make even more probable loop-seal defluidization than fluidizing gas without H_2O. To avoid this issue, several options could be suggested:

- The first choice would seem to change the fluidizing gas of the loop-seal. Air cannot be an option, since N_2 means impurities in the CO_2 stream difficult to eliminate before the CO_2 compression train. Fluidizing the loop-seal with steam would form CaO-OH, which actually enhances SO_2 capture (Wang et al., 2011). However, this compound is weaker and would favor attrition and segregation. Moreover, consequences of such high steam content inside the boiler must be carefully studied.
- Higher temperature in the loop-seal to avoid optimal conditions for the re-carbonation is not suitable for oxy-fuel combustion. This is narrowly related with what was demonstrated in Chpater 2, on the essential function of the

EHE: in oxy-fuel combustion, gases entering the furnace are reduced, compared to air-firing. To reach similar velocities, bed cross-sectional area is decreased. Less volume means less available steam-wall surface for the same fuel-input. Then temperature must be regulated by two additional ways:

  - Increasing solids concentration along the riser for enhancing heat transfer coefficient by increasing solids convection. This has an immediate effect: higher solids concentration increases wall layer density and so, shadow effect of solids diminishes radiation to be "seen" by the water-wall.
  - Heat transferred in the loop seal to an external heat exchanger could be intensified by further cooling of recycled particles, or by increasing mass flow of particles crossing the loop-seal.

- Avoiding calcination by keeping bed temperature under direct-sulfation conditions could be an interesting option. To reach high SO_2 capture efficiency as in indirect sulfation case, higher Ca:S ratio should be introduced. This would lead to higher solids circulation. The additional limestone needed means a minimum proportion to the total amount of solids elutriated from the riser.
- Increasing fluidization volume gas flow rate would allow CaO to be re-carbonated and also it would let enough CO_2 for proper fluidization. However, in practice this does not seem an easy option. The risk of either defluidization or gas by-pass to the cyclone is too high. The difference between the minimum CO_2 flow rate needed for bubbling conditions in the loop-sea and the total amount of CaO available for carbonation could be too short, if there were enough carbonation capacity of the CaO particles, and regulation would turn rather complicate.

The risk of loop-seal de-fluidization by re-carbonation of CaO has been reported by METSO Power, occurring in their 4 MW CFB boiler (Varonen et al., 2012). During the tests in which re-carbonation took place, limestone addition generated circulation problems in oxy-combustion, due to the recarbonation of CaO. In occasions, this reaction blocked the loop seal. Hence, all the circulation material was collected into the loop seal, dipleg and cyclone, which finally led to furnace temperature increase and sintering. They had confirmed the conditions of re-carbonation reactions at laboratory scale (Hyytiäinen et al., 2011). They

suggested that the safe operating window in oxy-mode must be defined and recarbonation problems were avoided if the process was controlled accordingly. Thus, the fourth option previously numbered, is the one selected for the modeling of the EHE. If recarbonation is likely to occur, fluidizing velocity will have to increase to prevent de-fluidization, and so, the operational window will be adequate.

4.5.2 EXTERNAL HEAT EXCHANGER SIMULATION

The sub-model for the external heat exchanger gets results from the CFB model developed in Chapter 2. The temperature of recycled solids was an input variable, for assuring the required average temperature along the boiler. It was a *black box* and calculation of the heat removed was calculated by energy balance with the flow of solids and the temperature difference. Now, the aim is to go into this device in depth. From the overall boiler simulation, data entering the EHE sub-model include the solids entrainment, the temperature of these solids, the composition of the flue gas, which will fluidized the EHE, and the amount of calcium-based components from the limestone. The overall sequence of programming the EHE is represented in Figure 4.22.

There are some external variables needed to complete the model. The geometrical configuration of the model was based on the one described by Man et al. (2012). They gave much detail about the arrangement of the different chambers and the fluidizing velocity. This makes possible to draw more realistic conclusions from the model itself. Based on this real EHE arrangement, the model is divided into three chambers. The first one has no tubes. It is fluidized initially with 0.5 m/s and has cross sectional area of 0.7 x 4.4 m. The second and the third chambers are the ones containing the tubes bundles. Their cross sectional areas are 4.2 m x 4.4 m and 3.5 m x 4.4 m, respectively and they are fluidized initially with a velocity of 0.3 m/s. Temperature of water entering the second chamber is 386ºC. The rest of temperatures are calculated in the simulation. As initial data, the heat exchanger effectiveness is also an input. It is an average value among those deduced from the data given in the paper, around 0.7. This effectiveness is defined as:

$$effectiveness_{EHE} = \frac{Q}{Q_{\max}} = \frac{Q_{water}}{c_{p,solids} m_{solids} \left(T_{solids,in} - T_{water,in}\right)} \qquad \text{Eq. 4.17}$$

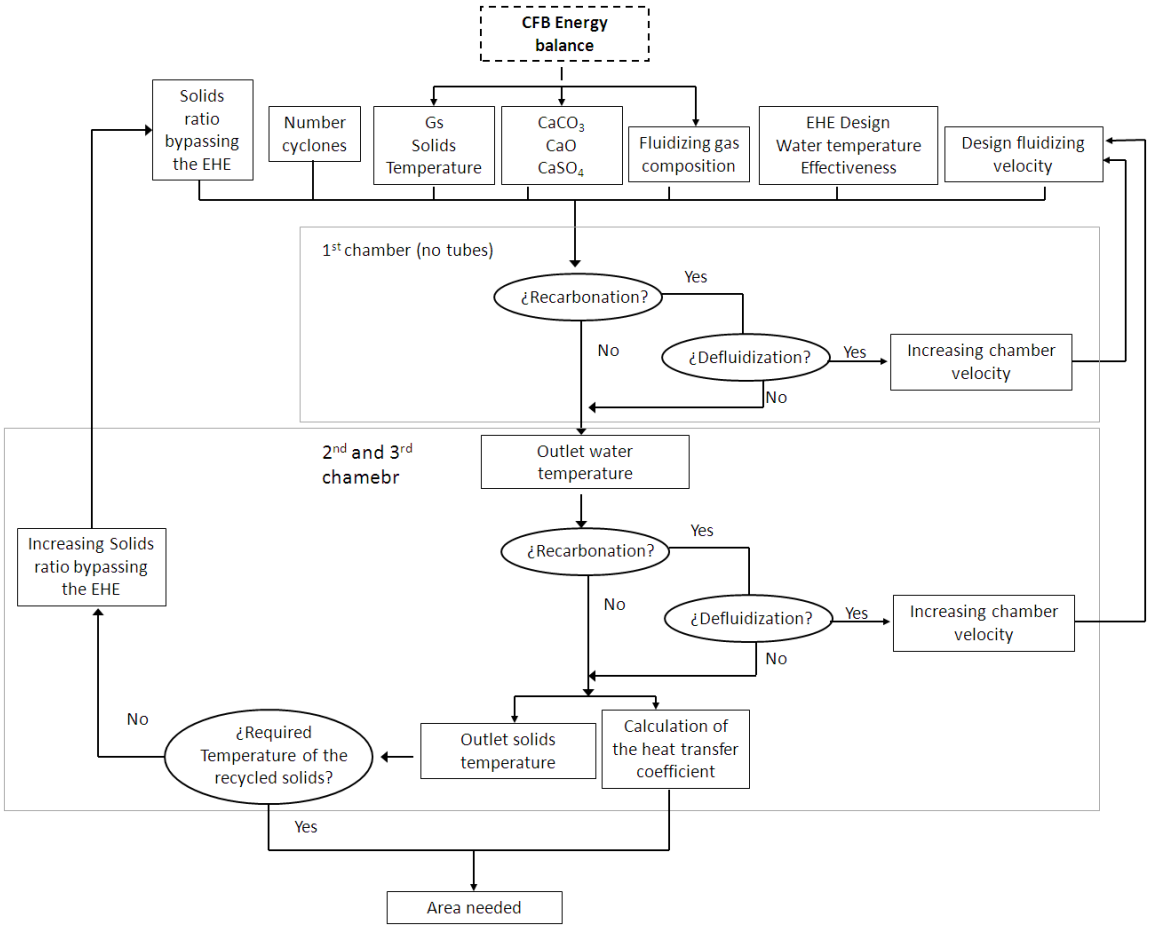

Figure 4.22. Modeling flow chart of the integration of an External Heat Exchanger into the global CFB model

Initially it is assumed that all the solids falling from the cyclone are conducted to the external heat exchanger. In the first chamber, there are no tubes, but conditions can favored the re-carbonation of CaO present in the solids, as previously explained. If this happens, to avoid de-fluidization, velocity must be increased. The re-carbonation energy is included when calculating the temperature of solids entering the second chamber.

Solids arriving at the second chamber, transfer energy to the water. The temperature of the water at outlet is calculated by the effectiveness value, with Eq. 4.17. If recarbonation takes and the chamber de-fluidized, the velocity is incremented, and the re-carbonation energy is included in the energy balance. This sequence is repeated in the following chamber. Finally, temperature of solids abandoning the EHE is calculated. If they are higher than required by the CFB model, part of the solids bypasses the EHE and temperature of solids entering back in the boiler is calculated by energy balance:

$$c_{p,s} m_{recycled} T_{requierd} = c_{p,s} m_{bypass} T_{solids,in} + c_{p,s} m_{EHE} T_{solids,out} \quad \text{Eq. 4.18}$$

The solids temperature and the heat transfer coefficient will establish the required area for reaching the specified temperature of solids. To attain the convergence, the key variable is the fraction of solids conducted through the EHE.

4.5.3 INTEGRATION RESULTS

To take into consideration the possibility of re-carbonation of CaO in the EHE, two different average bed temperatures in the boiler will be considered, to explore the model results. One of these temperatures will be high enough to form CaO in the boiler. This way, we could observe the increase on the fluidizing velocity in the EHE to cope with de-fluidization. The other temperature will be less than 900ºC, and the CaO available in the EHE would not bring any inconvenience.

Three different O_2 concentrations in the comburent inlet, 40%, 50% and 60%, are modeled here, at the two different temperature ranges mentioned above. The boiler geometry was kept the same in the three cases, with 96 m^2 cross sectional area, and 35 m height. For this reason, the fuel input in the simulations is 250 MW (air-firing), 450 MW (40% O_2), 620 MW (50% O_2) and 775 MW (60% O_2).The number of cyclones and EHE were 4 in all cases. The geometry and arrangement of the EHE has been kept the same for any case. This will allow a better comparison, isolating the influence of the EHE geometry. The heat transfer coefficient will be calculated as deduced in Eq. 3.34 and corrected with expression proposed in Eq. 4.16, by calculating the time that recycled solids take to cross every chamber. For the estimation of h_0, the fluidizing velocity was 3 times the one at minimum fluidization. This allowed a more realistic value for applying Eq. 4.16, since increasing Gs means also the corresponding increase on u_f. Higher O_2 concentrations, allows greater fuel input and the heat that the EHE must removed must augment.

The results from the simulations are synthesized in Figure 4.23 and Figure 4.24. Figure 4.23 shows the recycled solids flow in every case, with the corresponding value of the resulting heat transfer coefficient. The increase of heat transfer coefficient with O_2 concentration at inlet was due to the increase of elutriated solids needed to keep the adequate bed temperature. This was the reason why the heat transfer coefficient in the cases of lower bed temperature, between 850ºC and

880ºC was also higher, since so they were the solids recycled. In the 40% O_2 case, Gs for the lower and higher temperature range in the boiler were 11.6 and 9.3 kg/s m², but the solids conducted to the EHE were 28% and 35%, respectively. The time of solids to travel through the EHE, $t_{R,}$ was around 25 times that considered as the minimum, $t_{R,min}$. The enhancement of heat transfer coefficient due to the recycled solids was almost neglected. To asses this contribution, Figure 4.24 shows the values for h_0 and $h_{average}$, on the primary axle, and the heat transfer surface required to remove the appropriate heat flow, in the secondary axle.

In the cases of 50% and 60% O_2, Gs did not change for the two temperature ranges, being 16.8 kg/s m² and 19.4 kg/s m², respectively. To achieve the recycled solids temperature requirement, both parameters, the ratio of solids driven to the EHE and the solids temperature requirement, were adapted. In the 50% O_2 simulation, 40% of solids were cooled down to 498ºC in the EHE, to achieve 750ºC of the total solids flow back into the boiler. In this case, re-carbonation of fly-ashes took place in the first chamber, and fluidizing velocity was doubled to avoid de-fluidization. To keep direct sulfation in the boiler, and so, 855ºC average bed temperature, 45% of solids at 495ºC were mixed with the rest of solids and directed back into the boiler at 700ºC. In this case, as shown in Figure 4.24 heat transfer coefficient increased 26% from the value calculated if no solids crossed the EHE.

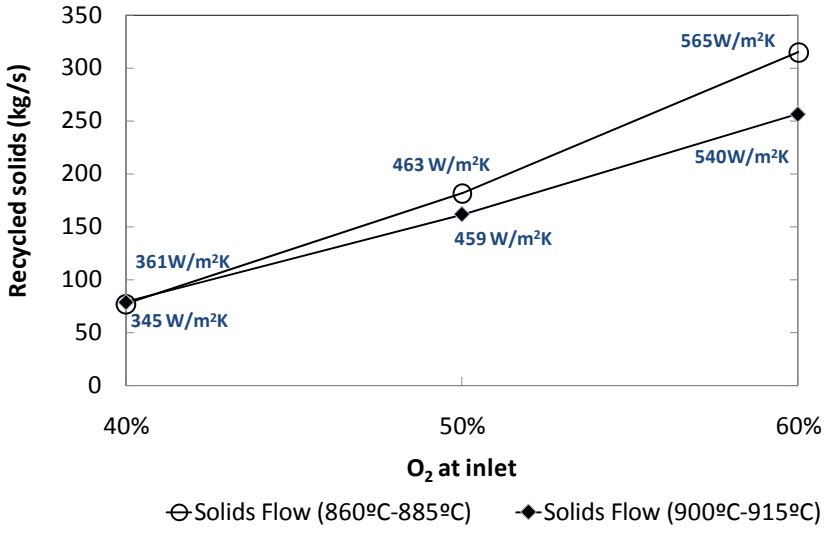

Figure 4.23. Results of recycled solids flow and heat transfer coefficients in the EHE

When inlet gas contained 60% O_2, boiler temperature was kept around 905ºC, reaching indirect sulfation conditions, by cooling 55% of recycled solids down to 442ºC, to reach 700ºC in the total solids recycled flow back into the boiler. This meant an increase of heat transfer up to 45%, compared to the coefficient for 40% O_2, since t_R was then 6 times the $t_{R,min.}$ The first chamber had to increase the fluidizing velocity up to 1.21 m/s, 2.4 times the design velocity of 0.5 m/s, to avoid defluidization. To diminish bed temperature down to 860ºC, 67.5% of solids from the cyclone were cooled down, and so, the total recycled solids back to the boiler were at 650ºC. In spite of this lower bed temperature, calcination took place for this conditions and part of the CaO found adequate carbonation conditions in the second chamber. Fluidizing velocity then was increment 0.86 m/s.

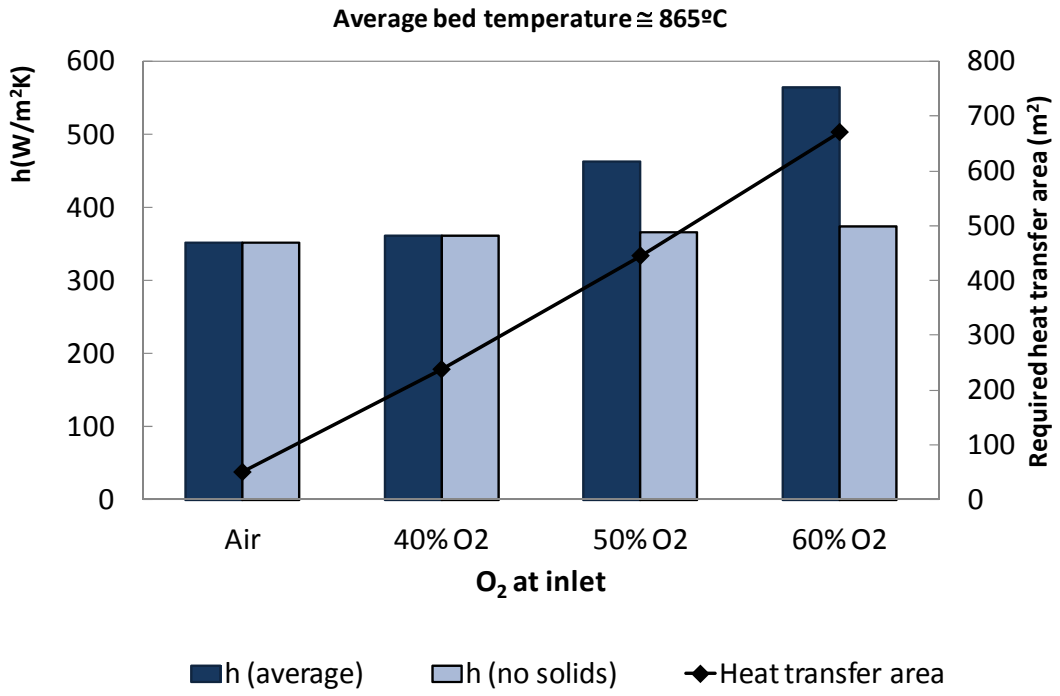

Figure 4.24. Results of heat transfer coefficients with and without recycled solids, and the calculated heat transfer surface required for the proper heat exchange

The required heat transfer surface in air-firing was only 50.3 m^2, one fourth of that needed in 40% O_2 case. In these two cases, the heat transfer coefficients got close values, 351 and 361 W/m^2K, respectively. Aiming to use similar boiler geometry for comparison, solids flow crossing the EHE in the AF case were only 18.8 kg/s, whereas in the 40% O_2 case, they were 76.9 kg/s.

In order to compare the heat transfer coefficients obtained in this work, with those proposed by other authors, in laboratory, or in the real EHE, Figure 4.25 indicates

the values obtained with fully empirical correlations by van Heerden et al. (1953) or Botterill et al. (1984); the semi-empirical approach for tubes bundle by Kim et al. (2003) or the expression deduced from the real EHE operation by Man et al. (2012). They are compared with the values predicted by the present study.

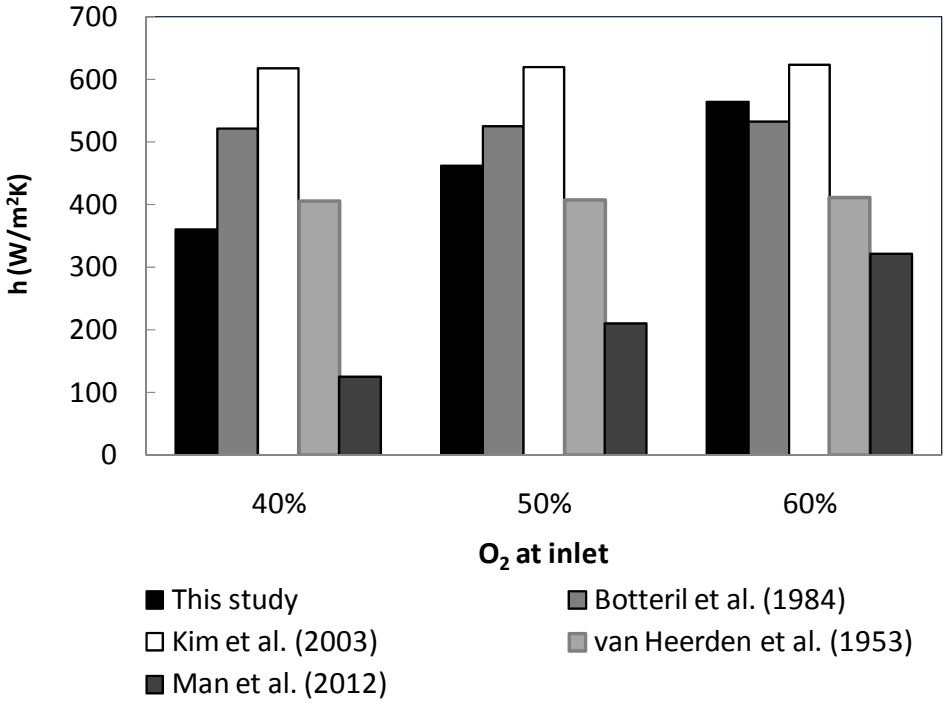

Figure 4.25. Heat transfer coefficients estimated by different authors

The values predicted by this study find within the range of values obtained from the literature. Only the correlation by Man et al. increases considerably, more than 2.5 times, the value at low O_2 concentration. The values obtained by the rest of expressions, varied only 0.2%-0.7% because the changes on the fluidizing gas conditions (density, conductivity and viscosity).

At the beginning of this work, it was highlighted the higher heat that would need to be externally removed in future oxy-fuel fluidized beds. The reason was the higher fuel power combustion and the lower heat transfer surface available inside the boiler. The increase of elutriated solids and the lower temperature, at which these solids will be recycled, allow exchanging more heat in the EHE. Far from being a drawback, according to the simulations results, the higher values of Gs will considerably increase the heat transfer coefficients in the EHE. We obtained increments up to 40% from the case of 40% O_2 at inlet to the case of 60% O_2 at

inlet. Therefore, heat transfer surfaces would be incremented only moderately to reach the higher heat removal requirements. On the other hand, however, the heat transfer surfaces will have to be more carefully located, to take the most advantage of heat exchange, looking at the increasing un-even distribution of local coefficients inside the EHE.

4.6 CONCLUSIONS

The EHE heat transfer surfaces of oxy-fuel CFB boilers were quantified for the first time, by means of a novel correction factor that takes into account the influence of increasing Gs, applied to a EHE simulation integrated into the overall CFB boiler model.

With the aim of obtaining the relation between the non-uniformity of heat transfer in the tubes bundle, and the average heat transfer coefficient in the overall EHE, a set of experiments was carried out in cold model of EHE. We could observe the effects of fluid-dynamics on heat transfer coefficients distribution along the EHE. It was found that the foreseeable increase on solids rate will bring additional drawbacks related to non-uniform fluidization among the sections of an EHE. In the experiments, higher cooling rates were observed when increasing gas velocity and solids flow rate. Up to certain fluidizing velocity, the heat is transferred to the tubes non-uniformly. At different heights of the tubes, the differences were only remarkable for the upper tubes row. In order to extrapolate this local heat transfer coefficients to an average value that can be implemented in a EHE, the obtained values were averaged.

The average heat transfer coefficient was proved to depend on the residence time of warm particles in the EHE. Thus, the heat transfer coefficient when no solids are crossing the EHE is the minimum value. A novel empirical correlation is proposed, to correct the heat transfer coefficient obtained when no solids are moving horizontally.

Thanks to this new expression, the heat transfer coefficient when no recycled solids are present can be modified, for including the enhancing effect of this solids flow. In order to look at the effect of this increase of heat transfer in a real EHE, a detail

model is developed to be integrated into the overall CFB model previously explained.

According to the modeling results, it is possible to reduce the heat transfer surface required for the desired heat exchange, due to the considerable increment heat transfer coefficients when increasing recycled solids in the oxy-fuel case. Further attention must be paid to the proper allocation of tubes bundles, to take better advantage of the trajectory placed by solids traveling along the EHE.

CHAPTER 5

SYNTHESIS, CONTRIBUTIONS AND RECOMMENDATIONS

5.1 SYNTHESIS

In spite of the stabilization of coal demand in developed countries, the role of coal in the next decades energy mix is still essential. Particularly relevant will be in the great developing economies, such as India or China, where this fuel is abundant and avoid external energy dependences. In parallel, the international community needs to drive its efforts towards politics that commit fossil fuels energetic companies to drop their CO_2 emissions drastically for 2015. In this regard, great advances have been made towards gaining plant efficiency and therefore, reducing the tones of CO_2 per produced kWh. Still, emissions need a more drastic reduction if we want to avoid an increment of atmosphere temperature higher than 2ºC. Here, the CO_2 capture and storage (CCS) technologies will have the potential of reducing up to 25% of CO_2 from stationary sources as soon as they will be commercially available.

Among the CO_2 capture technologies, grouping in pre-combustion, post-combustion and oxy-fuel combustion, this last one is receiving outstanding support by the national and European authorities. The possibility of implementing oxy-fuel combustion into circulating fluidized bed technology, contributes to approaching the concept of "clean-coal technology". Fluidized bed combustors have the outstanding feature of offering the possibility of burning a wide variety of fuels They have the possibility to capture SO_2 emissions, adding in-bed limestone. Their working temperature is lower than in pulverized fuel boilers, which avoids thermal NO_x formation. Additionally to these characteristics, already exploited under air-

firing, applying oxy-fuel combustion technology and being able to capture the CO_2 emissions from the coal combustion, or even from blends of coal and other fuels, makes oxy-fuel combustion in fluidized bed a great opportunity to turn the coal sustainable in the future power plant designs.

About the implications derived of applying oxy-fuel technology to a conventional CFB boiler, scarce literature exits, especially when considering high O_2 concentrations at inlet. A one dimensional model has been developed. The overall modeling strategy, in which the model has been based on, is explained in the first part of Chapter 2. It is based on the already known and validated air-firing semi-empirical expressions. The model has been divided into three sub-models interacting with each other: fluid-dynamics, combustion and energy balance of plant.

For attributing reliability to the developed model, the scarce public experimental measurements of real air-firing boilers have been compared with the model results. Additionally, three studies regarding the modeling of large oxy-fuel CFB boilers have also been used for comparing the model predictions. In spite of having insufficient information about the published models details, the model developed in this work fairly fits the predictions in the literature. This has allowed making the sensibility analysis, trying to draw the main consequences of oxy-fuel deployment in CFB boilers.

For retrofitting purposes, i.e. with no changes on an air-firing boiler configuration, the adequate O_2 proportion of oxygen at entrance should be around 30%. Higher O_2 concentrations lead to smaller cross sectional areas of the boiler. For a given fuel power required in a boiler, feeding 45% O_2 in the comburent, would reduce the cross sectional area down to 54% of the original one. This involves a reduction of heat transfer surface along the boiler walls of 23% approximately. The immediate consequence is the need of resorting to external heat transfer surfaces, i.e., external heat exchangers (EHE). This device would need to remove almost 50% of the total heat of combustion in the case of feeding comburent with 60% O_2 content.

The importance of the EHE resides not only in compensating the reduction of heat transfer surface in the riser, but in managing higher amount of elutriated solids. The simulations have shown that higher solids densities in the boiler will enhance heat transfer coefficients to the riser walls. For certain boiler geometry, if

increasing boiler load, higher recycled solids rate will be required. Feeding 60% of O_2 at inlet, fuel input can be increased from 600 to 800 MW if elutriated solids increase from 25 to 40 kg/m^{2}s. This refers us again to the higher solids crossing the EHE. An increase of 10% of heat removal will be required in this device for said changing load.

Applying EHEs to conventional boilers was not essential during air-firing operation. But for oxy-fuel combustion it was here demonstrated to be crucial for accomplishing the boiler energy balance. However, several operational and design uncertainties will need to be solved, before deploying first demonstration oxy-CFB boiler.

The design of the future EHE will imply two relevant distinguishing features of oxy-firing operation: the influence of gas composition on the determination of the heat transfer coefficients and the greater amount of elutriated solids, cooled down in the EHE. The CIRCE bubbling fluidized bed pilot plant presents the adequate bubbling working regime to obtain results of heat transfer coefficient for a wide range of oxy-fuel conditions and extracting further conclusions on possible effects of gas composition on heat transfer coefficients. The range of O_2 concentration at inlet reached values as high as 60%. Such a high concentration was scarcely achieved in pilot plants due, in most cases, to the limiting bed cooling capacity. Measurements of heat transfer coefficients were taken when cooling was needed to control the combustion temperature. Water could circulate through one or more of the four cooling jackets, depending on the cooling requirements. Heat transfer coefficients were indirectly measured by energy balance with the water mass flow and temperatures. There are no previous results on heat transfer measurements under oxy-fuel combustion, up to date.

The pilot plant is characterized by two important performance parameters: the fluidizing velocity and the bed temperature. These two parameters are common for all the fluidized bed plants working on combustion. Particularly for characterizing oxy-fuel combustion, the composition of the oxidant gas is the other key parameter in the plant operation. These three factors have been analyzed and their influence on heat transfer was examined. The three of them are, however, interrelated. O_2 concentration and bed temperature varied the gas density and thus, the fluidizing velocity. At the same time, the fluidizing velocity will affect the heat transfer coefficients and consequently, bed temperature would be influenced. For

accounting for this kind of dependences, non-dimensional numbers have been used for comparison. It was detected no dominant effect of non-dimensional numbers on the heat transfer. This is mainly offset by the different fluidization velocities in AF and OF operation. In the former, u_f was kept over 1 m/s, whereas OF required lower velocities, around 0.9 m/s. It was then determined the adequate semi-empirical correlations for the effective thermal conductivity and the residence time of particles at the heat transfer surface. Hence, a semi-empirical mechanistic approach is recommended for a good agreement with the experimental heat transfer coefficients obtained during oxy-fuel operation. It was demonstrated the relevance of the gaseous film resistance in the oxy-fuel tests, and a new empirical coefficient was deduced for both modes. As examined in Chapter 3, section 3.5, the recommended expressions to predict heat transfer coefficients during oxy-fuel combustion yield:

$$h = h_r + (1-\delta_b)\frac{1}{\frac{1}{h_{packet}} + \frac{1}{h_{film}}}$$

Where:

$$h_{packet} = \ldots$$
$$\ldots\left[\left(k_g\left(\frac{k_s}{k_g}\right)^{0.28-0.757\log\varepsilon-0.057\log\left(\frac{k_s}{k_g}\right)} + 0.1\rho_g C_g d_p u_{mf}\right)\rho_p(1-\varepsilon)c_{p,p}\left(0.7\delta_e\frac{d_b}{\delta_b u_b} + 6.52\delta_b\frac{d_c}{\delta_c u_c}\right)^{-1}\right]^{1/2}$$

$h_{film} = M\frac{k_g}{d_p}$ with M=6.51 for oxy-firing and M=*11.33* for air-firing

The larger amount of solids arriving at the EHE will influence the values and distribution of the average and local heat transfer coefficients, respectively. A review of the difficulties associated with the estimation of heat transfer to the tubes of a heat exchanger has been examined. By the use of a scaled-down EHE, it was possible to experimentally confirm the influence of heat transfer coefficients when horizontal movement of solids took place. The increase of solids rate stressed the inequalities of the local heat transfer coefficient, whereas the longer residence time taken by particles to travel through the EHE allows higher average heat transfer coefficient. The contribution of this parameter to the average heat transfer

coefficient was correlated by means of a new expression, as developed in Chapter 4, section 4.4:

$$H = 2.7324\ \Theta^{-0.322}$$

This expression allows modifying the heat transfer coefficient previously deduced for stationary conditions, and therefore, accounting for the enhancement of heat transfer when recirculation of solids takes place.

A real design of an EHE was then simulated and integrated in the existing CFB model previously developed. This is the first time that such a model is developed to predict the heat transfer area required in oxy-fuel operation. The EHE sub-model must fulfill the energy balance requirements previously set for the CFB model. The temperature, at which solids must be recycled back into the boiler, in order to keep the desired boiler temperature, is accomplished with this sub-model. The expressions for the heat transfer coefficient and the enhancement due to recycled mass flow of solids were included in the EHE sub-model. Hence, it was possible to determine the increase on the heat transfer surface, for different O_2 concentration in the oxidant stream, and two ranges of boiler temperature required. It was then recognized that, in spite of doubling the heat transfer surface requirements, when O_2 concentration increased 10%, the heat transfer surface increases less than expected if solids flow influence were not included in the heat transfer evaluation.

This thesis demonstrates that heat transfer surface design, arrangement and allocation, will differ in future oxy-fuel CFB boilers. Particularly, the heat transfer in the EHE will need address the influence of fluidizing gas composition and recycled solids, for an adequate and efficient heat exchanger configuration.

5.2 CONTRIBUTIONS

This thesis aimed to demonstrate that heat transfer surfaces design in oxy-fuel CFB boilers will have to be revised and adapted to the new mode of operation. Thus, the specific contributions are following summarized:

Chapter 2

- The contribution of this chapter is the oxy-fuel large-scale CFB model. The original simulation developed in this chapter has been based on the semi-

empirical expressions already validated for air-firing combustion. The estimations drawn from the model have been compared with air-firing CFB boilers data first, and with three oxy-fuel CFB models available in the literature.

- The heat share of heat removal in the overall CFB loop has been quantified, for the three parts of the heat balance of the plant: the boiler walls, the convection pass and the external heat exchanger. The heat transfer shares have been simulated for different O_2 concentrations at inlet and varying the boiler cross sectional area. It was also run for three different fuel loads, adapting the secondary air and the fluidizing velocity to the elutriated solids requirements; and modifying the temperature at which solids are recycled back into the boiler. The results of this study were published in Bolea et al. (2012b)
- It was here proposed the two key differences between the EHE of an air-firing and oxy-firing CFB boilers, that will influence heat transfer coefficient in the future EHEs: the fluidizing gas composition and the influence of increasing recycled solids rate

Chapter 3

- An original theoretical analysis of heat transfer during oxy-fuel in fluidized beds, was first carried out, considering the different models available in the literature for the air-firing case and assessing the potential influences of oxy-fuel combustion predicted by these approaches.
- In this chapter the heat transfer coefficients measured during oxy-fuel in the bubbling fluidized bed combustor in CIRCE are presented. As a relevant remark, the O_2 concentration in the oxidant stream ranged up to 60%. This high value is uncommonly found in the literature, and it requires a great cooling flexibility. This is the first time that heat transfer coefficients are quantified during oxy-fuel operation. Part of this analysis was included in the book *Oxygen-Enhanced Combustion* (Baukal Jr., 2013).
- The wide range of operational conditions allowed to compare the obtained heat transfer coefficients with the different non-dimensional numbers that accounts for the gas composition, gas properties, bed temperature and fluidizing velocity.

- The experimental results during air and oxy-firing operation were further treated in order to propose an appropriate approach that can predict the heat transfer coefficients to the walls during oxy-fuel combustion. The packet renewal model is recommended. The film thermal resistance was revealed as the differentiate term between air and oxy-firing heat transfer expressions. The empirical value for the film thermal resistance is proposed for both, air and oxy-firing modes.

Chapter 4

- A theoretically review of the literature on cold models and real EHE intended forecast the influence of increasing recycled solids on heat transfer. The existing cold model experiments of EHE did not account for a drastic increase of the solids flow rate, as it will be expected in EHE of large oxy-fuel CFB boilers, whereas the available data of real EHE exhibits a clear influence of Gs on heat transfer coefficients.
- A tests campaign was carried out in a cold EHE model, de-attached from the rest of the cold CFB loop and local heat transfer coefficients were measured in different tubes location. It was confirmed that uniformity of fluidization is lost when solids crossing the EHE are increase.
- The average heat transfer coefficient was related to the time that particles take to cross the EHE. Together with data from the literature, a new correlation to account for this contribution was deduced.
- An original EHE simulation was developed, for being integrated on the overall CFB simulation. The expressions for heat transfer prediction, previously deduced experimentally were implemented. The risk of EHE de-fluidization, for different O_2 concentration cases was also included in the EHE sub-model. This allowed quantifying the increments of heat transfer surfaces that will be needed in future EHE designs. These increments were moderated by the enhance of heat transfer coefficients, due to the solids recirculation.

5.3 RECOMMENDATIONS AND FURTHER WORK

This work aims to be an impulse towards the near term deployment of second generation of oxy-fuel CFB boilers. The large oxy-fuel CFB boiler model here developed must be the basis to accurately predict the changes in the heat transfer surfaces inside the boiler itself. To achieve this level of detail, an additional dimension in the model will be recommendable, also to account for the extended heat transfer surfaces, so as the hanging wing walls. The lately proposed combustion model of fuel particles in fluidized beds (Guedea et al., 2013) could be included to get a more precise allocation of the energy release cells. Additionally, the attrition phenomena that influence the sulfation reactions (Scala and Salatino, 2010) will have to be integrated into the model, to improving the contribution estimation of sulfation-calcination reaction into the boiler energy balance, and to further assess the influence on the re-carbonation reactions in the EHE.

The proper emplacement of heat transfer surfaces in the oxy-fuel CFB boilers and in their EHE devices will be one of the key issues to optimize the energy penalties associated to CO_2 capture technologies. The maximum efficiency of the boiler will reside on the proper steam circuit design for the new heat transfer areas configuration. This will contribute to the overall plant efficiency that would mean the turning point to allow oxy-fuel becoming commercially feasible. The O2GEN European Project aims to diminish the overall energy penalty of the oxy-fuel system to the half of the current state of the art. This will mean a joint effort between minimizing the electricity consumption by the Air Separations Unit; the integration of the CO_2 compression train with the whole system; and optimizing the boiler performance, from the basis of the study developed here.

In this work, it has been recognized the uncertainties associated to the appropriate way of estimating heat transfer coefficients and, additionally, the variation of the heat transfer coefficient with the location of the tubes, due to non-uniformities of fluidization in some areas of the EHE. It is urgent to solve this problem, developing a methodology to properly place the heat transfer tubes in the tubes bundles, although construction symmetry could be loose. The heat transfer coefficient will be influenced by the fluidizing gas composition as confirmed in this thesis and further experiments should be carried out similar to the ones run in CIRCE BFB, but with finer particle diameter, for resembling the conditions of the EHE. Additionally,

including horizontal immersed surfaces would be desirable, to ascertain the influence of the change of fluidynamics, affected by changes in the fluidizing gas composition.

Regarding the potential problems involved with the EHE device, when fluidized with RFG, it will be an essential issue to account for the potential corrosion problems derived from the presence of corrosive or acid substances in the fluidizing gas. This will lead to material corrosion issues and also to fouling of products of reactions with the bed material and elutriated solids. To acquire feasible results, experimentation must be carried out in oxy-fuel combustion with flue gas desulfurization, since the pollutant content in the diluting stream, will actively participate in the deposition and fouling, so as in the acid corrosion reactions.

5.4 PUBLICATIONS

The diffusion of some of the results was carried out by means of publication in papers in journals and conferences. The publications related to the performance of the present thesis are presented, from the results from the CFB modeling, to the results from the experiments carried out in the oxy-fuel fluidized bed pilot plant. Afterwards, they are also indicated some publications not related to oxy-fuel combustion, but with CO_2 capture and power plant integration.

International journal articles:

1. ***Bolea, I.**, L. M. Romeo and D. Pallarés (2012). The role of external heat exchangers in oxy-fuel circulating fluidized bed. Applied Energy 94(0): 215-223.*

   In this paper a large scale oxy-fuel circulating fluidized bed boiler has been modeled, in collaboration with Chalmers University. The main results of the sensitivity analysis were explained. This article is based on the Chapter 2 of the current thesis
2. *Romeo, L. M., L. I. Díez, I. Guedea, **I. Bolea**, C. Lupiáñez, A. González, J. Pallarés and E. Teruel (2011). Design and operation assessment of an oxyfuel fluidized bed combustor. Experimental Thermal and Fluid Science 35(3): 477-484.*

   In this paper the work carried out for the design and the operation of the oxy-fuel pilot plant, carried out by the whole oxy-fuel research team is

explained. Results of the oxy-fuel combustion of biomass and coal blends are shown. Section 3.3.2 is included in this article.

3. *Font, O., P. Córdoba, C. Leiva, L. M. Romeo,* ***I. Bolea****, I. Guedea, N. Moreno, X. Querol, C. Fernandez and L. I. Díez (2012). Fate and abatement of mercury and other trace elements in a coal fluidised bed oxy combustion pilot plant. Fuel 95(0): 272-281*

   In this article, the longest oxy-fuel tests were needed for the feasible samples gathering of ashes in the bed, cyclone and bag filter. Main trace elements, including mercury, were measured in collaboration with Institute of Environmental Assessment and Water Research (IDÆA-CSIC). Part of the measurements of heat transfer coefficients were obtained during the tests explained here.

4. *Ordorica-Garcia, G., M. Carbo****, I. Bolea*** *and M. Nikoo (2012). Technology Options and Integration Concepts for Implementing CO_2 Capture in Oil Sands Operations. Journal of Canadian Petroleum Technology* 51(5): 362-375.

   This was a joint collaboration between institutions from Canada, The Netherlands and Spain, aiming to look for the most suitable CO_2 capture technology integrated in any of the phases of the oil sands operations. The oxy-fuel state of the art in this paper is based on the Chapter 1 of this thesis.

5. *Lupiáñez, C., I. Guedea,* ***I. Bolea,*** *L. I. Díez, and L. M. Romeo, (2013). "Experimental study of SO_2 and NO_x emissions in fluidized bed oxy-fuel combustion." Fuel Processing Technology 106(0): 587-594.*

   This article analyzed the SO_2 and NO_x emissions during air and oxy-firing modes, for two different types of coal and blends of them. Several tests explained in this paper, were also used for the heat transfer measurements

During the last years, in parallel to the research carried out for the development of this thesis, the following papers were also published in international journals, related to the integration of CO_2 capture technologies in the overall power plant process:

6. Romeo, L. M., **I. Bolea** and J. M. Escosa (2008). Integration of power plant and amine scrubbing to reduce CO_2 capture costs. Applied Thermal Engineering 28(8–9): 1039-1046.

7. Romeo, L. M., S. Espatolero and **I. Bolea** (2008). Designing a supercritical steam cycle to integrate the energy requirements of CO_2 amine scrubbing. International Journal of Greenhouse Gas Control 2(4): 563-570.
8. Romeo, L. M., **I. Bolea**, Y. Lara and J. M. Escosa (2009). Optimization of intercooling compression in CO_2 capture systems. Applied Thermal Engineering 29(8–9): 1744-1751.
9. **Bolea, I.**, J. Uche and L. M. Romeo (2009). Integration of MED with captured CO_2 flue gas compression. Desalination and Water Treatment 7(1-3): 124-131.
10. Sanpasertparnich, T., R. Idem, **I. Bolea**, D. de Montigny and P. Tontiwachwuthikul (2010). Integration of post-combustion capture and storage into a pulverized coal-fired power plant. International Journal of Greenhouse Gas Control 4(3): 499-510

Conference proceedings involving oxy-fuel in fluidized bed:

A. Romeo, L. M., I. Guedea, **I. Bolea**, A. González, C. Lupiáñez, J. Pallares and L. I. Diez (2009). First Results in an Oxyfuel Combustion Fluidized Bed. 1st Oxyfuel Combustion Conference. Cottbus, Germany.
B. Guedea, I., **I. Bolea**, C. Lupiáñez, N. Cortés, E. Teruel, J. Pallarés, L. I. Díez and L. M. Romeo (2011). Control system for an oxy-fuel combustion fluidized bed with flue gas recirculation. Energy Procedia 4(0): 972-979.
C. Lupiáñez, C., I. Guedea, **I. Bolea**, J. Pallarés, L. I. Díez and L. M. Romeo (2011). Oxy-firing of high sulphur coal in CIRCE fluidized bed pilot plant. 5th International Conference on Clean Coal Technologies. Zaragoza, Spain.
D. Font, O., P. Córdoba, C. Leiva, L. M. Romeo, **I. Bolea**, I. Guedea, N. Moreno, X. Querol, C. Fernandez-Pereira and L. I. Díez (2011). Speciation and fate of mercury in oxy coal combustion. International Conference on Coal Science and Technology Oviedo, Spain.
E. **Bolea, I.,** C. Lupiáñez, I. Guedea, L. M. Romeo and L. I. Díez (2012). Direct Sulfation in oxy-fuel fluidzied bed boilers. 21st International Conference on Fluidized Bed Combustion, Naples, Italy.

Book contributions:

A. Romeo, L. M., L. I. Díez, P. Lisbona, A. González, I. Guedea, C. Lupiáñez, A. Martínez, Y. Lara and **I. Bolea** (2010). Captura y almacenamiento de CO_2. Zaragoza, Prensas Universitarias de Zaragoza.
B. Jia, L., Romeo, L. M., Díez, L. I., Guedea, I., **Bolea, I**. and Lupiañez, C. (2013). Oxy-fuel Fluidized Bed Combustion. In *Oxygen-Enhanced Combustion*, CRC Press. Taylor and Fracis: 649-674.

REFERENCES

Abdulally, I. F. and Randolph, N. J. (1989). *Fluidized Bed Steam Generation System And Method having an External Heat Exchanger*. Patent, U. S., Foster Wheeler Energy Corporation.

Adánez, J. and Diego, L. F. d. (1995). *Modeling of Carbon Combustion Efficiency in Circulating Fluidized Bed Combustors. 1. Selection of Submodels and Sensitivity Analysis*. Industrial & Engineering Chemistry Research 34(9): 3129-3138.

Adanez, J., Gayán, P., Grasa, G., de Diego, L. F., Armesto, L. and Cabanillas, A. (2001). *Circulating fluidized bed combustion in the turbulent regime: modelling of carbon combustion efficiency and sulphur retention*. Fuel 80(10): 1405-1414.

Aibéo, A. and Pinho, C. (2003). *Heat transfer Modelling in a Circulating Fluidised Bed Biomass Boiler*. International Conference of Renewable Energies and Power Quality. Vigo, Spain.

Al-Busoul, M. A. and Abu-Ein, S. K. (2003). *Local heat transfer coefficients around a horizontal heated tube immersed in a gas fluidized bed*. Heat and Mass Transfer 39(4): 355-358.

Alagöz, E. (2006). *Mathematical modeling of fluidized bed combustors with radiation model*, Middel East Technical University. Master of Science.

Alvarez, I., Muñoz, F., Lupion, M., Otero, P., Hotta, A., Kuivalainen, R. and Alvarez, J. (2011). *CIUDEN CFB boiler technological development*. 2nd Oxyfuel Combustion Conference. Queensland, Australia

Andersson, B.-Å. (1988). *Heat transfer in stationary fluidized bed boilers. PhD Thesis*. Chalmers University of Technology.

Andersson, B.-Å. and Leckner, B. (1992). *Experimental methods of estimating heat transfer in circulating fluidized bed boilers*. International Journal of Heat and Mass Transfer 35(12): 3353-3362.

Andersson, B. Å. (1996). *Effects of bed particle size on heat transfer in circulating fluidized bed boilers*. Powder Technology 87(3): 239-248.

Andersson, K. and Johnsson, F. (2006). *Flame and radiation characteristics of gas-fired O2/CO2 combustion*. Fuel 86(5-6): 656-668.

Anheden, M., Yan, J. and De Smedt, G. (2005). *Denitrogenation (or Oxyfuel Concepts)*. Oil & Gas Science and Technology 60(3): 485-495.

Arena, U., Chirone, R., D'Amore, M., Miccio, M. and Salatino, P. (1995). *Some issues in modelling bubbling and circulating fluidized-bed coal combustors*. Powder Technology 82(3): 301-316.

Barbucci, P. (2009). *CO_2 Capture and Storage- An utility view*. 3rd International Symposium on Capture and geological storage of CO2, Paris, France.

Baskakov, A. P. (1964). *The mechanism of heat transfer between a fluidized bed and a surface*. International Chemical Engineering 4(2): 320-323.

Baskakov, A. P. and Leckner, B. (1997). *Radiative heat transfer in circulating fluidized bed furnaces*. Powder Technology 90(3): 213-218.

Basu, P. (1999). *Combustion of coal in circulating fluidized-bed boilers: a review*. Chemical Engineering Science 54(22): 5547-5557.

Basu, P. (2006). *Combustion and gasification in fluidized beds*, Taylor & Francis.

Basu, P. and Nag, P. K. (1996). *Heat transfer to walls of a circulating fluidized-bed furnace*. Chemical Engineering Science 51(1): 1-26.

Baukal, C. E. (2000). *Heat transfer in industrial combusiton*, CRC Press LLC.

Baukal Jr., C. E. (2013). *Oxygen-Enhanced Combustion*, CRC Press. Taylor and Fracis.

Becher, V. (2008). *Controlled Staging with Non-Stoichiometric Burners for Oxyfuel Processes-Experimental Validation*. 2nd Young Researchers Forum on Oxyfuel Combustion, Gotheborg, Sweden.

Bolea, I., Lupiáñez, C., Guedea, I., Romeo, L. M. and Díez, L. I. (2012a). *Direct Sulfation in oxy-fuel fluidzied bed boilers*. 21st International Conference on Fluidized Bed Combustion, Naples, Italy.

Bolea, I., Romeo, L. M. and Pallarés, D. (2012b). *The role of external heat exchangers in oxy-fuel circulating fluidized bed*. Applied Energy 94(0): 215-223.

Botterill, J. S. M. (1989). *Fluidized Bed Heat Transfer*. Combustión en Lechos Fluidizados. COMETT, CEE, Zaragoza, Spain.

Botterill, J. S. M., Teoman, Y. and Yüregir, K. R. (1984). *Factors affecting heat transfer between gas-fluidized beds and immersed surfaces*. Powder Technology 39(2): 177-189.

BP (2011a). *BP Energy Outlook 2030*.

BP (2011b). *BP Statistical Review of World Energy*.

Breitholtz, C. and Leckner, B. (1997). *Heat balance over the fluid-dynamic boundary layer of a circulating fluidized bed furnace*. International Journal of Heat and Mass Transfer 41(8-9): 1013-1024.

Breitholtz, C., Leckner, B. and Baskakov, A. P. (2001). *Wall average heat transfer in CFB boilers*. Powder Technology 120(1-2): 41-48.

Breitholtz., C. and B., L. (2000). *Translation of heat transfer measurements from laboratory CFBs to the conditions of CFB-boilers*. IV Minsk International Forum on Heat and Mass Transfer, Minsk, Belarus.

Buhre, B. J. P., Elliott, L. K., Sheng, C. D., Gupta, R. P. and Wall, T. F. (2005). *Oxy-fuel combustion technology for coal-fired power generation*. Progress in Energy and Combustion Science 31(4): 283-307.

Burchhardt, U. (2009). *Experiences from Commissioning and Test Operation of Vattenfall's Oxyfuel Pilot Plant*. 1st Oxyfuel Combustion Conference, Cottbus, Germany.

Burnard, H. and Bhattacharya, S. (2011). *Power Generation from Coal. Ongoing Developments and Outlook*, International Energy Angency.

Coleman, H. W. and Steele, W. G. (1999). *Experimentation and Uncertanity Analysis for Engineers*, John Wiley & Sons, Inc.

Croiset, E. and Thambimuthu, K. V. (2001). *NOx and SO_2 emissions from O_2/CO_2 recycle coal combustion*. Fuel 80(14): 2117-2121.

Czakiert, T. (2011). *Personal communication*.

Czakiert, T., Bis, Z., Muskala, W. and Nowak, W. (2006). *Fuel conversion from oxy-fuel combustion in a circulating fluidized bed*. Fuel Processing Technology 87(6): 531-538.

Czakiert, T., Sztekler, K., Karski, S., Markiewicz, D. and Nowak, W. (2010). *Oxy-fuel circulating fluidized bed combustion in a small pilot-scale test rig*. Fuel Processing Technology 91(11): 1617-1623.

Chen, J. C. (2003). *Surface Contact---Its Significance for Multiphase Heat Transfer: Diverse Examples*. Journal of Heat Transfer. Max Jakob award lecture 125(4): 549-566.

Chen, J. C., Grace, J. R. and Golriz, M. R. (2005). *Heat transfer in fluidized beds: design methods*. Powder Technology 150(2): 123-132.

Chen, T.-P. and Saxena, S. C. (1977). *Mathematical modelling of coal combustion in fluidized beds with sulphur emission control by limestone or dolomite*. Fuel 65: 401-413.

Chen, Y. and Xiaolong, G. (2006). *Dynamic modeling and simulation of a 410 t/h Pyroflow CFB boiler*. Computers & Chemical Engineering 31(1): 21-31.

Cheng, L., Wang, Q., Shi, Z., Luo, Z., Ni, M. and Cen, K. (2007). *Heat transfer in a large-scale circulating fluidized bed boiler*. Energy Power Eng. China 1(4): 477–482.

Daki, D., Honing, G. v. d. and Valk, M. (1989). *Fragmentation and swelling of various coals during devolatilization in a fluidized bed*. Fuel 68: 911-916.

Davidson, J. F. (2000). *Circulating fluidised bed hydrodynamics*. Powder Technology 113(3): 249-260.

Davidson, J. F., Clift, R. and Harrison, D. (1985). *Fluidization*. London, Academic Press Inc.

de Diego, L. F., de las Obras-Loscertales, M., García-Labiano, F., Rufas, A., Abad, A., Gayán, P. and Adánez, J. (2011). *Characterization of a limestone in a batch fluidized bed reactor for sulfur retention under oxy-fuel operating conditions*. International Journal of Greenhouse Gas Control 5(5): 1190-1198.

de Diego, L. F., Rufas, A., García-Labiano, F., de las Obras-Loscertales, M., Abad, A., Gayán, P. and Adánez, J. (2012). *Optimum temperature for sulphur retention in fluidised beds working under oxy-fuel combustion conditions. In press*. Fuel(0).

de Souza-Santos, M. L. (2007). *A new version of CSFB, comprehensive simulator for fluidised bed equipment*. Fuel 86(12-13): 1684-1709.

Decker, N. and Glicksman, L. R. (1983). *Heat transfer in large particle fluidized beds*. International Journal of Heat and Mass Transfer 26(9): 1307-1320.

Di Natale, F., Lancia, A. and Nigro, R. (2008). *A single particle model for surface-to-bed heat transfer in fluidized beds*. Powder Technology 187(1): 68-78.

Diego, L. F. d., Londonot, C. A., Wang, X. S. and Gibbs, B. M. (1996). *Influence of operating parameters on NOx and N20 axial profiles in a circulating fluidized bed combustor*. Fuel 75(8): 971-978.

Dow, W. M. and Jakob, M. (1951). *Heat transfer between a verticl tube and a fluidized air-solid flow*. Chemical Engineering Progress 58: 637-648.

Duan, L., Zhao, C., Zhou, W., Qu, C. and Chen, X. (2011a). *Effects of operation parameters on NO emission in an oxy-fired CFB combustor*. Fuel Processing Technology 92(3): 379-384.

Duan, L., Zhao, C., Zhou, W., Qu, C. and Chen, X. (2011b). *O2/CO2 coal combustion characteristics in a 50 kWth circulating fluidized bed*. International Journal of Greenhouse Gas Control 5(4): 770-776.

Eddings, E. G., Okerlund, R. and Bool, L. E. (2009). *Pilot-scale evaluation of oxycoal firing in circulating fluidized bed and pulverized coal-fired test facilities*. 1st Oxyfuel Combustion Conference. Cottbus, Germany.

EIA (2011). *International Energy Outlook 2011. U.S. Energy Information Administration*.

Ergun, S. and Orning, A. A. (1949). *Flow through randomly packed columns and fluidized beds*. Fluid Industrial & Engineering Chemistry 41: 1179–1184.

Eriksson, M. and Golriz, M. R. (2005). *Radiation heat transfer in circulating fluidized bed combustors*. International Journal of Thermal Sciences 44(4): 399-409.

ExxonMobil (2012). *2012 The Outlook for Energy: A view to 2040*.

García-Labiano, F., Abad, L. F., de Diego, L. F., Gayán, P. and Adánez, J. (2002). *Calcination of calcium-based sorbents at pressure in a broad range of CO2 concentrations*. Chemical Engineering Science 57: 2381-2393.

García-Labiano, F., Rufas, A., de Diego, L. F., Obras-Loscertales, M. d. l., Gayán, P., Abad, A. and Adánez, J. (2011). *Calcium-based sorbents behaviour during sulphation at oxy-fuel fluidised bed combustion conditions*. Fuel 90(10): 3100-3108.

Gayan, P., Adanez, J., de Diego, L. F., García-Labiano, F., Cabanillas, A., Bahillo, A., Aho, M. and Veijonen, K. (2004). *Circulating fluidised bed co-combustion of coal and biomass*. Fuel 83(3): 277-286.

Glicksman, L. R. (2007). *Radiation Heat Transfer in Circulating Fluidized Beds*. The 12th International Conference on Fluidization - New Horizons in Fluidization Engineering, Vancouver, Canada.

Glicksman, L. R. and Decker, N. (1982). *Heat transfer from an immersed surface to adjacent particles in a fluidized bed; the role of radiation and particle packing*. 7th International Heat Transfer Conference, München, Germany.

Grace, J. R., Avidan, A. A. and Knowlton, T. M. (1997). *Circulating fluidized beds*, Blackie Academic and Professional.

Grewal, N. S. (1981). *A Generalized Correlation for Heat Transfer Between a Gas-Solid Fluidized Bed of Small Particles and an Immersed Staggered Array of Horizontal Tubes*. Powder Technology 30: 145-154.

Grewal, N. S. and Saxena, S. C. (1981). *Maximum heat transfer coefficient between a horizontal tube and a gas-solid fluidized bed*. Industrial & Engineering Chemistry Process Design and Development 20(1): 108-116.

Guedea, I., Díez, L. I., Pallarés, J. and Romeo, L. M. (2011). *Influence of O2/CO2 mixtures on the fluid-dynamics of an oxy-fired fluidized bed reactor*. Chemical Engineering Journal 178(0): 129-137.

Guedea, I., Pallarès, D., Díez, L. I. and Johnsson, F. (2013). *Conversion of large coal particles under O2/N2 and O2/CO2 atmospheres - Experiments and modeling*. Fuel Processing Technology 112: 118-128.

Gungor, A. (2009). *One dimensional numerical simulation of small scale CFB combustors*. Energy Conversion and Management 50(3): 711-722.

Gungor, A. and Eskin, N. (2008). *Two-dimensional coal combustion modeling of CFB*. International Journal of Thermal Sciences 47(2): 157-174.

Hack, H. and Shah, M. (2008). *Oxy-fuel Coal-Fired Combustion Power Plant System Integration*. 3rd International Oxy-Combustion Network Meeting, Yokohama, Japan.

Hamidipour, M., Mostoufi, N., Sotudeh-Gharebagh, R. and Chaouki, J. (2005). *Experimental investigation of particle contact time at the wall of gas fluidized beds*. Chemical Engineering Science 60(15): 4349-4357.

Hannaes, J., Renz, U. and van den Bleek, C. M. (1995). *The IEA model for circulating fluidized bed combustion*. 3th International Conference on Fluidized Bed Combustion. Henschel, K. J. 1: 287-296.

Harris, A. T., Thorpe, R. B. and Davidson, J. F. (2002). *Characterisation of the annular lm thickness in circulating fluidised-bed risers*. Chemical Engineering Science 57: 2579-2587.

Hartge, E.-U., Klett, C. and Werther, J. (2007). *Dynamic simulation of the particle size distribution in a circulating fluidized bed combustor*. Chemical Engineering Science 62(1-2): 281-293.

Hayhurst, A. N. and Lawrence, A. D. (1996). *The Amounts of NO, and N,O Formed in a Fluidized Bed Combustor during the Burning of Coal Volatiles and Also of Char*. Combustion and Flame 105: 341-357.

Heikkinen, M., Hiltunen, T., Liukkonen, M., Kettunen, A., Kuivalainen, R. and Hiltunen, Y. (2009). *A modelling and optimization system for fluidized bed power plants*. Expert Systems with Applications 36(7): 10274-10279.

Horio, M. (1997). *Hydrodynamics*. Circulating Fluidized Beds. Blackie Academic and Professional.

Howard, J. R. (1989). *Fluidized Bed Technology: principles and applications*, Taylor & Francis.

Hu, G., Dam-Johansen, K., Wedel, S. and Peter Hansen, J. (2006). *Review of the direct sulfation reaction of limestone*. Progress in Energy and Combustion Science 32(4): 386-407.

Huilin, L., Guangbo, Z., Rushan, B., Yongjin, C. and Gidaspow, D. (2000). *A coal combustion model for circulating fluidized bed boilers*. Fuel 79(2): 165-172.

Hyytiäinen, I., Mahlamäki, A., Palonen, M., Varonen, M. and Lemmetyinen, H. (2011). *Study of recarbonation in circulating fluidized bed combustion*. 10th International Conference on Circulating Fluidized Beds and Fluidization Technology. Rusnrive, Oregon, USA.

IEA (2010a). *Energy Technology Perspectives. Scenarios and Strategies to 2050. Executive Summary*.

IEA (2010b). *Power generation from coal. Measuring and reporting efficiency Performance and CO2 emissions*.

IEA (2011a). *CO2 emissions from fuel combustion. Hihlights*.

IEA (2011b). *World Energy Outlook 2011*.

IEA (2011c). *World Energy Outlook 2011. Resumen Ejecutivo*.

IPCC (2005). *Special Report Carbon Dioxide Capture and Storage*.

IPCC (2007). *Fourth Assessment Report: Climate Change*

IPCC (2010). *Understanding Climate Change. 22 years of IPCC assessment*.

Jäntti, T., Eriksson, T., Hotta, A., Hyppänen, T. and Nuortimo, K. (2007). *CFB Technology- Toward Zero CO_2 Emissions*. Varkaus, Finland.

Jia, L., Tan, Y. and Anthony, E. J. (2010). *Emissions of SO2 and NOx during Oxy-Fuel CFB Combustion Tests in a Mini-Circulating Fluidized Bed Combustion Reactor*. Energy Fuels 24(2): 910-915.

Jia, L., Tan, Y., Wang, C. and E.J., A. (2007). *Experimental Study of Oxy-Fuel Combustion and Sulfur Capture in a Mini-CFBC*. Energy & Fuels 21: 3160-3164.

Johansson, A., Johnsson, F. and Andersson, B.-A. (2006). *The Performance of a Loop Seal in a CFB Boiler*. Journal of Energy Resources Technology 128(2): 135-142.

Johansson, A., Johnsson, F. and Leckner, B. (2007). *Solids back-mixing in CFB boilers*. Chemical Engineering Science 62(1-2): 561-573.

Johnsson, F. (2010). *Oxyfuel CFB Combustion – discussion on challenges for development*. 60th IEA-FBC Meeting Göteborg, Sweden.

Johnsson, F. and Leckner, B. (1995). *Vertical distribution of solids in a CFB-furnace* 13th International Conference on Fluidized Bed Combustion. Orlando, Florida, USA.

Jordal, K., Anheden, M., Yan, J. and Strömberg, L. (2004). *Oxyfuel combustion for coal-fired power generation with CO_2 capture- Opportunities and challenges* 7th Internationa Conference on Greenhouse Gas Technologies, Vancouver, Canada.

Kather, A. (2007). *Oxy-fuel Process for Hard Coal with CO_2 Capture. A part of the ADECOS Project*. 2nd Workshop of the International Oxy-Combustion Research Network., Windsor CT, USA.

Kiga, T., Takano, S., Kimura, N., Omata, K., Okawa, M., Mori, T. and Kato, M. (1997). *Characteristics of pulverized-coal combustion in the system of oxygen/recycled flue gas combustion*. Energy Conversion and Management 38(Supplement 1): S129-S134.

Kim, S. W., Ahn, J. Y., Kim, S. D. and Hyun Lee, D. (2003). *Heat transfer and bubble characteristics in a fluidized bed with immersed horizontal tube bundle*. International Journal of Heat and Mass Transfer 46(3): 399-409.

Kim, S. W., Namkung, W. and Kim, S. D. (2001). *Solid Recycle Characteristics of Loop-seals in a Circulating Fluidized Bed*. Chemical Engineering Technology 24(8): 843-849.

Kohl, A. L. and Nielsen, R. D. (1997). *Gas Purification*, Gulf Professional Publishing.

Koornneef, J., Junginger, M. and Faaij, A. (2007). *Development of fluidized bed combustion--An overview of trends, performance and cost*. Progress in Energy and Combustion Science 33(1): 19-55.

Krzywanski, J., Czakiert, T., Muskala, W., Sekret, R. and Nowak, W. (2010a). *Modeling of solid fuel combustion in oxygen-enriched atmosphere in circulating fluidized bed boiler: Part 2. Numerical simulations of heat transfer and gaseous pollutant emissions associated with coal combustion in O2/CO2 and O2/N2 atmospheres enriched with oxygen under circulating fluidized bed conditions*. Fuel Processing Technology 91(3): 364-368.

Krzywanski, J., Czakiert, T., Muskala, W., Sekret, R. and Nowak, W. (2010b). *Modeling of solid fuels combustion in oxygen-enriched atmosphere in circulating fluidized bed boiler: Part 1. The mathematical model of fuel combustion in oxygen-enriched CFB environment*. Fuel Processing Technology 91(3): 290-295.

Kunii, D. and Levenspiel, O. (1991). *Fluidization Engineering*, Blutterworth-Heinemann.

Kurosaki, Y., Satoh, I. and Ishize, T. (1995). *Mechanisms of Heat Transfer Enhancement of Gas-Solid Fluidized Bed: Estimation of Direct Contact Heat Exchange From Heat Transfer Surface to Fluidized Particles Using an Optical Visualization Technique*. Journal of Heat Transfer 117(1): 104-112.

Kyungtae, P., Ikhyun, K., Namjin, J., Moongoo, J., Yukyung, L. and En Sup, Y. (2011). *Cost of energy analysis of integrated gasification combined cycle (IGCC) power plant with respect to CO_2 capture ratio under climate change scenarios*. Advanced Control of Industrial Processes (ADCONIP), 2011 International Symposium on.

Leckner, B. (1997). *Fluidized bed combustion: Mixing and pollutant limitation*. Progress in Energy and Combustion Science 24: 31-61.

Lee, D. K., Noh, D. S., Choi, K. B., Seo, D. M., Ko, C. B. and Lee, E. K. (2009). *Development of 0.1MW class Oxy-PC Swirl Burner with Primary O_2 Direct-injection*. 1st Oxyfuel Combustion Conference, Cottbus, Germany.

Lee, J.-M. and Kim, J.-S. (1999). *Simulation of the 200 MWe Tonghae thermal power plant circulating fluidized bed combustor by using IEA-CFBC model*. Korean Journal of Chemical Engineering 16(5): 640-645.

Levenspiel, O. and Walton, J. S. (1954). *Bed wall heat transfer in fluidized systems*. Chemical Engineering Progress Symposium Series 50(9): 1-9.

Lindsay, A. L. and Bromley, L. A. (1950). *Thermal Conductivity of Gas Mixtures*. Industrial & Engineering Chemistry 42(8): 1508-1511.

Liu, H., Katagiri, S., Kaneko, U. and Okazaki, K. (2000). *Sulfation behavior of limestone under high CO2 concentration in O2/CO2 coal combustion*. Fuel 79: 945-953.

Lu, J., Lu, X., Liu, H., Wang, H. and He, H. (2010). *Calculation and analysis of dissipation heat loss in large-scale circulating fluidized bed boilers*. Applied Thermal Engineering 30(13): 1839-1844.

Lu, J. D., Flamant, G. and Snabre, P. (1993). *Towards a generalized model for vertical walls to gas--solid fluidized beds heat transfer--I. Particle convection and gas convection*. Chemical Engineering Science 48(13): 2479-2492.

Luan, W., Bowen, B. D., Lim, C. J., Brereton, C. M. H. and Grace, J. R. (2000). *Suspension-to-membrane-wall heat transfer in a circulating fluidized bed combustor*. International Journal of Heat and Mass Transfer 43(7): 1173-1185.

Luan, W., Lim, C. J., Brereton, C. M. H., Bowen, B. D. and Grace, J. R. (1999). *Experimental and theoretical study of total and radiative heat transfer in circulating fluidized beds*. Chemical Engineering Science 54(17): 3749-3764.

Lupiáñez, C., Guedea, I., Bolea, I., Díez, L. I. and Romeo, L. M. (2012). *Experimental study of SO2 and NOx emissions in fluidized bed oxy-fuel combustion*. Fuel Processing Technology(0).

Lupiáñez, C., Guedea, I., Bolea, I., Pallarés, J., Díez, L. I. and Romeo, L. M. (2011). *Oxy-firing of high sulphur coal in CIRCE fluidized bed pilot plant*. 5th International Conference on Clean Coal Technologies. Zaragoza, Spain.

Man, Z., Haibo, W., Qinggang, L., Yunkai, S. and Guoliang, S. (2012). *Heat transfer characteristics of fluidized bed heat exchanger in a 300 MW CFB boiler*. Powder Technology 222(0): 1-7.

Masoumifard, N., Mostoufi, N., Hamidi, A.-A. and Sotudeh-Gharebagh, R. (2008). *Investigation of heat transfer between a horizontal tube and gas–solid fluidized bed*. International Journal of Heat and Mass Transfer 29: 1504-1511.

Mathur, A., Saxena, S. C. and Chao, A. (1986). *Heat transfer from an immersed vertical tube in a gas-fluidzied bed*. Industrial & Engineering Chemistry Fundamentals 25(1): 156-163.

Mattisson, T. A. and Lyngfelt , A. (1999). *The reaction between limestone and SO2 under periodically changing oxidizing and reducing conditions – effect of temperature and limestone type*. Termochimica Acta 325: 59-67.

McCauley, K. J., Farzan, H., Alexander, K. C., McDonald, D. K., Varagani, R., Prabhakar, R., Tranier, J.-P. and Perrin, N. (2008). *Commercialization of Oxy-Coal Combustion: Applying Results of a Large 30 MWth Pilot Project*. 9th International Conference on Greenhouse Gas Control Technologies, Washington, D.C., U.S.A.

Mickley, H. S. and Fairbanks, D. F. (1955). *Mechanism of heat transfer to fluidized beds*. AIChE Journal 1(3): 374-384.

Mills, A. F. (1995). *Transferencia de calor*, Irwin.

Molerus, O., Burschka, A. and Dietz, S. (1995a). *Particle migration at solid surfaces and heat transfer in bubbling fluidized beds--I. Particle migration measurement systems*. Chemical Engineering Science 50(5): 871-877.

Molerus, O., Burschka, A. and Dietz, S. (1995b). *Particle Migration at solid surfaces and heat transfer in bubbling fluidized beds- II. Prediction of heat transfer in bubbling fluidized beds*. Chemical Engineering Science 50(5): 879-885.

Myöhänen, K., Eriksson, T., Kuivalainen, R. and Hyppänen, T. (2012). *Design and modelling of a 330 MWe Flex-Burn CFB for oxygen-fired and air-fired combustion*. 21st International Conference on fluidized bed combustion, Naples, Italy.

Nsakala, N., Liljedahl, G. N. and Turek, D. G. (2004). *Greenhouse gas emissions control by oxygen firing in Circulating Fluidized Bed Boilers. Phase II-Pilot scale*

testing and updated performance and economics for oxygen fired CFB with CO_2 capture. Final Technical Progress Report, ALSTOM Power Inc.

Ochs, T., Oryshchyn, D., Woodside, R., Summers, C., Patrick, B., Gross, D., Schoenfield, M., Weber, T. and O'Brien, D. (2009a). *Results of initial operation of the Jupiter Oxygen Corporation oxy- fuel 15 MWth burner test facility*. Energy Procedia 1(1): 511-518.

Ochs, T., Patrick, B., O'Brien, D., Oryshchyn, D., Summers, C., Gerdemann, S., Woodside, R., Carney, C., Schoenfield, M. and Turner, P. (2009b). *Oxy-Natural Gas Firing of the Jupiter Oxygen Oxy-Fuel Test Facility*. 34th International Technical Conference on Coal Utilization & Fuel Systems, Clearwater, Florida, USA.

Oka, S. N. (2003). *Fluidized Bed Combustion*, Marcel Dekker Inc.

Okazaki, K. and Ando, T. (1997). *NOx reduction mechanism in coal combustion with recycled CO2*. Energy 22(2-3): 207-215.

Ozawa, M., Umekawa, H., Matsuda, T., Takenaka, N. and Matsubayashi, M. (1998). *Flow Pattern and Heat Transfer in Tube Banks of a Simulated FLuidized Bed Heat Exchanger*. JSME International Journal 41(3): 720-726.

Pallarès, D. and Johnsson, F. (2006). *Macroscopic modelling of fluid dynamics in large-scale circulating fluidized beds*. Progress in Energy and Combustion Science 32(5-6): 539-569.

Park, C. K. and Basu, P. (1997). *A model for prediction of transient response to the change of fuel feed rate to a circulating fluidized bed boiler furnace*. Chemical Engineering Science 52(20): 3499-3509.

Patil, D. J., Smit, J., Van Sint Annaland, M. and Kuipers, J. A. M. (2006). *Wall-to-bed heat transfer in gas-solid bubbling fluidized beds*. AIChE Journal 52(1): 58-74.

Peña, J. A. P. (2011). *Bubbling Fluidized Bed (BFB), when to use this technology?* Industrial Fluidization South Africa. Jojannesburg, South Africa.

Pidwerbecki, D. and Welty, J. R. (1995). *Heat transfer to a horizontal tube in the splash zone of a bubbling fluidized bed, an experimental study of particle size effects*. Experimental Thermal and Fluid Science 10(3): 307-317.

Pikkarainen, T. (2007). *Small scale fluidized bed experiments under oxygen combustion conditions*. 2007 International Conference on Coal Science and Technology, Nottingham, UK.

Qiu, K. and Lindqvist, O. (2010). *Direct sulfation of limestone at elevated pressures*. Chemical Engineering Science 55: 3091-3100.

Rabinovich, E. and Kalman, H. (2011). *Flow regime diagram for vertical pneumatic conveying and fluidized bed systems*. Powder Technology 207(1–3): 119-133.

Redemann, K., Hartge, E. U. and Werther, J. (2009). *A particle population balancing model for a circulating fluidized bed combustion system*. Powder Technology 191(1-2): 78-90.

Rodriguez, O. M. H., Pécora, A. A. B. and Bizzo, W. A. (2002). *Heat recovery from hot solid particles in a shallow fluidized bed*. Applied Thermal Engineering 22(2): 145-160.

Romeo, L. M., Bolea, I. and Escosa, J. M. (2008). *Integration of power plant and amine scrubbing to reduce CO2 capture costs*. Applied Thermal Engineering 28(8–9): 1039-1046.

Romeo, L. M., Bolea, I., Lara, Y. and Escosa, J. M. (2009a). *Optimization of intercooling compression in CO2 capture systems*. Applied Thermal Engineering 29(8–9): 1744-1751.

Romeo, L. M. and Cortés, C. (1998). *Simulation of a full-scale pressurized fluidized bed combustor by using semi-empirical pilot plant correlations*. Revue Générale de Thermique 37(10): 862-873.

Romeo, L. M., Díez, L. I., Guedea, I., Bolea, I., Lupiáñez, C., González, A., Pallarés, J. and Teruel, E. (2010a). *Design and operation assessment of an oxyfuel fluidized bed combustor*. Experimental Thermal and Fluid Science In Press, Corrected Proof.

Romeo, L. M., Díez, L. I., Guedea, I., Bolea, I., Lupiáñez, C., González, A., Pallarés, J. and Teruel, E. (2011). *Design and operation assessment of an oxyfuel fluidized bed combustor*. Experimental Thermal and Fluid Science 35(3): 477-484.

Romeo, L. M., Díez, L. I., Lisbona, P., González, A., Guedea, I., Lupiáñez, C., Martínez, A., Lara, Y. and Bolea, I. (2010b). *Captura y almacenamiento de CO2*. Zaragoza, Prensas Universitarias de Zaragoza.

Romeo, L. M., Guedea, I., Bolea, I., González, A., Lupiáñez, C., Pallares, J. and Diez, L. I. (2009b). *First Results in an Oxyfuel Combustion Fluidized Bed*. 1st Oxyfuel Combustion Conference. Cottbus, Germany.

Saastamoinen, J., Tourunen, A., Pikkarainen, T., Häsä, H., Miettinen, J., Hyppänen and Myöhänen, K. (2006). *Fluidized bed combustion in high concentrations of O2 and CO2*. 19th FBC Conference, Vienna, Austria.

Santos, S. (2009). *Challenges in the Development of Oxy-Coal Combustion Power Plant with CO_2 Capture*. Asia Pacific Programme (APP). Oxyfuel Working Group Capacity Bldg. Course, Daejeon, South Korea.

Santos, S. and Haines, M. (2005). *Oxy-fuel Combustion Application for Coal Fired Power Plant*. Inaugural Workshop of the International Oxy-Combustion Research Network., Cottbus, Germany.

Santos, S. and Haines, M. (2007). *Oxy-fuel Combustion: Progress and Remaining Issues*. . 2nd Workshop of the International Oxy-Combustion Research Network., Windsor CT, USA.

Sarofim, A. (2007). *Oxy-fuel Combustion: Progress and Remaining Issues*. . 2nd Workshop of the International Oxy-Combustion Research Network., Windsor CT, USA.

Scala, F., Chirone, R. and Salatino, P. (2011). *Recent Research on Fluidized bed Oxy-fuel combustion at Naples*. 63rd IEA FBC meeting, Ponferrada, Spain.

Scala, F. and Salatino, P. (2010). *Flue gas desulfurization under simulated oxyfiring fluidized bed combustion conditions: The influence of limestone attrition and fragmentation*. Chemical Engineering Science 65(1): 556-561.

Scheffknecht, G. (2009). *Research Perspective- Review of the Current Understanding, Identifying Research Gaps*. 1st Oxyfuel Combustion Conference, Cottbus, Germany.

Scheffknecht, G., Grathwohl, S., Lemp, O., Schnell, U., Maier, J., Kluger, F., Krohmer, B., Moenckert, P. and Stamatelopoulos, G. N. (2009). *Highly Flexible Burner Concept for Oxyfuel Cobustion*.

Schmidt, A. and Renz, U. (2005). *Numerical prediction of heat transfer between a bubbling fluidized bed and an immersed tube bundle*. Heat and Mass Transfer 41: 257-270.

Schoenfield, M. and Menendez, M. (2012). *Oxy-fuel burner and integrated pollutant removal research and development test facility*, Jupiter Oxygen Corporation.

Seddigh, S., Pallarès, D., Johnsson, F., Varonen, M., Hyytiäinen, I., Ylä-Outinen, V. and Palonen, M. (2011). *Assessment of Oxyfuel Circulating Fluidized Bed Boilers – Modeling and Experiments in a 5 MW Pilot Plant*. 2nd Oxyfuel Combustion Conference. Queensland, Australia, IEG GHG.

Seddighi, S., Pallarès, D. and Johnsson, F. (2010). *One-dimensional modeling of oxy-fuel fluidized bed combustion for CO2 capture*. Fluidization XIII: New Paradigm in Fluidization Engineering, Gyeong-ju, Korea.

Seevam, P. N., Downie, M. J. and Race, J. M. (2008). *The Next Generation of CO_2 Pipelines*. IEA Summer School 2008, Vancouver, Canada.

Seltzer, A., Fan, Z. and Hack, H. (2009). *Design of a Flexi-Burn™ Pulverized Coal Power Plant for Carbon Dioxide Sequestration*. 34th International Technical Conference on Coal Utilization & Fuel Systems, Clearwater, Florida, USA.

Shaul, S., Rabinovich, E. and Kalman, H. (2012). *Generalized flow regime diagram of fluidized beds based on the height to bed diameter ratio*. Powder Technology 228(0): 264-271.

Shen, L., Johnsson, F. and Leckner, B. (2004). *Digital image analysis of hydrodynamics two-dimensional bubbling fluidized beds*. Chemical Engineering Science 59(13): 2607-2617.

Sims, R. E. H., Schock, R. N., Adegbululgbe, A., Fenhann, J., Konstantinaviciute, I., Moomaw, W., Nimir, H. B., Schlamadinger, B., Torres-Martínez, J., Turner, C., Uchiyama, Y., Vuori, S. J. V., Wamukonya, N. and Zhang, X. (2007). *Energy supply*. Climate Change 2007. Mitigation. Contribution of Working Group III to the Fourth

Assessment Report of the Intergovernmental Panel on Climate Change. Cambridge University Press.

Smart, J., O'Nions, P., Riley, G. and Jamiesion, E. (2009). *Radiative and Convective Heat Transfer in Oxy-Coal Combustion*. 1st Oxyfuel Combustion Conference, Cottbus, Germany.

Snow, M. J. H., Longwell, J. P. and Sarofim, A. F. (1988). *Direct Sulfation of Calcium Carbonate*. Industrial & Engineering Chemistry Research 27: 268-273.

Sotudeh-Gharebaagh, R., Legros, R., Chaouki, J. and Paris, J. (1998). *Simulation of circulating fluidized bed reactors using ASPEN PLUS*. Fuel 77(4): 327-337.

Spero, C., Chpman, L. and Montagner, F. (2011). *Callide Oxy-fuel Project. Stage 1-Capture at Callide A Power Station Comissioning Experience.* 2nd Oxyfuel Combustion Conference. Queensland, Australia

Spero, C. and Montagner, F. (2007). *Oxy-combustion Technology in the World Scene*. Coal21 Conference, NSW, Australia.

Stanmore, B. R. and Gilot, P. (2005). *Review—calcination and carbonation of limestone during thermal cycling for CO2 sequestration*. Fuel Processing Technology 86: 1707-1743.

Stringer, J. (1995). *Practical experience with wastage at elevated temperatures in coal combustion systems*. Wear 186-187: 11-27.

Sturgeon, D. (2009). *Official Opening of the OxyCoal™ Clean Combustion Test Facility. Technical Seminar*.

Sun, P., Grace, J. R., Lim, C. J. and Anthony, E. J. (2007). *Removal of CO2 by Calcium-Based Sorbents in the Presence of SO2*. Energy & Fuels 21: 163-170.

Sunderesan, S. R. and Clark, N. N. (1995). *Local heat transfer coefficients on the circumference of a tube in a gas fluidized bed*. International Journal of Multiphase Flow 21(6): 1003-1024.

Svensson, A., Johnsson, F. and Leckner, B. (1996). *Bottom bed regimes in a circulating fluidized bed boiler*. International Journal of Multiphase Flow 22(6): 1187-1204.

Tchunko, S., Toporov, D., Föster, M. and Kneer, R. (2008). *Stabilising Swirl Pulverised Coal Flames under Oxyfuel Conditions*. 2nd Young Researchers Forum on Oxyfuel Combustion, Gotheborg, Sweden.

Thunman, H., Niklasson, F., Johnsson, F. and Leckner, B. (2001). *Composition of Volatile Gases and Thermochemical Properties of Wood for Modeling of Fixed or Fluidized Beds*. Energy & Fuels 15: 1488-1497.

Tondl, G., Penthor, S., Wöß, D., Pröll, T., Höltl, W., Rohovec, J. and Hofbauer, H. (2011). *From Oxygen enrichement to Oxyfuel combustion*. 63rd IEA FBC meeting, Ponferrada, Spain.

Total (2007). *Project Information Dossier. Lacq CO_2 capture and storage Pilot Project*.

Umekawa, H., Ozawa, M., Takenaka, N. and Matsubayashi, M. (1999). *Visualization of bed material movement in a simulated fluidized bed heat exchanger by neutron radiography*. Nuclear Instruments and Methods in Physics Research Section A: Accelerators, Spectrometers, Detectors and Associated Equipment 424(1): 77-83.

UNFCC (1992). *United Nations Framework Convention on Climate Change*.

van Heerden, C., Nobel, A. P. P. and van Krevelen, D. W. (1953). *Mechanism of Heat Transfer in Fluidized Beds*. Industrial & Engineering Chemistry 45(6): 1237-1242.

van Ommen, J. R. and Mudde, R. F. (2007). *Measuring the Gas-Solids Distribution in Fluidized Beds - A Review*. 12th International Conference on Fluidization. Vancouver, Canada.

Varonen, M. (2011). *4 MWth Oxy-CFB Test Runs*. 63rd IEA FBC meeting, Ponferrada, Spain.

Varonen, M., Hyytiäinen, I., Palonen, M. and Ylä-Outinen, V. (2012). *Results of oxyfuel combustion tests in 4MWth CFB pilot boiler*. 21st International Conference on fluidized bed combustion. Naples, Italy.

Vepsalainen, A., Myohanen, K., Hyppanen, T., Leino, T. and Tourunen, A. (2009). *Development and Validation of a 3-Dimensional CFB Furnace Model*. 34th

International Technical Conference on Coal Utilization & Fuel Systems. Clearwater, Florida, USA.

Wagialla, K. M., Elnashaie, S. S. and Fakeeha, A. H. (1990). *Review on heat transfer in gas solid fluidized beds*. Chemical Engineering 2(2): 331-346.

Wall, T., Liu, Y., Spero, C., Elliott, L., Khare, S., Rathnam, R., Zeenathal, F., Moghtaderi, B., Buhre, B., Sheng, C., Gupta, R., Yamada, T., Makino, K. and Yu, J. (2009). *An overview on oxyfuel coal combustion--State of the art research and technology development*. Chemical Engineering Research and Design 87(8): 1003-1016.

Wang, C., Jia, L., Tan, Y. and Anthony, E. J. (2008). *Carbonation of fly ash in oxy-fuel CFB combustión*. Fuel 87: 1108-1114.

Wang, C., Jia, L., Tan, Y. and Anthony, E. J. (2011). *Influence of Water Vapor on the Direct Sulfation of Limestone under Simulated Oxy-fuel Fluidized-Bed Combustion (FBC) Conditions*. Energy & Fuels 25: 617-623.

Wang, Q., Luo, Z., Fang, M., Ni, M. and Cen, K. (2003). *Development of a new external heat exchanger for a circulating fluidized bed boiler*. Chemical Engineering and Processing 42(4): 327-335.

Wang, Q., Luo, Z., Li, X., Fang, M., Ni, M. and Cen, K. (1999). *A mathematical model for a circulating fluidized bed (CFB) boiler*. Energy 24(7): 633-653.

Wang, W., Lu, B., Zhang, N., Shi, Z. and Li, J. (2010). *A review of multiscale CFD for gas-solid CFB modeling*. International Journal of Multiphase Flow 36(2): 109-118.

Wen, C. Y. and Leva, M. (1956). *Fluidized bed heat transfer; a generlaized dense phase correlation*. AIChE Journal 2(4): 482-488.

Wen, C. Y. and Yu, Y. H. (1966). *Mechanics of fluidization*. Chemical Engineering Progress Symposium Series 62: 100-111.

Werdermann, C. C. and Werther, J. (1993). *Solids flow pattern and heat transfer in an industrial-scale fluidized bed heat exchanger*. The 12th International Conference on Fluidization - New Horizons in Fluidization Engineering, New York, USA.

Werner, A. (2001). *Solids distribution as a basis for modeling of heat transfer in circulating fluidized bed boilers*. Experimental Thermal and Fluid Science 25(5): 269-276.

Werther, J. (1999). *Measurement techniques in fluidized beds*. Powder Technology 102(1): 15-36.

Werther, J., Hartge, E.-U., Ratschow, L. and Wischnewski, R. (2009). *Simulation-supported measurements in large circulating fluidized bed combustors*. Particuology 7(4): 324-331.

White, V., Armstrong, P. and Fogash, K. (2009). *Oxygen supply for Oxyfuel CO_2 capture*. 1st Oxyfuel Combustion Conference, Cottbus, Germany.

Wilke, C. R. (1950). *A Viscosity Equation for Gas Mixtures*. The Journal of Chemical Physics 18(4).

Wilsoon, J., Maxwell, C., Degenstein, N., Sah, M., Li, J., Venkateswaran, V., Eddings, E. and Adams, J. (2009). *Oxygen Transport Membrane Based OxyCombustion for CO_2 Capture from Coal Power Plants*.

Wirth, K. E. (1994). *Prediction of heat transfer in circulating fluidized beds*. 4th International Conference on Circulating Fluidized Beds. Pennsylvania

Wirth, K. E. (1995). *Heat Transfer in Circulating Fluidized Beds*. Chemical Engineering Science 50(13): 2137-2151.

Wu, Y., Wang, C., Tan, Y., Jia, L. and Anthony, E. J. (2011). *Characterization of ashes from a 100 kWth pilot-scale circulating fluidized bed with oxy-fuel combustion*. Applied Energy In Press, Corrected Proof.

Xavier, A. M. and Davidson, J. F. (1985). *Heat Transfer in Fluidized Beds: Convective heat transfer in fluidized beds*. Fluidization. Academic Press.

Xie, D., Bowen, B. D., Grace, J. R. and Lim, C. J. (2003). *Two-dimensional model of heat transfer in circulating fluidized beds. Part II: Heat transfer in a high density CFB and sensitivity analysis*. International Journal of Heat and Mass Transfer 46: 219-2205.

Yamada, J., Kurosaki, Y. and Nagai, T. (2001). *Radiation Heat Transfer Between Fluidizing Particles and a Heat Transfer Surface in a Fluidized Bed*. Journal of Heat Transfer 123(458-465).

Yan, J., Faber, R., Jacoby, J., Anheden, M., Giering, R., T., S., Ross, G., Stark, F. and Kosel, D. (2009). *Flue-gas cleaning Processes for CO2 Capture from Oxyfuel Combustion- Experience of FGD and FGC at 30 MWth Oxyfuel Combustion Pilot*. 1st Oxyfuel Combustion Conference, Cottbus, Germany.

Yang, H., Yue, G., Xiao, X., Lu, J. and Liu, Q. (2005). *1D modeling on the material balance in CFB boiler*. Chemical Engineering Science 60(20): 5603-5611.

Yusuf, R., Halvorsen, B. and Melaaen, M. C. (2012). *An experimental and computational study of wall to bed heat transfer in a bubbling gas-solid fluidized bed*. International Journal of Multiphase Flow 42(2): 9-23.

Zabrodsky, S. S. (1966). *Hydrodynamics and heat transfer in fluidized beds*, The M.I.T Press.

Zarghami, R., Mostoufi, N., Sotudeh-Gharebagh, R. and Chaouki, J. (2007). *Analysis and modeling of particle-wall contact time in gas fluidized beds*. Chemical Engineering Science 62(17): 4573-4578.

Zhang, N., Lu, B., Wang, W. and Li, J. (2010). *3D CFD simulation of hydrodynamics of a 150 MWe circulating fluidized bed boiler*. Chemical Engineering Journal 162(2): 821-828.

Ziegler, E. N., Koppel, L. B. and Brazelton, W. T. (1964). *Effects of Solid Thermal Properties on Heat Transfer to Gas Fluidized Beds*. Industrial & Engineering Chemistry Fundamentals 3(4): 324-328.

Zijerveld, R. C., Koniuta, A., Johnsson, F., Marzocchella, A., Schouten, J. C. and Bleek, M. v. d. (1997). *Axial Solids Distribution and Bottom Bed Dynamics for Circulating Fluidized Bed Combustor Application*. AIChE Symposium Series 93(317): 97–102.